High Temperature Filtration in Biomass Combustion and Gasification Processes

by

Håvar Risnes

A thesis submitted to
The Norwegian University of Science and Technology
for the degree of
Doktor Ingeniør

August 2002
The Norwegian University of Science and Technology
Faculty Engineering Science and Technology
Department of Thermal Energy and Hydropower

URN:NBN:no-3322

URN:NBN:no-3322

NTNU
The Norwegian University of Science and Technology
Norges teknisk-naturvitenskapelige universitet

Report no.
2002:08
Classification
Open

POSTAL ADDRESS
NTNU
DEPARTMENT OF THERMAL
ENERGY AND HYDROPOWER
Kolbjørn Hejes vei 1A
N-7491 TRONDHEIM

TELEPHONE
Switchboard NTNU: +47 73 59 40 00
Department office: +47 73 59 27 00
Hydropower section: +47 73 59 38 57

TELEFAX
Department office: +47 73 59 83 90
Hydropower section: +47 73 59 38 54

Title of report HIGH TEMPERATURE FILTRATION IN BIOMASS COMBUSTION AND GASIFICATION PROCESSES	Date August 2002 No. of pages/appendixes 183/238
Author Håvar Risnes	Project manager Johan E. Hustad
Division Faculty of Engineering Science and Technology Department of Thermal Energy and Hydropower	Project no.
ISBN nr. 82-471-5463-3/2002:66	Price group
Client/sponsor of project The Nordic Council of Ministers' Energy Research Program on Biomass combustion, Vang Filter Technology and ReaTech.	Client's ref.

Abstract

High temperature filtration in combustion and gasification processes is a highly interdisciplinary field. Thus, particle technology in general has to be supported by elements of physics, chemistry, thermodynamics and heat and mass transfer processes. This topic can be addressed in many ways, phenomenological, based on the up stream processes (i.e. dust/aerosol formation and characterisation) or apparatus oriented.

The efficiency of the thermochemical conversion process and the subsequent emission control are major important areas in the development of environmentally sound and sustainable technology. Both are highly important for combustion and gasification plant design, operation and economy.

This thesis is divided into four parts:

I. High temperature cleaning in combustion processes.
II. Design evaluations of the Panel Bed Filter technology.
III. Biomass gasification
IV. High temperature cleaning of biomass gasification product gas

The first part validates the filter performance through field experiments on a full scale filter element employed to a biomass combustion process and relates the results to state of the art within comparable technologies (i.e. based on surface filtration). The derived field experience led to new incentives in the search for a simplified design featuring increased capacity. Thus, enabling both high efficiency and simplified production and maintenance. A thorough examination of design fundamentals leading to the development of a new filter geometry is presented.

It is evident that the up-stream process has significant influence upon the operation conditions of a filter unit. This has lead to a detailed investigation of some selected aspects related to the thermochemical conversion. Furthermore, the influence of fuel characteristics upon conversion and product gas quality is discussed.

The last part discusses the quality of biomass gasification product gas and requirements put upon the utilisation of this gas in turbines, diesel engines or other high temperature applications. Filtration experiments conducted on product gas derived from wood gasification are reported and discussed.

	Indexing Terms: English	Indexing Terms: Norwegian
Group 1	Heat Engineering	Varmeteknikk
Group 2	Filtration	Filtrering
Selected by author	Solid Fuels	Faste brensler
	Combustion	Forbrenning
	Gasification	Forgassning

URN:NBN:no-3322

Preface

The work presented in this thesis has been performed at the Norwegian University of Science and Technology (NTNU), Faculty of Engineering Science and Technology, Department of Thermal Energy and Hydro Power. In addition considerable time has been spent at ReaTech in Denmark and Åbo Academy University, Faculty of Chemical Engineering, Combustion Research Group, Finland.

This work originates from the desire to increase the knowledge and understanding of high temperature filtration in biomass combustion and gasification processes.

I direct a sincerely thank you to all of my financial contributors. Main financial contributor has been the Nordic Council of Ministers' Energy Research Program on Biomass combustion, funding scholarship. However, Vang Filter Technology and ReaTech have also contributed financially.

I want to thank my academic advisors, Professor Johan E. Hustad and Professor Otto K. Sønju, for their assistance and for making it possible for me to conduct this work, and for encouraging me to publish my work within the scientific community.

I wish to thank Lasse Holst Sørensen and Jan Fjellerup at ReaTech for many valuable discussions concerning fuel reactivity and equilibrium modelling. Furthermore, Associate Professor Rainer Backman at Åbo Academy University is acknowledged for his guidance and support on aspects concerning equilibrium modelling. I also would like to thank my other friends at Åbo Academy University and the Technical University of Denmark for inspiration and for their friendship.

The scientific staff at the Department of Thermal Energy and Hydropower deserves thanks for their help, encouragement, inspiring discussions and critical comments. Special thanks goes to my fellow-Ph.D. students Maria Barrio and Klaus Zepter whom I shared the boat with during this study. Furthermore, Anders Liang and Hans Kritian Odland deserves a sincerely thank you for their patient and accurate work on the development of the new filter design. The support from the technical staff in the laboratory regarding design and modifications of experimental equipment is acknowledged, especially Oddmund Rydningen, Halvor Flatberg, Geir Haugness, Nils Skei and Helge Laukholm. Without their support the comprehensive experimental program carried out in this thesis would not have been possible.

URN:NBN:no-3322

Table of contents

URN:NBN:no-3322

1 Introduction

Fossil fuels such as coal, oil and gas are by far the major energy carriers utilised in the global energy production. However, growing concern for the environmental impact of increased CO_2 accumulation in the atmosphere has resulted in renewed interest in the utilisation of renewable energy carriers. Combustion and gasification of bio-fuels in advanced CHP plants represents an interesting and important alternative in this respect.

Although being CO_2 neutral, utilisation of these fuels requires efficient systems for the removal of other gaseous and particulate emissions. This has made product gas cleaning an objective of much research world-wide and represents the motivation for this work, where the focus has been directed upon the utilisation of the Panel Bed Filter.

This novel gas cleaning concept utilises the transient behaviour of granular filtration and operates in surface filtration mode. Louvered walls, somewhat resembling Venetian blind, hold a sand bed in a tall relatively narrow "panel". These louvers expose a large number of sand surfaces upon which the fly ash is deposited, forming a filter cake. The filter is periodically cleaned, by releasing a short pressure pulse, acting in the reverse direction to normal flow.

1.1 Background

Gasification makes efficient electricity production possible through advanced thermal conversion of the biomass into a secondary fuel for utilisation in integrated gasification combined cycle (IGCC) or fuel cells. For these processes, environmentally sound feedstocks are biomass materials, like wood, agricultural residues, municipal waste and energy crops. Conversion of these fuels by gasification facilitates the removal of environmentally hazardous impurities and their precursors from the gas before it is combusted. Thus, very high demands are put on the hot gas cleanup unit and the product gas must comply with strict regulations with respect to both alkali metals and particulate matter.

Alkali metals tend to participate in the formation of submicron aerosols. The capture of these submicron aerosols must proceed by impaction, interception or further particle growth by condensation. Gas cooling increases the collection efficiency by inducing further condensation and particle growth. Formation of stable and super micron particles, significantly enhances filter performance. Unfortunately, the cooling of the product gas results in lower overall power efficiency.

In the case of biomass, the flue gas should be cooled below some 400-550 °C for an adequate removal of alkali metals (Kurkela 1996). At the biomass-fired IGCC plant in Värnamo, the fuel gas is cooled to 350-400 °C (process pressure about 18bar) before filtration to ensure the longevity of the gas turbine (Engstrom 1998). For advanced facilities using biomass, the matter of optimising the hot gas cleanup system with respect to both filtration efficiency and overall power efficiency remains to be solved satisfactorily.

1.2 Thesis objective

The overall objective of this work has been to contribute to the future development of the Panel Bed Filter technology, with general emphasis on high temperature biomass combustion and gasification processes in particular.

The validation of the Panel Bed Filter versus state of the art within technologies based on surface filtration/dust cake formation, is motivated on the lack of comparative studies and the voluminous work conducted within this field during the last decades.

Design evaluations was introduced upon recently acquired field experience, which re-vitalised the interest of a design featuring simplicity with respect to production and maintenance, as well as rigidity in operation and increased filter competitiveness.

The process of product gas cleaning is still one of the major technical challenges with regard to the utilisation of biomass producer gas in gas-fired engines or gas turbines. The complexity of the contaminants in special, being closely coupled to the conversion process itself, motivated the work on the more fundamental processes involved in the thermochemical conversion of biomass fuels. And thereby contribute to increased knowledge about fuel conversion, the release of inorganic compounds and the interaction within these processes, as well as the interaction between gasifier/combustor and the down stream equipment (e.g. heat exchangers and filters).

Furthermore, operational experience and scientific publications concerning high temperature filtration of biomass gasification product gas is rather limited. This motivated the experimental work on high temperature filtration and contaminant characterisation.

1.3 Summary

The filtration experiments embrace investigations conducted on a full-scale filter element (about 1100 m^3/h) and two laboratory scale filter units (about 1-5 m^3/h) for high temperature filtration. The filtration activity involved design, construction and operation of the two laboratory scale filter units. And govern filter capacity enhancement through the development of a new and simplified design.

Chapter 2

Field tests, on the single filter element of commercial design were successfully conducted at typical operating condition. Measured filtration efficiency is comparable with bag house filters. The applied filtration velocities (up to 14 cm/s) are extremely high compared with bag filters (normally operating at about 1.0 to 2.5 cm/s). Measured pressure drop over the sand filter shows, despite this, that it is possible to work within the same field as bag filters, i.e. from 900 to approximately 2200 Pa.

Average dust concentration downstream of the filter unit was measured to be well below 5 mg/Nm^3. Measured filtration efficiency at 190 °C and 9 cm/s corresponds to a filter efficiency above 99.83%, verified in a full-scale pilot plant. Calculated average specific cake resistance (K_2') equals 6.5 (± 0.1) $\cdot 10^4$ [s^{-1}] at operating conditions, which is within the range found in the literature.

The Panel Bed Filter concept has been successfully demonstrated in full scale operation, and more detailed filtration behaviour has been studied. Filter cake data have been obtained at very high filtration velocity and reasonable pressure drops. Very low dust concentrations are observed.

Chapter 3

New front louver geometry has been developed; featuring reduced manufacturing costs, simplified production and maintenance, and enhanced filter capacity. The novel front louver design features 2 to 3 fold increase in filter capacity, compared to the original Wishbone design, and the measured filtration efficiency was generally above 99.9%. The reported filtration experiments cover a range of superficial velocities from about 4-20 cm/s and raw dust concentrations from 1 to 11 g/m^3. Sand (AFS30) with a mass median diameter of about 500 μm (d_p < 200 μm removed) has been used in all filtration experiments.

Special attention has been directed upon the cleaning action applied and the resulting sand spill distribution, emphasising upon the pressure pulse induced motion of sand. Applying a variety of cleaning pulse shapes, and operating the filter on-line/off-line gave no significant effect upon the resulting puffback uniformity as seen in the laboratory scale filter units.

Furthermore, removing the second (coarse) sand layer (applied in the commercial scale filter) imposes restrictions concerning the filter capacity. As too high filtration velocities (e.g. due to process fluctuations) and uneven velocity profiles both can lead to fluidisation of the unbounded bed of granular media.

Chapter 4

The great diversity among biomass fuels and its impact upon the gasification process and down stream equipment are discussed. And investigations are made in order to produce operational data for the *C-CO$_2$* and the *C-H$_2$O-H$_2$* gasification of biomass (wood and straw) chars and coal chars. The char reactivity was thermogravimetrically determined using pre-pyrolysed char samples, at atmospheric pressure and sample temperatures in the range from 700 to 1000 °C.

The influence of the inherent ash forming elements upon gasification behaviour of five straw chars is investigated. This work focuses beside fuel characterisation on the effect of quantitative addition of calcium to straw samples and its influence on agglomeration, sintering, corrosion and fuel gasification reactivity. A brief summary and conclusion of the papers presented on this topic is given below.

CO2 reactivity of chars from wheat, spruce and coal

Measurement and modelling of *CO$_2$*-gasification reactivity is presented for two biomass chars: Danish wheat straw and Norwegian spruce char; and a dense metallurgical coke from Longyear coal. The reactivity was thermogravimetrically determined using 4-10 mg of pre-pyrolysed char samples, *CO$_2$*-partial pressure (0.03-1 bar) and sample temperature (700-1000 °C). Char reactivity (R) is expressed by separating the effects arising from true kinetics (r_C) and structural development ($f(X)$), the resulting function: $R = r_C \cdot f(X)$. r_C is modelled by n^{th} order kinetics

For all fuels tested the n^{th} order kinetic models gives a good representation of the thermogravimetrically determined CO_2-reactivity. Since normalised reactivity was approximately independent of conversion, for each char, one reaction order, and activation energy could be estimated for the whole range of temperatures and CO_2 partial pressures. Applying n^{th} order kinetics the following kinetic parameters were obtained (atmospheric experiments): apparent activation energies (E) for wheat straw char; 205.6 kJ/mol, spruce char; 219.9 kJ/mol and Longyear coke; 233.1 kJ/mol, the respective reaction orders equals 0.59, 0.36 and 0.51. However, the results indicated that a more complex mechanism must be considered if the results, even for a single pure gas, are to be extrapolated to their limits for the purposes of modelling reactor data under realistic conditions.

Steam gasification of wood char and the effect of hydrogen inhibition on the chemical kinetics.

Gasification kinetics parameters have been derived for birch and beech char samples pyrolysed under identical conditions. Reactivity experiments were made in steam-hydrogen-nitrogen mixtures at atmospheric pressure. Reactivity profiles have been obtained in the temperature range from 750 °C to 950 °C, for H_2O partial pressures of 0.05-1.0 bar and H_2 partial pressures of 0.1-0.3 bar. Assuming n^{th} order kinetics for pure steam experiments, the activation energy and the reaction order are E = 211 kJ/mol and n = 0.51 for beech and E = 237 kJ/mol and n = 0.57 for birch.

A kinetic expression based on Langmuir-Hinshelwood kinetics fairly describes the observed hydrogen inhibition effect on the steam-carbon reaction. The differences between the kinetics determined for the two fuels are relatively small and partly due to the origin and quality of the raw wood. The kinetic parameters obtained are presented using a kinetic compensation diagram; they are compared with literature data and discussed. The influence of the calculation procedure on the results is discussed, it is concluded that: i) The definition of the reactivity will not affect the activation energy or the reaction order calculation. ii) The method to select a representative reactivity value from one experiment has more influence on the frequency factor than on the activation energy and reaction order. The accuracy of the calculation might also be affected.

Calcium addition in straw gasification

The present work focuses beside fuel characterisation on the effect of quantitative addition of calcium to straw samples and its influence on agglomeration, sintering, corrosion and fuel gasification reactivity. The equilibrium program FACT was used for the theoretical evaluation under atmospheric gasification conditions in a temperature range of 700 to 1000 °C. Char reactivity was measured in two thermogravimetric analyzers and subsequently the ashes were analysed using scanning electron microscopy, X-ray diffraction and time resolved in-situ synchrotron X-ray powder diffraction. Equilibrium calculation predicts the significant formation of a molten catalytic and corrosive salt phase and a silicate-oxide slag. Calcium may be added dry or impregnated as calcium carbonate, calcium oxide and calcium-acetate and additionally together with an organic matrix. When properly added, calcium to a large extent binds silicon producing calcium silicates e.g. as Ca_2SiO_4 and Ca_3SiO_5 and

to minor extent potassium as potassium calcium silicates, e.g. $K_4CaSi_3O_9$ and K_2CaSiO_4. Hereby the addition of sufficient amounts of calcium favours the formation of potassium (and calcium-) carbonate rich salt mixture formation while silicate slag formation is reduced.

Chapter 5

Generally cooling of biomass gasification product gas to below some 550 °C results in the alkali level being reduced to acceptable limits while further cooling might introduce operational problems due to tar condensation. The critical temperature limit beyond which tar condensation will cause operational problems within the filter system is highly dependent upon gasifier operation.

A high temperature granular bed filter unit has been designed and connected to an air blown stratified downdraft biomass gasifier (fuelled with birch pellets). Filter cake formation upon a free horizontal surface of unbound filter media (sand with a mass mean particle diameter of about 500 μm) is successfully demonstrated at about 500 °C. (Preliminary measurements estimate the tar and particle content of the raw product gas to be about 3-5 g/Nm^3 and about 10 g/Nm^3 respectively). No melt formation was detected either through ashing, heat treatment or through visual inspection, applying scanning electron microscope. This reveals char particles with a clearly bimodal size distribution and a Ca rich ash.

Application of catalytic material within the bed efficiently reduced the content of tars and higher hydrocarbons. Despite the relatively low filtration temperature (535 °C) no catalyst deactivation was observed after three hours of filter operation.

It is important to stress the operational differences between the simplified filter construction (simple particle accumulation) used in this study and continuous operation of a filter system operating in surface filtration mode (e.g. the panel bed filter). Long term operation of this latter system typically incorporate accumulation of micron/sub-micron particles within the filter vessel and extensive mixing of the contaminants due to the mechanisms involved in filter regeneration (e.g. particle re-entrainment). These parameters, especially in combination with elevated filtration temperature, typically allow the system to approach global equilibrium to a greater extent.

Reference:

Engstrom, F. (1998) *Hot gas clean-up Bioflow ceramic filter experience.* Biomass and Bioenergy, v 15, n 3, pp. 259-262.
Kurkela, E. (1996) *Formation and removal of biomass-derived contaminants in fluidized-bed gasification processes.* Espoo 1996, Technical Research Centre of Finland, VTT Publications 287. 47p. + app. 87 p.

2 The Panel Bed Filter in application to high temperature combustion processes.

2.1 Introduction

The main purposes of flue gas cleaning are to reduce the stack emissions of combustion aerosols and to protect sensitive downstream equipment from hot corrosion and erosion. Furthermore, the emission of submicron aerosols may constitute a health hazard due to respiratory deposition. Different technologies are applied for flue gas cleaning in existing combustion plants for heat and power production. The focus in this study is on the granular Panel Bed Filter technology.

The major advantage of a granular bed filter is its potential for use in hot gas cleaning operations and for combined removal of particles and harmful gaseous components. The disadvantage is the complexity of the solid handling and regeneration process.

An overall review of particle cleaning technologies is followed by a brief introduction to the Panel Bed Filter working principle and a review of surface filtration theory. Special attention is given to the experiments and theory concerning the properties of the filter cake and the influence of filter regeneration upon filter stability and efficiency. Only cleaning by means of a pressure pulse is considered in this work.

The objective of this part is to validate filter performance through field tests conducted on a commercial scale filter module. And evaluate the results based on state of the art within filter technologies operating in surface filtration mode.

2.2 Overall review of existing particle cleaning technologies

In Figure 2.1a schematic presentation is given for the various gas cleaning strategies and available technologies. The choice of which filter to use is a complicated optimisation problem involving emissions, reliability and costs. The Panel Bed Filter technology can be utilised both for dry scrubbing and for hot gas conditioning and typically compete with baghouses, ESP, ceramic and metallic filters. A detailed analysis of wet scrubbing and ESP technologies is beyond the scope of this work.

Multi cyclones is the most common, and often the only, gas cleaning device installed in Norwegian combustion facilities. This fairly simple device removes sand, dust and fly ash particles larger than about 20 μm. However, additional filters have to be installed in order to comply with new and stricter regulations for particle removal. In more advanced cycles (e.g gasification) efficient filtration of the product gas is necessary for protection of downstream equipment.

Enhanced particle removal can be accomplished using barrier filters (e.g. fibrous, ceramic, metallic or granular), electrostatic filters or wet scrubbers. These filters often have very high mass collection efficiencies (> 99%) and virtually all of the coarse particles like fly ash are removed from the flue gas. Figure 2.2a shows that the Panel Bed Filter typically has filtration efficiency in the upper range, and filter capacity higher than the reported values for fabric filters, while comparable to the upper range reported for rigid media filters. The corresponding pressure drop is an order of magnitude lower than those reported for rigid media filters (Figure 2.2b) but

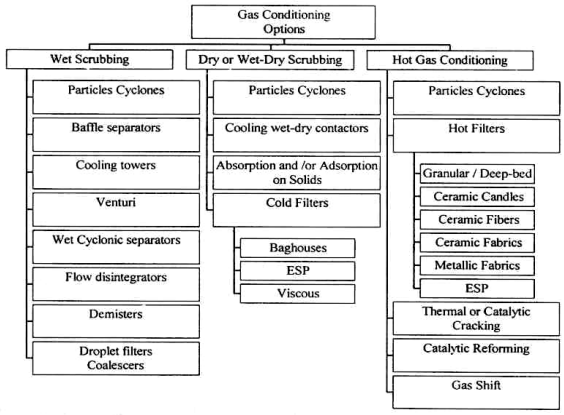

Figure 2.1: Schematic representation for various gas cleaning technologies (Milne et al. 1999)

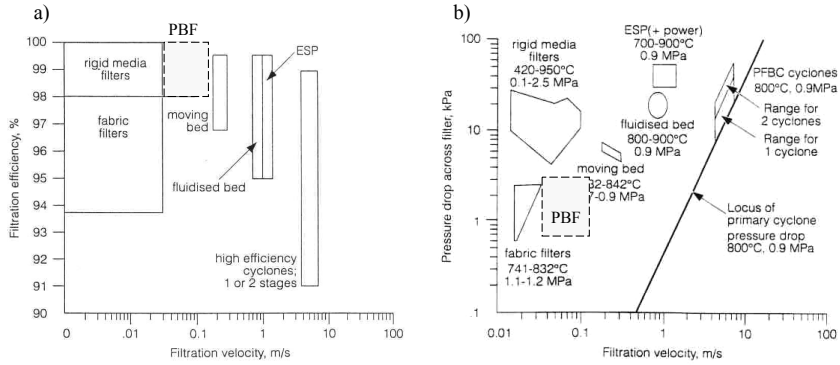

Figure 2.2: Relative performance of the PBF: efficiencies (a) and pressure drop ranges (b) of particulate filters at HTHP conditions (Orignial figure in: Thambimuthu (1993)

comparable with fabric filters. Noting that the operating temperature rather than the pressure is the more significant variable influencing the pressure drop, dust separation and retention process in a filter, the filtration data obtained at ambient and high temperature conditions can be compared with those measured at HTHP conditions.

A granular bed filter consists essentially of a stationary or moving layer of granular solids (granule diameter typically about 1 mm). The principal collection mechanisms are inertial impaction and agglomeration, which result from the highly tortuous path inside the granular structure. The less important collection mechanisms are diffusion (for sub-micron particles), interception (a geometrical effect) and electrostatic, magnetic or acoustic fields, which are illustrated in Figure 2.3a. Besides particle capture, particle re-entrainment occurs, resulting from particle rebound. Particle capture is considered irreversible for all particles except those collected in the inertial regime; i.e. an impacting particle can rebound only when the Stokes' number is sufficiently large (Kuo et al. 1998).

Most granular filters are based on the principle of deep bed filtration (particle penetration deep into the filtration medium) and the purification degree has been relatively poor for particle sizes in the range 0.1-5 μm. The collection efficiency of a barrier filter, as a function of particle size, is presented in Figure 2.3b. Especially the

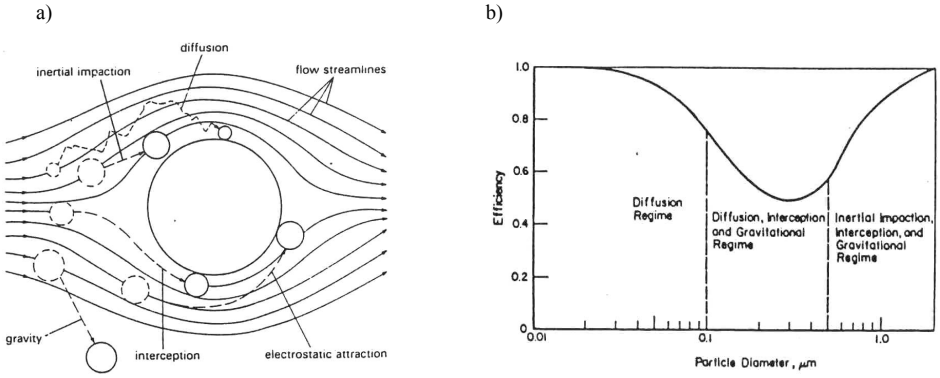

Figure 2.3: a) Separation mechanisms in a granular bed filter and b) collection efficiency of a typical barrier filter as a function of particle size (Zevenhoven (1992) and Lee & Schmidt (1984) respectively, both in Kuo et al. 1998).

range from 0.1-1 μm shows reduced efficiency. Collection efficiencies for submicron aerosols in conventional filtration units are significantly lower than the reported overall mass collection efficiencies.

However, granular filtration in a fixed bed is inherently a time dependent process (Tien, 1989). As the filtration process proceeds (Figure 2.4) the filter medium structure undergoes a continuous change due to accumulation of deposited particles. If the granular filtration is prolonged, the filter becomes increasingly clogged (Squires & Pfeffer 1970, Lee 1975 and Tsubaki & Mori 1997). Q_0' denotes the total number of particles required for the porosity of the filter cake (ε_p) to be equal to that of the particle deposit within the filter. After the filtration Q_0', the filter cake with a porosity of ε_p grows continuously and the pressure drop shows a tendency to increase linearly with increasing deposit, suggesting that surface filtration should become the dominant mechanism (Tsubaki and Mori 1997). Figure 2.4 also includes a schematic presentation of the filter cake formation as described by Lee (1975): *i*) clean bed filtration (poor efficiency), *ii*) rooting-cake filtration (forms the foundation of a surface filter cake) and *iii*) surface-cake filtration (very high efficiency).

The Panel Bed Filter utilises this transient behaviour of granular filtration and operates in surface filtration mode. The size of the sand grains and the speed of the gas impinging on the filter surface are important parameters with regard to the formation of the filter cake and the efficiency of the filter.

The majority of the work published on the fundamental mechanisms relevant for surface filtration originates from investigations conducted on fibrous and rigid ceramic/metallic filters.

2.2.1 Commercial scale Panel Bed Filter element

Figure 2.5 shows a cross section of a commercial scale Panel Bed Filter element and the principle for the construction of the filter is illustrated.

All sand has an angle of repose fixed on the basis of the dimension of the sand grains and the distribution of size. By placing the louvers at a common distance adapted to the angle of repose for the fine sand, the sand remains stable between the louvers. A large number of these louvers defines a wall, somewhat resembling

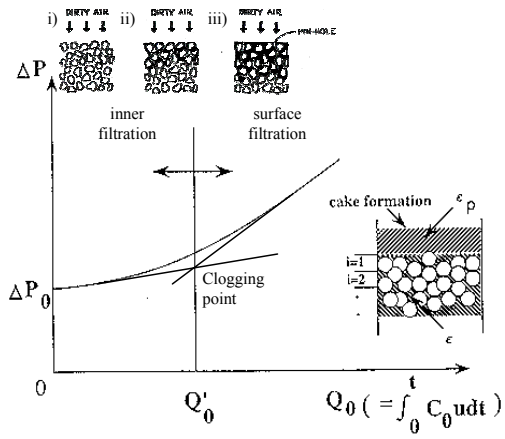

Figure 2.4: Schematic pressure drop versus inlet particle load illustrating different filtration regimes. (Figure derived from Lee (1975) and Tsubaki & Mori (1997).)

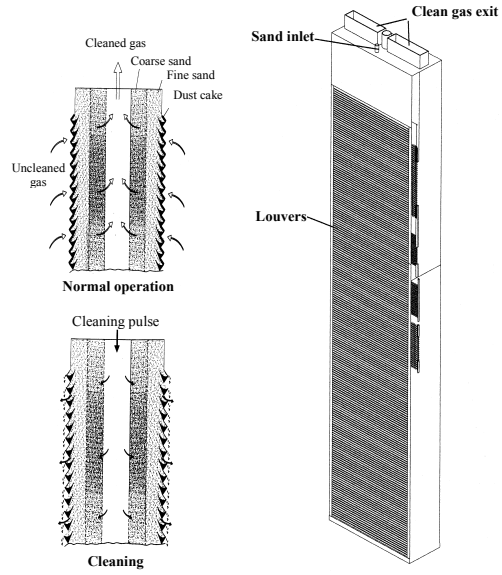

Figure 2.5: The design of a commercial scale filter element (Nos 1997): height of approximately 3500 mm, width of 600 mm and a thickness of 250 mm. This size provides a filter area of approximately 3.25 m^2. The cross sections of the filter illustrate normal filtration mode (upper left) and pulse cleaning mode (lower left). The full scale filter element is shown to the right.

venetian blind, and holds the sand bed in a tall relatively narrow "panel". Gas flows in the horizontal direction across the sand bed, and the dust in the gas deposits forming a filter cake upon the sand surfaces at the gas-entry "face" of the panel.

There are two layers of sand along each outer surface. A layer of fine sand on the outside and a layer of coarse sand on the inside facing the clean gas duct in the centre. The fine layer (typically $x_{50,3} \leq 500$ μm) rests against the front louvers and is supported by a coarser layer (typically $x_{50,3} \approx 1000$ μm). Separation of the layers is accomplished by a wire-mesh.

When the filter cake has built up to a thickness whereby resistance over the filter has reached its desired maximum value. The filter is cleaned by stopping circulation and transmitting a short pressure pulse, with duration of only a few milliseconds, into the filter element in the reverse direction to normal flow. The pressure wave generates a body movement in the sand bed and the sand moves slightly horizontally between the louvers. As a result, some of the sand together with the filter cake falls from the filter element, thereby cleaning the filter surface. The mixture of dust and sand is precipitated into a hopper for dust separation and sand recirculation.

Figure 2.6 shows the erected pilot plant, capacity of 30000 m^3/h at 200 °C. Each filter element is suspended from a dividing sheet between pure and contaminated gas at the top of the filter housing. Thus, a design similar to the approach usually applied for bag-house filters and ceramic / metallic filters.

In general, the main parameters controlling the operational characteristics of cake forming filter systems might be categorised into five groups Figure 2.7 (Schmidt and Pilz 1996). These include the filter system configuration, the filter medium characteristics, the operational parameters, the characteristics of the particles and those of the gas in which they are dispersed. These parameters are discussed in the following sections.

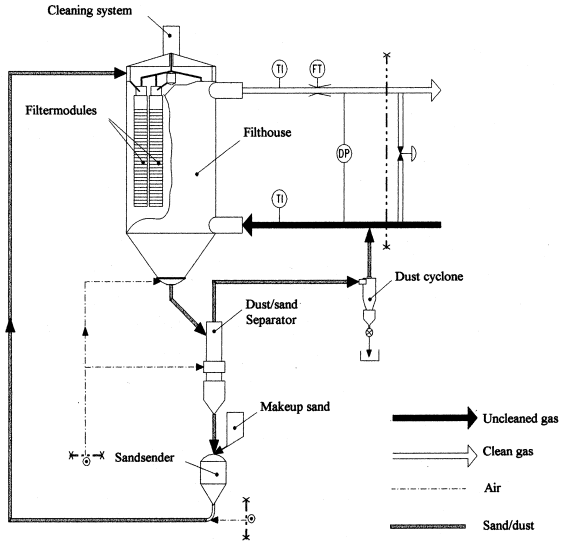

Figure 2.6: Full-scale pilot plant, flow-sheet (Nos 1997).

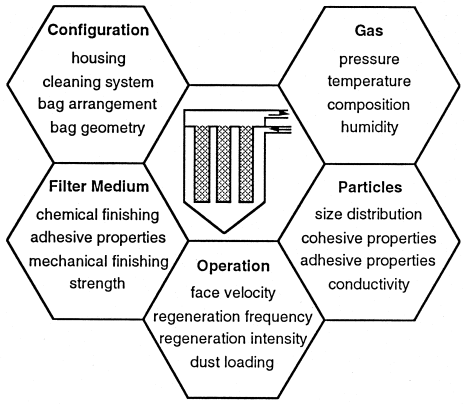

Figure 2.7: Parameters influencing the operational behavior of cake-forming filters, Schmidt and Pilz (1996).

2.3 Surface filtration theory

The high filtration efficiency characteristic of surface filtration has to be balanced against the amount of dust collected and the resulting pressure drop. Thus, periodical regeneration must be applied. This is achieved by releasing a pressure pulse in the reverse direction of bulk flow.

Figure 2.8 illustrates the course of stable filtration (pressure build up and periodical cleaning). The pressure drop measured at any time, during ideal operation, is the sum of three effects: i) the pressure drop ΔP_0, within the passages of the vessel; ii) the constant pressure drop, ΔP_F, caused by the filters; and iii) the time dependent pressure drop, $\Delta P_C(t)$, caused by the growth of the filter cakes.

Section 2.3.1 discusses the time dependent pressure drop and the parameters involved in the dust cake formation. A literature review gives a condensed summary of relevant experimental and theoretical work. Filter regeneration and filtration efficiency is discussed in Section 2.3.2 and parallels drawn between the Panel Bed Filter and fibrous, ceramic and metallic filters. Finally (Section 2.3.3) a brief discussion of particle sedimentation within the filter vessel and its influence upon filter operation is given.

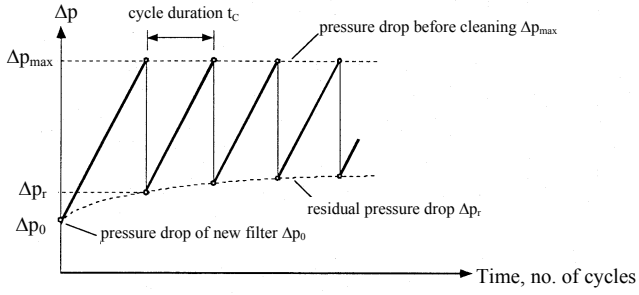

Figure 2.8: Pressure drop vs. elapsed time (University of Karlsruhe, 1999)

2.3.1 Filter cake characteristics.

On-line measurements of cake thickness during filter-system operation have not been feasible in most systems. However, when the pressure drop across the filter system, the gas flow rate, and the particle concentration in the incoming gases are measured, these data can be used to calculate the mass of filter cake on each filter. Several models have been developed to improve the prediction of pressure loss, but the general approximation, for a plain filter, remains simple:

$$\Delta P = \Delta P_{Filter} + \Delta P_{Cake} \qquad (2.1)$$

Applying K_1 as the specific resistance of the filter medium itself, including deposited particles and K_2 as the specific cake resistance, *Eq.* 2.1 can be rewritten as

$$\Delta P = K_1 \mu U_S + K_2 \mu U_S \overline{W}_A \qquad , where\ \overline{W}_A = c U_S t_c \qquad (2.2)$$

Where μ is the gas viscosity, U_S – the mean gas velocity across the filter surface and W_A equals dust load. It is common to combine the specific resistance and viscosity, and replace K_1 and K_2 (in *Eq.* 2.2) with

$$K_1' = \mu K_1 \text{ and } \qquad K_2' = \mu K_2 \qquad (2.3)$$

$$K_2' = \frac{\Delta P_{Cake}}{t_c U_S^2 c} \qquad (2.4)$$

The concept held by most investigators is that once a substantial layer has formed, the true K_2 value of the dust is reflected regardless of the supporting media. Hence, K_2' is mainly determined by the filter cake structure and closely related to the physical properties of the dust itself. Dennis et al. (1981) compared laboratory and field derived K_2 values and found the former to provide the best estimates, despite that data adjustments may be required due to scale factors and aerosol generation effects.

The vast majority of research conducted on cake forming filters originates from ceramic, metallic and bag house filters. However, the early findings of Squires and Pfeffer (1970), Paretsky (1972), Lee (1975) and Lee et al. (1977) all report evidence for efficient filtration by establishing filter cakes upon sand. Lee (1975) and Lee et al. (1977) studied the pressure build up due to filter cake formation in a granular panel bed filter. Values for the specific resistance as derived from the reviewed literature and the recent publication by Risnes and Sønju (2001), are given in Table 2.1. Generally the variation within one dust quality (e.g. coal fly ash) is found to be about one order of magnitude. Decreasing particle diameter results in a higher specific resistance as does increasing filtration velocity.

Increasing filtration temperature results in increased viscosity of the gas, i.e. leading to a higher pressure drop. This effect highly influences K_2' (= μ K_2). Thus, K_2 might be a more representative parameter when comparing the specific cake resistance derived from various filtration temperatures. As K_2 is closer connected to the structure of the dust cake.

Table 2.1: Specific Cake resistance K_2', literature review

Dust	*Filter temp.* [°C]	d_p [μm]	c [g/m^3]	v_f [cm/s]	K_2'·10^{-5} [s^{-1}]
Fly ash-bark combustion Risnes and Sønju (2001) granular, Panel Bed Filter	~190	$X_{50,3}$ = 12.3; $X_{95,3}$ = 62.2	1	18	0.65 ± 0.01
Steinkohle-flughashe Pilz (1995) (Ceramic filter element)	ambient-850°C	3 ≤$X_{r,3}$≤100	-	3	1.5-1.7$^{\xi}$
Coal fly ash Dennis (1981) Fabric filters	*ambient	2.42-11.3 MMD	-	1-1.5	0.63-6.35
Lignite fly ash Dennis (1981) Fabric filters		8,85 MMD		1	0.8
Coal fly ash Dennis, 1978 fabric	*ambient	9	5-10	0.5-2.5	0.63-0.78Us^0.5
Coal fly ash Cheng et al 1998	*ambient	6.28 MMAD	1.36-1.96	1-9	0.91-2.83 ($\propto V_f^{0.52}$)
Coal fly ash Dennis 1981 fabric	*ambient	-	27.6	4.17	1.08
Fly ash Wayne 1976 Fabric filter	75F, air	5.2	1.3*e-5g/cm3	1.58	0.1-0.2
Coal fly ash Dennis, 1980 fabric	*ambient	4.2	27.6	4.17	0.77Us^0.5
Limestone Cheng et al 1998	*ambient	2.53 MMAD	2.83-3.40	1-9	3.65-8.44 ($\propto V_f^{0.38}$)
Limestone Klingel, 1981, 1983	*ambient	$X_{50,3}$= 5	1-10	4.2-8.3	0.69-1.45$^{\chi}$
Limestone Schmidt, 1995b**	*ambient	$X_{50,3}$=3.5	-	2.8-4.58	0.9-0.98 (dP_{max} = 1000Pa)-
Chalk & PVC Morris, K. 1987, fabric		*1.5****	-	2.8-4.58 3.33	1.05-1.2 (dP_{max} = 2000Pa) 1
Talc Dennis, 1980 fabric	*ambient	2.8	3.5	4.33	5.3
Talc Dennis (1981) Fabric filters	*ambient	2.77 MMD	-	1.33	3.5
SAE-fine Cheng et al 1998	*ambient	MMAD = 3.88	2.78-3.72	1-9	2.15-5.52 ($\propto V_f^{0.43}$)
Granite Dennis (1981) Fabric filters	ambient	1.23-9.21 MMD	-	1	7.4
Quarz Hajec (1997) (Metal fiber fleece & ceramic fiber fleeze)	ambient-600°C	$X_{50,0}$ = 0.7; $X_{90,0}$=2.74	25	2.5	0.216 (0°C) - 0.036(700°C)
					Units actually in Pahm/g?
Quartz Peukert, 1998 ceramic fiber fleece, metal fiber fleece	ambient-600°C	$X_{50,0}$ = 0.70; $X_{90,0}$=2.74	25	2.5	0.06(0°C) - 0.001(700°C)
Quartz Peukert, 1998 metal wire mesh	estimated	$X_{50,0}$ = 0.70; $X_{90,0}$=2.74	25		0.03(0°C) - 0.007(700°C)
Quartz Peukert, 1998 metal fiber fleece	up to 700°C	$X_{50,0}$ = 0.70; $X_{90,0}$=2.74	25		4(0°C) - 0.06(700°C)
Fumed Silica Peukert, 1998 metal fiber fleece	ambient	$X_{50,0}$ = 0.53; $X_{90,0}$=1.66	1		2 (ambient)
NOTE: The graph published by Peukert gives K_2' in units of 1/s. However, this is believed to be erroneous. The real unit for the graph as published is believed to be [Pahm/g] i.e. 36E5 [1/s]. Thus in accordance with values published TU-Karlsruhe 1999 (Short course in filtration fundamentals)		Recalculating to 1/s gives:	Quarz Quarz Quarz Fumed Silica		K_2' *10^{-5} [1/s]: 2.16 (0°C) – 0.036(700°C) 1.08(0°C) – 0.25(700°C) 144(0°C) – 2.16(700°C) 72 (ambient)
Silica Hajec (1997) (Metal fiber fleece)	ambient-600C	$X_{50,0}$ = 0.53; $X_{90,0}$=1.6	1	2.5	100 (0°C) 1.8(700°C)
NaCl, NH_4Cl ,Al_2O_3 Novic (1992) (47mm HEPA-filter)	*ambient	0.5-2	-	2.45-3.0	2-20, $K_2 \propto 1/d_p$
$^{\Psi}$Carbon Black Morris, K. 1987, fabric	*ambient	mostly sub micron	-	3.33	4-10
Specific cake resistance reported in modeling studies					
Dittler, 1999, v59, p. 299-303		-	-	5	1.2
Schmidt, 1995c	*ambient	-	5	4.4	2.16 (2.36-2.59)
Fly ash Ellenbecker 1979 fabric filter		-	-	10	0.25
Coal fly ash Dennis, 1979 fabric	*ambient	-	-	-	0.77Us^0.5

* Temperature level not mentioned in the article, assumed to be ambient

** Influence of relative gas humidity: no significant effect up to about 60%, decreasing for higher humidities due to capillary condensation.

*** PVC and chalk were found to have broadly similar particle size distributions. PVC particle density is approximately half of chalk but the resulting cake has similar voidage.

$^{\chi}$ The following dependency of the specific cake resistance upon the superficial filtration velocity can be estimated from the data published by Klingel (1983) K_2' (U_s) = 6.26E-03 U_s^3 - 9.36E-02 U_s^2 + 5.91E-01 U_s - 5.98E-01

$^{\Psi}$ Cakes of carbon black are very thick and fluffy. They tend to penetrate deeply into the filter and clog the pores.

$^{\xi}$ Reports K_2' being constant and K_2 decreasing upon increasing filtration temperature. While Hajec (1997) and Peukert 1998 reports the decreasing K_2' as function of increasing temperature, i.e. opposite to Pilz (1995).

Peukert (1998) and Hajec and Peukert (1997) both state that K_2' is decreasing significantly with temperature, while the results published by Pilz and Löffler (1995) shows the opposite trend. Furthermore, Pilz and Löffler find K_2 to be decreasing with increasing temperature. It is believed that the results published by Pilz and Löffler has a typographical error, i.e. When K_2' is mentioned this is really K_2, and vice versa. Concluding these observations gives a clearly decreasing K_2' with increasing temperature.

Furthermore, it is interesting to note the dependency of the K_2' values upon filter medium in the publication by Peukert (1998). Peukert relates these differences to the nature of the porosity of the filter media.

Parameters involved in the dust cake formation have been identified as the dust cake porosity and mass, the particle size (including size distribution and shape) and the operating conditions (e.g. superficial velocity and temperature). Numerous empirical, semi-empirical and non-empirical models have been applied in the prediction of the specific cake resistance K_2'. Klingel (1983) gives a systematic review.

Real-time information on the dust cake growth rate, especially when the cake passes through a compression phase is scarce. Lee (1975) and Lee et al. (1977) studied filter cakes formed upon a granular filter and found that deposits put down at low air velocities (about 2.5 cm/s) were fluffy and porous, while deposits put down at higher velocities (above 10 cm/s) tended to be denser and more compact. Abbot (Abbot 1980, ref. in Klingel (1983)) reported compression of the fly ash dust cake at pressure losses of about 1300-2000 Pa, with a local maximum at dP = 1500 Pa, no further densification occurred above 1700 Pa. Likewise Klingel (1983) found compression (Us = 4.2 cm/s) in limestone (d_p = 5 μm) filtration at a pressure loss of about 1500 Pa. Endo et al. (1998b) found compression of the dust layer (2 μm AC-fine) at a pressure drop of 3-18 kPa (3.29-26 cm/s). Generally the interparticulate forces are low at the top and high at the bottom of the filter cake.

Japuntich et al. (1994) studied the pressure gradient with mass loading of monodisperse (stearic acid, 1 to 5 μm) particles upon a flat fibrous filter media. And found the smaller particles to give higher penetration and higher pressure drop. Schmidt (1991, 1993) developed a method to freeze the limestone dust cake structure for subsequent microscopic examination. Using this technique, Schmidt (1995, 1993) found that the porosity of dust cake layer (d_p ~ 2 μm) decreased with increasing pressure loss and the local area porosity increased with increasing filter medium loading. Aguiar and Coury (1996) studied dust cakes of limestone (d_p = 2.5, 3.3, 6.9 and 10.7 μm). And found cake porosity to be increasing considerably with decreasing particle diameter. An expression for the pressure drop in a compressible cake was developed with good agreement with image analysis and pressure loss measurements. Endo et al. (1998a and 1998b) measured the real-time pressure drop and height of dust cake (alumina particles (0.7 μm), AC-fine (2 μm), mixtures of these and pure 2.3 μm talc powder) at fixed parameters. And derived an analytical expression to correlate dust cake porosity with the physical properties of the particles (the particle size distribution and particle shape), heights of the dust cake layer, and the operating conditions (the filtration flow rate and pressure drop). The initial dust cake height increased linearly with the loading time, but decreased as the height had build up to several hundred micrometers, indicating compression as the drag force acting on the

dust particles became slightly higher than the strength of the cake layer. Polydispersity and shape-factor significantly affected filter loading. Kono et al. (1998) used elutriated particles (30wt%carbon and 70wt%ash) from an IGCC plant to prepare filter cakes in a laboratory-scale apparatus. The filter cake porosity was found to depend on filtration velocity, but largely independent of temperature (25-515 °C).

Höflinger et al. (1994) simulated collection of spherical particles on a filter and compared load and shear forces between the particles. The work could only provide a qualitative explanation, due to the uncertainty in estimating the shear force between particles in the dust cake. Höflinger (1995) also estimated the relationship between the total cake thickness and the total pressure drop. This simulation was based on the division of a dust cake layer into three layers (loose incompressible, compressible and compressed incompressible). For each layer a different porosity could be given and the pressure drop of each layer was then calculated. A fitting parameter, the volume loading data, was required for the general application. Schmidt (1996) published modelling results on porosity variations within the dust cake and the effect of cake compression. Stöklmaier and Hoflinger (1998a) used the same approach and simulated compression effects in a 2-D dust cake. The estimated pressure drop and number of particles in the clean gas showed good qualitative agreement with experimental data. Stöklmaier and Hoflinger (1998b) examined the long-term behaviour of a needle-felt filter and discussed filter blinding as due to the build-up of a second compressible cake within the filter medium.

Sørhuus (1997) modelled bag-house filtration of SiO_2 dust (U_S = 1.7 cm/s, primary d_p = 0.1 μm) by introducing a highly bimodal size distribution, thereby taking into account the accumulation of dust within the filter vessel and the formation of secondary particles through agglomeration and re-entrainment.

Schulz (1988) related the pressure build-up curves to the structure of the filter media and described three typical cases (Figure 2.9): i) open/porous media, ii) dense surface with relative few pores and iii) intermediate between i and ii. The longest cycle time is obtained for case i.

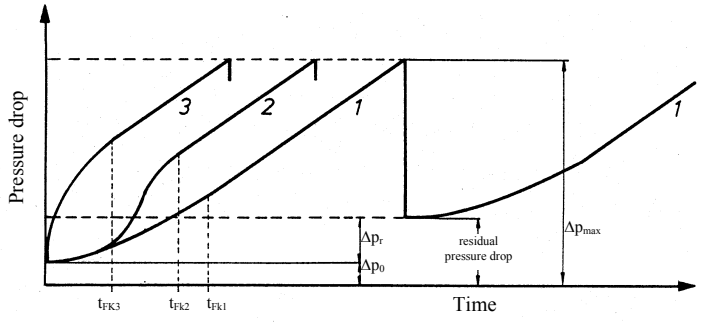

Figure 2.9: Influence of the filter media structure upon the resulting pressure build up: 1) Porous filt, 2) fleece and 3) smooth woven filter, Schulz (1988)

$$\Delta P_{Filter} = K_1^{'} \cdot U_S^n \tag{2.5}$$

$$\Delta P_{Cake} = K_2^{'} \cdot \overline{W_A} \cdot U_S^{n_C} \Rightarrow \Delta P_{Cake} = K_2^{'} \cdot c \cdot U_S^{n_C+1} \cdot t_c \tag{2.6}$$

Where the effect of U_S is greater for the dust cake ($n_C > 2$) than the clean filter media ($1 \leq n \leq 2$; 1 for pure laminar and 2 for turbulent flow). $n_C = 2$ requires a homogeneous dust quality and negligible compression. Hence, n_C might be larger than 2 even if complete regeneration is achieved. Leith and First (1977) (in Schulz (1988)) reports the pressure drop to be proportional to $U_S^{2.34}$, where n_C is larger than 2 due to the effect of re-entrainment.

An alternative approach is to express the pressure loss due to the build up of a filter cake as, Schulz:

$$\Delta P_{Cake} = K_2^{'}(U_S) \cdot c \cdot U_S^2 \cdot t_c \tag{2.7}$$

Table *2.*1 also includes some estimates for the dependency of the specific cake resistance upon the superficial filtration velocity. Dennis (1978 and 1979), Cheng and Tsai (1998) and Klingel (1981 and 1983) all find the specific cake resistance to increase with increasing face velocity (U_S). However, the correlations published by Dennis and Cheng & Tsai are downward sloping, while Klingel finds and upward sloping trend. This despite the fact that both Cheng and Klingel operates within the same velocity range and applies limestone of approximately the same particle diameter.

2.3.2 Filter regeneration and filtration efficiency.

Filter regeneration and filter stability depends on both the nature of the dust cake (thickness, adhesion forces and degree of compressibility), propagation and distribution of the pressure pulse within the filter element, the defined maximum allowable pressure drop, and pulsating frequency. It also heavily influences upon the plant's efficiency, as typically 60-90% of the emissions is related to this phase (Klingel 1983 and Schmidt 1995a/b). A schematic presentation is given in Figure 2.10. Additional particle penetration either proceeds via straight through, seepage or pinhole plugs. Furthermore, a high pulsating frequency (i.e. short filtration periods) results in enhanced degree of particle penetration into the filter media and typically leads to both a rapid increase in the residual pressure drop and low filter efficiency. The higher the dust mass, i.e. the thicker the deposit layer, the higher the cleaning efficiency (Morris et al. 1987; Sievert and Loeffler 1987; Seville et al. 1989; Berbner and Löffler 1994)

Tank pressure, valve-opening times and diameter, blow-tube arrangement and whether the cleaning is operated on/off-line can control the intensity and shape of the pressure pulse. On-line cleaning generates an ejector (jet-pump) effect. Thus, surplus air will be entrained into the filter element from the clean air side. This reduces the demand for pressurised air and has lead to the development of alternative filter inlet geometry's (venturies/ejectors).

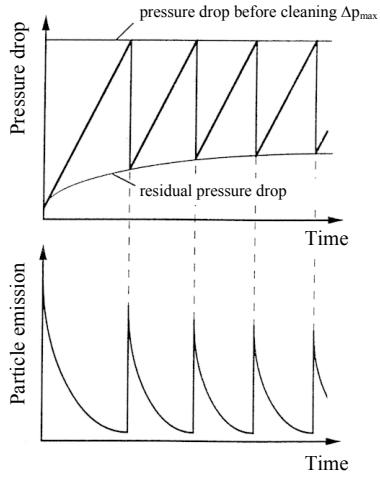

Figure 2.10: Schematic representation of the time-dependent pressure loss and clean gas concentration trends during several filtration cycles, Schmidt (1995a)

Based on experiments conducted in a model filter (75x305 mm) and a full scale filter element (305x3050 mm) Lee (1975) and Lee et al. (1977) concluded that regeneration of the PBF by means of a pulse-jet is a transient soil mechanics failure phenomenon Schulz (1988) also discussed the effect of changing filtration velocity upon the resulting pressure loss and models the pressure loss through the filter and filter cake as caused by transient aerodynamic drag forces. Lee (1975) defined "t_a" the active puffback time or the active time which is the time period the pressure drop across the sand bed is greater than the minimum pressure drop (dP_{min}) required to cause sand spill. The reported values for dP_{min} is found to be within the range 500-870 Pa, and appeared not to be a function of the sand size. Figure 2.11a illustrates Lee's definition of active time in terms of an idealised "triangular" curve of puffback pressure difference versus time. The sand spill did not depend upon the peak pressure, nor upon the area of this idealised triangle.

Figure 2.11a also illustrates the propagation of the cleaning pulse through the full-scale filter element (off-line cleaning). A packet of puffback gas travels downward from top to bottom of the clean side, and as it moves, gas leaks forward through the panel bed and into the space on its dirty side. A more thorough description of these mechanisms is given in Chapter 3.

Klingel (1983) characterized the propagation of the cleaning pulse through a fibrous filter element (including the blow tube arrangement) during on-line cleaning, Figure 2.11b. In order to have a measure for the cleaning intensity the so-called pressure impulse P_D (Figure 2.11) was introduced.

$$P_D = \int_{t_1}^{t_2} P(t)dt \qquad (2.8)$$

The pressure impulse P_D is given by the integral between the positive pressure signals and the line of pressure compensation (dP = 0 Pa). The pressure impulse P_D takes not only the intensity of the pressure signal into account, but also its duration, so that a measurement for the positive portion of the pressure traces is accomplished.

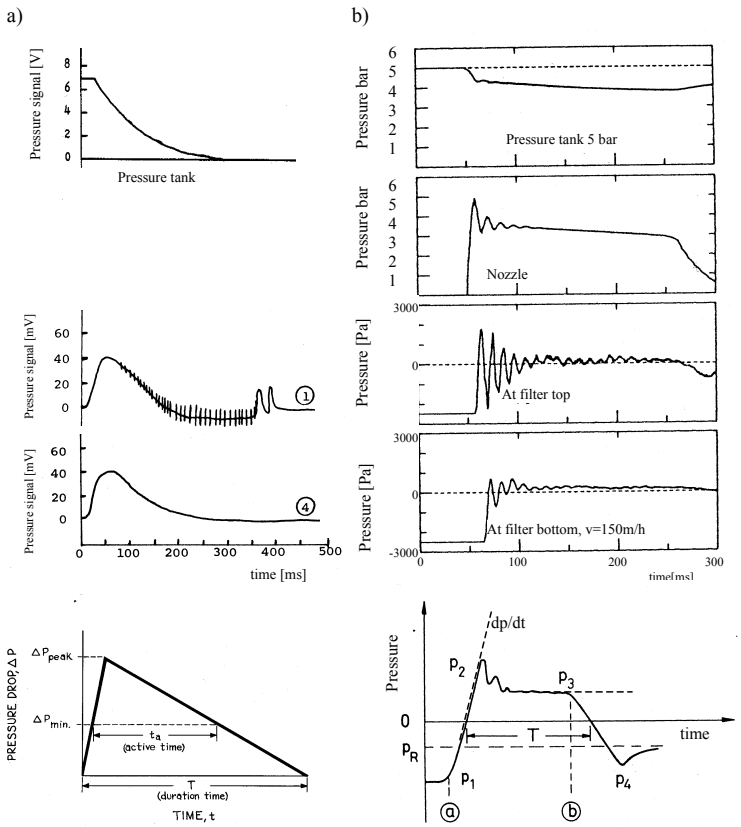

Figure 2.11: The propagation of a pressure pulse from the pressure vessel through the blow tube arrangement (and nozzle) and filter element. a) Lee et al. (1977) off-line cleaning of a full scale (3500 mm) Panel Bed Filter element. Including a schematic representation of the active time theory. b) Klingel (1983) on-line cleaning of a fibrous filter element. Including characterization of the pressure pulse (P_2-pressure peak, P_3-quasistationary pressure level, P_4-residual pressure, a-opening of the pressure valve and b-closing of the pressure valve).

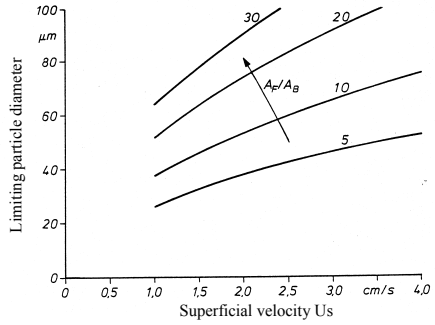

Figure 2.12: Sedimentation velocity, Schulz 1988

However, this takes no account of any negative component, which may be negating the effect of the cleaning pulse. Rothwell (1986) resolved the pressure pulse into positive and negative components and defined the resultant of the specific impulse being the sum of these two components.

$$\int_{t=0}^{t} P(t)dt\,, \text{ P being zero at t=0} \qquad (2.9)$$

Furthermore, the quality of the overpressure pulse used to release the cake in pulse-jet filters depends on the form of the injector and the jet-injector separation. By restricting the throat of the injector, the peak filtration velocity can be restricted. According to Rothwell (1990), the first 5 ms of the overpressure pulse are critical for cake detachment.

Seville et al. (1989) found that cake detachment, from a fabric filter, occurs when it experiences a tensile stress sufficient to overcome either the strength of the adhesive bond between the cake and the filter medium (or a residual dust layer) or the internal cohesion of the cake itself. The median cake detachment stress σ_{50} is usually in the range 20-100 Pa for fibrous filters and at least an order of magnitude higher for rigid ceramic media (Koch et al. 1996). This corresponds well with reported values for rigid ceramic media: 100-10000 Pa (Schmidt 1998). The cleaning stress should be independent of cake areal mass if true surface filtration occurs.

Dittler reported in-situ measurements (1998) and modelling (Dittler and Kasper (1999)) of cake thickness and the distribution of the remaining cake fraction after regeneration (patchy cleaning) of rigid ceramic filters. This phenomenon was also modelled by Ferer and Smith (1997, 1998a/b) and Duo et al. (1997a/b).

2.3.3 Particle sedimentation within the filter vessel

After each backpulse, the particle concentration in the vessel will increase significantly for a short period of time (Shmidt et al. 1998a/b, Sørhuus 1997). In the re-entrainment fraction model some fraction of the resulting filter-cake fragments returns to the filter surface. The fraction of re-entrained particles is a function of the size distribution of the cake fragments. In the limit that the time for re-entrainment goes to zero the reentrainment becomes indistinguishable from incomplete cleaning.

The vertical raw gas velocity (w_B) in a large scale filter plant can be expressed as proportional to the ratio between the filter area (A_F) and the cross section of the filter house (A_B).

$$w_B = w \cdot \frac{A_F}{A_B} \qquad (2.10)$$

Schulz (1988) reported considerable variation in the ratios (5-30) applied in existing filter plants. The sedimentation velocity is mainly influenced by the particle diameter ($\propto d_p^2$), and must be higher than w_B in order to get an efficient removal of the dislodged dust. The limiting particle size for on-line cleaning as function of the superficial velocity is given in Figure 2.12. Hence, characteristic dust properties as particle diameter and agglomeration tendency are important parameters when

considering on-line cleaning. A low sedimentation velocity might favour off-line cleaning on the expense of a less continuous filtration process.

2.4 High temperature filtration

Filtration temperature influences on gas density and the dynamic viscosity:

$$\Delta p = K_O \cdot \eta_G^m \cdot w^n, \qquad \eta_G = \nu \cdot \rho_G \qquad where\ \eta_G \propto\hat{}\ T^{0.7} \tag{2.11}$$

According to Darcy, m is equal to 1, but experimental findings support a value greater than unity, Schulz (1988). Assuming constant mass flow, and re-writing the expression gives:

$$\Delta p = K_O \cdot \eta_G^m \cdot \left[\frac{\dot{m}_G}{A_F \cdot \rho_G} \right]^n \tag{2.12}$$

Assuming ideal gas and temperatures up to about 500 °C, the effect of increased temperature can be expressed as:

$$\nabla p = \frac{\Delta p}{\Delta p_0} = \left(\frac{\eta_G}{\eta_{G_0}} \right)^m \cdot \left(\frac{\rho_{G_0}}{\rho_G} \right)^n = \left(\frac{\eta_G}{\eta_{G_0}} \right)^m \cdot \left(\frac{p_0 T}{p T_0} \right)^n \tag{2.13}$$

Jo and Raper (1997) (in Schulz (1998) found the magnitude of the increase in dP at high temperature to be less than expected from the viscosity alone, and related this to flow slippage (more porous filter cake). Increased temperature might also result in enhanced dust stickiness and dust cake porosity.

However, high temperature, in general, leads to reduced filter efficiency at a given mass flow of gas. Only collection within the diffusion regime (particles smaller than approx. 0.5 μm) becomes more effective with increasing temperature, inversely proportional to gas density. This can be of significant importance when extremely fine condensation aerosols (e.g. heavy metals and inorganic salts) are to be collected. However, for larger particles subject to the influence of inertial forces, a drop in separation efficiency is to be expected due to increasing drag forces. Under cake filtration conditions, high collection efficiencies may also be attained at temperatures up to 800 °C (Peukert et al. 1991).

A more thorough discussion of special factors relevant for high temperature filtration is given Chapter 5 (high temperature cleaning of biomass gasification product gas).

2.5 Evaluation of the Panel Bed Filter system for high temperature applications

Field tests were undertaken on a full-scale single filter element (about 1200 m^3/h) of commercial design on combustion flue gas from a 5 MW bark-boiler. Results from the filtration experiments, in total 80 hours of operation, show a reduction in the dust concentration from approx. 1 g/Nm^3 at the filter inlet to an average dust content of 1.7 mg/Nm^3 at the filter outlet (average filtration efficiency equal to 0.9983). The filter unit was operated at approximately 190 °C, with a superficial filtration velocity

ranging from 4 to 15 cm/s. The pressure drop over the sand filter shows that even if filtration speed is increased dramatically, it is possible to work within the same field as bag filters, i.e. from 900 to approximately 2200 Pa. Calculated average specific cake resistance (K_2') equals 6.5 (± 0.1) $\cdot 10^4$ [s^{-1}] at operating conditions, which is within the range found in the literature (Table 2.1).

The results obtained from the field tests on this single element have been verified in a full-scale pilot plant with a capacity of approx. 30000 m^3/h operating at 200 °C.

The Panel Bed Filter concept has been successfully demonstrated in full scale operation, and more detailed filtration behaviour has been studied. Filter cake data have been obtained at very high filtration velocity and reasonable pressure drops. Very low dust concentrations are observed.

A more detailed description of the field tests and the pilot plant is found in Paper I: Evaluation of a novel granular bed filtration system for high temperature applications.

2.6 Discussion and conclusions

Granular filtration in a fixed bed is inherently a time dependent process. The Panel Bed Filter utilises this transient behaviour of granular filtration and operates in surface filtration mode. Thus, this report especially emphasis upon regenerateable filter systems operated in surface filtration mode. The high filtration efficiency characteristic of surface filtration has to be balanced against the amount of dust collected and the resulting pressure drop.

A comprehensive literature review on the key parameters influencing upon the time dependent pressure drop is given. The specific filter cake resistance K_2' is mainly determined by the filter cake structure and closely related to the physical properties of the dust itself. Dennis et al. (1981) compared laboratory and field derived K_2 values and found the former to provide the best estimates, despite that data adjustments may be required due to scale factors and aerosol generation effects. Generally the variation within one dust quality is found to be about one order of magnitude.

Parameters involved in the dust cake formation have been identified as the dust cake porosity and mass, the particle size (including size distribution and shape) and the operating conditions (e.g. superficial velocity and temperature). Decreasing particle diameter results in a higher specific resistance ($\propto 1/d_p$) as does increasing filtration velocity ($K_2' = K_2'(U_s)$). Furthermore, increasing filtration temperature results in a decreasing K_2'. It is interesting to note the dependency of the K_2' values upon filter medium in the publication by Peukert (1998). Peukert relates these differences to the nature of the porosity of the filter media.

The reviewed articles give both experimental and theoretical evidence of cake compression. Cake porosity is known to decrease towards the cake-filter interface, and with filtration time. This can be due to either cake compression (increasing with increasing dP) or due to particle migration, thus resulting in an upward sloping pressure loss curve. Pinholes are seen as sudden falls in the pressure drop.

Filter regeneration and filter stability depends on both the nature of the dust cake (thickness, adhesion forces and degree of compressibility), propagation and distribution of the pressure pulse within the filter element, the defined maximum allowable pressure drop, pulsating frequency and whether the filter is operated with

on- or off- line cleaning. It also heavily influences upon the plant's efficiency, as typically 60-90% of the emissions is related to this phase (Klingel 1983 and Schmidt 1995a/b).

Lee (1975) found that the pressure pulse had to generate a pressure drop across the granular Panel Bed Filter had to exceed a threshold value ($500 < dP_{min} < 870$ Pa) in order to cause sand spill. (These tests were conducted on a clean filter bed, i.e. no filter cake.) Seville et al. (1989) found that cake detachment, from a fabric filter, occurs when it experiences a tensile stress sufficient to overcome either the strength of the adhesive bond between the cake and the filter medium (or a residual dust layer) or the internal cohesion of the cake itself. The median cake detachment stress σ_{50} is usually in the range 20-100 Pa for fibrous filters (Koch et al. 1996) while Schmidt (1998) reported 100-10000 Pa for rigid ceramic media. The cleaning stress should be independent of cake areal mass if true surface filtration occurs.

After each backpulse, the particle concentration in the vessel will increase significantly for a short period of time. In the re-entrainment fraction model some fraction of the resulting filter-cake fragments returns to the filter surface. The fraction of re-entrained particles is a function of the size distribution of the cake fragments. A low sedimentation velocity might favour off-line cleaning on the expense of a less continuous filtration process.

High temperature, in general, leads to reduced filter efficiency at a given mass flow of gas. Only collection within the diffusion regime ($d_p < 0.5$ μm) becomes more effective with increasing temperature, inversely proportional to gas density. While a drop in separation efficiency is to be expected for larger particles (inertial dominated regime). Under cake filtration conditions, high collection efficiencies may also be attained at temperatures up to 800 °C (Peukert et al. 1991).

The field tests reported within this chapter demonstrate successful operation of a commercial scale Panel Bed Filter element. Stable operation, i.e. a stable residual pressure drop was maintained within a wide range of filtration velocities (U_S = 4-14 cm/s). Filter capacity (325 m^3/m^2h) and efficiency at design conditions is typically comparable to or higher than those reported for fabric and rigid media filters.

Capacity and efficiency has been verified in an industrial scale pilot plant connected to a 5 MW bark boiler, designed for a capacity of 30000 m^3/h at 200 °C.

References

Aguiar, M. L. and Coury, J. R. (1996) *Cake formation in fabric filtration of gases,* Industrial & engineering chemictry research v 35, n 10, Okt 1996, pp. 3673-3679.

Berbner, S. and Löffler, F. (1994) *Investigations on the course of pulse jet cleaning of rigid ceramic filter media*, Staub-Reinhaltung der Luft v 54, 1994, pp. 297-303.

Cheng, YH. and Tsai, C. J. (1998) *Factors influencing pressure drop through a dust cake during filtration.* Aerosol Science and Technology 29, 1998, pp. 315-328.

Dennis, R., Cass, R. W. and Hall, R. R. (1978) *Dust dislodgement from woven fabrics versus filter performance.* JAPAC, 28, 1, 1978, pp. 47-452.

Dennis, R. and Klemm, H. A. (1979), JAPAC, 29, 230

Dennis, R. and Klemm, H. A. (1980) *Modelling concepts for Pulse Jet filtration,* JAPAC, 30, 1, 1980, pp. 38-43.

Dennis, R. and Dirgo, J.A. (1981) *Comparison of Laboratory and Field Derived K2 Values for Dust collected on Fabric Filters.* Filtration & Separation 18, 1981, 5, pp. 394-396/417.

Dittler, A., Gutmann, B., Lichtenberger, R., Weber, H. and Kasper, G. (1998) *Optical in situ measurement of dust cake thickness distributions on rigid filter media for gas cleaning*. Powder Technology v 99, 1998, pp. 177-184.

Dittler, A. and Kasper, G. (1999) *Influence of regeneration behaviour and regeneration pattern on the residual pressure drop of rigid filter media*. Gefahrstoffe – Reinhaltung der Luft v 59, 1999, pp. 299-303.

Duo, W., Kirkby, N. F., Seville, J. P. K. and Clift, R. (1997a) *Patchy cleaning of rigid gas filters - I. A probabilistic model.* Chemical Engineering Science, v 52, n 1, jan. 1997, pp. 141-151.

Duo, W., Seville, J. P. K., Kirkby, N. F., Büchele, H. and Cheung, C. K. (1997b) *Patchy cleaning of rigid gas filters - II. Experiments and model verification.* Chemical Engineering Science, v 52, n 1, jan. 1997 pp. 153-164.

Endo, Y., Chen, D-R and Pui, D.Y.H. (1998a) *Bimodal aerosol loading and dust cake formation on air filters.* Filtration and Separation, v 35, n 2 Mar 1998, pp. 191-195.

Endo, Y., Chen, D-R and Pui, D.Y.H. (1998b) *Effects of particle polydispersity and shape factor during dust cake loading on air filters*. Powder Technology, v 98, 1998, pp. 241-249.

Ellenbecker, M. J. and Leith, D. (1979) *Theory for dust deposit retention in a Pulse-Jet fabric filter.* Filtration and Separation, v 16, n 6, 1979, pp. 624-629.

Ferer, M. and Smith, D. H. (1997) *A simple model of the adhesive failure of a layer: Cohesive effects*. Journal of Applied Physics, v 81, n 4, 15. Feb. 1997, pp. 1737-1744.

Ferer, M. and Smith, D. H. (1998) *Modeling of backpulse filter cleaning; The small particle filter cake fragments.* Aerosol Science and Technology, v 29, 1998, pp. 246-256.

Ferer, M. and Smith, DH (1998) *Transition from continuous to discontinuous material failure in a simple model of an adhesive layer*. Physical Review E, v 58, n 6, Des. 1998, pp. 7071-7078.

Hajec, S. and Peukert, W. (1997) *Comparison of ceramic and metallic filter units for high temperature filtration.* Chemie Ingenieur Technik, v 69, n 3, Mar. 1997, pp. 341-345.

Höflinger, W., Stocklmayer, Ch. and Hackl, A. (1994) *Model calculation of the compression beahviour of dust filter cakes.* Filtration and Separation, v 31, n 8, Dec. 1994, pp. 807-811.

Höflinger, W. and Stocklmayer, C. (1995) *Investigations about the layered structure of dust filter cakes.* Staub Reinhalt. Luft, n 55, 1995, pp. 423-428.

Japuntich, D.A., Stenhouse, J.I.T. and Liu, B.Y.H (1994) *Experimental results of solid monodisperse particle clogging of fibrous filters.* Journal of Aerosol Science, v 25, n 2, Mar. 1994.

Jo, Y. M. and Raper, J. A. (1997) *Experimental study of airborne particulate filtration using thin ceramic composite membrane filters.* Process Safety and Environmental

Protection: Transactions of the Institution of Chemical Engineers, IChemE Rugby Engl , Part B, v 75, n 3, Aug. 1997, pp. 164-170.

Klingel, R. and Löffler, F. (1981) *Influence of selected parameters on pulse jet fabric filter efficiency.* Proc. Filtech ¨81 Conference, The Filtration Society, London.

Klingel, R. and Löffler, F. (1983) *Influence of cleaning conditions on outlet dust concentration of a pulse jet fabric filter.* 2nd Conference in Fabric Filter Technology for Coal Fired Power Plants, Mar. 1983, Denver, Colorado, USA.

Klingel, R. and Löffler, F. (1983) *Dust collection and cleaning efficiency of a Pulse-Jet filter.* Filtration and Separation, v 20, n 3, 1983, pp. 205-208.

Klingel, R. (1983) *Untersuchung der partikelabscheidung aus gasen an einem schaluchfilter mit druckstossabreinigung,* Fortschr.-Ber. VDI Reihe 3 Nr. 76. Düsseldorf 1983.

Kono, H. O., Jordan, B., Ohtake, T. and Duane, H. S. (1998) *Formation and Measurement of the porosities, tensile strengths, and deformation coefficient of gasification filter cakes at operating temperatures and pressures.* Aerosol Science and Technology, v 29, 1998, pp. 236-245.

Koch, D., Seville, J., and Clift, R. (1996) *Dust cake detachment from gas filters.* Powder Technology, v 86, n 1, Jan. 1996, pp. 21-29.

Kuo, J-T., Smid, J., H, S.-S. and Chou, C.-S. (1998) *Granular bed filter technology.* Proceedings of the National Science Council, Republic of China, Part A: Physical Science and Engineering, v 22, n 1, Jan. 1998, Natl Sci Counc Taipei Taiwan, pp. 17-34.

Lee, K. C. (1975) *Filtration of redispersed power-station fly ash by a Panel Bed Filter with puffback.* The City University of New York, Ph,D. thesis, 1975.

Lee, K. C., Rodon, I., Wu, M. S., Pfeffer, R. and Squires, A. M. (1977) *The panel bed filter*" , EPRI AF-560, Final report, may 1977.

Milne, T.A., Abatzoglou, N. and Evans, R.J. (1999) *Biomass gasifier "tars". Their nature, formation and Conversion.* NREL/TP-570-25367, November 1998.

Morris, K., Allen, R. W. K. and Clift, R. (1987) *Adhesion of cakes to filter media.* Filtration and Separation, v 24, n 1, Jan-Feb 1987, pp. 41-45.

Nos, P. (1997*) Panel Bed Filter, Industrial gas cleaning*, Norsk Energi, v 74, n 1

Novick, V.J., Monson, P.R. and Ellison, P.E. (1992) *The effect of solid particle mass loading on the pressure drop* J. Aerosol. Sci.

Paretsky, L. (1972) *Filtration of aerosols by granular beds*, Ph.D. Dissertation, The City University of New York, 1972.

Peukert, W. and Loeffler, F. (1991) *Influence of temperature on particle separation in granular bed filters.* Powder Technology, v 68, n 3, Dec. 1991, pp. 263-270.

Peukert, W. (1998) *High temperature filtration in the process industry.* Filtration and Separation v 35, n 5, Jun. 1998, pp. 461-464.

Pilz, T. and Loeffler, F. (1995) *Influence of adhesive and cohesive particle properties in filtration on surface filters.* Chemie Ingenieur Technik, v 67, n 6, Jun. 1995, pp. 745-749.

Risnes, H. and Sønju, O. K. (2001) *Evaluation of a novel granular bed filtration system for high temperature applications*. In proceedings: Progress in Thermochemical Biomass Conversion, September 2000, Tyrol, Austria, pp. 730-742.

Rothwell, E. (1986) *The design and operating characteristics of reverse-jet assemblies for Pulse Jet dust collectors.* Fourth World Filtration Congress, Ostend, Belgium, 22-25 April, 1986, Part 1, pp. 2.43-2.53.

Rothwell, E. (1990) *Pulse-driven injectors for fabric dust filters III. Comparative performance of model and commercial assemblies.* Filtration and Separation, v 27, n 55, Sept-Oct 1990, pp. 345-349.

Schmidt, E. (1991) *Elektrische Beeinflussung der Partikelabscheidung in Oberflächenfiltern.* Dissertation, University of Karlsruhe, 1991.

Schmidt, E. and Loeffler, F. (1991) *Analysis of dust cake structures.* Particle & Particle Systems Characterization, v 8, n 2, Jun. 1991, pp. 105-109.

Schmidt, E. (1993) *Comperssion of dust cakes formed on filter media.* Staub-Reinhaltung der Luft, v 53, n 10, Oct. 1993, p. 369-376.

Schmidt, E. (1998) *Experimental investigations into the detachment of differently structured particle layers from surfaces.* Chemical Engineering & Technology, v 21, n 1, Jan. 1998, pp. 26-29.

Schmidt, E. (1995a) *Experimental investigation into the compression of dust cakes deposited on filter media.* Filtration and Separation, v 32, n 8, Sept. 1995, pp. 789-793.

Schmidt, E. (1995b) *Simulation of the flow conditions on a filter bag during dust separation.* Staub-Reinhaltung der Luft, v 55, 1995, pp. 467-469.

Schmidt, E. and Pilz, T. (1995) *Raw gas conditioning and other additional techniques for improving surfce filter performance. Part 2: Impact of relative gas humidity, electrostatic and acoustic factors.* Staub-Reinhaltung der Luft, v 55, 1995, pp. 65-70.

Schmidt, E. (1996) *Simulation of three-dimensional dust structures via particle trajectory calculations for cake-forming filtration* Powder Technology v 86, n 1, Jan. 1996, pp. 113-117.

Schmidt, E. and Pilz, T. (1996) *Raw gas conditioning and other additional techniques for improving surfce filter performance*. Filtration and Separation, v 33, n 5, May 1996, pp. 409-415.

Seville, J. P. K. Cheung, W. and Clift, R. (1989) *Patchy-cleaning interpretation of dust cake release from non-woven fabrics.* Filtration and Separation, v 26, n 3, May-Jun 1989, pp. 187-190.

Schulz, R. (1988) *Untersuchungen zur Staubabscheidung aus Gasen mit Filtrationsabscheidern bei hohen temperaturen und hohen drücken.* Fortschr.-Ber. VDI Reihe 3 Nr. 156. Düsseldorf 1988.

Sievert, J. and Loeffler, F. (1987) *Dust cake release from non-woven fabrics.* Filtration and Separation, v 24, n 6, Nov.-Dec. 1987, pp. 424-427.

Sievert, J. and Loeffler, F. (1987) Filtration and Separation, v 24, pp. 110.

Smith, D. H., Powell, V. and Ahmadi, G. (1998a) *Analysis of operational filtration data part II: Incomplete cleaning of candle filters.* Powder Technology, v 97, 1998, pp. 139-145.

Smith, D. H., Powell, V., Ahmadi, G. and Ferer, M. (1998b) *Analysis of operationalfiltration data part III: Re-entrainment and incomplete cleaning of dust cake.* Aerosol Science and Technology, v 29, 1998, pp. 224-235.

Squires, Am and Pfeffer, R. (1970*) Panel bed filters for simultaneous removal of fly ash and sulfur dioxide-1.* JAPCA v 20, n 8, 1970, pp. 534-538.

Stöcklmayer, Ch. and Hoflinger, W. (1998) *Simulation of the regeneration of dust filters.* Mathematics and Computers in Simulation v 46, n 5-6, Jun. 1998, pp. 601-609.

Stöcklmayer, Ch. and Höflinger, W. (1998) *Simulation of the filtration behavour of dust filters.* Simulation Practice and Theory, v 6, 1998, pp. 281-296.

Sørhuus, A. (1997) *Flow resistance in cakes formed on the bags in a reverse air cleaned filter for microsilica.* Dr.ing. thesis, Dep. of Metallurgy, The Norwegian University of Science and Technology, MI-report 1997:44

Thambimuthu, K.V. (1993) *Gas cleaning for advanced coal-based power generation*. IEA Coal Research, London (ISBN 92-9029-211-3) 163p.

Tsubaki, J-I. and Mori, H. (1997) *New correlations for predicting the transient behavior of granular filtration.* Journal of Chemical Engineering of Japan, v 30, n 2, 1997, pp. 239-245.

Tien, C. (1989) *Granular filtration of aerosols and hydrosols* Butterworths Series in Chemical Engineering, ISBN 0-409-90043-5, 365p.

University of Karlsruhe (TH) *Short Course – Fundamentals of hot gas filtration 1999.* Inst. für Mechanische Verfahrenstechnik und Mechanik.

Wayne, T.D. LaRosa, P.J. and Noll, K. (1976) *The generation and evaluation of fabric filter performance curves from pilot plant data.* Filtration and Separation, Nov./Des. 1976, pp. 555-560.

Zevenhoven, C.A.P. (1992) *Particle charging and granular bed filtration for high temperature application* Ph.D. (Eng.) thesis (public defense Dec. 3, 1992) Delft University of Technology, the Netherlands Delft University Press 1992 (ISBN 90-6275-822-3), 288 p.

Paper I:
Evaluation of a novel granular bed filtration system for high temperature applications. In proceedings: Progress in Thermochemical Biomass Conversion, September 2000, Tyrol, Austria, pp. 730-742.

Evaluation of a novel granular bed filtration system for high temperature applications.

H. Risnes and O. K. Sønju
Department of thermal energy and hydropower, The Norwegian University of Science and Technology, Trondheim, Norway

ABSTRACT: Panel Bed filter is a new alternative for particle removal. The filter is based on the use of sand or other granulated material as a filtration medium, and is operating in surface filtration mode. The concept was developed in the United States* and further developed in Norway.

Studies were undertaken to test a full-scale single filter element (1150m^3/h) of commercial design on combustion flue gas from a 5MW bark-boiler. Results from the field filtration experiments, in total 80 hours of operation, show a reduction in the dust concentration from approx. 1g/Nm^3 at the filter inlet to an average dust content of 1.7mg/Nm^3 at the filter outlet (average filtration efficiency equal to 0.9983). The filter unit was operated at approximately 190°C, with a superficial filtration velocity ranging from 4 to 15 cm/s. The results obtained from the field tests on a single element has been verified in a full scale pilot plant with a capacity of approx. 30,000m^3/h operating at 200°C.

Further, a lab scale filter unit, based on the German filtration standard VDI-3926, type 2, has been built for testing on biomass gasification gases, at higher temperatures.

INTRODUCTION

The fast increase in severity concerning environmental legislation has provoked a renewed interest in particle removal from gas streams. Emphasizing on the collecting of micrometer particles and tolerance to fluctuations in the gas stream conditions. Also the potential usage of alternative energy carriers has recently attracted considerable attention. Substantial effort has, therefore, been directed toward developing advanced technology for power generation with high efficiency and reduced emissions. Power systems, such as the integrated gasification combined cycle (IGCC) and pressurized fluidized-bed combustion (PFBC, requiring gas turbines), are widely anticipated as future technologies to produce electricity and steam from coal and biomass. Removal of particulate and other emissions is required for these processes, to protect the gas turbines against erosion and corrosion. To maintain high thermal efficiency, the gas cleaning should be carried out at high temperatures (at least 350°C for IGCC and 750°C for PFBC). Thambimuthu[1] and Clift and Seville[2] have published extensive reviews of gas cleanup at high temperatures.

* A. M. Squires, Professor at Virginia Polytechnic Institute & State University

For particle cleanup; cyclones, impact separators, fabric and fiber filters, granular beds, and electrostatic percipitators for low-temperature gas cleaning have been widely used in the industry. However, for hot gas filtration with ceramic filters, the long-term durability, alkali corrosion, cleanability, thermal shock, and particulate penetration into filter media has been recognized as major concerns. Traditional bag filters are sensitive to high temperature and hot particles, electrostatic percipitators have a relatively high cost of installation in smaller plants and multi-cyclone cleaners are not sufficiently efficient to meet the new purification demands.

The term "granular bed filter" describes devices in which particles are removed from a fluid by passing it through a bed of an unbonded granular medium. Granular bed filters are cleaned in situ, as described by Coury et al.[3], or alternatively the medium may be displaced intermittently, as in the "panel bed" configuration described in this paper. The objective of this paper is to describe and evaluate field tests conducted on a new type of cake forming granular bed filter element, of commercial design, and relate these findings to an existing pilot plant of full scale.

Sand filters have also numerous advantageous properties compared with electrostatic percipitators and bag filters:

- The filter material is easy accessible and cheap to replace, insensitive to hot particles, temperature fluctuations and corrosive elements in the flue gas.
- Compactness, due to a superficial filtration velocity which is up to 10 times higher than for bag filters
- Granulated material can be added to the filter to provide chemical processing of the gas.
- Measured filtration efficiency is at least equal to or better than for bag filters.

The Panel Bed Filter exposes a large number of sand surfaces for collecting deposits of fly ash. Louvered walls, somewhat resembling venetian blind, hold a sand bed in a tall relatively narrow "panel". Gas flows in the horizontal direction across the sand bed, and the dust in the gas deposits forming a filter cake upon the sand surfaces at the gas-entry "face" of the panel.

Cake filtration occurs when the deposit layer becomes thick enough so that the properties of the dust cake, rather than the supporting medium, determine filtration characteristics. Besides particle properties and forces, such as electrostatic forces, the structure of the dust cake can be influenced by fluid conditions such as gas velocity and temperature and the geometry of the filter medium. The dust loading process for cake forming filters generally proceeds through four regimes: i) clean filter filtration, ii) initial depth filtration regime, iii) transition filtration regime, and iv) dust cake filtration regime. Under high particle loading conditions, the process will often pass through the first three regimes in a very short time to reach the dust cake filtration regime.

For a low and stable conditioned pressure loss, successful pulse cleaning of the filter is clearly essential. There are two parts to this problem: i) the geometry and reservoir pressure of the cleaning system must be selected to deliver the required conditions for dust cake removal at the filter surface, and ii) the magnitude of the cleaning action which is necessary to detach the cake must be known.

THEORY

The pressure loss across the dust layer during filtration as well as the energy necessary to remove the deposited layer in the cleaning cycle are strongly related to filter cake properties, including cake porosity. The porosity can, in principle, be estimated from macroscopic values of the pressure drop across the dust layer for a given gas flow rate, if the total cake mass is known (Darcy's law). Generally the cake porosity is known to decrease; i) with increasing particle size, ii) towards the cake-filter interface and iii) as cake grows with time, for a given position within the cake[4-9].

On-line measurements of cake thickness during filter-system operation have not been feasible in most systems. However, when the pressure drop across the filter system, the gas flow rate, and the particle concentration in the incoming gases are measured, these data can be used to calculate the mass of filter cake on each filter. The overall pressure drop can be modeled as[10,11]:

$$\Delta P = \Delta P_{Filter} + \Delta P_{Cake} \qquad (1)$$

Applying K_1 as the specific resistance of the filter medium itself, including deposited particles, and K_2 as the specific cake resistance, *Eq.* 1 can be rewritten as

$$\Delta P = K_1 \mu v_f + K_2 \mu v_f \overline{W}_A \quad \text{, where } \overline{W}_A = c v_f \Delta t \qquad (2)$$

Where μ is the gas viscosity, v_f – gas velocity across the exposed filter cake surface and W_A equals dust load. It is common to combine the specific resistance and viscosity, and replace K_1 and K_2 (in *Eq.* 2) with

$$K_1' = \mu K_1 \quad \text{and} \quad K_2' = \mu K_2 \qquad (3)$$

$$K_2' = \frac{\Delta P_{Cake}}{t_c v_f^2 c} \qquad (4)$$

K_2' is mainly determined by the filter cake structure; thus closely related to the physical properties of the dust itself.

THE WORKING PRINCIPLE

Fig. 1 shows a cross section of a filter element and the principle for the construction of the filter is illustrated. The figure shows that the outer surface of the filter element consists of louvers. There are two layers of sand along each outer surface. A layer of fine sand on the outside and a layer of coarse sand on the inside facing the clean gas duct in the center. The sand fractions are physically separated.

All sand has an angle of respose fixed on the basis of the dimension of the sand grains and the distribution of size. By placing the louvers at a common distance adapted to the angle of respose for the fine sand, the sand remains stable between the louvers. In this way the open sand surface is exposed to the dust containing gas.

Most granular filters are based on the principle of deep bed filtration (particle penetration deep into the filtration medium) and the purification degree has been relatively poor for particle sizes in the area 0.1-5μm.

The Panel Bed Filter differs from other granular filters in that filtration takes place on the surface of the granular medium, through the building up of a filter cake with "roots" in the outside layer of sand. The size of the sand grains and the speed of the gas impinging on the filter surface are important parameters with regard to the formation of the filter cake and the efficiency of the filter.

When the filter cake has built up to a thickness whereby resistance over the filter has reached its desired maximum value. The filter is cleaned by stopping circulation and transmitting a short pressure pulse, with duration of only a few milliseconds, into the filter element in the reverse direction to normal flow. The pressure wave fluidizes the sand and the sand moves slightly horizontally between the louvers. As a result,

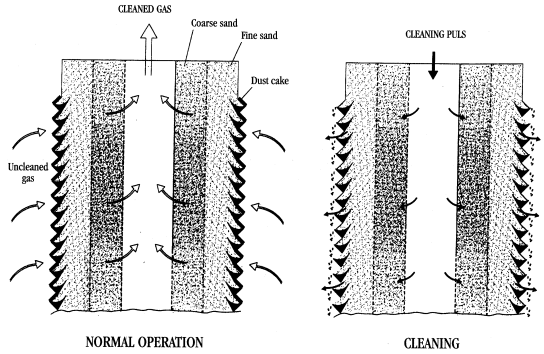

Fig. 1 Cross section of a filter element and the principle for the construction of the filter.

some of the sand together with the filter cake falls from the filter element, thereby cleaning the filter surface. The mixture of dust and sand is percipitated into a hopper for dust separation and sand recirculation.

EXPERIMENTAL

SET-UP

Field tests were conducted on a slip-stream connected downstream of the multi-cyclone, on a 5MW-bark fired boiler. The instrumentation of the set-up was as indicated in *Fig.* 2. Connections for isokinetic dust sampling (gravimetrical determination) were mounted on the upstream and downstream side of the filter unit. The following signals were connected to the data acquisition unit for continuous sampling of: Pressure difference, between filter inlet and outlet (PT1); volume flow (torbar pitot-tube installed downstream of the filter (PT2)); temperature at the isokinetic sampling points (TT1-inlet / TT4-outlet) and connections for pressure difference measurements (TT2-inlet / TT3-outlet). The volume flow measurement is located close to TT4.

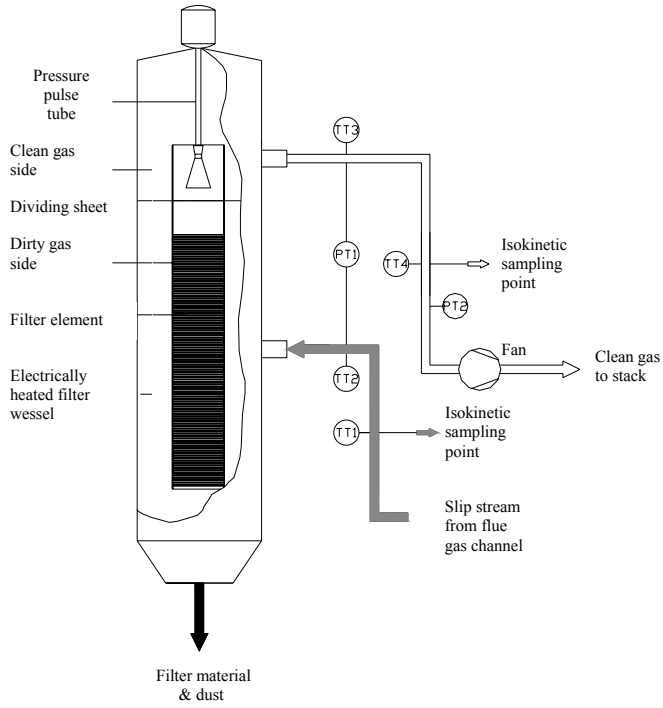

Fig. 2: Flow-sheet for the experimental set-up during the filtration experiments.

THE FILTER ELEMENT

Fig. 3 shows a cross section of a filter element. The design is quite similar to that of bag-house filters and ceramic / metallic filters. Each filter element is suspended from a dividing sheet between pure and contaminated gas at the top of the filter housing.

The filtration experiments were conducted on a full-scale filter element: height of approximately 3500mm, width of 600mm and a thickness of 250mm. This size provides a filter area of approximately 3.25 m^2.

EXPERIMENTAL RESULTS

FILTER CAKE FORMATION AND FILTER REGENERATION

The Panel Bed Filter unit was successfully operated for 80 hours on flue gas from a 5 MW bark boiler. Stable operation was maintained, despite significant fluctuations in flue gas dust concentration (at the filter inlet, c = 600-1200mg/Nm^3) and filter operation ($4 \leq U_s \leq 14$cm/s). The observed unstability in dust load makes extraction of exact values for the specific cake resistance less accurate.

The influence of filtration velocity on resulting pressure build up and cycle-time is illustrated in *Fig.* 4. Note that the displayed offset in the base pressure loss for a clean filter (t=0) has been used to enhance readability

Measured pressure build up versus accumulated amount of fly ash is shown in *Fig.* 5 a). Calculated fly ash accumulation is based on averaged dust load measured gravimetrically during the respective filtration cycle. Observed pressure loss is close to ideal behavior for surface filtration (i.e. incompressible cake formation and constant dust concentration). Calculated specific cake resistance is shown in *Fig.* 5 b).

Fig. 6 shows the variation in K_2' and residual pressure drop during six hours of operation. K_2' is calculated from *Eq.* 4. Calculated mean specific cake resistance equals $6.5 \cdot 10^4$ [s^{-1}], with a standard deviation of approx. 15%. v_f is defined as the velocity across the exposed filter surface ($v_f \approx 2\ U_s$). Observed fluctuations in pressure build-up did not result in any increase in the residual pressure drop. The residual pressure drop could be maintained at a constant level. The average filtration efficiency was 0.9983. Filter regeneration was conducted with off-line pulsing (P_{tank} = 2barg and total sand spill of 10 kg).

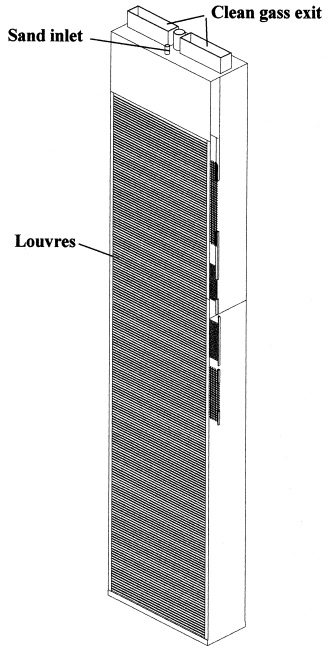

Fig. 3: The design of a commercial scale filter element.

Table 1 Commercial PBF-filter element: operating conditions during the field tests.

Operating conditions	
Filter material	Olivine sand (AFS50) Virgin and circulated up to three times
Mean filter temperature	190°C
Volume flow	500-2000 m^3/h
Superficial velocity (U_s)	4-14 cm/s
Fly ash from a bark boiler	$X_{50,3}$ = 12.3 μm; $X_{95,3}$ = 62.2 μm
Fly ash concentration	600-1200mg/Nm^3
Duration of pressure pulse	approx. 30 ms
Tank volume	5-10 liters
Tank pressure	1-2 barg
Sand spill during cleaning	approx. 10 kg

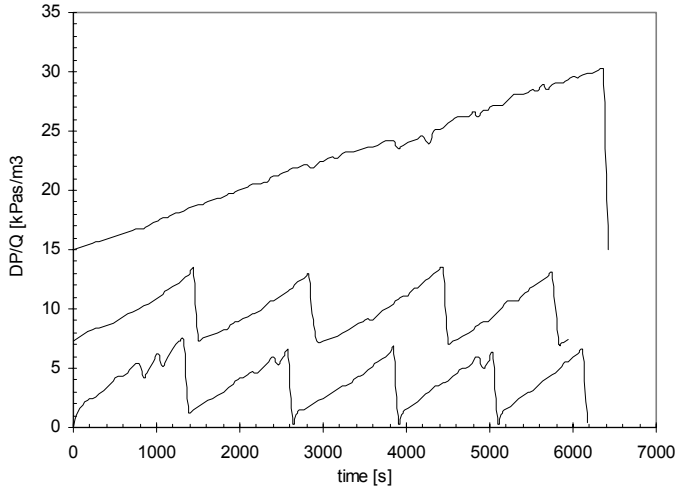

Fig. 4 Comparison of the pressure build-up at three different operating conditions (4 (top curve), 8.9 and 10.8 (bottom curve) cm/s).

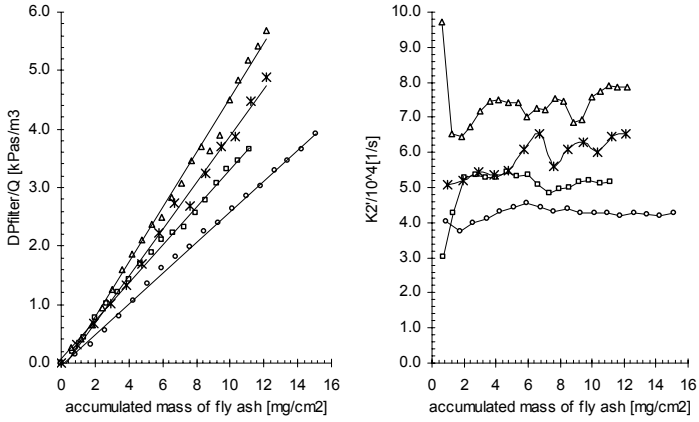

Fig. 5 (a) Pressure build-up and (b) Calculated specific cake resistance at operating conditions close to design load. (Δ - v_f = 17cm/s, c = 962 mg/Nm^3; ∗ - 21.3cm/s, 1226 mg/Nm^3; □- 23.1cm/s, 810mg/Nm^3; ○ - 18.8cm/s, 1261 mg/Nm^3)

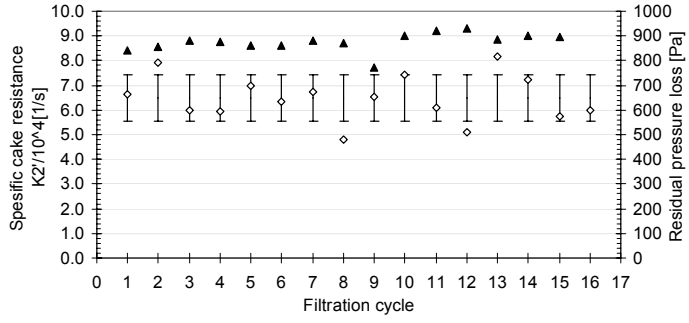

Fig. 6 variations in specific cake resistance and residual pressure loss during a filtration cycle (cycle time varied from 20 to 27 minutes, within this series).

RESULTS AND DISCUSSION

The calculated specific cake resistance (K_2'), for design conditions, is found to be within the range of published values, see *Table* 2. Note the high value of v_f applied in the present work. Due to the significant fluctuations in the flue gas dust concentration calculated values should be considered as being of approximate nature.

Fig. 7 a) shows both base and maximum pressure loss (just before and after regeneration respectively) for some sample filtration series. The base pressure loss (ΔP_0) shows a linear dependency of U_s. Increase in the residual pressure drop due to depth filtration, dust re-entrainment and fractional cleaning is well known to cause serious filter degrading and may lead to total filter blinding. During the 80 hours of field operation such systematic degrading effects has not been observed.

Normally bag house filters operate with superficial velocities in the range 0.1-2 cm/s and ΔP_0 approximately equal to 900Pa. Superficial filtration velocities typical for the Panel Bed Filter, is approximately ten times higher than for traditional fabric filters. Thus, the Panel Bed Filter can operate at substantial higher filtration velocities at comparable pressure loss and filtration efficiency (above 98%).

Filtration efficiency as discussed above, has been verified in a commercial scale filter plant. This pilot plant, *Fig.* 8, includes a system for discontinuous separation of dust from the used filter bed material. The cleaned bed material is re-circulated by pneumatic transport to sand silos located at the top of the filter vessel. A summary of typical operating conditions, at design load, is given in *Table* 3. Compared to the field-testes described above, this system represents a scale up by a factor of 27. A picture of the filter plant is given in *Fig.* 9.

In addition the development of this filter concept for a bark fired bolier application, a research program has been undertaken for evaluation of high temperature applications such as biomass gasification gases. For this purpose, a laboratory filter test unit for application at temperatures higher than >550°C, has been built. The filter closely resembles the system described in VDI-3926, type 2 [13]. Tests on this unit will be started shortly.

Table 2 Comparison to literature values, derived at approximately 200°C

Dust	d_p [µm]	c [g/m^3]	v_f [cm/s]	$K_2' \cdot 10^{-5}$ [s^{-1}]
Present work	$X_{50,3}$ = 12.3; $X_{95,3}$ = 62.2	1	18	0.65 ± 0.01
NaCl, NH_4Cl, Al_2O_3 (HEPA-filter)[12]	0.5-2		2.45-3.0	2-20
Steinkohle-flughashe (Ceramic filter element)[10]	$3 \leq X_{r,3} \leq 100$		3	1.5-1.7
Silica (Metal fiber fleece)[11]	$X_{50,0}$ = 0.53; $X_{90,0}$=1.6	1	2.5	0.028
Quarz (Metal fiber fleece & ceramic fiber fleeze)[11]	$X_{50,0}$ = 0.7; $X_{90,0}$=2.74	25	2.5	0.001

Table 3 Commercial PBF-filter element: operating conditions during the field tests.

Operating conditions		
Flue gas origin:		Bark boiler of 5 MW
Filter matieral		Olivine sand (AFS50)
Filter temperature		approx. 200°C
Number of filter elements		27
Design load:	Superficial velocity (U_s)	9 cm/s
	Volume flow	approx. 30,000 m^3/h
Fly ash concentration (after multi-cyclone)		1000mg/Nm^3

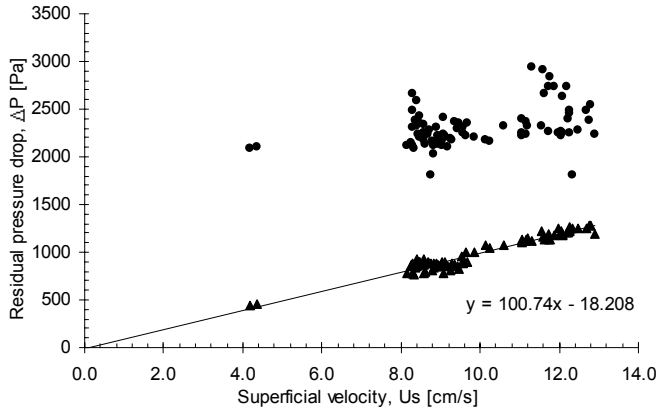

Fig. 7 Operational range for the Panel Bed Filter, pressure loss before (•) and after (▲) regeneration.

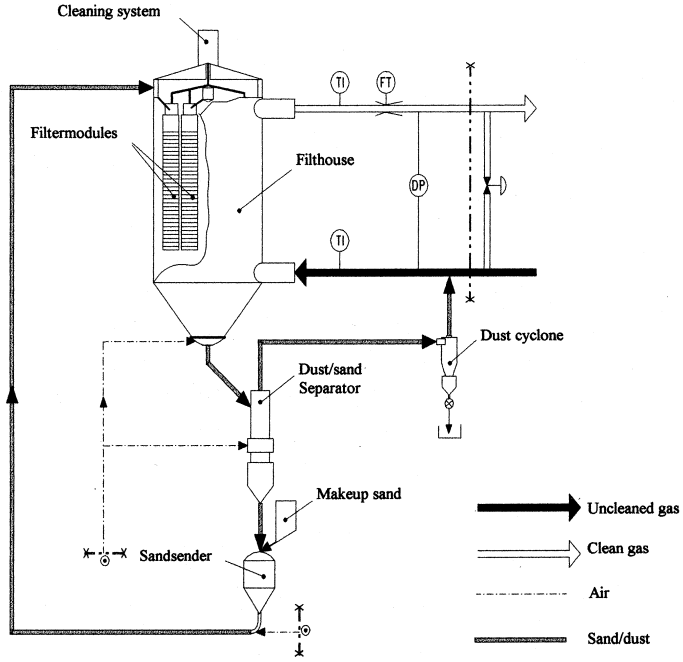

Fig. 8 Full-scale pilot plant, flow-sheet.

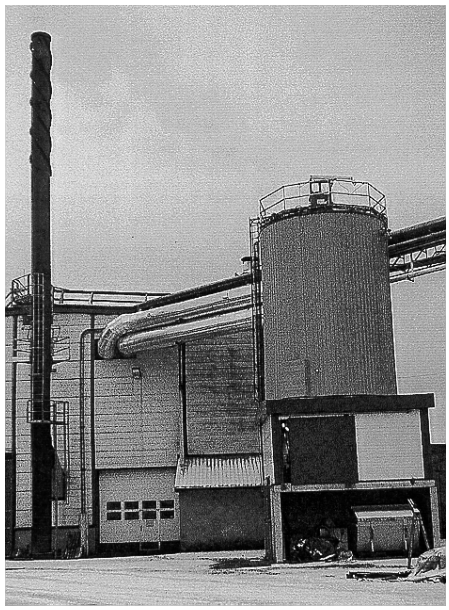

Fig. 9 The commercial scale pilot-plant, capacity of 30,000 m^3/h. The filter vessel is seen at the right side, with the 5MW boiler house located in the background.

CONCLUSION

Field tests, on a single filter element of commercial design, have been successfully conducted at typical operating condition. Measured filtration efficiency is comparable with bag house filters, for filtration velocities up to 14 cm/s. The applied filtration velocities are extremely high compared with bag filters which normally operates in the area of 1.0 to 2.5 cm/s. The pressure drop over the sand filter shows that even if filtration speed is increased dramatically, it is possible to work within the same field as bag filters, i.e. from 900 to approximately 2200 Pa.

Average dust concentration downstream of the filter unit was measured to be well below 5 mg/Nm^3. Measured filtration efficiency at 190°C and 9 cm/s corresponds to a filter efficiency above 99.83%, verified in a full-scale pilot plant. Calculated average specific cake resistance (K_2') equals 6.5 ($\pm$ 0.1) $\cdot 10^4$ [s^{-1}] at operating conditions, which is within the range found in the literature. A more detailed study of the filter cake behavior will be carried out with the new laboratory unit.

The Panel Bed Filter concept has been successfully demonstrated in full scale operation, and more detailed filtration behavior has been studied. Filter cake data have been obtained at very high filtration velocity and reasonable pressure drops. Very low dust concentrations are observed.

NOMENCLATURE

ΔP – pressure loss [Pa]
ΔP_0 – pressure loss across a clean filter element [Pa]
ΔP_{Filter} – pressure loss across filter material, including deposited particles [Pa]
ΔP_{Cake} – pressure loss across filter cake [Pa]
Q – volume flow [m^3/h]
K – specific resistance [s^{-1}]
W_A – accumulated dust mass [g/m^2]
t – time [s]
U_s – superficial filtration velocity [cm/s]
v_f – average gas velocity thorough filter cake [m/s]
c – dust concentration in flue gas [kg/m^3]
μ – gas viscosity [Pa s]

REFERENCES

1. Thambimuthu, K. V. (1993) Gas cleaning for advanced coal-based power generation. IEACR/53, IEA Coal Research, London
2. Clift, R. & Seville, J. P. K. (1993) Gas cleaning at high temperatures. Blackie Academic & Professional, New York
3. Coury, J.R., Thambimuthu, K.V. & Clift, R. (1987) Capture and rebound of dust in granular bed filters. Powder Technology v 50 n 3 p 253-265
4. Aguiar, M. L. & Coury, JR. (1996) Cake formation in fabric filtration of gases. Industrial & engineering chemictry research Vol. 35, No. 10, p 3673-3679
5. Höflinger, W., Stocklmayer, Ch. & Hackl, A. (1994) Model calculation of the compression beahviour of dust filter cakes. Filtration and Separation v 31 n 8 p 807-811
6. Kono, H. O., Jordan, B., Ohtake, T. & Duane, H. S. (1998) Formation and Measurement of the porosities, tensile strengths, and deformation coefficient of gasification filter cakes at operating temperatures and pressures. Aerosol Science and Technology v 29 p 236-245
7. Rothwell, E. (1985) Analysis of fabric dust filtration. I: Model observation of dust cake formation. Filtration and Separation v 22 n 5 p 318-324
8. Schmidt, E. & Loeffler, F. (1991) Analysis of dust cake structures. Particle & Particle Systems Characterization v 8 n 2 p 105-109
9. Stöcklmayer, Ch. & Höflinger, W. (1998) Simulation of the filtration behavior of dust filters. Simulation Practice and Theory v 6 p 281-296
10. Pilz, T. & Loeffler, F. (1995) Influence of adhesive and cohesive particle properties in filtration on surface filters. Chemie Ingenieur Technik Vol. 67, Nr. 6, p 745-749
11. Hajek, S. Peukert, W. (1997) Comparison of ceramic and metallic filter units for high temperature filtration Chemie Ingenieur Technik Vol. 69, Nr. 3, Mar 1997, side 341-345
12. Novick, V.J., Monson, P.R. & Ellison, P. E. (1992) The effect of solid particle mas lading on the pressure drop in HEPA filters. J. Aerosol. Sci., Vol. 23, No. 6. p 657-665
13. VDI-Richtlinie 3926 Testing of filter media for cleanable filters, Beut Verlag, Berlin, 1994.

3 The Panel Bed Filter – Design evaluations

The original filter concept described by Squires and Pfeffer (1970) consisted of two sets of louvers defining a single bed of thickness about 25 mm. Field experience has re-vitalised the interest in this design due to its simplicity with respect to production and maintenance. Removal of the coarse sand box and the two sets of wire mesh, not only reduce the pressure loss, but also incorporate enhanced rigidity as the potential of filter blinding by dust migration is reduced. However, Lee (1975) experienced fluidisation in this first design, at a superficial velocity of approximately 15 cm/s or by the building up of a filter cake (pressure drop of about 3500 Pa). This phenomenon emphases the importance of characterising the upper stability limit, i.e. maximum filter load (U_S) below which no bed particles are entrained into the clean gas duct.

Furthermore, reducing the number of louvers per filter unit and simultaneously enhance the filter surface (i.e. increased dust load capacity) increases the filter competitiveness through cost effective production and plant compactness.

Evaluation of the filter design has been based on the original work conducted by Squires and Pfeffer (1970) and Lee (1975) and Lee et al. (1977). The Wishbone louvers, herein used as reference geometry, resemble the louver developed by Lee et al. (1977). In order to verify filter performance state of the art within cake forming filters has been reviewed (Chapter 2) and links established to newly developed filtration standards (VDI/ISO).

3.1 Review of the Panel Bed Filter design fundamentals

This section give a brief summary of the investigations conducted by Lee and co-workers (Lee 1975 and Lee et al. 1977) on a model filter (75x305 mm) and a full scale filter element (305x3050 mm). These filters had three columns of louvers, which defined two separate sand beds. The Folla design (Paper I) represents a modification of this design, by incorporating a simplified front louver design and replacing the remaining two sets of louvers with two sets of wire-mesh.

The mechanisms governing the regeneration of the panel bed filter is outlined and the performance of different louver geometries and operating conditions upon filter performance is discussed.

3.1.1 General

Lee (1975) and Lee et al. (1977) concluded that regeneration of the PBF by means of a pressure pulse is a transient soil mechanics failure phenomenon caused by transient aerodynamic drag forces. The spill of bed material was found to be a result of a body movement of the entire sand bed, and closely related to the characteristics of the granular media. The different stages as identified by Lee (1975) are illustrated in Figure 3.1: a) t = 0; grains thrown out, *b*) grains jump up from the inner edge of the gas-entry surface, local failure (at surface, lasts 10-100 ms), c) body failure (the whole bed moves forward in a plug flow with a slightly downward motion) and separation, d) local failure and de-separation, a small amount of sand falls from the outer edge of

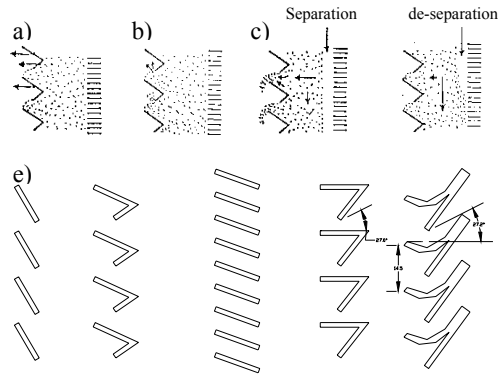

Figure 3.1: The mechanisms of puff-back: a) sand grain thrown out, b) first stage, sand grains jump up, c) second stage: body failure and separation, d) third stage: Local failure and de-separation e) a summary of the front louvers investigated by Lee (1975) and Lee et al. (1977)

the gas-entry surface, major motion of the bed is downward. Both stage c) and d) lasts several times longer than stage b), and no sharp separation was found. Lee (1975) concluded that only the first stage, local failure, occurs at low pulse intensity.

Only the outermost layer of sand (0.3-0.8 g/cm^2 of free sand surface ref. Squires, 0.15 ref. Lee et al. 1977) is to be removed upon puff-back.

Also included in Figure 3.1 is the series of dirty face louvers tested by Lee. The louvers were designed so that the angle of the louver opening for the sand free surface with the horizontal (the louver surface angle) was 27° (the angle of repose for sand ranges from 30-35° depending on the sand properties). Louver #1 was the first louver used in studying the panel bed filter. Design #2 has a converging section that concentrates the puff-back airflow. And the upper part of the louver plate holds the dirty sand near the surface without letting the dirty sand fall into the bed during puff-back stage d) . Louver #3 was designed in order to increase the sand free surface area, but gave poor puff-back results. Also louver #4 failed as the sand appeared to jam the opening during puff-back. Design #2 was found to be the best in Lee's report from 1975. However, the work published in 1977 concluded that the wishbone front louvers (design #5) combined with inclined back louvers gave improved performance.

An unexpected benefit of the inclined louvers was a marked increase in the puff-back spill at a given puff-back intensity. Also, they increased the range of sand spill for which the spill was reasonably uniform along the height of the panel bed.

3.1.2 Active time theory

The cause of puff-back sand spill is due to the pressure drop across the bed. Typical pressure pulse data as obtained with side shot puff-back (off-line) is shown in Figure 3.2: a) the pressure decay in the puff-back bottle and b) the pressure pulse measured just behind the filter bed. Note the relative long pressure rise time.

The reported values for the minimum pressure drop (dP_{min}) required to cause sand spill was found to be about 530 Pa for sideshot and about 830 Pa for downshot puff-back. The difference in dP_{min} of the two different puff-back configurations was

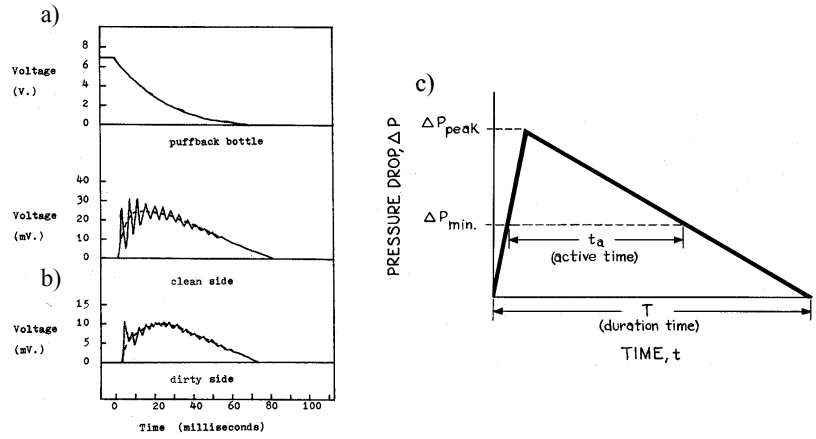

Figure 3.2: Characterization of the pressure pulse by Lee (1975) a) Typical side shot cleaning pulse and b) The active time theory discussed in connection to an ideal triangular cleaning pulse.

believed to be due to the difference in rise time of the pressure curve. A fast rise time (i.e. downshot) resulting in more soil resistance due to elastic and plastic deformation of the sand, requiring a higher dP_{min}.

It was not possible to determine an exact value for the full-scale element (downshot) but dP_{min} was estimated to be about 600 Pa (Lee et al. 1977). dP_{min} appeared not to be a function of the sand size. Sand spill at any given time elevation of the panel bed depended only upon active time "t_a" and NOT upon the peak pressure difference achieved at the particular elevation (see Figure 3.2c).

Deposition of fly ash on the sand surface decreased the permeability of the sand bed and resulted in a higher pressure build up on the clean air side. Thus, giving a higher puff-back intensity (higher active time) for the same puff-back set-up.

A practical upper limit on active time appeared to be about 50 ms. At long active times, beyond about 150 ms, the sand spill at first exhibits the body motion characteristics of puff-back, but changes to the spill characteristic of blowback and tends to generate a large sand spill at the topmost few gas-entry surfaces.

3.1.3 Puff back uniformity tests

Lee found the porosity variation in the filter bed to result in non-uniform soil strength and hence non-uniform sand spill. (A lower initial porosity will have higher soil strength and vice versa.) Loosening of the sand bed by a high intensity puff-back decreased the soil strength and increased the porosity, but below the plane of failure the sand remained stationary and packed at the original density.

High puff-back intensity resulted in slightly more sand spill near the top than at the bottom. Lee suggested introducing a relative displacement of front vs. back louvers in order to overcome this problem. The low porosity at the topmost louver space during puff-back was found to be of minor importance.

Figure 3.3a illustrates some typical uniformity profiles as obtained by Lee (1975).

3.1.4 Experimental results from the filtration of redispersed fly ash

Lee concludes that dirty sand a filter better than clean sand, and that fly ash is being filtered by a fly ash filter cake (i.e. in surface filtration mode). Compared to filter cakes formed at high filtration velocities (> 10 cm/s), lower velocities (< 5 cm/s) led to fewer and smaller pin-holes resulting in a higher efficiency, but with a higher porosity tending to reduce the efficiency. (The importance of Brownian diffusion increases with decreasing velocity.) Lee (1975) reported that less fly ash was required to establish roots for the filter cake at higher velocities.

Lee et al. (1977) reports that the autohesivity of fly ash or its adhesivity toward sand to be less at 150 °C than at atmospheric temperature. And suggested that this might be due to the absence of capillary forces arising from the presence of moisture at lower temperatures. Lee also speculates in whether a measured minimum in the penetration curve at 315 °C reflected a greater tendency for fly ash re-entrainment at the higher temperature.

The experiments conducted by Lee revealed little difference in filtration behaviour of fly ash deposits put down upon silicon carbide, copper shot or upon sand (297-420 μm / 40-50 mesh). Fly ash filtration efficiency in the PBF begins to deteriorate at filtration cycle times longer than optimum. Figure 3.3b gives an example of stable filtration of redispersed fly ash (150 °C, 7.7 cm/s and a raw gas dust concentration of about 12 g/m^3) applying sand 297-420 μm (40-50 mesh) as filter material (Lee et al. 1977). Only the pressure drop for the clean bed, just before regeneration and just after regneration is given (i.e. not the pressure build up curve). The maximum pressure build up was 250-340 Pa in Lee (1975) and 400-1900 Pa in Lee et al. (1977). The ratio of dust over granules (discharged upon each puff-back) is also included in (b).

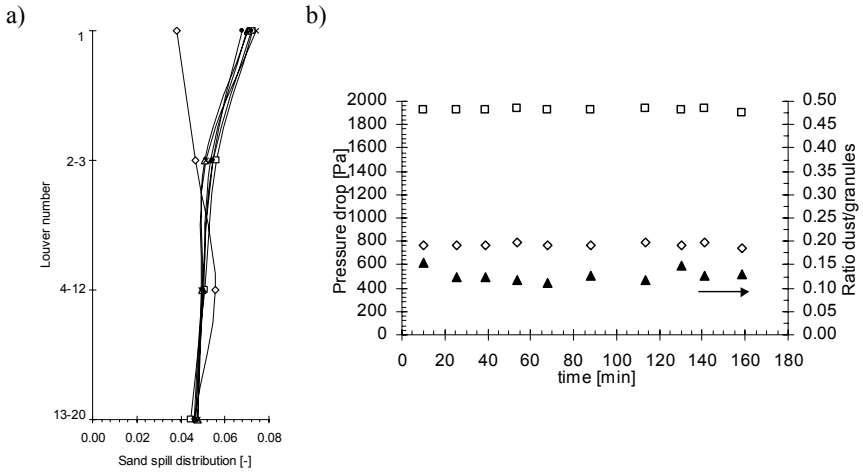

Figure 3.3: Results from the laboratory scale filter unit (75x305 mm) operated by Lee: a) Typical sand spill uniformity (420-590 μm / 30-40 mesh, Louver # 2) as obtained by Lee (1975) and b) stable filtration of redispersed fly ash (150 °C, 7.7 cm/s and a raw gas dust concentration of about 12 g/m^3) applying sand 297-420 μm (40-50 mesh) as filter material (Lee et al. 1977).

3.1.5 Penetration studies with a 1.1micron aerosol on surface deposits of fly ash.

Paretsky (1972), Lee (1975) and Lee et al. (1977) gave data for the penetration of a surface deposit of fly ash resting upon a horizontal bed of sand by their dilute 1.1 micron aerosol (polystyrene microspheres) 10^{-5} g/cm^3. (Deposition of incremental amounts of fly ash while flowing air downward at 5.5 cm/s.) Lee's dilute aerosol penetration gave the first strong signal that the autohesive properties of a dust and its adhesive properties toward granular medium are important factors in successful application of the panel bed filter.

Furthermore, Lee (1975) found that a deposit on 297-420 μm (40-50 mesh) sand was coherent and unblemished. A deposit on 590-840 μm (20-30 mesh) sand tended to develop "pinholes" or "craters" after the deposit reached a given density, whereupon the penetration tended to remain about the same upon further additions of fly ash to the deposit. No coherent deposit formed at all on 420-1885 μm (10-40 mesh) sand. Similarly, no coherent deposit of Teflon powder (3-8 microns) formed upon 590-840 μm (20-30 mesh) sand. The maximum pressure drop across the filter cake was about 9000 and 20000 Pa in Lee (1975) and Lee et al. (1977) respectively. Some typical pressure build-up curves are shown in Figure 3.4.

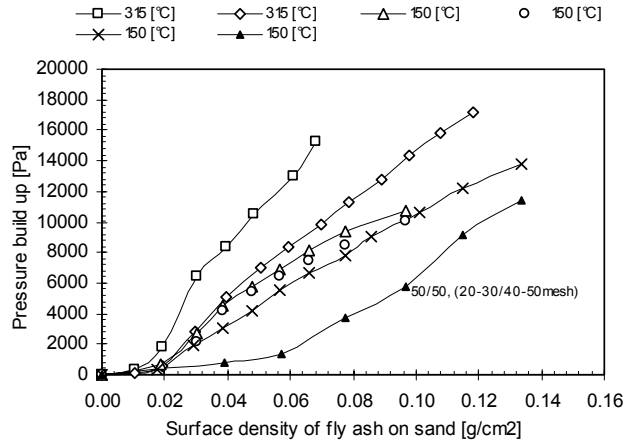

Figure 3.4: Pressure build up when depositing redispersed fly ash (15.2 cm/s) upon 297-420 μm (40-50 mesh) sand in the horizontal bed unit operated by Lee et al. (1977). Note the difficulties in establishing a filter cake when using the mix of 297-420 μm (40-50 mesh) and 590-840 μm (20-30 mesh) sand.

Lee describes a typical tree stage pressure build-up: i) Penetration. The sand grains at the surface of the sand bed become coated with fly ash, and toward the end of this period, the surface takes on a pitted appearance. ii) Filling the pits. Development of deposit coherency, i.e. fly ash fills the pits betweeen sand grains resulting in a relatively smooth surface. iii) Surface filtration. The fly ash deposit continues to grow with a smooth surface.

3.2 Experimental equipment and test procedures

Three primary goals were defined for the experimental work: i) develop a new louver geometry featuring increased pitch (i.e. distance between two individual louvers) and enhanced effective filter surface, ii) evaluate the stability limits relevant for the single bed concept (e.g. upper stability limit) and iii) evaluate filter performance (new vs. old design) at elevated temperatures. This section describes the different test units built and the operation procedures developed in order to accomplish these goals.

Two test units were built in order to develop the new louver design: the Puff-Back Unit (PBU) and the small scale Panel Bed Filter (PBF). The PBU was used to establish a qualitative description of the pulse-jet induced motion of sand between two adjacent louvers. The small-scale PBF unit resembles the small-scale test unit operated by Lee (1975) and Lee et al. (1977) and is comparable with the standard test rig described in the German standard VDI 3926, type 2. The design is highly flexible and incorporate an easy to change louver rack (filter area equal to about 80x300 mm), variable bed thickness (from 30 mm and upward) and allows for a relative displacement of the front vs. back louvers. Additionally a rack of louvers can replace the coarse sand box.

The effect of the relative displacement of the front vs. back louvers upon bed stability was investigated in the transparent test unit and compared with fluidisation tests conducted in a small fluidised bed.

Filter performance at 200 °C was evaluated in the high temperature panel bed filter (resembles the transparent test unit) and the horizontal bed unit. The former was applied in the evaluation of filter performance (filter cake formation, regeneration and filter efficiency) during continuous operation, while the latter was used to evaluate the filter cake formation upon a free horizontal surface of sand.

A rotating brush particle dispenser described in the German standard VDI 3491 was used to redisperse the various test dusts.

A schematic presentation of these test units is given below.

3.2.1 Transparent test-unit for louver evaluations, The Puff-Back Unit.

A simplified drawing of the test unit is shown in Figure 3.5. A solenoid valve connected to a pressure vessel generated the cleaning pulse. The vessel was filled with pressurised air through the first electric valve, and subsequently released through the solenoid valve (off-line cleaning). The electric valve was closed during release of the pressure pulse. A cone (inclusive angle 16° vertical and 10° horizontal) preserves the uniformity of the shock wave as the cross section increases. The test section consists of two layers of granular material with replaceable louvers in front (i.e. comparable to the commercial filter element of Folla design). To enable visual inspection, and minimise the influence of wall friction, one of the sidewalls was made out of glass. The replaceable louver rack is 80 mm wide, and 64 mm high. The unit is mounted onto a stand and vibrations are absorbed through leaf springs.

The louver-rack typically consisted of three louvers, defining two flow channels / sand surfaces. Only the uppermost channel was used for performance evaluation, due to reduced edge effects.

3.2.2 The small scale Panel Bed Filter, transparent unit.

The transparent unit was used to evaluate the effects of scale up (from the Puff-back unit) upon the bed stability and uniformity of sand spill. The exchangeable filter section is made out of plexi glass and has a filtration area 80 mm wide and about 300 mm high. Its flexible design allowed replacement of front louvers, comparison of coarse-sand box vs. a set of back-louvers and effect of bed thickness. The scale of this unit is the same as the first set-up introduced by Lee (1975).

Compressed air at about 0.7 MPa passes through a filter (FL01), removing moisture and oil from the air. Dry air passes a reduction valve and the volume flow rate is controlled by a rotameter. Both the inlet and outlet section is horizontally arranged (tapered steel cones with rectangular cross-section, inclusive angle 30° vertical and 6° horizontal).

The transducer data were taken with piezoelectric differential pressure transducers (Kulite XTE 190, 0.35 bar differential). The pressure difference between the clean side pressure and the pressure in the laboratory is used to analyse the data.

The applied front louvers results in an upward directed gas flow through the filter bed. This can lead to locally high gas velocities at the uppermost back louver. A vertical upward displacement of the back louvers can compensate for this effect and enhance filter stability.

The limiting filtration velocity ($U_{S,max}$) was determined by provoking bed destabilisation. Three characteristic velocities were defined: *i*) first bed movement, *ii*) first grain entrained and *iii*) continuous sand spill. The experimental set-up is shown in Figure 3.6.

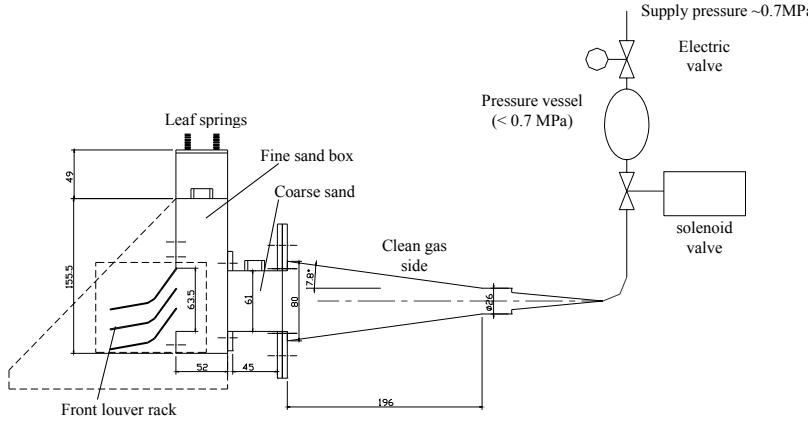

Figure 3.5: Transparent test-unit for evaluation of the pressure pulse induced motion of granular media between to adjacent louvers. Developed in co-operation with A. M. Squires, Professor at Virginia Polytechnic Institute & State University.

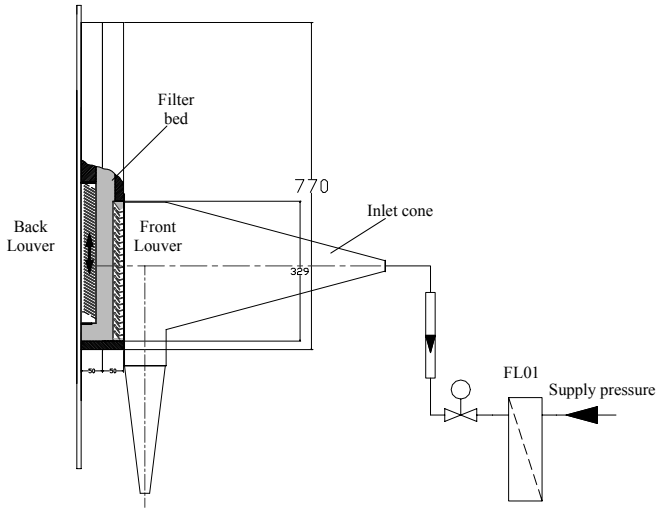

Figure 3.6: Experimental set up for the bed stability tests conducted in the transparent test unit. Compressed air at about 7 bar passes through a filter (FL01), removing moisture and oil from the air. Dry air passes a reduction valve and the volume flow rate is controlled by a rotameter.

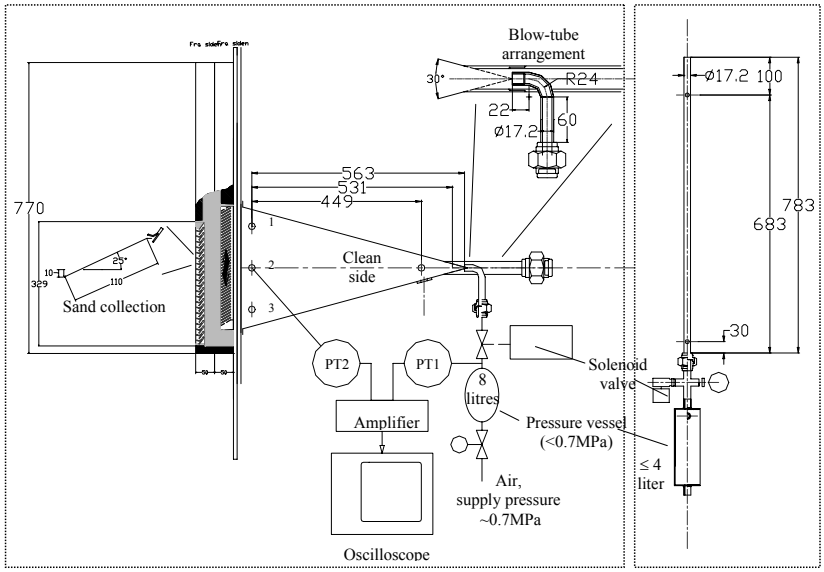

a) b)

Figure 3.7: a) Transparent test unit used for the characterisation of puff-back uniformity and the influence of the pressure pulse generation. (Method for sand collection is indicated on the drawing.) b) Vertical test tube used to characterise the pressure system/valve.

All uniformity tests were conducted as off-line pulsing with side shot puff-back (Figure 3.7). The connection between the pressure vessel and the air supply was open during pressure pulse generation. Uniformity of the pressure-pulse was checked by a series of simultaneous pressure pulse measurements between two out of the three pressure taps: top, middle and bottom of the panel bed louver area (Rudberg 2000). No difference could be seen between the different locations. The pressure data used in the evaluation of the sand spill distribution were all taken at the middle point of the panel bed louver area (position 2).

A special sand collection unit was build in order to enable a detailed analysis of the sand spill distribution. And the sand removed upon puff-back was collected from all louvers separately, but simultaneously. The sand from each louver was carefully measured and displayed as fraction of the total sand spill.

The cause of puff-back sand spill is due to the pressure drop across the bed. Typical data on side shot puff-back as used in this study is shown in Figure 3.8: a) the pressure pulse measured just behind the filter bed and b) the pressure decay in the puff-back bottle. Comparing the pressure pulse generated in the vertical pipeline, and the pulse measured just before the filter bed clearly shows the damping of the pulse, introduced by the large volume in the outlet section. Thus, resulting in a less sharp pressure rise (also observed by Lee (1975)).

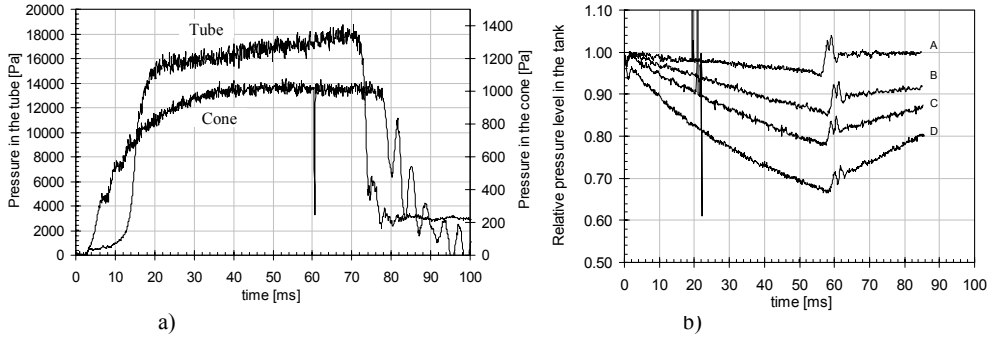

Figure 3.8: a) comparison of a pressure pulse generated in the vertical tube and a pressure pulse measured just behind the filter. b) Relative pressure level as function of tank volume. (Pressure tank volume for case A, B, C and D is 4, 2, 1 and 0.5 litres respectively.)

3.2.3 Cylindrical fluidised bed

The fluidised bed (inner diameter = 0.085 m and 0.215 m) set up was as indicated in Figure 3.9. Distance between inlet cone and filter is about two times the filter diameter. The experiments were conducted with the bed materials as described above. Pressurised air was supplied through a reduction valve and volume flow rate adjusted in a rotameter. 20 and 40 mm bed heights were used.

Bed collapse was studied by gradually increasing the superficial velocity until fluidisation occurred. The interpretation of these tests is based on the identification of the limiting velocity ($U_{s,max}$) which has 3 characteristic values: i) the first bed movement (local fluidisation of a few grains), ii) the first bubble and iii) continuous bubbling.

The various bed materials investigated are described in section 3.2.6.

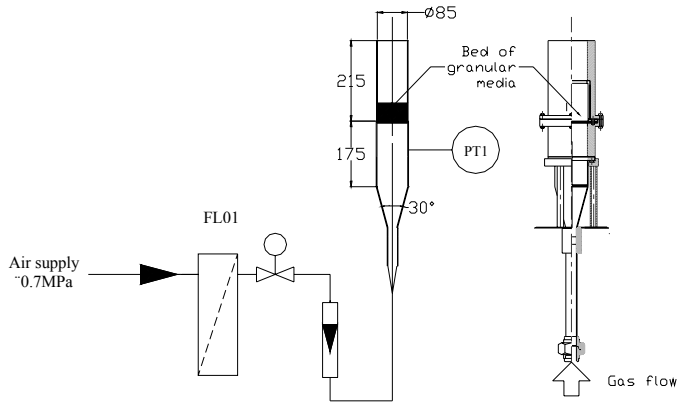

Figure 3.9: Circular fluidised bed used for determining fluidisation velocities. Compressed air at about 7 bar passes through a filter (FL01), removing moisture and oil from the air. Dry air passes a reduction valve and the volume flow rate is controlled by a rotameter.

3.2.4 High temperature Panel Bed Filter Unit

The design of the laboratory scale high temperature filter unit is shown in Figure 3.10. Compressed air at about 0.7 MPa passes through Domnick Hunter filters FL01-FL03. The first filter removes moisture and oil from the air while FL02 and FL03 remove coarse and fine particles respectively. Dry air leaving the last filter enters the pressure reduction valve at the particle dispenser inlet. The air carries the dispersed particles through the horizontal raw gas channel (d_i 8 mm, length about 2300 mm) and into the test unit. Both the inlet and outlet section is horizontally arranged (tapered cones with rectangular cross-section, inclusive angle 30° vertical and 6° horizontal). The exchangeable filter section has a filtration area 80 mm wide and about 300 mm high. Figure 3.11 shows the filter section with wishbone and L10-56 louvers installed (louver inlet and outlet section inclined 56° and declined 10° respectively). A rotating brush particle dispenser of type RBG 2000 (Palas gmbh) ensures constant feed rate (0.04-400 g/h) and good dispersion.

The cleaning system comprise a pressure tank (8 l and less than 0.7 MPa), a diaphragm valve that generates the pressure pulse (duration typically < 100 ms) and a ¾'' blow tube with an exchangeable nozzle. The spent solid was collected from the bottom of the collection bin (in the dirty side of the panel bed) through a ball valve. The bed material was separated from the dust by regeneration in a high efficiency separator (delivered by TelTek). The particle size distribution is given in Figure 3.13.

A total filter (ø 225 mm) is installed down-stream of the outlet section for the gravimetric determination of the dust concentration in the clean gas. The total filtration efficiency is determined by amount of dust collected on the total filter and the amount of dust fed to the test section during the test period.

The gas was cooled in a water-cooled steel condenser before entering the volume flow control and measurement system, which consists of a reduction valve and a critical nozzle (ø5 mm) installed upstream of the blower. The volume flow rate and raw gas concentration is kept constant throughout the filtration cycle.

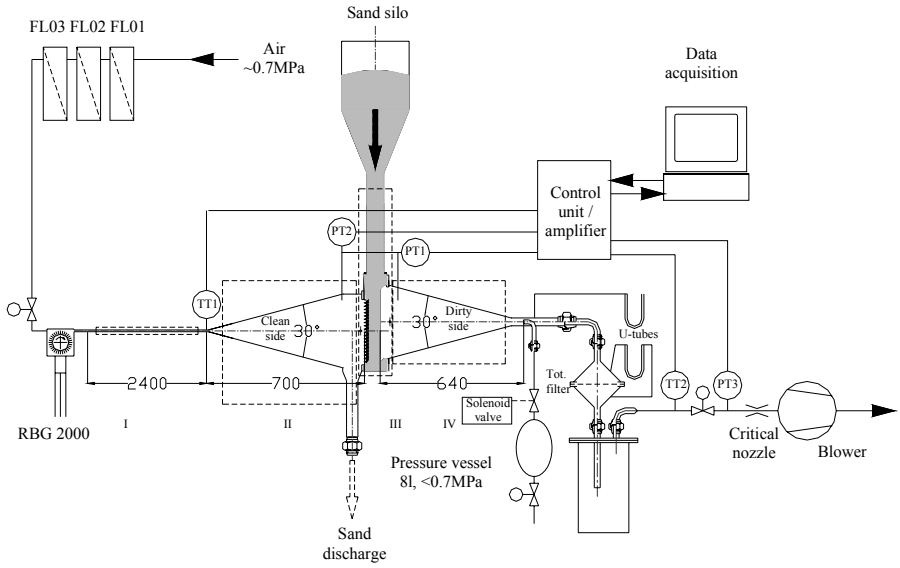

Figure 3.10: High temperature panel bed filter, layout and instrumentation.

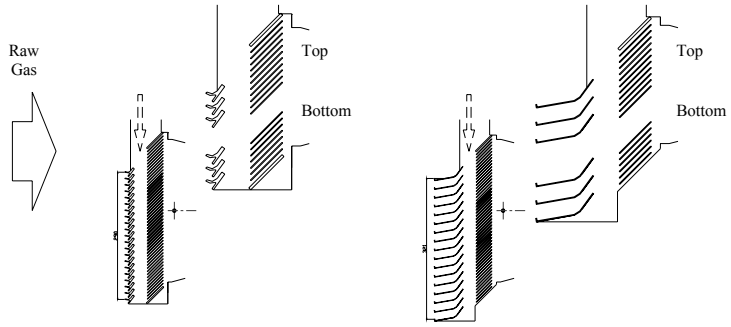

a) b)

Figure 3.11: High temperature filter unit, illustration of the vertical displacement of the back louvers: installation of a) the wishbone and b) the L10-56 louver. The dotted arrows indicate where sand enters the filter bed.

The maximum differential pressure at which the filter is cleaned has been chosen as either 1000 Pa above the clean filter pressure drop, or a total pressure drop of 2000 Pa. The differential pressure is recorded continuously.

Signals used to evaluate the filter operation includes: pressure difference between the dirty and clean gas sides of the filter (PT1); the relative pressure in the test section (PT2); volume flow (absolute pressure (PT3) at the inlet of a critical nozzle installed downstream of the filter); and the temperature at the inlet of the test section (TT1).

The heating system is divided into four zones: i) raw gas channel (heating element of about 1800 mm), ii) inlet cone, iii) filter section and iv) outlet cone. All zones ii-iv is kept isothermal at the desired filtration temperature. While the measured raw gas temperature (TT1) is used to regulate zone i (set point equal to the desired filtration temperature).

3.2.5 The horizontal bed filter.

Figure 3.12 is a schematic diagram of the experimental set up, which we have developed, based on a similar unit operated by Lee et al. (1977). Compressed air at about 0.7 MPa passes through Domnick Hunter filters FL01-FL03. The first filter removes moisture and oil from the air while FL02 and FL03 remove coarse and fine particles respectively. Dry air leaving the last filter enters the pressure reduction valve at the particle dispenser inlet. The air carries the applied dust through a vertical tube (d_i = 6 mm and about 2300 mm long) before it enters the test section. A back-up filter was placed directly beneath the filter (ø 142 mm).

Tapered entrance and exit sections precede and follow the sand bed that is retained on a wire screen. The internal angle of the upper tapered section was about 6°, while 15° was applied in the outlet section. The objective of the tapered section is to provide for deceleration and acceleration of gas flowing to and from the sand bed with reduced loss of dust particles by deposition on the walls of the gas passages.

The sand bed (ø 85 mm) rests inside a glass tube and upon a wire mesh. The tube sits inside a metal sleeve in which there are three rectangular windows for viewing the bed and fly as deposits on the bed. The sleeve forms a continuous metal structure together with the tapered inlet and exit sections. The glass tube is held in place by gasket material.

The volume flow control and measurement system consisted of a reduction valve and a calibrated nozzle (ø 5 mm) installed upstream of the blower. The volume flow rate and raw gas concentration is kept constant throughout the complete filtration cycle.

A rotating brush particle dispenser of type RBG 2000 (Palas gmbh) ensures constant feed rate (0.04-400 g/h) and good dispersion.

The following signals were recorded continuously, and used to evaluate the filter operation: The relative pressure just above the filter surface (PT1); the pressure difference between the dirty and clean gas sides of the filter (PT2); the volume flow (calculated based on the absolute pressure (PT3) at the nozzle inlet); and the temperature measured just beneath the wire-mesh (TT1).

The heating system consisted of three separate heating elements (Figure 3.13): i) the vertical pipeline, ii) the inlet cone and iii) the test section. The heating elements were placed concentric around each part of the system. Thus, heat transfer was accomplished through natural convection and radiation (no direct contact between heating elements and filter unit). All heating elements were used during the pre-

heating of the system. While the element surrounding the test section was switched off during filtration. (This heating element is shaped as a coil and generates a significant electromagnetic field at the filter). The filtration temperature was maintained by regulating element i via TT1 and manually adjusting element ii. TT1 was kept isothermal at the desired filtration temperature.

The main difficulties experienced in the operation of this filter unit were to establish a homogeneous sand bed. Therefore, the filter bed was partly fluidised prior to each experiment, in an attempt to get uniform bed porosity. However the sand surface was slightly concave upward, i.e., the bed was slightly deeper at the circumference than at the centre. Furthermore, the initial feeding rate was difficult to control, and tended to be slightly discontinuous during the first minute of operation (these problems were also discussed by Lee (1975) and Lee et al. (1977)).

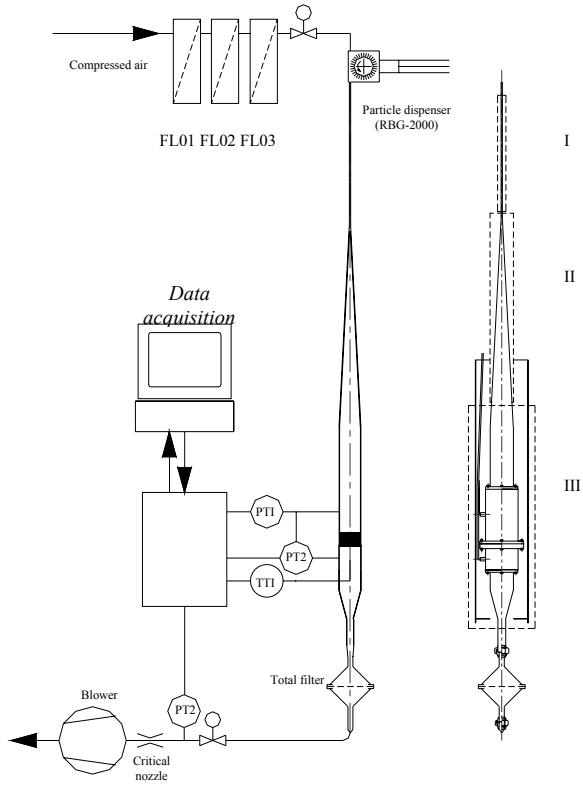

Figure 3.12: Experimental set-up: Deposition of standard dust qualities upon a horizontal free surface of sand. The different heating sections are indicated in the right figure.

3.2.6 Characterisation of the bed materials applied in this study

Parameters as size distribution, bulk density, angularity, angle of repose and hardness all significantly influence the filter operability through bed stability, louver performance and filter efficiency. The size distribution and corresponding specific densities for the granular media used in this work is given in Figure 3.13.

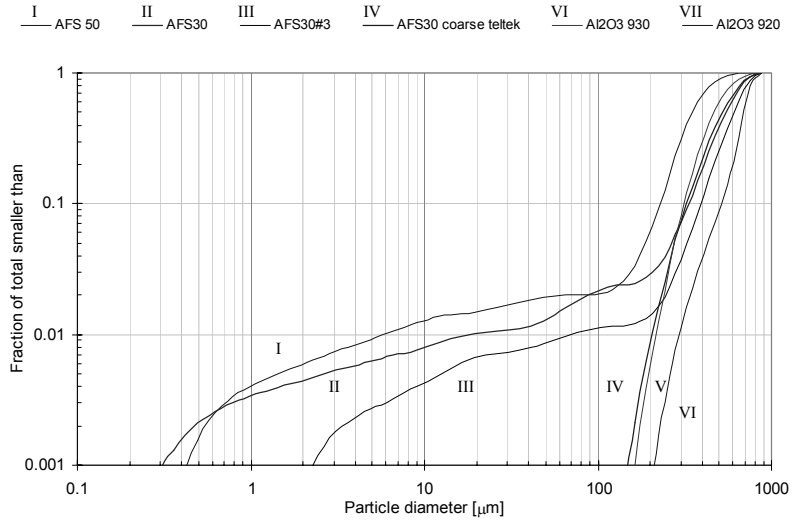

Figure 3.13: Particle size distributions for the different bed materials used in this study. Specific densities: Olivin sand (AFS) about 3400 kg/m^3; Aluminium oxide (Al_2O_3, from North Alcoa) about 3500 kg/m^3.

3.2.7 Experiments

The following sections presents the data derived from the various experiments conducted in connection to the filter design evaluations. The experimental data derived from the filter bed stability evaluations are reported first (in Section 3.3). Followed by the louver geometry evaluations and puff-back uniformity tests (3.4) and finally the filtration experiments (3.5). The latter section is divided into the following sub-sections: description of the applied dust qualities (3.5.1), the test matrix (3.5.2), panel bed filtration data (3.5.3) and deposition of dust upon a free horizontal surface of sand (3.5.4). Summary and conclusions is given in Section 3.6.

3.3 Filter bed stability

Replacing the coarse sandbox with a rack of louvers introduces the need of defining a maximum filtration velocity, as velocity fluctuations and uneven velocity profiles can lead to local fluidisation and entrainment of bed material into the clean gas duct.

The limiting filtration velocity ($U_{S,max}$) was determined by provoking bed destabilisation in the small-scale PBF units (Section 3.3.1). Three characteristic velocities were defined: *i*) first bed movement, *ii*) first entrainment and *iii*) continuos sand spill. Additional experiments were conducted in order to relate these velocities to fluidisation mechanisms (Section 3.3.2).

3.3.1 Stability tests in the small scale PBF units

Both the Wishbone and L10-56 louver results in an upward directed flow through the filter bed, resulting in local high velocities at the uppermost back louvers. A vertical displacement of the back-rack was therefore necessary to obtain an even flow distribution across the back louvers.

Most of the experiments were conducted in the transparent unit, experimental arrangement as illustrated in Figure 3.6, using AFS30#3 as filter bed material. The relative position of the back louver-rack was adjustable and vertical displacement of up to 80 mm was tested. Zero and four cm displacement results in the relative positions as shown in Figure 3.14. The superficial velocity and differential pressure as measured when the first sand grain was entrained out of the bed is presented in Figure 3.15a and b. The latter figure also includes arrows indicating the effect of the vertical displacement. These experiments shows that it is possible to minimise the top effect and create a more uniform velocity distribution across the outlet, recognised through a more uniform fluidisation over the back louvers. And thereby obtain a significant increase in the maximum filtration velocity before destabilisation occurs. The results indicate an optimum displacement of about 40 mm.

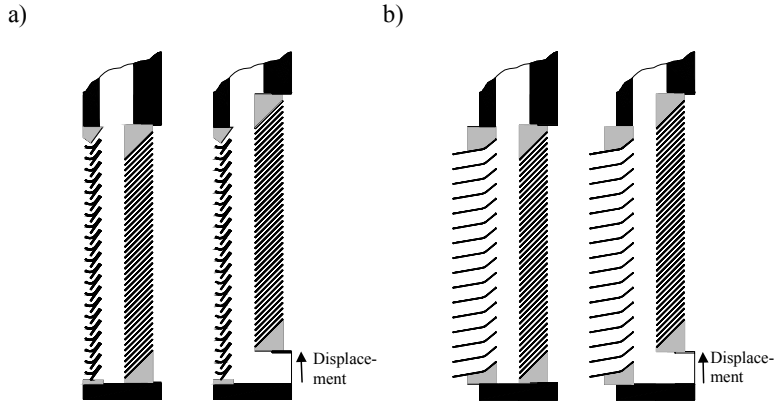

Figure 3.14: Transparent test unit: Relative position of front vs. back-rack for zero and four cm displacement. a) Wishbone and b) L10-40

a)

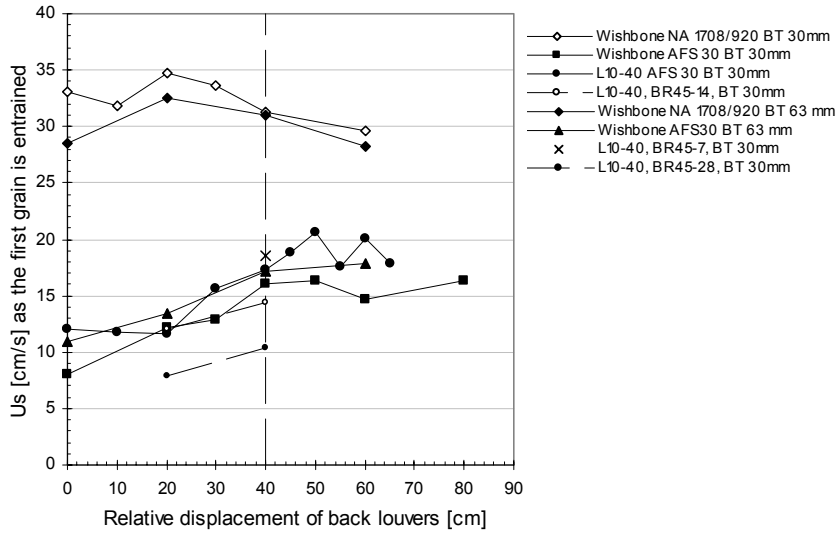

b)

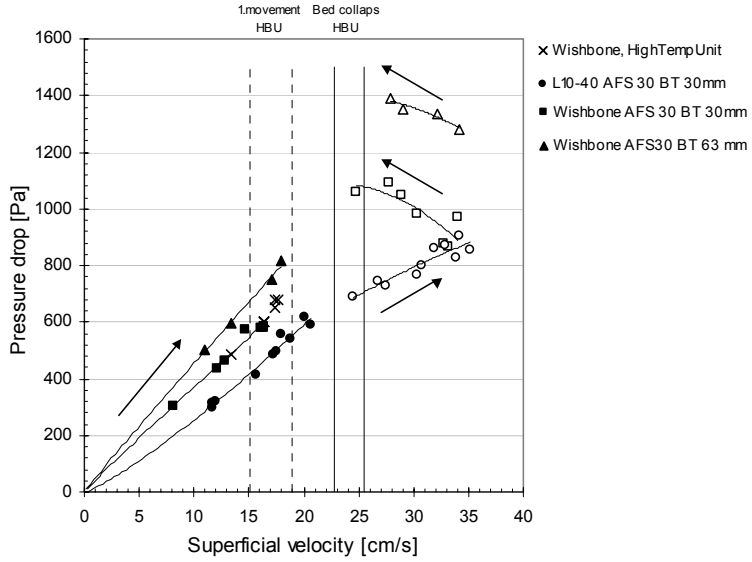

Figure 3.15: Effect of relative displacement of back vs. front louvers (Wishbone and L10-40) upon bed destabilisation. a) The superficial velocity at which the first grain is entrained from the filter bed increased upon elevation of the back louvers. b) Superficial velocity vs. pressure drop for the different configurations. (The arrows indicate the effect of increasing the vertical displacement of the back louvers upon both pressure drop and limiting filtration velocity ($U_{s,max}$). The velocity ranges indicated for 1. bed movement and bed collaps corresponds to the experiments conducted in the the cylindrical fluidised bed.

Despite the improved uniformity in the flow, the sand spill tended to be dominant in the upper part of the louver area. This might be due to higher bed porosity at the topmost louvers resulting in higher gas velocities within this region.

Increasing the distance between the front and back louvers (i.e. the filter bed thickness, BT) from 30 to 63 mm (Figure 3.15a and b) resulted in a higher pressure loss. However, no significant increase was measured in $U_{S,max}$. Applying the more open L10-40 louver geometry (identical to the L10-56 louver except that the back part is inclined 40° as in the R-2 design) raised the upper stability limit by approximately 30%, as compared to the Wishbone louver. Furthermore, decreasing the back louver pitch also lead to a significant increase in $U_{S,max}$. The different back louver configurations are denoted as BR 45-7, BR 45-14 and BR 45-28 for 7, 14 and 28 mm pitch respectively. BR 45 indicates that the louvers in the back rack were inclined 45°, the louvers were 25 mm long. Increased porosity at the interface between the filter media and the louver surface is assumed to contribute to the observed stability increase, as well as the more uniform sand surface towards the clean air side. (Note the transition region between first entrainment and continuous sand spill, Figure 3.15b.)

Additional tests has been conducted with an alternative bed material, consisting of Al_2O_3 rich and close to spherical particles (Norton Alcoa Proppants, NA 1780/920, $X_{50,3}$ about 700 microns). Similar particles have been used in earlier filtration studies conducted by Engebretsen (1984). This material has a narrower particle size distribution, slightly higher specific density and larger particle diameter than the applied sand quality. A twofold increase in $U_{s,max}$ was observed, and the dependency of the vertical displacement of the back-rack significantly decreased. Actually, by increasing the vertical displacement to above some 20 mm resulted in decreased $U_{s,max}$. Using a bed thickness of 30 or 63 mm had no significant effect upon $U_{s,max}$.

Bed destabilisation was suppressed in the high temperature unit by applying a combination of vertical displacement and increased height of the clean air side louver section, se illustration in Figure 3.11. (The height of the dirty and clean side louver sections were practically identical for the transparent test unit used in the stability tests.) A stability test conducted in the high temperature unit, wishbone configuration, is included in Figure 3.15b. A maximum in the limiting filtration velocity ($U_{s,max}$) of about 17 cm/s corresponds well with the earlier findings from the transparent unit.

3.3.2 Fluidisation velocity determination (the cylindrical fluidised bed)

The stability tests in the transparent test unit were compared to fluidisation tests conducted in the cylindrical fluidised bed, described in section 3.2.3. The fluidisation tests include both 2 and 4 cm bed thickness. And each of the bed materials described in section 3.2.6 was used.

Increasing the bed thickness had only minor influence upon the fluidisation velocity. The initial tests were conducted with AFS30#3 (fine fraction removed) as to obtain a point of reference to the tests conducted in the transparent unit. Resulting velocities for the first bubble and continuous bubbling are included Figure 3.15b. The scattering seen in the experimental data is reflected in the depicted velocity range. These velocities correspond very well to the maximum values found for the limiting

filtration velocity ($U_{s,max}$) defining first entrainment and continuous sand spill in the transparent test unit.

3.4 Puff-back experimental data.

The objective of this part is to develop a new louver design, incorporating larger sand surface area and efficient regeneration (i.e. uniform sand spill). Thus, characterise the influence of pressure pulse shape and intensity vs. total amount of sand spill and spill uniformity.

Section 3.4.1 discusses the characteristic features of the louver geometry and the development of a novel louver design through tests in the puff back unit. Section 3.4.2 discusses the puff-back uniformity tests conducted in the transparent panel bed filter. The uniformity was quantified by weighing the sand spill from each louver. The obtained results were verified in the high temperature filter unit prior to start-up of the filtration experiments. The bed stability evaluations (maximum filter load before bed collapse) is discussed in Section 3.4.3

3.4.1 Development of an alternative louver geometry

The main criteria for this development have been defined as: i) reduced number of louvers (increased pitch) , ii) enhanced exposed sand surface area and iii) simplified geometry. Thus, increasing filter capacity thorough enhanced mass load and increased cycle duration.

A digital video camera and the transparent Puff-Back unit was used in studying the relationship between louver geometry and the characteristics of the pressure pulse induced sand motion between two adjacent louvers. Sand (Olivin Afs50) was used as filter bed material during these tests. The sand motion was clarified by the addition of coloured sand. (The olivine sand change colour from grey to brown when heated up to about 700 °C)

In order to enable detailed analysis of the sand movement all the tests were videotaped. Both pictures and short movies were made. The short movie files gave good information on the shock-wave propagation and the sand movement. How many puff-backs needed to replace the sand resting upon one louver is dependent on the length and free surface of the louver. Even though the wall effects are reduced the movement near the wall is slower than in the middle of the louver. The pictures are therefore only giving a qualitative and not quantitative idea of the sand movement. To verify that there are no significant end-effects that affect the puff-back in the studied louver duct, additional tests were also made in a rack containing five louvers (four ducts).

Figure 3.16 illustrates some characteristic features for the louver geometry development. The louvers are designed so that the angle of the louver opening should be less than the angle of repose of sand. The angle of repose for sand ranges from 30-35° and depends on the sand properties. Lee applied 27° for the angle of the louver opening (Wishbone), while about 30° was used for the novel L10-56 louver design.

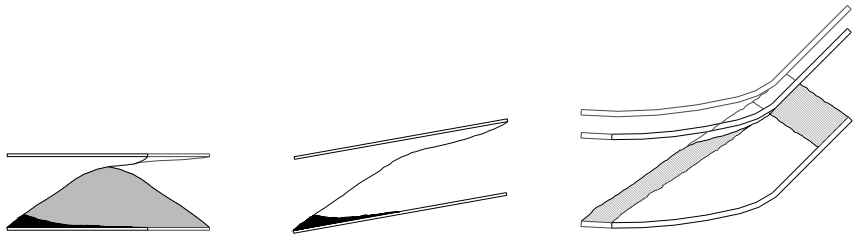

a) b) c)

Figure 3.16: Characteristic features of some simple louver geometries a) the horizontal plate b) the inclined plate and c) the R-2 louver. The gray lines indicate the maximum configuration, i.e. the maximum pitch possible before de-stabilisation. Shaded area illustrates the effect of decreasing the louver pitch.

When stabilised between two adjacent louvers, the granular material defines an inclined surface at an angle equal to or larger than the angle of repose. Thereby defining the maximum ratio between filter face and the exposed sand surface. The simplest design tested consisted of an array of horizontal plates (Figure 3.16a). An inclined louver (Figure 3.16b, inclined 10°) was introduced in order to enlarge the surface area even further. However, the puff-back experiments revealed the build up of a stagnant zone at the louver tip and a small gap was formed between the upper louver and the granular material.

Furthermore, a significant downward motion of bed material follows the discharge of bed material (Figure 3.1d). This is especially pronounced behind the uppermost louvers in a full-scale (3500 mm high) filter element. Thus, ensuring a stable sand front is important in order to eliminate transportation of dust into the filter bed.

These problems were minimised by the R-2 design (Figure 3.16c). Where the sand front is stabilised by inclining the back end 40°, slightly more than the angle of repose, and the dead end zone minimised by introducing the elliptic front part. To ease the manufacturing of the louver a simpler geometry was developed, the L10-56 louver (Figure 3.17a). This louver is a combination of the inclined louver and the R-2 louver. However, the initial 40°angle of the back end was increased to about 56° (same as for the wishbone louver).

Figure 3.17 gives a comparison of the Wishbone design as developed by Lee et al. (1977), the Folla louver (applied in the tests reported in Chapter 2, Paper I) and the novel R-2 and L10-56 louvers. A picture of the latter louver installed into the Puff-Back unit is also included.

Figure 3.17b shows that there is an air slit between the filter bed material and the uppermost louver, just after the bend (also seen in Figure 3.16), this slit can be minimized by shortening the foremost part of the lover (inclined 10°). However, instabilities might be introduced and even the smallest inaccuracy in the manufacturing could lead to adverse sand leakage. Thus, optimum louver length is related to the stability, e.g. the angularity, of the bed material.

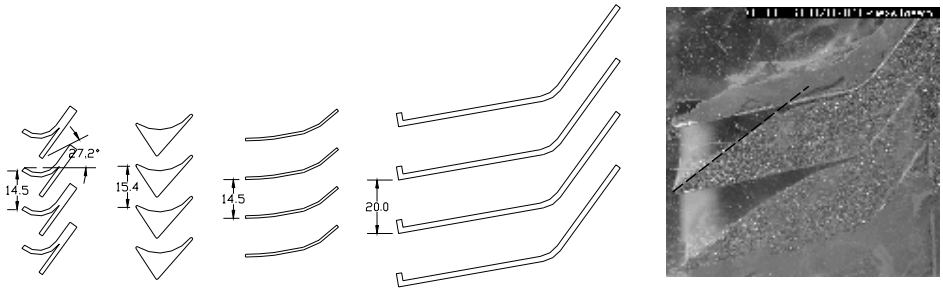

a) b)

Figure 3.17: a) Comparison of (from left to right) the Wishbone, Folla, R-2 and L10-56 louver b) Picture of the L10-56 louver installed into the transparent Puff-Back Unit. Developed in co-operation with A. M. Squires, Professor at Virginia Polytechnic Institute & State University

3.4.2 Puff-back uniformity tests

The initial puff-back test series were conducted in the small-scale transparent panel bed filter with a coarse sand box instead of back louvers. The coarse sand box was utilised in order to establish a point of reference towards the work conducted by Lee (1975) and Lee et al. (1977) and the commercial Folla design. Choosing the coarse sand box as a reference also eliminates additional effects imposed by the back louvers. However, verification of sand spill uniformity as conducted in the high temperature filter unit includes the effect of a set of back louvers (50 mm steel plates inclined 45° and arranged with a pitch of 7 mm).

The test unit used for the characterisation of puff-back uniformity and the influence of the pressure pulse generation is shown in Figure 3.7. The reported sand spill uniformity tests include Wishbone, Folla and L10-56 front louvers.

In order to obtain a uniform sand spill the pressure rise time on the clean side should be as fast as possible. This can be done by increasing the tank pressure, puff-back valve orifice area, increasing the valve opening rate, and decreasing flow resistance between the puff back tank and filter. In the present study puff-back intensity and duration is controlled by tank pressure and the valve opening time. (The tank volume was chosen to be 8 litres in order to obtain a close to constant pressure within the pressure vessel. The applied pressure valve was a FESTO CPE14 in all experiments except experiment number 220101#11, where a larger valve was used (FESTO CPE24).)

The range of pulse shapes utilised in this study is shown in Figure 3.18a (measured just behind the back louvers, PT1, Figure 3.10). The pulse duration was less than 100 ms in all tests and applied puff-back tank pressure varied between 0.3 and 0.6 MPa. The objective behind using such a variety of pulse shapes was to investigate whether this influenced upon puff-back uniformity.

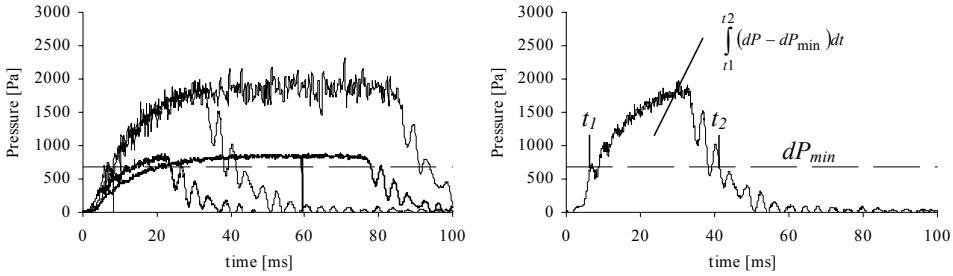

a) b)

Figure 3.18: a) Typical cleaning pulses as measured just behind the coarse sand box. b) Derivation of the specific impulse [Pa s] (dP_{min} – estimated threshold value)

Figure 3.19 gives the resulting uniformity profiles as derived for a) the Folla, b) and c) the Wishbone and d) the L10-56 louver. a), b) and d) was conducted with a coarse sand box, while c) and e) was conducted in the high temperature unit. The high temperature unit incorporated back louvers 50 mm long, inclined 45° and with a pitch of 7 mm.

Sand spill uniformity is found to be relatively independent of pressure pulse generation (i.e. intensity and shape). The Folla louver, Figure 3.19a, typically shows a decreasing sand spill for the uppermost louvers. The initial tests with the Wishbone louver, Figure 3.19b was conducted on the louvers used by Engebretsen (1984) and reveals a significant variation between the different louvers. This variation was found to be louver specific, i.e. the variations followed the louvers as their location was changed. The correlation between louver dimension "C" and the resulting uniformity profile is included in Figure 3.19b. Based upon these results a new set of louvers was made, Figure 3.19c. This louver was only tested in the high temperature unit and shows a clear tendency to give highest sand spill at the top and bottom of the louver area. The relatively large sand spill at the top and bottom of the louver rack might be attributed to the slightly larger cross section across the back louvers compared to the front louver area (see Figure 3.11). Figure 3.19d illustrates the sensitivity of the L10-56 louver geometry upon sand spill uniformity as the peak value for louver number 5 shifts to louver space number 10 as these to louvers change position (as seen for the old Wishbone louver). Figure 3.19e shows the result obtained with the high temperature filter unit. This latter profile represents the most uniform profile obtained, regardless of louver design. It should be noted that only a very limited number of uniformity test was conducted for this louver after installation in the high temperature filter.

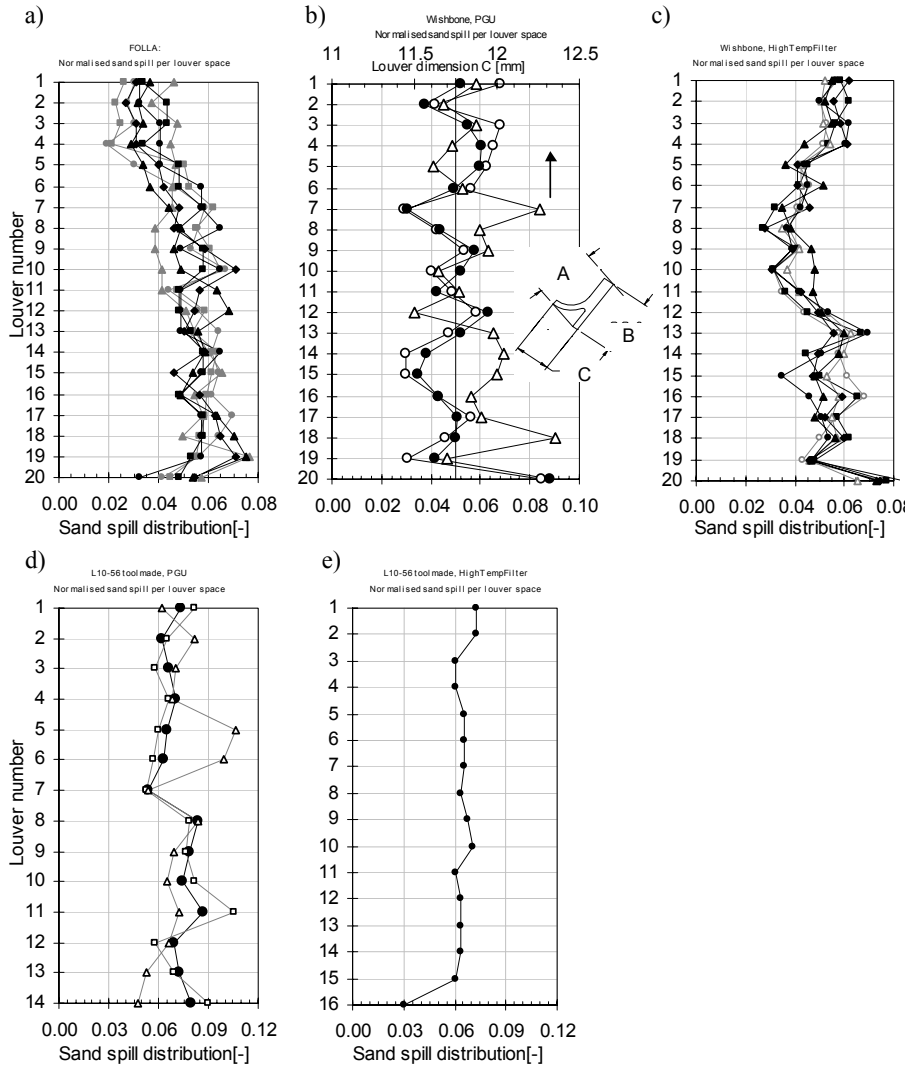

Figure 3.19: Sand-spill uniformity test. a) Folla, b) & c) Wishbone and d) & e) L10-56. (The normalised sand spill is calculated as the amount of sand collected from one louver over the total amount of sand discharged upon puff-back.)

The present work support the theory of a threshold value, and estimated values (Table 3.1) is found to be in the range 500-900 Pa, and fairly independent on the filter configuration. The correlation towards the active time is questionable. However, a strong correlation was found between the average of the normalised sand spill and the resultant of the specific impulse (Figure 3.20):

$$\int_{t1}^{t2}(dP - dP_{\min})dt \qquad (3.1)$$

Where $t_1 - t_2$ denotes the time at which the pressure exceeds and falls below the defined failure pressure (dP_{min}). It is interesting to note that this dP_{min} corresponds quite well to the transitional region determined during the stability tests (discussed in Section 3.3).

Figure 3.20b also includes correlations extracted from Lee (1975) (solid lines – downshot, dashed lines – sideshot). Note that the sandspill decreases with increasing particle diameter, for the same active time.

Despite a skilled operator and accurate handling of the equipment some scattering in the experimental data is to be expected. However, reproducibility in the different set-ups was high. Figure 3.21 shows that the standard deviation of the normalized sand spill vs. specific sand spill for the different configurations is roughly constant and between 0.010 and 0.015. (The specific sand spill is calculated as the amount of bed material discharged from one louver vs. the total amount of discharged upon the same puff-back.) Wishbone/Cs clearly deviates from the others. This is primarily due to very low reproducibility in the louver design, as discussed in connection with Figure 3.19b.

Table 3.1: Comparison of sand spill ranges, active time and threshold value for the different configurations.

		Sandspill		dtactive	
	Terskelverdi	max	min	max	min
Louvertype	[Pa]	[g/cm^2]	[g/cm^2]	[ms]	[ms]
Folla/Cs	800	0.98	0.10	78	31
Wishbone PBF/Br	670	0.50	0.04	58	19
Wishbone/Cs, AFS 30:	900	1.10	0.16	82	25
L10-56 toolmade/Cs	750	1.42	0.34	52	37
L10-56 toolmade/Ny-rigg PBF, AFS 30:	500				

Note: The sand spill is calculated versus the exposed gas entry surface (approximate value).

a)

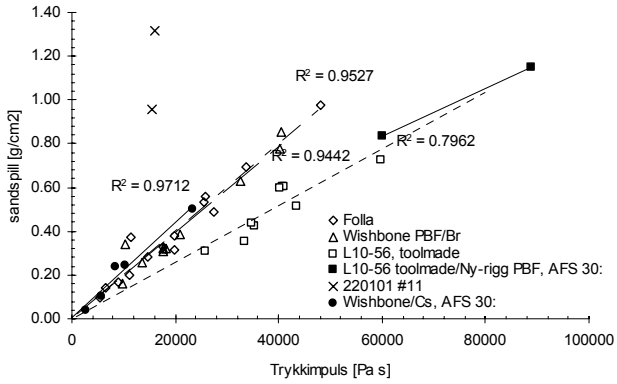

b)

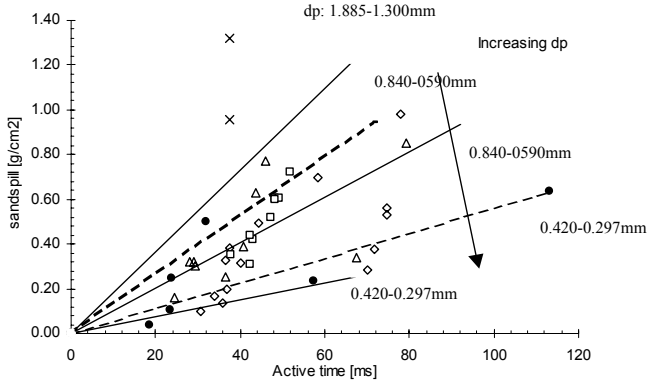

Figure 3.20: Sand spill correlation: average normalised sand-spill vs.: a) Pressure impulse [Pa·s] and b) active time [ms]. (Calculated vs. the exposed sand surface area, approximate values.) The arrow in b) indicates the effect of an increased threshold value (dP_{min}). Correlations extracted from Lee (1975) (solid lines – downshot, dashed lines – sideshot) shows decreasing sand spill with increasing particle diameter.

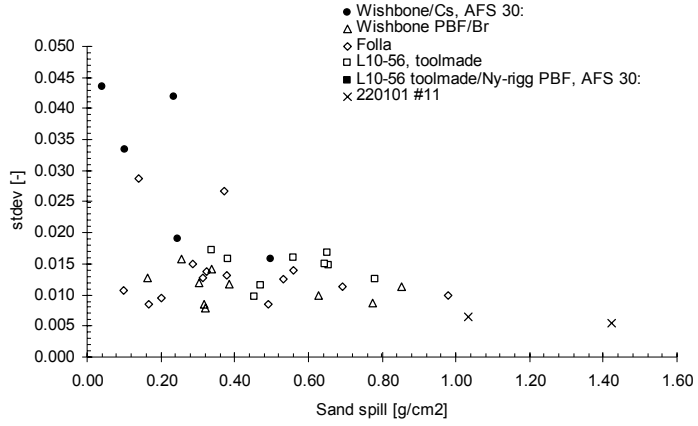

Figure 3.21: Standard deviations calculated for the specific sand spill. (Calculated vs. the exposed sand surface area, approximate values.)

3.5 Filtration experiments

In addition to the characteristics of the granular filter media (e.g. size distribution, angularity and specific weight) both dust quality as well as operation conditions (e.g. superficial velocity, defined maximum pressure loss and the efficiency of filter regeneration) all significantly affects filter operation. The main focus of this section has been to evaluate the Panel Bed Filter stability at typical field operation conditions and compare the observed performance with state of the art within alternative filter technologies operating in surface filtration mode.

All experiments has been conducted at about 200 °C, in two different test units and on two different front louver geometries. Superficial filtration velocities ranged from 4 to 20 cm/s. Four dust qualities, raw dust concentration ranging from 1 to 11 g/m^3, and one sand quality (AFS30, fine fraction removed in a high efficiency separator prior to the experiments) has been used in these experiments. A more detailed description of the dust qualities and bed material utilized in this study is given in section 3.5.1.

More than 140 hours of accumulated filtration experience is documented.

3.5.1 Use of standard dust qualities

In total four standard dust qualities have been used in order to characterise the high temperature filter units. Three of these dusts have been found in the German VDI-3926 standard: two high purity aluminium oxides supplied by Condea Chemie gmbh (Pural NF, $X_{50,3}$ = 18.3 μm; Pural SB, $X_{50,3}$ = 74.9 μm) and Micro-calcilin supplied by LTG gmbh ($CaCO_3$, estimated particle diameter from the supplier: $X_{50,3}$ = 3.8 μm), the last dust quality is the SAE-fine test dust (ISO 12103-1, $X_{50,3}$ = 12.6 μm; 68-76wt% SiO_2 and 10-15wt% Al_2O_3). The mean particle diameters as indicated are obtained by laser diffraction analysis (in a Malvern analyser) on particles suspended in water.

These particle measurements and the loose bulk and compact bulk densities of the various dusts are included in Table 3.2. Loose and compact bulk densities are measured as the dust is loaded into the piston reservoir, without compaction and in small increments with compaction. The particle sizes and bulk densities as given by the supplier are given for comparison. The accumulative size distribution (volume basis) for the various dusts and the applied filter bed material is included in Figure 3.22.

Both micro-calcilin, PuralNF and SAE-fine had very much the same compression effects, and appeared visually similar. However, PuralNF gave some problems in the particle feeder, and caused complete blocking of the particle feeder when operated with top-cover type A. Stable operation was obtained with top-cover type B installed. Pural SB is typically free flowing and did not cause any problems in the particle feeder, but it has a relatively large particle diameter.

Table 3.2: Key parameters for the tested dust qualities

	SAE PTI standard12103-1	Pural NF	Pural SB	$CaCO_3$	Fly-ash Folla
Particle size measurements*					
$X_{50,3}$	12.6	18.3	74.9		31.7
$X_{95,3}$	41.1	37.1	110.9		102.8
as received from supplyer					
$X_{50,3}$	9****	5.5***	45***,**	3.8	
Density measurements:					
Measured in the laboratory					
-Loose bulk density, dry [kg/m3]	677	508	725		
-Compact bulk density, dry [kg/m3]	1053	692	790	1026	
-Compact/loose	1.34	1.27	1.09		
From supplyer:					
Loose bulk density		500	730		

*Malvern analysis, particles suspended in water
**Cilas particle size analysis (Laser diffraction)
*** approximate value ($X_{51.7,3}$ = 45µm)
****Coulter(R) Multisizer

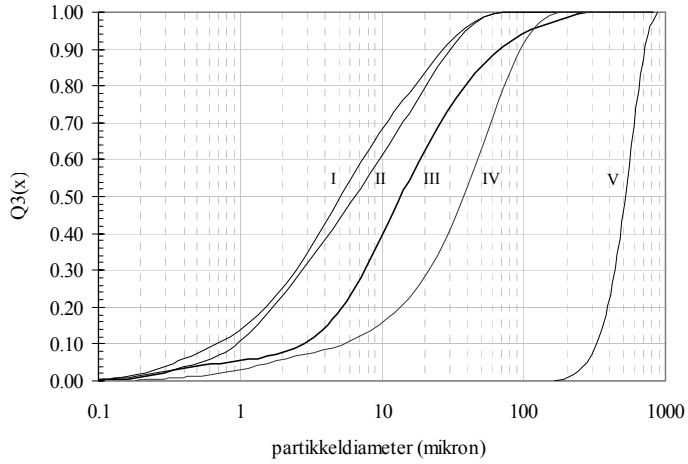

Figure 3.22: Particle size distributions as measured by a Malvern particle sizer (laser diffraction) on particles suspended in water. From left to right (at $X_{50,3}$): SAE-fine, Pural NF, Fly ash Folla, Pural SB and finally the filter bed material (Olivin AFS30, fine fraction removed in a cyclone prior to the filtration experiment).

Table 3.3: Summary of filtration tests conducted in the high temperature panel bed filter (filtration temperature about 200 °C).

dust	file	dt	Us	q	dP_{clean}	dP_r	dP_{max}	Feed rate [mm/h]	C_{raw}	Cycles	Discharged material upon puff-back Theoretical, average values tot	ex. Dust	dust/sand	Apparent outlet dust conc	eff.
	Exp#	[min]	[cm/s]	[m^3/h]	[Pa]	[Pa]	[Pa]	average	[g/m^3]		[g/cm^2]	[g/cm^2]	[-]	[mg/m^3]	[-]
Wishbone															
SAE	020201#1	707.4	4.44	3.70	241	239	1214	13.31	3.07	17	0.70	0.64	0.093		
	020201#2	313.2	4.57	3.82	250	298	1227	27.11	6.07	15	0.50	0.43	0.134		
	020201#3	89.8	8.63	7.21	461	429	1399	94.94	11.26	16	0.62	0.55	0.102	5.55	0.9995
	10201	355.2	8.75	7.31	399	399	1380	27.87	3.26	18	-	-	-		
	310101	165.7	13.67	11.42	400	413	1470	51.44	6.15	14	0.75	0.73	0.090		
NF	030201#1	40.0	5.37	4.49	447	452	1353	70.00	8.68	2.5					
	060201#1	496.4	5.30	4.42	303	340	1291	18.23	2.29	11	0.81	0.75	0.078	5.05	0.9978
	060201#2	259.1	5.30	4.43	313	315	1312	37.95	4.77	10	0.83	0.83	0.084	9.35	0.9980
	050201#1	101.6	8.55	7.14	563	478	1412	29.43	2.29	4					
		298.7	8.57	7.16					2.32	12				6.48	0.9972
		197.1	8.59	7.17				30.33	2.35	8	0.78	0.69	0.111		
	050201#2	133.0	10.25	8.56	513	552	1515	70.44	4.58	13	0.63	0.58	0.088	12.63	0.9972
SB	030201#1	60.0	8.71	7.28	437										
	080201#1	184.5	10.09	8.42	459	503	949	57.74	4.69	3	1.03		0.327		
	070201#1	190.0	10.15	8.48	507	617	1499	57.26	4.62	2.5	0.89		0.384		
max			10.25						11.26						
min			4.44						2.29						
	Total	56.8	[h]												
	Exp#	[min]	[cm/s]	[m^3/h]	[Pa]	[Pa]	[Pa]	mm/h average	[g/m^3]		[g/cm^2]	[g/cm^2]	[-]	[mg/m^3]	[-]
L10/56															
SAE	080301#1	352.7	4.84	4.46	310	520	1981	27.01	5.18	4	0.16	0.09	0.452	1.38	0.9997
	030301#1	346.7	4.86	4.47	293	486	1288	27.21	5.20	6	0.23	0.18	0.204	-3.17	1.0006
	080301#2	224.8	7.34	6.76	469	807	1994	40.00	5.06	6	0.16	0.13	0.167	1.09	0.9996
	090301 #1-4	871.7	7.40	6.82	390	619	1970	40.14	5.03	22	0.36	0.31	0.133	1.81	0.9996
	270201#1	216.3	8.57	7.90	368	446	1372	42.86	4.64	7	0.54	0.50	0.074	3.02	0.9993
	280201#1	417.1	8.60	7.92	394	496	1396	21.42	2.31	8	0.58	0.48	0.066	1.21	0.9995
	070301#1	380.8	9.74	8.97	500	766	1995	27.49	2.62	9	0.18	0.16	0.111	1.53	0.9990
	060301#1	789.9	9.89	9.12	483	664	1488	13.43	1.26	16	0.20	0.19	0.097	-0.43	1.0003
	070301#2	176.9	9.98	9.19	514	666	1952	53.54	4.98	8	0.19	0.15	0.189	3.01	0.9994
	020301#2	355.6	10.02	9.24	512	649	1519	27.21	2.52	16	0.21	0.19	0.086	3.12	0.9988
	070301#3	354.6	10.03	9.25	510	737	2001	27.29	2.52	9	0.19	0.15	0.173	1.75	0.9993
	020301#1	318.3	10.69	9.85	486	509	1455	27.16	2.36	9	0.50	0.47	0.057		
	280201#2	298.9	12.77	11.77	549	693	1537	32.47	2.36	18	0.25	0.23	0.066	3.92	0.9983
NF	180301#1	234.4	4.47	4.12	301	0	1979	40.78	5.51	3	0.33		0.190	4.18	0.9992
VDI	20501		4.80	4.42				24.00	4.49				#DIV/0!		
	030501#2		9.75	8.99				55.22	5.08				#DIV/0!		
	030501#1		9.77	9.00				111.10	10.20				#DIV/0!		
	Total	85.1	[h]												
Wishbone + L10/56		141.9	[h]												

The amount of discharged material upon puffback is calculated vs. the exposed filter surface (approximate values).

3.5.2 Test matrix.

A summary of the filtration experiments conducted in the Panel Bed Filter is listed in Table 3.3. While those conducted on the Horizontal bed filter are listed in Table 3.4.

The first panel bed filter tests were performed with Wishbone louvers in order to get a point of reference between this work, Lee (1975) and Lee et al. (1977). The standard dust qualities SAE-fine, Pural NF and Pural SB were used in these tests. Superficial velocity and inlet dust concentration was between 4-10 cm/s and 2-11 g/m^3 respectively. While the novel L10-56 louver was evaluated at 4-13 cm/s and 1-10 g/m^3, applying SAE-fine, Pural NF and Micro-Calcilin. The experiment include about 57and 85 hours of operation on the Wishbone and L10-56 louvers respectively.

The rugged construction of the horizontal bed unit (Figure 3.12) combined with a simple sampling procedure represents an easy way to obtain reference data (e.g. K_2') for a preliminary evaluation of the filter capacity and applicability. The experiments conducted in this unit include deposition of SAE-fine and Micro-Calcilin at about 200 °C. Applied superficial filtration velocities were about 15 and 20 cm/s and dust load about 2.5 and 5 g/m^3.

The filter was re-generated on-line in all filtration experiments. In order to reach sufficient cleaning intensity a larger solenoid valve was used in these experiments (Festo CPE24) than in the puff-back uniformity tests (Festo CPE14). The valve opening times also had to be increased. Exact measurement of the resulting pressure pulse (shape, peak pressure and duration) at operating conditions was not possible at present.

Main focus in the present work has been to verify filter cake formation, obtain stable filtration and compare the resulting pressure build up rates obtained in the panel bed filter and the horizontal bed unit. Furthermore, examining filter performance by the use of standard dust qualities ease comparison with other filter technologies and supports the evaluation of the experiments on raw gasification product gas presented in Chapter 5. Exact penetration measurements were beyond the scope of this work.

Table 3.4: Summary of the experiments conducted in the horizontal bed unit.

	File	$T_{filter,average}$	U_s	c	dust feeder
	Exp#		[cm/s]	[g/m^3]	[mm/h]
SAE-fine	190401	227	21.0	5.0	24.8
	180401	198	15.1	5.2	18.7
	230201	215	14.7	4.3	15.0
VDI	210401	200	21.4	4.6	24.4
	200401	223	15.1	4.9	18.1
	220401	206	21.3	2.4	12.9

3.5.3 Panel bed filtration data

A comparison of Wishbone and L10-56 when filtering SAE-fine dust (about 5 cm/s and 5 g/m^3) is given in Figure 3.23. The duration of each filter test was limited by the maximum load capacity of the rotating brush feeder. One extended filter test (about 900 minutes of semi-continuous filtration) was conducted for the L10-56 louver at 7.5 cm/s and 5 g/m^3 (Figure 3.24). The dust reservoir (RBG piston) was refilled three times (as indicated in the figure) during this test. Therefore the filter was operated for approximately one hour on particle free air after each refill, in order to re-establish stable air flow and filter temperature. No additional cleaning pulse was applied during this period.

A summary of the filtration experiments is given below. Relevant figures are included in Appendix: I.1) pressure build up vs. time, I.2) change in cycle time and residual pressure drop vs. elapsed time and specific filter cake resistance vs. time. The most important experimental parameters are given in Table 3.3 (a more extensive table is given in appendix I.3).

The filtration test series on the Wishbone louver was conducted successfully with a close to linear pressure build up rate. The initial cake forming period seems to be short and a close to linear pressure build up rate was quickly established. However, sudden drops in the pressure difference across the filter cake are seen at high pressure losses. This effect is especially pronounced above some 1000 Pa pressure build up. This behaviour is similar to what would be expected for pinhole formation.

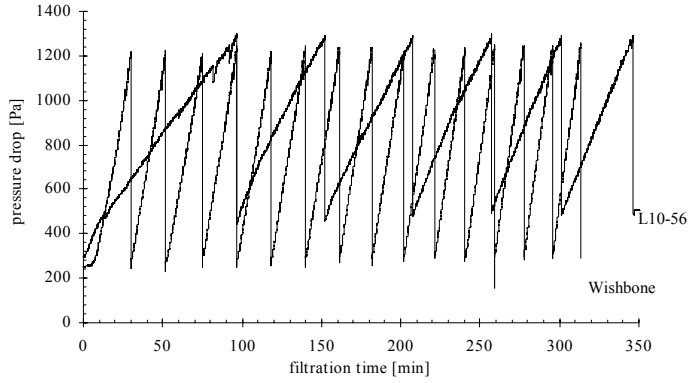

Figure 3.23: Illustration of the enhanced filter capacity as compared to the design developed by Lee et al. (1977) Comparison of Whishbone louvers (high frequency curve) and the new L-10-56 louvers (low frequency curve).

A marked decrease in the cycle duration and increase in the residual pressure drop is observed during the first 2-3 cycles. However, stable conditions were obtained for both louver geometries. The build up of the residual pressure loss (dP_r) is shown in Figure 3.25. The residual pressure drop is significantly higher for the L10-56 as compared to the Wishbone louver. This might be partly related to the relatively large sand spill applied for the Wishbone louver. Which might have resulted in removal of the roots established within the outermost filter bed layer.

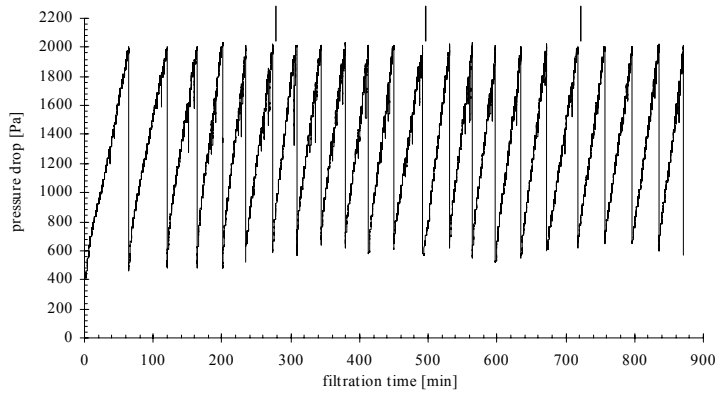

Figure 3.24: Extended filter test for the novel L10-56 louver. The drop lines indicate dust reservoir re-filling.

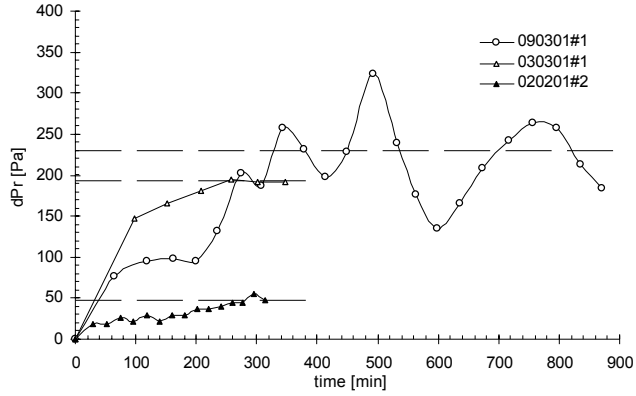

Figure 3.25: Comparison of the residual pressure drop as function of filtration time for the novel L10-56 louver and the Wishbone louver. The experiments shown here corresponds to those shown in figure 3.23 and 3.24. (Circles and open triangle refers to the novel L10-56 louver.)

The PuralNF dust is highly agglomerative and cased unplanned shut-down due to serious blocking problems in the particle feeder during the first filtration tests (030201#1 and 050201#1). This explains the instabilities observed in these tests. Successful operation was achieved after cleaning of the brush and changing to the special top cover (type B, different air jet nozzle for dispersing of the solids from the RBG2000 brush head). The standard top cover (type A) was used for all the other dust qualities. Despite these problems, Pural NF and SAE fine gives much the same pressure build up rate.

The experiments with PuralSB gave no problems with the particle feeding or filter regeneration, but the resulting pressure drop was low. This is believed to be due to the large particle diameter ($X_{50,3}$ = 74.9 μm). As already noted in Chapter 2, increasing particle diameter gives a lower resulting pressure drop ($dP \propto 1/d_p$ (Novic et al. 1992)). But it will also significantly affect particle concentration due to

sedimentation in the inlet cone. A downward-sloping pressure increase is observed at the very beginning of experiment number 070201#1. This effect was not reproduced in the consecutive test run.

The experiments conducted on the L10-56 louver shows a significantly longer cycle time at otherwise comparable test conditions. Except from this, the pressure build up was typically downward-sloping in the initial phase, but became linear at a total pressure drop of about 1000 Pa (dependent of superficial filtration velocity).

Instabilities in the filter operation were encountered in some of the initial experiments. Especially pronounced is this in experiment 280201#2, 020301#2 and 060301#1. All having a typically downward sloping pressure build up during the whole cycle.

It is known from the literature that a downward sloping pressure build up rate is typical for incomplete cleaning. A typical example of this is seen in experiment number 080301#1, first cleaning pulse. It should be noted that this insufficient cleaning is more likely caused by instabilities in the pressure valve than filter blinding. We experienced several times that the pre-adjusted sand spill decreased if there was a long period between each pulse, even on particle free gas.

Micro-calcilin: Was only tested for the L10-56 louver. The resulting pressure build up was very similar to that seen for Pural SB. Indicating a larger particle diameter than given from the supplier.

The extended test (SAE-fine) was conducted at about 7.5 cm/s, closer to normal field operation conditions (Paper I: about 9 cm/s) than what is suggested in the VDI-3926 standard (5 cm/s).

The pinhole-formation like pressure drops seems to be more pronounced for the L10-56 louver as compared to the wishbone louver, note however that the maximum pressure drop across the filter cake is significantly higher than for the wishbone louver. Similar “pinhole” effects were observed for the higher pressure drop utilised in an initial test on the Wishbone louver. This experiment is not shown here due to an error in the data acquisition system. Thus, filter cake pressure drops significantly exceeding 1000Pa are only documented for the novel L10-56 louver. It should be noted that a closer examination has to be taken in order to determine whether these pressure drops are due to pinhole formation or simply due to instabilities in the gas flow through the particle generator.

The total sand spill, including accumulated dust, in each puff-back was between 60-107 grams (about 0.43-0.83 g/cm^2 exposed sand surface) for the Wishbone louver and between 74-254 grams (about 0.09-0.50 g/cm^2) for the L10-56 louver. Note that these values are average values. Thus, variations in the sand spill between the different regenerations might have occurred.

3.5.4 Deposition of dust upon a free horizontal surface of sand

In order to verify the mechanisms governing the formation and retention of a filter cake on the surface of a granular solid, we ran some preliminary experiments whereby SAE-fine and Micro-Calcilin was deposited on a free horizontal surface of sand (Olivin AFS30, Figure 3.22).

The experiments conducted in the panel bed filter were influenced by particle sedimentation in the inlet cone. Resulting in an underestimation of the derived

specific cake resistances. Particle sedimentation in general proceeds through two routes: sedimentation and diffusion. The former is significantly reduced in the horizontal bed unit, as the particle containing gas flow vertically through both the raw gas line and the filter itself. Rudberg (2000) studied the distribution of monodisperse particles within this filter unit, applying numerical simulations in the CFD code flow-3D. And concluded that particles exceeding 10 microns had a clear tendency to accumulate near the centre of the filter surface, due to strong inertial forces. While smaller particles was mainly influenced by diffusion and tended to distribute evenly across the filter.

Only 6 experiments (Table 3.4) have been conducted in this filter unit. These experiments include deposition of SAE-fine and Micro-Calcilin at about 200 °C. The resulting pressure drop curves are shown in Figure 3.26. Applied maximum pressure drop across the filter cake was about 9000-15000 Pa. The accumulated pressure loss across the fly ash deposit is calculated by subtracting the pressure loss of the clean bed.

Some preliminary results are obtained, despite the limited number of tests conducted. The SAE-dust gives significantly higher pressure drops as compared to Micro-Calcilin.

These experiments confirm Lee's earlier finding that a filter cake is formed as fly ash is put down upon a free horizontal surface of sand.

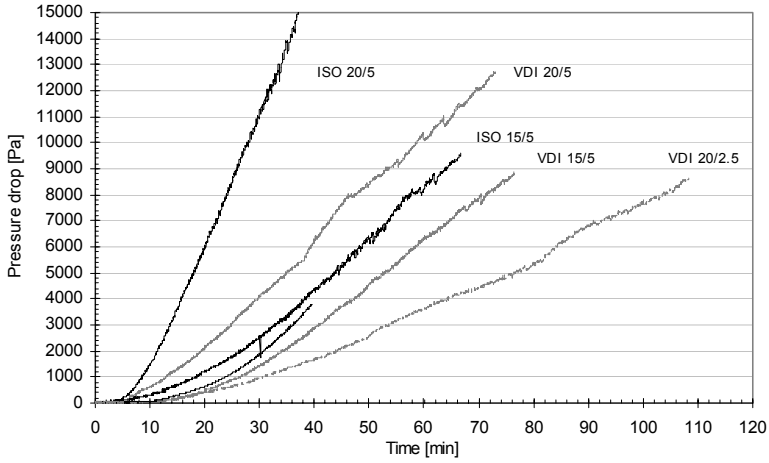

Figure 3.26: Resulting pressure drop for the ISO (black) and VDI (dark grey) dust qualities. (Notation: "dust type" Us [cm/s] / c [g/m^3])

3.6 Summary and conclusions

The overall goal for the ongoing filter development is to increase the filter competitiveness through cost effective production and plant compactness. Developing a louver geometry featuring reduced manufacturing costs, simplified production and maintenance, and enhanced filter capacity is part of this work.

A series of experiments has been designed in order to study the pressure pulse induced motion of sand between two adjacent front louvers, applying the design fundamentals as given by Lee (1975) and Lee et al. (1977). These experiments verified Lee's results and a simplified louver geometry incorporating the above-mentioned criteria were developed.

Furthermore, the second (coarse) sand layer (applied in the commercial scale filter, Paper I) has been removed and replaced by a new set of louvers. This imposes restrictions concerning the filter capacity. As too high filtration velocities (e.g. due to process fluctuations) and uneven velocity profiles both can lead to fluidisation of the unbounded bed of granular media.

The applied front louvers results in an upward directed gas flow through the filter bed, resulting in local high velocities at the uppermost back louvers. This effect was especially pronounced when using sand (AFS 30) as filter bed material. Incorporating vertical displacement of the back louvers vs. front louvers resulted in a significant improvement of filter bed stability. A similar effect was not observed in the experiments were spherical particles (NA 1708/920) replaced sand. (Note that these particles had a narrower particle size distribution.) This shows that bed stability and optimum displacement of the back-louvers is dependent upon the characteristics of the applied bed material.

Experiments indicate that the stability limit can be closely related to the theoretical minimum fluidisation velocity (U_{mf}). Hence, being a strong function of the physically properties of the bed media (e.g. specific density, angularity and particle size distribution).

Despite a skilled operator and accurate handling of the equipment some scattering in the puff-back uniformity data is to be expected. However, reproducibility in the different set-ups was high.

Applying a variety of cleaning pulse shapes gave no significant effect upon puff-back uniformity. The present work support the theory of a threshold value, and estimated values (Table 3.1) is found to be in the range 500-900 Pa, and fairly independent on the filter configuration. It is interesting to note that this dP_{min} corresponds quite well to the transitional region determined during the stability tests. A correlation towards the active time is questionable. However, a strong correlation was found between the average of the normalised sand spill and the resultant of the specific impulse.

An accurate measurement of the actual filter sand surface is difficult. This influences upon the calculation of the specific sand spill (g/cm^2) and partly describes the different gradients found when correlating this with the pulse intensity. The geometrical similar Folla and Wishbone louvers follow practically the same correlation. But significantly higher pulse intensity is required to cause the same sand spill for the novel L10-56 louver. However, an accurate determination of the actual sand surfaces is complicated. The sand surface in the Folla and Wishbone louvers is calculated as shown in Figure 3.17. Thus, as the actual sand surface is slightly higher

than the theoretical, while the opposite is seen for the L10-56 louver. Taking this into account would slightly reduce the difference in the slopes. Note that the filter bed is deeper for the L10-56 louver, which might also explain the need of a higher intensity at otherwise similar conditions.

The standard deviation of the normalised sand spill vs. specific sand spill for the different configurations is roughly constant and between 0.010 and 0.015. The uniformity profile obtained on the novel L-10-56, when installed into the high temperature filter unit, represents the most uniform profile obtained regardless of louver design.

Main focus in the present filtration experiments has been to verify filter cake formation, obtain stable filtration and compare the resulting pressure build up rates obtained in the panel bed filter (two different front louver geometries) and the horizontal bed unit. All experiments has been conducted at about 200 °C.

Both high temperature filter units built in connection to this work are based on similar units operated by Lee (1975) and Lee et al. (1977). Furthermore, the PBF unit is comparable with the German filtration standard VDI-3926, type 2. A standardised powder dispersion generator (VDI 3491) was used for a constant, continuous and reproducible generation of polydisperse solid aerosols from bulk material. Several standard test dust qualities (ISO-SAE fine, VDI-Pural NF, VDI-Pural SF and VDI-Micro Calcilin) was used to document filter performance and enable comparison between the novel L10-56 louver, the original Wishbone louver and published values from fabric filters and rigid ceramic and metallic filters. Furthermore, these ease comparison with other filter technologies and supports the evaluation of the experiments on raw gasification product gas presented in Chapter 5.

Superficial filtration velocities ranged from about 4 to 20 cm/s and raw dust concentration from 1 to 11 g/m^3. Only one type of bed material (AFS30, fine fraction removed in a high efficiency separator prior to the experiments) has been used in these experiments.

Comparison between the experiments conducted in the laboratory scale high temperature PBF-unit and the Folla experiments (Paper I) are given in Figure 3.27. In the experiments on the Wishbone louver the maximum pressure drop before regeneration was defined as 1000Pa above the pressure drop for the clean filter. An additional series where the maximum pressure drop was set to 2000Pa was conducted on the L10-56 louver. Hence, the chosen operating conditions allows comparison to these experiments.

The shape of the initial pressure build up rate is slightly different for the two louver geometries. The initial pressure build up rate is typically close to linear for the wishbone louver, while it was typically down-ward sloping for the L10-56 louver. Similar effects were observed by (Schulz 1988), who attributed them to the nature of the filter media itself (open loose vs. dense filter surfaces, see Section 2.3.1). A downward sloping pressure build up is also known to be the effect of incomplete cleaning (Section 2.3.2). In our case it seems more likely that this effect is a combination of cleaning efficiency and the considerable geometrical differences between the two filter configurations, as the filter media (sand) is the same in all experiments.

The stability of the filter cake decreased as the pressure build up exceeded about 1000Pa. Seen as sudden drops in the pressure loss. Similar pressure drops is seen in the experiments reported on the commercial scale unit (Paper I). This

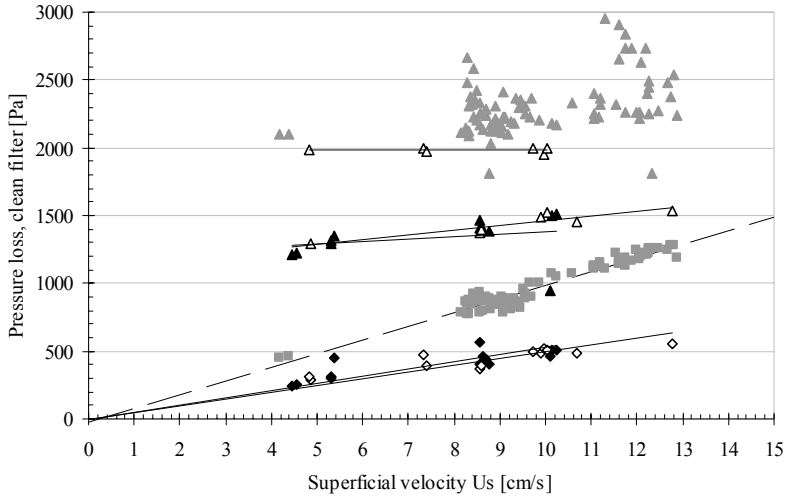

Figure 3.27: Maximum pressure drop before regeneration vs. clean/cleaned filter pressure drop, as a function of superficial velocity. The velocity and pressure loss ranges applied in the small-scale panel bed filter is compared with the experimental conditions applied in the commercial scale filter element. (Triangles – dP_{max}; Rectangular symbols- dP_{clean}; Filled black symbols for Wishbone, open symbols for L10-56 and grey symbols for Folla louvers (Risnes and Sønju (2001)).

behaviour is similar to what would occur if pinholes were formed. However, as mentioned earlier, a closer examination should be taken in order to verify whether this is due to real pinhole formation of simply due to instabilities in the flow through the particle feeder.

Increasing the maximum allowable pressure build up (i.e. longer cycle duration) resulted in less visible dust on the total filter, in accordance with theory. Apparent filtration efficiency as measured for the Wishbone louver was generally above 0.997 (outlet dust concentration below 10 mg/m^3, with one exception (12.63 g/m^3)), while it was generally above 0.999 (outlet dust concentration below 5 mg/m^3 in all experiments) for the L10-56 louver.

The experiments conducted in the panel bed filter were influenced by particle sedimentation in the inlet cone. Sedimentation is significantly reduced in the horizontal bed unit, where the particle containing gas flow vertically through both the raw gas line and the filter itself.

Only 6 experiments have been conducted in this filter unit. These experiments include deposition of SAE-fine and Micro-Calcilin at about 200 °C. Some preliminary results are obtained, despite the limited number of tests conducted.

Particle sedimentation, i.e. reduced filter capture efficiency, results in an underestimation of K_2' and partly explains that the derived K_2' values being significantly lower than those found in the reviewed literature (Table 2.1, chapter 2.3.1).

K_2' typically depicts an increasing trend during operation when calculated on the whole pressure build up range in the Panel Bed Filter (less pronounced for the Wishbone compared to the L10-56 louver). This effect is significantly reduced when calculated between 70-90% pressure build up.

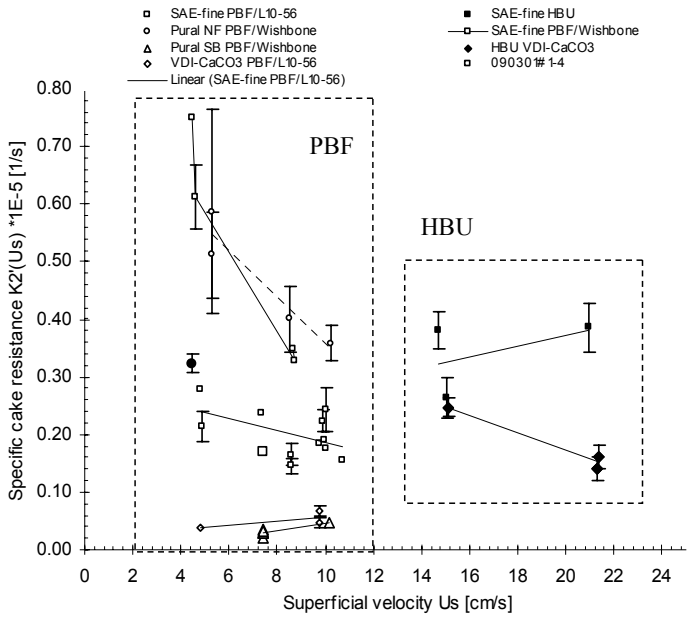

Figure 3.28: Comparison of values for the specific cake resistance as derived in the PBF and HBU respectively.

Note that the superficial velocity applied for the K_2' is derived based on the filter face area, and not the active filter surface, i.e. the exposed sand surface. The ratio between the exposed sand surfaces for the two louvers is significant. As discussed earlier (Section 3.4) the louver construction is based on the angle of repose for the applied bed material. However, this angle might change as the dust cake roots are established, resulting in a reduction of the exposed sand surface area. A theoretical area ratio (based on the angle of repose) for the wishbone and L10-56 louver is about 3.5 (A_W/A_L).

Increasing filtration temperature, from ambient conditions up to 200 °C, will reduce K_2' with roughly 50% (Table 2.1, Chapter 2).

The conducted filtration tests cover a wide range of operation conditions. Stable operation was successfully obtained for both louver geometries at 200 °C, i.e. no signs of filter blinding were observed. Comparison of the two louvers shows a capacity increase of about 2-3 times (Figure 3.23 and 3.28) for the novel L10-56 louver (the capacity increase apparently decreases at higher filtration velocities). The gravimetrically determined filter efficiency is above 0.999. The pressure build up ranged from 1000 to 1700 Pa for the panel bed filter, and up to 17000 Pa in the horizontal bed filter. The corresponding values were 250-340 Pa in Lee 1975 and 400-1900 Pa in Lee et al. 1977.

These filtration tests were conducted with on-line cleaning while Lee (1975), Lee et al. (1977) and Risnes and Sønju (2001) used off-line cleaning.

The specific of the resulting impulse correlates very well against the specific sand spill for the wide variety of pressure pulses evaluated in this work. The active time theory seems to give the best results for geometrically similar cleaning pulses. The porosity variations discussed by Lee is not further evaluated in this work. Lee found dP_{min} not to be a function of sand size and reported an upper limit for t_a of about 50ms.

Lee suggested applying a relative displacement in order to increase bed stability and sand spill uniformity. The present work supports this solution. However, the optimum displacement is closely related to. The filter stability limit ($U_{S,max}$) is closely related to louver configuration and the applied bed material. Experiments with AFS30 shows an upper stability limit at a face velocity of 17-20 cm/s. This is close to the 15 cm/s found for the preliminary unit operated by Lee (1975).

This work (deposition of dust upon Olivin sand, $X_{50,3}$ = 545 μm) documents the formation of pin-holes as the pressure drop exceeds about 1000 Pa. No pin-hole formation is reported by Lee from the filtration experiments conducted in the horizontal bed unit on 297-420 μm (40-50 mesh) sand, while experiments on 590-840 μm (20-30 mesh) sand showed pin-hole formation above a critical pressure build up. Pin hole formation increased with increasing face velocity. Lee also showed that a higher mass loading was necessary to establish a filter cake upon a 50/50 mixture of 20-30 and 40-50 mesh sand as compared to 20-30 mesh sand. These results indicate that the bed material used in this work (AFS30) has a particle diameter close to maximum if stable filtration is to be reached.

References

Engebretsen, T. (1984) *Sandfilter for rensing av høytemperatur røykgass – laboratorieforsøk med FeSi-støv*. Project report 3/84. Dep. of thermal energy and hydro power, The Norwegian University of Science and Technology.

Lee, Kun-chieh (1975) *Filtration of redispersed power-station fly ash by a Panel Bed Filter with puff-back*. The City University of New York, Ph.D. Thesis.

Lee, K. C., Rodon, I., Wu, M. S., Pfeffer, R. and Squires, A. M. *The panel bed filter* , EPRI AF-560, Final report, May 1977.

Novick, V.J., Monson, P.R. and Ellison, P.E. (1992) *The effect of solid particle mass loading on the pressure drop* J. Aerosol. Sci.

Paretsky, L. (1972) *Filtration of aerosols by granular beds*, Ph.D. Dissertation, The City University of New York, 1972.

Risnes, H. and Sønju, O. K. (2001) *Evaluation of a novel granular bed filtration system for high temperature applications*. In proceedings: Progress in Thermochemical Biomass Conversion, September 2000, Tyrol, Austria, pp. 730-742.

Rudberg, Ø. (2000) *Theoretical and experimental investigation of a granular filter coupled to a biomass gasifier.* Diploma thesis, Dep. for thermal energy and hydropower, The Norwegian University of Science and Technology, ITEV-report 00:74.

Schulz, R. (1988) *Untersuchungen zur Staubabscheidung aus Gasen mit Filtrationsabscheidern bei hohen temperaturen und hohen drücken.* Fortschr.-Ber. VDI Reihe 3 Nr. 156. Düsseldorf 1988.

Squires, Am. and Pfeffer, R. (1970*) Panel bed filters for simultaneous removal of fly ash and sulfur dioxide-1.* JAPCA v 20, n 8, 1970, pp. 534-538

VDI-Richtlinie 3926 *Testing of filter media for cleanable filters*, Beut Verlag, Berlin, 1994.

4 Biomass gasification

The driving force of the development of gasification technology is the need for higher power-to-heat ratios in cogeneration, since the demand for electricity increases more rapidly tan the heat demand.

The use of biomass derived fuels, as substitutes for conventional fossil fuels, in large and medium scale power production, demands examination of several aspects, both operational and environmental. These aspects include ease of fuel handling, fuel conversion rate, propensity for producing aerosol or gaseous pollutants, and the tendency of inorganic components to cause fouling or corrosion of burner and boiler surfaces.

The objectives of this chapter is to give a brief description of biomass conversion processes for power production and to discuss the most important parameters associated with gasification reactivity in particular, such as the influence of fuel composition, reactor temperature and gas concentrations upon fuel reactivity. Thereby enhance the understanding of the basic mechanisms involved in thermochemical conversion of biomass, contribute to improved reactor modelling and increase the accuracy in the prediction of product gas quality. Furthermore, to contribute to optimised filter design and operation and ensure that the gas cleaning requirements are met.

Char conversion is typically the rate-limiting step during combustion and gasification of solid fuels. Biomass char reactivity is relatively high compared to coal char, and the low-density residue char particles are easily elutriated from the bed in fluidised gasifiers or combustors. Furthermore, volatile and mobile potassium and sodium alkali salt melts may form sticky layers on the ash and bed particles and react with Si and Ca hereby forming highly viscous oxide/silicate slag with low melting temperature eventually leading to agglomeration and sintering within the gasifier. Additionally heat transfer surfaces and high-temperature filters are corroded from deposits primarily composed of alkali-salt chlorides, carbonates, and hydroxides and in combustion additionally also sulphates.

In this chapter special attention has been devoted to biomass char (from wood and straw) and the reactivity towards CO_2 and H_2O/H_2. Furthermore, the influence of the inherent inorganic ash forming elements (in straw gasification) and the effect of calcium addition upon gasification reactivity and sintering behaviour has been investigated both experimentally and theoretically. A detailed description of this work is given in the included papers (Paper II, Paper III and Paper IV).

4.1 Introduction to thermochemical biomass conversion

There are four thermochemical methods suitable for the conversion of biomass: pyrolysis, gasification, liquefaction or direct combustion, and the primary products can be gas, liquid, solid char and/or heat dependent on the conversion process and technology employed. Secondary higher value products may be produced by additional processing. In principle, most of the petroleum derived chemicals currently being used can be produced from biomass, but some will require rather circuitous

synthesis routes. An overview of achievements and prospects for biomass heat and power production is given in a recent European Commission report (EUR 18029).

The great variations in moisture content, ash and chemical composition (especially nitrogen, sulphur and chlorine) give rise to large variations in conversion behaviour and pollutant emissions from biomass systems.

Viewing the chemical composition of biomass compared to peat and coals, the biomass fuels are high in the O/C – and H/C ratios. These high ratios are responsible for the biomass fuels being more volatile than coals and peat, and high O/C – ratios give lower heating values for the biomass fuels.

Both combustion and gasification can be described as a two-stage process. First the solid substance goes through devolatilisation. Decomposing the biomass into volatile components (CO, H_2, CH_4 and higher hydrocarbons), typically occurring between 300 °C and 500 °C. This stage is schematically illustrated in equation 4.1.

$$Biomass \xrightarrow{heat} soid(char) + liquid(tar) + gas(CH_4, H_2, CO, CO_2) + inorganics \quad (4.1)$$

Secondly the gases and the remaining charcoal (~15 wt% for wood) is oxidised. These processes can occur sequentially or in parallel depending on conditions such as fuel particle size, excess air ratio and temperature.

The heating value of biomass gasification product gas (mainly CO, H_2, CH_4, CO_2 and N_2) highly depends upon the gasification medium. Generally the product gas can be classified as: Low Calorific Value gas (5 MJ/Nm^3); Medium Calorific Value gas (10-15 MJ/Nm^3) and High Calorific Value gas (30 MJ/Nm^3). LCV gas is produced by air gasification, MCV gas by oxygen or oxygen/steam mixture. While HCV gas can be produced via catalytic methanisation of MCV gas.

4.2 Biomass gasification

In a gasifier biomass is converted at 800-1200 °C to combustible gases (H_2, CO, CH_4 and hydrocarbons), condensable tars, nitrogen compounds (NH_3, HCN) and solid products through reactions with gaseous media such as air, steam and/or oxygen. The final product distribution largely depends on gas-feedstock contact type and process conditions.

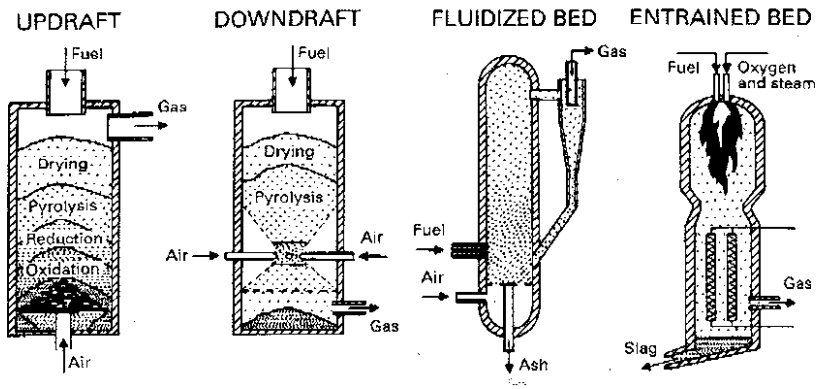

Figure 4.1: Gasifier types, Kurkela et al. 1993.

In principle, all main gasifier types shown in Figure 4.1 can be used in syngas production from biomass.

Fixed bed (updraft/downdraft), fluid bed, and entrained flow refer to the motion of the solids within the gasifier. In this work, special focus is directed towards the characteristics of the fixed-bed downdraft and fluidised bed gasifier.

The fixed-bed downdraft gasifier is suitable for small-scale engine applications with dense, high-quality feedstocks such as pellets and briquettes, hog fuel, or high-quality wood chips. In the ideal reactor, the pyrolysis products pass through a hot-char-containing combustion zone, in which the tars are cracked thermally and oxidised. In theory, the organic vapours from downdraft gasifiers should be burned totally, whereas in practice the amount of tars is mainly a function of the temperature, the efficiency of the combustion zone, and the channelling of the bed.

In a fluidised bed gasifier the fuel particles (mm size particles) are fed into a hot bed of particles suspended by upflowing gases. The characteristics of this reactor type are: a) even temperature distribution through the reactor b) good mixing of solids and gases c) the presence of fuel bed and bed particles, which also can be used to catalyse gasification reactions d) high content of particulates and relatively low tar concentration due to cracking reactions (Kurkela (1996)).

4.3 Gasification kinetics and reactivity

The oxidising, or gasifying, agents are air, oxygen, steam and CO_2. CO_2 is produced during the pyrolysis and early oxidation processes and generally not externally added. Because of biomass moisture, and steam from pyrolysis in downdraft gasification, steam will always be present in gasification whether steam or air is used as gasification agent. Hydrogen and carbon monoxide are products of gasification and their effect on the reaction is also relevant.

The most common reaction for conversion of carbon is combustion with oxygen, represented with the overall reaction:

$$C + O_2 \leftrightarrow CO_2 \qquad (4.2)$$

Combustion is an exothermic reaction which takes place under oxidative conditions. Because the reaction gives off heat, it is self-perpetuating provided that enough oxygen or air is available. However, the studies presented here focus on the gasification with CO_2:

Boduard reaction:

$$C + CO_2 \leftrightarrow 2CO \qquad \Delta H_R = +160{,}9 \text{ kJ/mol} \qquad (4.3)$$

and gasification with steam:

Water gas reaction:

$$C + H_2O \leftrightarrow H_2 + CO \qquad \Delta H_R = +118{,}4 \text{ kJ/mol} \qquad (4.4)$$

Gasification by carbon dioxide and steam are both endothermic reactions. Hence, the heat necessary in order for them to occur is normally provided through partial combustion, alternatively by indirect heating.

A comparison of the reaction rate between carbon and oxygen, steam and carbon dioxide gives the relative reaction rates (at 800 K and 0.1 atm (Laurendau (1978)):

$$\underset{10^5}{O_2} >> \underset{3}{H_2O} > \underset{1}{CO_2} \qquad (4.5)$$

4.3.1 Reactivity determination

For a solid fuel, the char reactivity towards a reactive gas is usually defined in terms of the conversion rate per remaining mass**,** Laurendau (1978):

$$R = -\frac{1}{m}\frac{dm}{dt} = \frac{1}{1-X}\frac{dX}{dt} \qquad (4.6)$$

where m is the mass of the organic portion of the sample, dm/dt is the conversion rate and X is the degree of conversion, $X = (m\text{-}m_0)/m_0$.

A voluminous literature exists regarding the reactivity of carbon in its various forms ranging from charcoal, coke to carbon filaments. Although this literature provides valuable information related to specific aspects of char reactivity, there is a need for further information on the reactivity of different substrates, under a variety of conditions.

-Gasification by CO_2

The proposed Langmuir-Hinshelwood kinetics expression for the gasification reaction (CO_2 and CO gas mixture) is given by, Laurendau (1978):

$$r_C = \frac{k_{1f} P_{CO2}}{1 + aP_{CO2} + bP_{CO}} \qquad (4.7)$$

This complex rate expression can describe both, saturation by the reactant gas (a) and inhibition by the product gas (b). However, the simpler n^{th} order reaction scheme might be applicable at low CO ratios:

$$r_C = k P_{CO2}^n \quad , \; k = k_0 \cdot \exp(-E/RT) \qquad (4.8)$$

-Gasification by steam

Steam (H_2O) gasification is more complex than carbon dioxide (CO_2) gasification because not only H_2O is involved but also H_2, CO_2 and CO due to the equilibrium of the water gas shift reaction. Hüttinger and Merdes (1992) give a comprehensive description of the models proposed in the literature for the carbon-steam reaction. Basically, there are two models of the reaction mechanism: the oxygen exchange model and the hydrogen inhibition model.

In this work, the kinetic parameters have been obtained according to the oxygen exchange model, and also according to n^{th} order kinetics:

$$r = \frac{k_{1f} p_{H2O}}{1 + aP_{H2O} + bP_{H2}} \qquad (4.9)$$

$$r_C = k P_{H_2O}^n \quad , \; k = k_0 \cdot \exp(-E/RT) \qquad (4.10)$$

4.3.2 Effect of minerals on the gasification reactivity, catalytic effects

The gasification of carbon/char is controlled mainly by: intrinsic reactivity of carbon/char; pore structure; and catalytic effect of mineral impurities. The relevant catalysts in biomass gasification are K, Ca, Mg, and Na.

Kannan (1990) found for a range of biomass chars (pyrolysed at 750 °C) that silica deactivates K by forming catalytic inactive potassium silicate. Moilanen and Kurkela (1995) found that the inverse correlation between biomass silica content and char reactivity were most significant at high fuel conversions. Moilanen et al. (2001) showed that during the pyrolysis stage the total amount of potassium, K_{tot}, and the water soluble potassium, K_{ws}, levels were reduced to (X, K_{tot}, K_{ws}) = (0, ~90%, ~75%). During char gasification the values were (0.5, ~85%, 50%) and (1, ~80%, ~15%).

For calcium catalysed gasification reactions, the proposed active intermediates include $CaCO_3$, CaO, CaO_2 and Ca_xO_y. However, Ca shows severe deactivation in particular ascribed to sintering due to calcium carbonate formation. Leboda et al. (1998) deposited around 1.44% calcium ions on the surface of active carbons produced from plum stones treated by mineral acid and organic solvent. Ion exchange was made by oxidizing the surface by nitric acid and then adding Ca ions using a calcium acetate solution. The reactivity increased significantly in the order: R(raw sample) < R(impregnate sample) < R(ion exchanged sample). The same conditions, however, also favour the reactivity of Ca towards other inorganic species like Si, which is often abundant in biomass. Dependent of the fuel composition the addition of very small or

moderate amounts of Ca may, however, together with Si and K lead to eutectics at even lower temperatures than those of Si and K alone.

4.4 Ash, the inorganic fraction in biomass

There is far greater diversity in ash composition than in the organic composition in bio-fuels. The ash forming elements (Ca, K and Si normally accounts for 60/90% of the ash calculated as oxides) are mainly organically/ionically bounded to the fuel matrix, or contained as very fine salt particles. An extensive chemical characterisation of biomass fuels is given by Nordin (1994).

Volatile and mobile potassium and sodium alkali salt melts may form (low-viscosity) sticky layers on the ash and bed particles (typically consisting of sand, dolomite, lime or limestone) and react with Si and Ca hereby forming highly viscous slag with low solidus temperatures eventually leading to sintering and defluidisation. Additionally heat transfer surfaces are corroded from deposits containing primarily alkali salt chlorides, carbonates, hydroxides and in combustion additionally also sulphates.

Operational measures to decrease the tendency of agglomeration and sintering and salt deposition in a fluidised bed are: 1) avoiding hot spots, 2) decreasing process temperatures, 3) fuel refinement (extraction of Na, K), 4) co-firing with fuels with less problematic ashes, 5) modifying the bed material size distribution and composition or 6) using additives. Additives typically react with a part of the slag-producing species converting them into compounds with high solidus temperatures. One example is kaolin depleting the mobile catalysts from the carbon surfaces hereby reducing the char reactivity as well as the sintering tendency.

4.5 Ideal multiphase equilibrium model

In global equilibrium analysis, the process of interest, or a certain part of an overall process, is treated as an equilibrium reactor to which known amounts of all elements considered are introduced. Given the temperature, pressure, and a set of possible chemical compounds, the equilibrium composition of the reactor can be found. Several equilibrium reactors at, say, different temperatures, can be connected together and the mass flows between them can be controlled to simulate more complicated systems.

The equilibrium state can be described as the final limit beyond which no further reaction can take place. No kinetic (time dependent) factors are taken into account. Equilibrium analysis gives first hand information about which phases are likely to appear at different over-all, or local conditions. It also provides quantitative information about amounts and composition of phases present.

There are some weaknesses in today's models, which mainly are due to lack of experimental multicomponent data. Thus, extrapolation into higher order composition regimes are uncertain. An excellent review on state of the art, possibilities and application is given by Backman and Nordin (1998). A review of multicomponent chemical equilibrium programs commercially available is given by Bale and Eriksson (1990).

How well the results from an equilibrium calculation describes the real system is dependent on the thermodynamic data used in the calculations. Therefore, new predictions should always be related to previous or new experimental validations.

In energy conversion systems a gas phase is always involved. Its impact is significant, because it provides the actual oxygen potential which affect the formation of oxidized or reduced species. The gas-to-condensed ratio is also important because this ratio determines how much of a volatile component that can evaporate.

- experimental data

The condensed phases in bioash chemistry seem to belong to either of two chemically distinctive systems, an oxide/silicate system, K_2O-CaO-SiO_2, or a salt mixture system. The former consist of a silicate melt and a number of stoichiometric solid compounds, and the latter consist of a liquid. The K_2O-CaO-SiO_2 system is experimentally determined by Morey et al. (1930). They found 7 ternary solid compounds in addition to the binary substances. Most of these compounds are in the silica rich corner of the ternary diagram. The lowest solidus temperature (720 °C) is found on the $K_2O.2CaO.9SiO_2$ liquidus in the binary $K_2O.4SiO_2$ – $CaO.SiO_2$ system. At higher Ca-contents the first melting temperature increases above 1000 °C.

The most important calcium salts formed in biomass conversion systems are carbonate, sulfate (mainly in combustion) and chlorine. In fluctuating conditions the carbonisation/recarbonisation cycle can significantly affect fouling and sintering of deposits (Backman and Nordin (1998)).

- modelling

The sublattice models are, in general, utilised for calculations on salt solutions while the quasichemical model is more suitable when oxides are analysed. The quasichemical model has shown particularly good agreement on binary systems containing silicates and oxides. Ternary and multicomponent systems can be approximated solely from the subsidiary binary systems or they can be described with ternary, quarternary etc. parameters, found from the optimisation together with the binary parameters. The equations do not involve a detailed structure and they therefore remain general, but mathematically useful in practise.

To obtain the solution parameters, non-ideal solutions models must be used. Many of the binaries and some of the ternaries in the multicomponent system of interest K_2O-CaO-SiO_2-Na_2O-MgO-FeO-Al_2O_3 have been described recently with the quasi-chemical model (Wu et al. (1995), Eriksson and Pelton 1993, Eriksson et al. 1993). The solution parameters for the binaries K_2O-SiO_2 and CaO-SiO_2 have been determined using the quasi-chemical model (Pelton and Blander (1986) and Wu et al. (1993)). No experimental data is available, at least in the FACT-database (Bale (2000)) on the ternaries. But by combining these two binaries a first estimate of the melting properties of ternary systems can be made. These have been added to the K_2O-CaO-SiO_2 ternary to enhance the accuracy in the estimation of the melting properties.

4.6 Summary

Improved fundamental knowledge about the processes involved in the thermochemical biomass conversion will clarify the interaction between product gas contaminants and the operational conditions within the gasifier, and consequently supports a successful implementation of hot gas cleaning systems. Although the available literature provides valuable information related to specific aspects of char reactivity, there is a need for further discussion of the validity range of the determination and extrapolation of reactivity data for coal and biomass.

A brief summary of the included papers is given below. This work presents experimentally determined (i.e. by thermogravimetry) char reactivity parameters obtained from atmospheric gasification of biomass chars in mixtures of CO_2 and H_2O/H_2 in nitrogen. Selected char samples derived from a variety of biomass qualities, ranging from well-defined heartwood to highly problematic straws are investigated. The influence of ash chemistry upon char reactivity has also been discussed thorough experiments combined with theoretical evaluations.

Paper II presents investigations made in order to produce operational data for the gasification reactivity for biomass chars (derived from spruce and wheat straw). Furthermore, the differences between these chars and a dense metallurgical coke (from Longyear coal) are illustrated.

Comparing conversion rates at a given conversion (eg. initial rate) is frequently done in kinetic studies. In most cases the initial 10% or 50% of the conversion is used for evaluating the kinetic parameters. For most chars of coal, lignite and peat, the reactivity decreases with increasing conversion or time, whereas for most chars of biomass it increases. (Reactivity can also exhibit a maximum or a minimum.) However, reactivity measured versus conversion may, in order to obtain kinetics, be sought split into a chemical kinetics term (r_c), and a structural profile ($f(X)$, where X is the degree of conversion). The structural profile is often implicitly or explicitly with success assumed to summarise the effect of available internal surface, available active/reactive sites and pore-evolution and to be invariant over the relevant T-P domain. Note that only if the invariant structural profile assumption is approximately valid a reference profile (R_{ref}) can be used to eliminate the structural profile to form a normalised reactivity (R_n) and to determine kinetics up to a constant.

The n^{th} order kinetic model give a good representation of the thermogravimetrically determined CO_2-reactivity. (Note that no CO was externally added during these experiments.) Since normalised reactivity was approximately independent of conversion for each char, one reaction order and activation energy could be estimated for the whole range of temperatures and CO_2 partial pressures studied.

The following kinetic parameters were obtained (atmospheric experiments): apparent activation energies (E) for wheat straw char; 205.6 kJ/mol, spruce char; 219.9 kJ/mol and Longyear coke; 233.1 kJ/mol, the respective reaction orders equals 0.59, 0.36 and 0.51. In the investigated temperature and CO_2-partial pressure range, using normalised reactivity (R_n) and the reactivity at 20, 40, 60 and 80% conversion (R_{X20}, R_{X40}, R_{X60} and R_{X80}) for kinetics determination gave similar results, as expected in the case of an invariant structural profile $f(X)$. However, O_2 and CO_2 give reactant specific and different reactivity profiles. For the Longyear coke partial pressure dependent reactivity profiles were measured and discussed.

Paper III presents the kinetic parameters and reactivity profiles for steam gasification of birch and beech char. The inhibition effect of hydrogen is also studied using externally added hydrogen and Langmuir-Hinshelwood kinetics. The same birch char has been used for CO_2/CO gasification (Barrio and Hustad (2001)).

Apart from their origin there was also other differences between the woods. The beech sample, received as wood chips, whose surface had been exposed to the ambient and that partially contains bark. The birch sample came from the heartwood of a wood log that had been cut into small cubes of 1x1x1 cm (i.e. bark free).

All the kinetic parameters obtained were compared with those found in literature, with and without hydrogen inhibition, by means of a kinetic compensation diagram. Most of the values were found to lie within the same line what might be a sign of consistency in spite of the disparity in activation energies. The differences between kinetic parameters can also be due to parameters not studied in this investigation like the number of active sites or the effect of temperature on the active sites behaviour.

The reactivity was evaluated at i) 20, ii) 50 and iii) 80% conversion, iv) as the average reactivity (20-80% conversion), v) assumption of structural profile and vi) based on the time for 80% conversion. Regarding the uncertainty of the calculation, definitions ii), iv) and v) seem to give more precise results and it is interesting to notice that the error of the reaction order calculation did not depend on how the representative reactivity value was defined.

The kinetic parameters for the n^{th} order kinetic model (for the pure steam gasification experiments) give activation energies between 228-238 kJ/mol and reaction orders between 0.54 and 0.58, with one exception. The frequency factors are somewhat more scattered, lying between $5 \cdot 10^7$ and $3 \cdot 10^8$.

The influence of the inherent ash forming elements in straw and calcium addition upon steam gasification reactivity (thermogravimetrically determined at 850 °C) and sintering behaviour of five straw chars is investigated in Paper IV. The equilibrium program FACT (Bale et al. (2000)) was used for the theoretical evaluation under atmospheric gasification conditions in a temperature range of 700 to 1000 °C.

Calcium was added to the straw samples before pelletising. The reactivity seems only little affected by the addition of the calcium solution. This indicates that calcium does not contribute much as a catalyst compared to the fuel potassium, during most of the observed carbon gasification reaction. Nor does it affect the behaviour of the water-soluble potassium catalyst, until late in the process, in support to the observations made by Moilanen et al. (2001). However, calcium participates significantly during the inorganic element transformations.

Analysis of the ash residues obtained from the gasified samples clearly show enrichment by calcium. A number of silica containing crystalline compounds are observed through x-ray powder diffraction, including binary Ca-Si (Ca_2SiO_4, and Ca_3SiO_5) and ternary K-Ca-Si (K_2CaSiO_4, $K_4CaSi_3O_9$ and $K_4CaSi_3O_9$) and K-Al-Si ($KAlSiO_4$ and $K_{1.25}Al_{1.25}Si_{0.75}O_4$).

In-situ synchrotron X-ray powder diffraction studies (during the heating of a char sample at 20 ^oC/min in an oxygen flow) of the inorganic fractions shows that the added calcium is greatly reactive and that this is particular so at the end of the conversion of the carbonaceous phase. Between 500 and 550 °C the small angle background completely disappeared and K_2CaSiO_2 and one or more calcium silicate

phases was detected (Ca_2SiO_4/Ca_3SiO_5). This is in accordance with the results from the SEM-EDX and X-ray powder diffraction studies.

4.7 Conclusions

In this chapter special attention has been directed towards the gasification of biomass char. The diversity among the ash content and inorganic compositions of these chars is especially pronounced, representing highly different properties with respect to ash fusion/agglomeration and catalytic influence upon the char reactivity.

A simple n^{th} order reaction scheme and an assumption about invariant reactivity development versus char conversion (structural profile $f(x)$) was successfully applied for gasification reactivity determinations, conducted at atmospheric conditions, in different partial pressures of CO_2 in N_2 and H_2O in N_2. Since all representative reactivity definitions are related to a fixed degree of conversion (or a fixed interval), the difference between the defined reactivities will be a multiplying factor, independent of temperature and pressure, and therefore absorbed in the frequency factor. Underlining the importance of analysing the influence of the reactivity definition upon the resulting kinetic parameters.

The activation energies derived from the n^{th} order kinetic model lies between 205-233 kJ/mol for CO_2 gasification and 228-238 kJ/mol for H_2O gasification. Reaction orders lay within 0.36-0.59 and 0.54-0.58 for CO_2 and H_2O gasification, respectively.

External addition of hydrogen, together with steam, resulted in significant inhibition and Langmuir-Hinshelwood kinetics was used to take this into account. The reactivity development versus conversion was found to be consistent within one fuel/reactant combination, but different reactants gives reactant specific reactivity profiles. Note that significant melt formation, due to reactions among the inorganic components present in the raw fuel, might influence upon the validity of the structural profile assumption (discussed in Paper II).

Steam gasification experiments conducted on various straws and compared to global equilibrium analysis (discussed in Paper IV) document the positive influence of the novel Ca-based additive, by significantly reducing sintering and agglomeration (i.e. the generation of potassium rich silicate/oxide slag and liquid salt melts) while preserving fuel reactivity. Availability of the added Ca is shown to depend on how it is added to the raw fuel. The observed reactivity indicates that Ca mainly reacts with the fuel ash at higher conversion levels. The results also indicate that the Ca-additive mainly reacts with fuel Si, producing binary calcium silicates, and to a minor extent with fuel potassium. Thus Ca, suppressing the formation of a catalytic inactive liquid oxide/silicate melt, has an indirectly catalytic effect as K is now found in a liquid salt melt as KCl/K_2CO_3. Global equilibrium calculation shows that the increased salt formation is mainly due to carbonate formation.

References

Backman, R. and Nordin, A. (1998) *High temperature equilibrium calculations of ash forming elements in biomass combustion/gasification systems - state of the art, possibilities and applications.* International Biomass Ash Workshop, Technical University of Graz, Austria, October 1-2, 1998.

Bale, C. W. and Eriksson, G. (1990) *Metallurgical thermochemical databases – a review*, Can. Met. Quar., v 29, n 2, 1990, pp. 105-132.

Bale, C. W., Pelton, A. D. and Thompson, W. T. (2000) FACT-Win® Version 3.05, Software with extensive Thermochemical Database, Ecole Polytechnique de Montreal, Quebec, Canada. H3C3A7

Barrio, M. and Hustad. J. E. (2001) *CO_2 gasification of birch char and the effect of CO inhibition on the calculations of chemical kinetics.* In proceedings: Progress in Thermochemical Biomass Conversion, September 2000, Tyrol, Austria, pp. 32-46.

Eriksson, G. and Pelton, A.D. (1993) *Critical evaluation and optimization of the thermodynamic properties and phase diagrams of the CaO-Al2O3, Al2O3-SiO2, and CaO-Al2O3-SiO2 Systems*, Metallurgical transactions B, v 24B, Oct. 1993, pp. 807

Eriksson, G., Wu, P. and Pelton, A. D. (1993) *Critical evaluation and optimization of the thermodynamic properties and phase diagrams of the MgO-Al2O3, MnO-Al2O3, FeO-Al2O3, Na2O-Al2O3 amd K2O-Al2O3 systems*. Calphad, v 17, 1993, pp. 189-205.

EUR 18029 (1999) *Biomass conversion technologies – achievements and prospects for heat and power production.* Luxembourg – Office for Official Publications of the European Communities, 1999, ISBN 92-828-5368-3, 178p.

Hüttinger, K.J. and Merdes, W.F. (1992). *The carbon-steam reaction at elevated pressure: formations of product gases and hydrogen inhibitions,* Carbon, v 30, n 6, pp. 883-894.

Kannan, M.P. and Richards, G.N. (1990). *Potassium catalysis in air gasification of cellulosic chars.* Fuel, v 69, pp. 999-1006.

Leboda R., Skubiszewska-Zieba, Grzegorczyk (1998). Carbon v 36, pp. 417-425.

Laurendeau, N-M. *Heterogeneous kinetics of coal char gasification and combustion. Prog. Energy Combust.* Sci., 1978.

Kurkela, E., Stahlberg, P. Laatikainen, J. and Simell, P. (1993) *Development of Simplified IGCC-Process for biofuels: Supporting Gasification Research at VTT*, In: Bioresource Technology United Kingdom, 1993, v 46 (1-2), pp. 37-47.

Kurkela, E. (1996) *Formation and removal of biomass-derived contaminants in fluidized-bed gasification processes.* Espoo 1996, Technical Research Centre of Finland, VTT Publications 287, 47p.

Morey, G. W., Kracek, F. C. and Bowen, N. L. (1930) *The ternary system K2O-CaO-SiO2* Journal of the Society of Glass Technology, pp. 149-187.

Moilanen, A. and Kurkela, E. (1995) *Gasification reactivities of solid biomass fuels*. Am. Chem. Soc. Div. of Fuel Chem., v 40, n 3, Preprints of Papers Presented at the 210th ACS National Meeting Chicago, August 20-24, 1995 Chicago, pp. 688-693.

Moilanen, A., Sørensen, L.H., Gustafsson, T.E, Laatikainen-Luntama, J. and Kurkela, E. (2001) *Characterisation method of biomass ash for gasification.* In: Progress in Thermochemical Biomass Conversion, September 2000, Tyrol, Austria, pp. 122-136.

Nordin, A (1994) *Chemical elemental characteristics of biomass fuels*. Biomass and Bioenergy, v 6, n 5, 1994, pp. 339-347.

Pelton, A. D. and Blander, M. (1986) *Thermodynamic analysis of ordered liquid solutions by a modified quasichemical approach - application to silicate slags.* Met. Trans. B., v 17B, 1986, pp. 805-815.

Wu, P., Eriksson, G. and Pelton, A. (1993) *Optimization of the thermodynamic properties and phase diagrams of the Na2O-SiO2 Systems*. J. Am,. Ceram. Soc., v 76, n 8, pp.2059-2064.

Wu, P., Eriksson, G. and Pelton, A. (1995) *Critical evaluation and optimization of the thermodynamic properties and phase diagrams of theCaO-FeO, CaO-MgO, CaO-MnO, FeO-MgO, FeO-MnO, and MgO-MnO systems*. J. Am. Ceram. Soc., v 76, n 8, pp. 2065-2075.

Paper II:
CO2 reactivity of chars from wheat, spruce and coal.
In proceedings: Progress in Thermochemical Biomass Conversion, September 2000, Tyrol, Austria

CO2 reactivity of chars from wheat, spruce and coal

H. Risnes, L. H. Sørensen* and J. E. Hustad
Department of thermal energy and hydropower, The Norwegian University of Science and Technology, Trondheim, Norway
** ReaTech c/o Center for Advanced Technology (CAT), Frederiksborgvej 399, Postbox 30, DK-4000 Roskilde*

ABSTRACT: Measurement and modelling of CO_2-gasification reactivity is presented for two biomass char species: Danish wheat straw (d_p<150μm, prior to devolatilisation) and Norwegian spruce char (d_p< 63μm); and a dense metallurgical coke from Longyear coal (d_p < 45 μm). The reactivity was thermogravimetrically determined using 4-10 mg of pre-pyrolysed char samples, CO_2-partial pressure (0.03-1 bar) and sample temperature (700-1000°C). Char reactivity (R) is expressed by separating the effects arising from true kinetics (r_C) and structural development ($f(X)$), the resulting function: $R = r_C \cdot f(X)$. r_C is modelled by n^{th} order kinetics. $f(X)$ was separated from r_C by normalising R with respect to a reference profile (R_{ref}). Over the considered pressure and temperature range, reactivity varies considerable, but the structural profile is in general approximately invariant, i.e. each sample apparently exhibits consistently the same structural evolution for a broad span of kinetic conditions as one prerequisite for good kinetics determination. The structural profile is dependent on reactant gas (O_2 or CO_2) and different for each carbonaceous material. Significant structural profile invariance to conversion and CO_2 partial pressure was illustrated for a Longyear coke at 1000°C. Applying nth order kinetics, for $r_C(X=0.5)$, the following kinetic parameters were obtained: apparent activation energies (E_a) for wheat straw char; 205.6 [kJ/mol], spruce char; 219.9 [kJ/mol] and Longyear coke; 233.1 [kJ/mol], the respective reaction orders (n) equals 0.59, 0.36 and 0.51.

INTRODUCTION

Use of biomass, being a renewable energy source, for heat and power production has become more interesting due to a growing concern for both man made pollution and future energy demand. Gasification is one of the more promising technologies for thermochemical conversion of solid fuels, i.e. biomass, waste and coal (TERES[1] and Bridgewater[2]). To use biomass-derived fuels in gasification processes, as substitutes for conventional fossil fuels, demands examination of several aspects, both operational and environmental. These aspects include ease of handling, gasification reactivity, propensity for producing aerosol or gaseous pollutants, and the tendency of inorganic components to cause fouling or corrosion of burner and boiler surfaces.

Char conversion is typically the rate-limiting step during combustion and gasification of solid fuels. The magnitude and variation of char reactivity during gasification are, therefore, of primary concern when comparing results from different

solid fuels such as coal and biomass. Although this literature provides valuable information related to specific aspects of char reactivity, there is a need for further discussion of the validity range of the determination and extrapolation of reactivity data for coal and biomass.

Experimental data for CO_2 gasification of chars have been reported using TGA, fixed bed, laminar flow (drop tube), entrained flow or fluidised bed reactors. The mechanism of this reaction is not yet fully understood. It is generally believed that CO_2 adsorption on the surface of char (oxygen transfer) followed by CO desorption (carbon removal) are the main steps determining the apparent rate[3-6]. This mechanism can be further simplified by proposing the Langmuir-Hinshelwood type rate expression[7]. For the following discussion a simple nth order reaction is sufficient. The reviewed literature reports both fractional values of n [8-15] and alternative reaction schemes[3,16-32] (e.g. 1st order and Langmuir-Hinshelwood type expressions). Most of the experimental studies[4,8,9,16-23,31,32] are directed towards a packed-bed gasification, with very limited work on single particle behaviour[10,11,24-26,33-36].

Kinetic parameters from selected publication on CO_2 reactivity are shown in *Table* 1. A wide span of apparent activation energies is published: for biomass chars, 80.3 kJ/mol [8] -318 kJ/mol [23] and for coal chars, 79 kJ/mol [38] -359.5 kJ/mol [39]. Some of the discrepancy can be explained as due to different experimental procedures (such as sample load, particle size and sample preparation) and the application of different analysing equipment. Concerning the latter one, the potential role of systematic errors in temperature measurements among various thermobalances is evident[40]. Variations might also be explained by different extraction procedures, lack of accuracy caused by the approximations used in the different computational methods and the kinetic compensation effect.

Many researchers have tried to correlate the kinetic rates of carbon gasification to the many physical and chemical properties of the different materials used. Despite of this a universal rate expression does not exist. Furthermore it is difficult to find data operational for reactor simulations in the relevant temperature and partial pressure ranges. In particular the variation of the reactivity with conversion due to structural variations is not dealt with, i.e. the structural profile is seldom explicitly given.

In the present paper investigation are made in order to produce operational data for the gasification reactivity for biomass chars and coal chars. Furthermore the differences between chars derived from biomass and coal is illustrated. Thermogravimetric analyses have been used to obtain information about the kinetic values of the C-CO_2 reaction.

THEORETICAL

For a solid fuel, the char reactivity towards a reactive gas is usually defined in terms of the conversion rate per remaining mass[7]:

$$R = -\frac{1}{m}\frac{dm}{dt} = \frac{1}{1-X}\frac{dX}{dt} \qquad (1)$$

where m is the mass of the organic portion of the sample, dm/dt is the conversion rate and X is the degree of conversion, $X = (m\text{-}m_0)/m_0$. The reactivity is measured versus

Table 1 Summary of kinetic parameters available in the literature. Experiments conducted under conditions (fixed bed of particles, particle size, temperature and pressure ranges etc.) comparable to this work.

Char origin	$ln(k_0)$ *[1/min]*	E_a [kJ/mol]	n [-]	P_{CO2} [atm]	d_p [μm]	m_s [mg]
Wheat straw*	19.67	205.6	0.59	-1	<150	5
Spruce*	20.96	219.9	0.36	-1	<63	5
Longyear coke*	18.66	233.1	0.51	-1	<45	10
Birch[12]	19.04	215	0.38	-1	32-45	5
Eukalyptus kraft lignin[16]		230-233	- ***	1	45-53	10
Coal[28]	22.73 22.96	189 212	- ***	1	105-74	5 (pp)
Coal[13]	16.45	212.9	0.89	0.21-1	75-125	2
Coal[30]		213-251	- ***	100****	<100	<63
Coal[14]		238.6	0.5-0.6	0-1	45-73	3
Carbons[3]		243 +/-13	- ***		106-250	50
Coal[37]		243-260	- ***	1	<75	20-50

* -This work, ** -Prior to devolatilisation *** -No reaction order dependency is given, **** -kPa

conversion and may in order to obtain kinetics be sought split into a chemical kinetics term (r_c), and a structural profile ($f(X)$). The structural profile is often implicitly or explicitly with success assumed to summarise the effect of available internal surface, available active/reactive sites and pore-evolution and to be invariant over the relevant T-P domain[41,42]. For CO_2 gasification one then finds $R = r_c(T, P_{CO2}) \cdot f(X)$. To illustrate that the invariant structural profile assumption is not always valid one may instead write

$$R = r_C\left(T, P_i, c_r\right) f\left(X, \boldsymbol{P}, T, c_f\right) \tag{2}$$

Where c_f is a structural parameter that counts available reactive carbon sites and c_r is a coefficient that account for distribution of reactive carbon sites types and catalytic effects and thus a variation in c_r may change kinetic parameters. The gas composition vector ($\boldsymbol{P}$) in $f(X)$ may beside the CO_2 partial pressure also include such gas partial pressures as KOH since the likelihood that a catalytic site is activated is a function of the partial pressure of the catalyst, the site-catalyst attraction forces and the temperature. Since from *Eq.* (2) the structural profile invariance 'SPI' assumption is by no means obvious we suggest that a temperature and partial pressure range are always given for the validity of the structural profile invariance assumption. Only if the invariant structural profile assumption is approximately valid a reference profile (R_{ref}) can be used to eliminate the structural profile to form a normalised reactivity (R_n) and to determine kinetics up to a constant

$$R_n = < \frac{R(X)}{R_{ref}(X)} > \tag{3}$$

The proposed Langmuir-Hinshelwood kinetics[43] expression for the gasification reaction (CO_2, N_2 and CO gas mixture) is given by[7]:

$$r_C = \frac{k_{1f} P_{CO2}}{1 + aP_{CO2} + bP_{CO}} \qquad (4)$$

This more complex rate expression can describe both, saturation by the reactant gas and inhibition by the product gas. However, for to obtain data in the present work no external CO was added to the reactant gas and the simpler nth order reaction scheme was applicable

$$r_C = k P_{CO2}^n \quad , \; k = k_0 \cdot \exp(-E/RT) \qquad (5)$$

Both E and n were calculated using the Marquart-Levenberg least square algorithm. The sum $SS = \sum w (R_{calc}-R_{exp})^2$ was explicitly used to minimise effects of non-uniform errors. By applying the weight function $w = 1/R^2_{exp}$ all data points are considered equally significant.

Char reactivity versus conversion

Comparing rates at a given conversion (eg. initial rate) is frequently done in kinetic studies. In most cases the initial 10% or 50% of the conversion is used for evaluating the kinetic parameters. For most chars of coal, lignite and peat, the reactivity decreases with increasing conversion or time, whereas for most chars of biomass it increases. Reactivity can also exhibit a maximum or a minimum. Tancredi et al.[20] and Rodriguez-Mirasol et al.[44] explains the steep reactivity increase at high conversion levels, often seen for biomass chars, as a result of an increasing catalytic effect of the metallic constituents of the inorganic matter present in the char. McKee et al.[45] found the activity of alkali and alkaline earth metal salts to decrease in the order *Cs>K>Na>Li>>Ba>Sr>Ca*, in catalytic gasification. Alkali metals being approximately ten times more active than alkaline earth metals. (Also observed for a lignite char and graphite). Moilanen[46] correlated gasification rates and ash composition, and found that especially the rates at higher fuel conversions seemed to decrease with increasing silica content in the fuel. This indicates that catalytic active ash components can loose their activity due to reactions with silica, or due to sintering behaviour.

To derive the kinetics for a char or coke, with respect to a specific reactant gas, the normalised reactivity R_n must be constant and hence the structural profile $f(X,\mathbf{P},T,c_f)$ invariant at all the relevant experimental conditions.

Defining f(X)

In the following the structural function is simplified and described as a function of X only (i.e. $f(X)$). $f(X)$ is calculated from the experimental values in the range $0.1 \leq X \leq 0.9$ and extrapolated for $X<0.1$ and $X>0.9$. The structural profile is modelled through a polynomial $f(X) = A_0+A_1X+A_2X^2+A_3X^3+A_4X^4+A_5X^5+A_6X^6$. R_n is defined as the average value of the normalised profile times the reactivity of the reference profile at 50% conversion. Thus the reactivity is modelled as:

$$R = r_C \cdot f(X) \qquad (6)$$

, where $f(X=0.5)$ is defined to be 1.0. The uncertainty in measured reactivity is often large for low degrees of conversion (X), before the particles pore structure has opened up and experimental conditions have settled. The uncertainty in the measured reactivity will also increase as m goes to zero. Kinetics determinations are therefore limited to values of the normalised reactivity (R_n) within the conversion interval from $X = 0.2$ to 0.8.

EXPERIMENTAL SECTION

Reactivity profiles were measured vs. conversion over a broad range of temperatures and carbon dioxide partial pressures for all three chars. A reference reactivity profile (R_{ref}) was chosen and used to eliminate the structural profile in the relevant experiments. Kinetic parameters are calculated by using both the normalised reactivity (R_n) and the reactivity at 20, 40, 60 and 80% conversion (R_{X20}, R_{X40}, R_{X60} and R_{X80}). Calculated reactivities are compared.

INSTRUMENTAL

In the atmospheric experiments an "SDT 2960, TA-instruments simultaneous differential and thermal gravimetric analyser" were used to determine the CO_2-gasification reactivity under isothermal conditions. The samples were kept isothermal for 10 minutes in N_2 at 150°C, before the sample temperature was increased (heating rate 30°C/min) to the defined reaction temperature and switching to the N_2/CO_2 mixture. The gas flow used was 400 ml/min. Ash was determined by increasing the temperature to 1000°C for complete conversion.

SAMPLES

The investigations are made on two biomass chars derived from wheat straw and spruce, and a dense metallurgical coke derived from Longyear coal. Sample loading was around 4 mg for the biomass samples and 10 mg for the Longyear coke. Wheat samples were prepared from a batch of wheat straw bales. The straw was grounded to a particle size < 150 μm and pyrolysed in a pressurised entrained flow reactor (2-3s at 900°C and 15 bar N_2[47]). The char derived from spruce (d_p < 63 μm) was produced at atmospheric conditions. The Longyear coke (d_p < 45 μm) was prepared from cooking a high volatile coal at approximately 1000°C for several hours[41,48,49]. In all cases nitrogen was used for the devolatilisation.

Kinetics are determined based on gasification experiments made at atmospheric conditions, and CO_2-partial pressures equal to 0.03, 0.20, 0.50 and 1.0 bar. The

gasification temperature varied between 700 and 1000°C, in steps of 50 degrees. For each char the reference reactivity profile was measured over a broad conversion interval.

RESULTS

EXPERIMENTAL EVALUATION OF GASIFICATION REACTIVITY

Isothermal experiments

Reactivity profiles obtained from all three chars are evaluated by using the normalisation procedure. The quality of this procedure is indicated by the calculated standard deviation (σ) relative to the reference profile: *a*) Wheat straw: 11 out of 14 experiments shows $\sigma < 5.8\%$, *b*) Spruce: 9 out of 12 shows $\sigma < 5.9\%$ and c) Longyear coke: experiments below 1000°C shows an extremely good fit, $\sigma < 2.4\%$. At 1000°C $f(X)$ changes dramatically for Longyear coke, as the CO_2 partial pressure is reduced from 1.0 to 0.03bar. (The calculated standard deviations are based on R_n ($0.2 \leq X \leq 0.8$) and a step size of $\Delta X = 0.002$.)

Wheat straw*:* A total of 14 isothermal and isobaric runs were made at atmospheric conditions. Gasification temperatures were 700, 750, 800 or 850°C and CO_2-partial pressure were 0.03, 0.20, 0.50 or 1.0 bar. Rathmann et al.[47] investigated CO_2-gasification reactivity for wheat straw at pressurised conditions and found the effect of the total pressure to be insignificant, at a constant CO_2 partial pressure. Sørensen[39] obtained the same conclusion from combustion (O_2) reactivity studies. However, external addition of carbon monoxide, resulted in decreased gasification reactivity and a change in the reactivity profile. In the present study the same char sample as used by Rathmann[47] was investigated at atmospheric conditions.

Spruce: Kinetic parameters for a Norwegian spruce char are calculated based on 12 isothermal experiments. No marked effect of *CO*-inhibition or CO_2-saturation seems to be present between 750-850°C and 0.03-1.0 bar CO_2.

Longyear coke: Because of the dramatically change of reactivity profile at 1000°C, experimental data obtained at 1000°C and 0.20 and 0.03bar CO_2 are not used to determine the kinetic parameters but added to the plot in order to show the error that may otherwise be introduced.

Evaluation of the structural profile

Fig. 1 shows a comparison of the reference profiles normalised to the reactivity at $X = 0.2$. This reveals a pronounced difference in the development of the overall reactivity as a function of conversion. For the spruce char the overall reactivity increases with a factor of 2.8 between $X = 0.2$ and 0.8, while wheat straw char and Longyear coke gives 1.0 and 1.2 respectively.

For the Longyear coke the reactivity profile at 1000°C showed an unexpected behaviour. At 1.0 bar CO_2, $f(X)$ approximately equals the reference profile observed at lower temperatures (increasing with conversion, $R_{0.8}/R_{0.2} = 1.2$), while the profile at 0.03

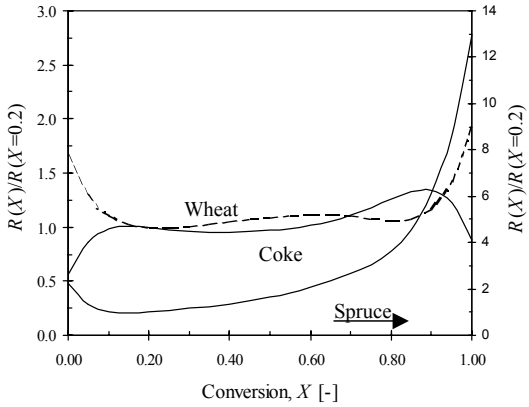

Fig. 1 Comparison of different reactivity profiles from the analysed chars.

bar shows a marked decrease ($R_{0.8}/R_{0.2}$ = 0.4). In the former case activation and the latter case deactivation of the char is observed (*Fig. 2*). The profile obtained at 1000°C and 0.2 bar is also shown in Figure 2. The reactivity profiles obtained at 1000°C were validated. The CO_2 reactivity profile at 0.03 bar CO_2 and 1000°C is fairly similar to the O_2 reactivity profile obtained in air at 600°C by Sørensen[41]. This indicates that the same sites may eventually be non-catalytic and be responsible for the pore and site evolution in both these cases. Alternatively a time dependent deactivation may take place for T≥1000°C.

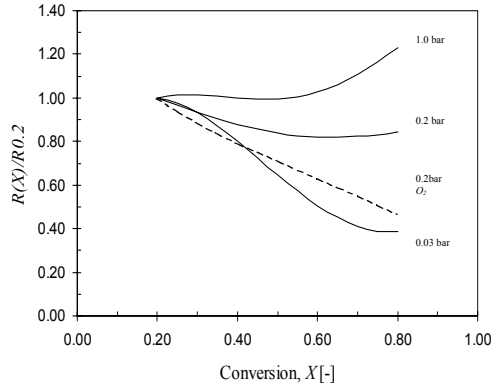

Fig. 2 Changing reactivity profile for the Longyear coal, at 1000°C.

DISCUSSION

The results obtained from the kinetic determination are shown in *Table 2* and *Fig. 3*. Experimental values and the results from *n*th order kinetics are shown in *Fig. 4*. Taken into account the wide span of E_a (79 kJ/mol [38]-359.5 kJ/mol [39]) and n (0-1) reported in the literature the results reported in this study is found to be within a relatively narrow range. Our results are in general agreement with the data shown in *Table 1* (205.6-233.1 vs. 189-260 kJ/mol and. 0.36-0.59 vs. 0.38-0.89 respectively). Miura[50], in his review, reported activation energies for coal chars in the range 190-210 kJ/mol.

The structural profiles of both biomass chars show consistency within the studied temperature and pressure range. This result is in agreement with earlier findings[51]. Our reactivity profiles obtained under different reactants (e.g. CO_2 and O_2) gives reactant specific reactivity profiles. Which is consistent with Salatino[13] and Floess[51].

Table 2 Reference profile $f(X)$, and kinetic parameters for *n*th order kinetics. Standard deviation is calculated, assuming 95% confidence interval and given in *%(±)*. Experimental data are assumed to be normal distributed.

	ln(k$_0$)[1/min]	*E[kJ/mol]*		*n [-]*			*f(X)*
Wheat straw			(±)		(±)	A_0	1.2334E+00
X=0.2	18.21	193.8	3.8	0.52	0.02	A_1	-3.7472E+00
X=0.4	19.68	205.9	0.2	0.60	0.02	A_2	2.1309E+01
X=0.6	20.03	208.6	0.3	0.62	0.03	A_3	-7.2306E+01
X=0.8	20.41	213.1	0.6	0.55	0.04	A_4	1.4679E+02
$R_{c,norm}$(X=0.5)	19.67	205.6	0.3	0.59	0.02	A_5	-1.5311E+02
						A_6	6.1511E+01
Spruce			(±)		(±)	A_0	1.5399E+00
X=0.2	20.07	215.3	0.4	0.35	0.02	A_1	-1.9650E+01
X=0.4	21.03	222.0	0.3	0.37	0.02	A_2	1.5876E+02
X=0.6	20.65	215.4	0.7	0.40	0.04	A_3	-5.9680E+02
X=0.8	21.11	215.6	0.7	0.34	0.04	A_4	1.1513E+03
$R_{c,norm}$(X=0.5)	20.96	219.9	0.4	0.36	0.02	A_5	-1.0900E+3
						A_6	4.0332E+02
Longyear			(±)		(±)	A_0	5.7762E-01
X=0.2	18.81	234.2	0.3	0.52	0.02	A_1	8.9778E+00
X=0.4	18.98	236.4	0.3	0.51	0.03	A_2	-6.2449E+01
X=0.6	18.29	228.8	8.3	0.51	0.03	A_3	2.0354E+02
X=0.8	18.95	233.5	0.3	0.52	0.02	A_4	-3.4601E+02
$R_{c,norm}$(X=0.5)	18.66	233.1	0.6	0.51	0.02	A_5	2.9850E+02
						A_6	-1.0232E+02

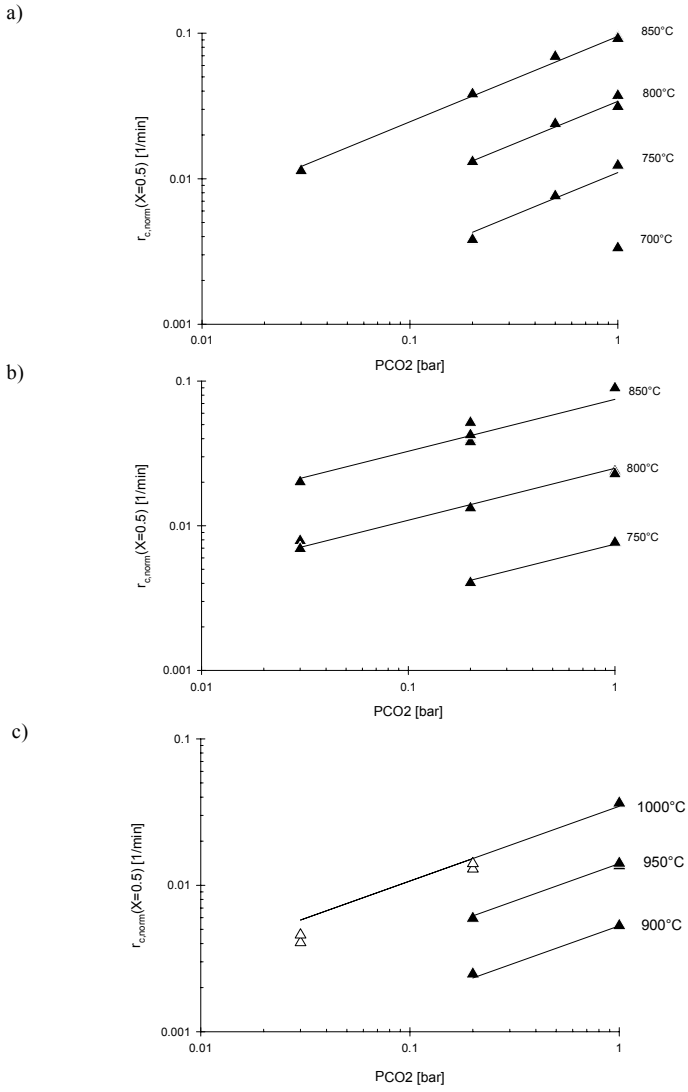

Fig. 3 Reactivity ($r_{c,norm}$ (X=0.5) = $r_C(T, P_{CO2}) \cdot f(X$=0.5)) for a) wheat straw char, b) spruce char and c) longyear coke, presented in a log(R)-log(P_{CO2}) diagram (Δ = experiments not included in kinetic analysis). Solid line: reactivity as calculated by the nth order kinetic model.

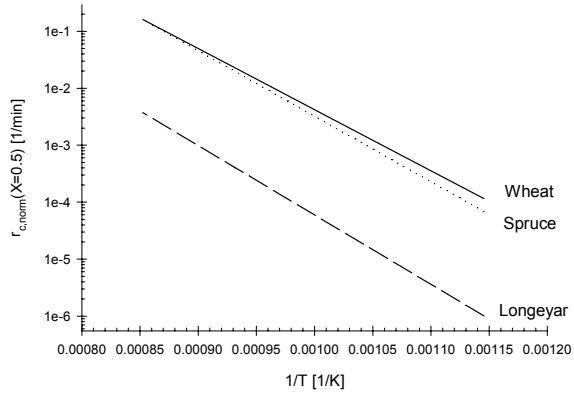

Fig. 4 Comparison of the obtained reactivity (at $X = 0.5$) for char from wheat spruce, and coke ($P_{CO2} = 0.5$bar).

The observed shift in the reactivity profile for the Longyear coke was highly unexpected. A similar effect has not been found in the reviewed literature. Introduction of mass transfer effects would be expected to result in the reverse effect, i.e. increasing char reactivity at higher degrees of conversion. We suggest that the observed effect is caused either by a shift in reactive site distribution, by thermal annealing or a time dependent deactivation of the catalytic sites. Thus, the parameters in c_f and c_r in *Eq*. 2 can not be ignored This observed behaviour illustrates that the reactivity profile and thus kinetic data for the Longyear coke cannot be extrapolated to beyond $T \geq 1000$°C. A more precise description of this phenomena demands further investigations.

A comparison of the reactivity of wheat, spruce and Longyear coke is shown in *Fig.* 4. The two biomass chars exhibit almost identical reactivity while the reactivity for the much more dense metallurgical coke is clearly lower. This is in general agreement with the reviewed literature.

CONCLUSION

For all fuels tested the *n*th order kinetic models gives a good representation of the thermogravimetrically determined CO_2-reactivity. Since normalised reactivity was approximately independent of conversion, for each char, one reaction order, and activation energy could be estimated for the whole range of temperature and CO_2 partial pressures. Applying *n*th order kinetics the following kinetic parameters were obtained (atmospheric experiments): apparent activation energies (E) for wheat straw char; 205.6 [kJ/mol], spruce char; 219.9 [kJ/mol] and Longyear coke; 233.1 [kJ/mol], the respective reaction orders equals 0.59, 0.36 and 0.51. In the investigated temperature (T) and CO_2-partial pressure (P_i) range, using normalised reactivity (R_n) and the reactivity at 20, 40, 60 and 80% conversion (R_{X20}, R_{X40}, R_{X60} and R_{X80}) for kinetics determination gives similar results, as expected in the case of an invariant structural profile *f(X)*. O_2 and CO_2 give reactant specific and different reactivity profiles. For the Longyear coke partial pressure dependent reactivity profiles were

measured and discussed. A simple nth order reaction and an invariant structural profile assumption was used under the evaluation of experimental data. (see *Eq*. 6). However, the results indicated that a more complex mechanism, e.g. *Eq*. 2, must be considered if the results, even for a single pure gas, are to be extrapolated to their limits for the purposes of modelling reactor data under realistic conditions.

REFERENCES

1. TERES (1994) The European Renewable Energy Study; Prospects for renewable energy in the European Community and Eastern Europe up to 2010 (ALTENER PROGRAM). Main report made for the "Commission of the European Communities, Directorate General for Energy (DGXVII). Brussels, Belgium
2. Bridgewater A. V. (1995) Fuel, **74**, p. 631-635
3. Freund, H. (1985) Fuel, **64**, p. 657-660
4. Ergun, S. (1956) Phys. Chem., **60**, p.480-485
5. Walker Jr., P. L., Rusinko Jr. F. & Austin L.G. (1959) Advan. Catalysis., **11**, p. 133
6. Matsui, I., Kunii, D. & Furusawa, T. (1987) Ind. Eng. Chem. Res., **26**, p. 91-95
7. Laurendeau, N-M. (1978) Prog. Energy Combust. Sci.
8. Plante, P., Roy, C. & Chornet, E. (1988) The Canadian Journal of Chemical Engineering, **66**, p. 307-312
9. DeGroot, W. & Shafizadeh F. (1984) Fuel, **63**
10. Standish, N. & Tanjung A.F.A. (1988) Fuel **67**
11. Groeneveld, M. J. & van Swaaij, W.P.M. (1980) Chem. Eng. Sci. **35**, p. 307-313
12. Barrio, M & Hustad, J. E. CO2 gasification of birch char and the effect of CO inhibition on the calculation of chemical kinetics. *This conference*
13. Salatino, P., Senneca, O. & Masi, S. (1998) Carbon, **36**, p. 443-452
14. Hampartsoumian, E., Murdoch, P.L., Pourkashanian, M., Trangmar, D.T. & Williams, A. (1993) Combustion science and technology, **92**, p. 105-121
15. Roberts, D.G. & Harris, D.J. (2000) Energy & Fuels **14**, p. 483-489
16. Rodriguez-Mirasol, J., Cordero, T. & Rodriguez, J. J. (1993) Carbon, **31**, p. 53
17. Dutta, S., Wen, C. Y. & Belt, R. J. (1977) Ind. Eng. Chem., Process Des. Dev., **16**, p. 20-30
18. Salles, J. E. F., De Castro, L. F. A. & Tavares, R. P. (1985) Metallurgia-ABM, **41**, 15
19. Li, J. & van Heiningen, A R. P. (1990) Ind. Eng. Chem. Res., **29**, p. 1176
20. Tancredi, N., Cordero, T., Rodriguez-Mirasol, J. & Rodriguez, J. J. (1996) Fuel, **75**, p. 1505-1508
21. DeGroot, W. & Richards, G. (1989) Carbon **27**, p. 247-252
22. Turkdogan, E. T. & Vinters, J. V. (1970) Carbon, **8**, p. 39
23. Blackwood, J. D. & Ingeme, A. J. (1960) Austral. J. Chem., **11**, p.194-209
24. Capart, R., Gelus, M., Lesgourgues, M. & Li, Z. (1989) Pyrolysis and gasification, London (UK) Elsevier Applied Science, p. 593-597
25. Dasappa, S., Paul, P. J., Mukunda, H. S. & Shrinivasa, U. (1994) Chem. Eng. Sci., **49**, p. 223-232
26. Whitty, K. J. (1997) Ph.D. dissertation, Åbo Academy, Combusiton Research Group Report , R97-3
27. Zamalloa, M., MA, D. & Utigard, T.A. (1995) ISIJ International, **35**, p. 458-463
28. Kovacik, G., Chambers, A. & Ozum, B. (1991) Canadian Journal of Chemical Engineering, **69**, p. 811-815

29. Wu, P.-C., Lower, W. E. & Hottel, H. C. (1988) Fuel, **67**, p. 205-214
30. Radovic, L. R., Jiang, H. & Lizzio, A. A. (1991) Energy & Fuels, **5**, p. 68-74
31. Kasaoka, S., Sakata, Y., Shimada, M. & Matsutomi, T. (1985) Journal of Chem. Eng. of Japan, **18**, p. 426-432
32. Mulhen, H. J., Heek, K. F. & Juntgen, H. (1985) Fuel, **64**, p. 944-949
33. Mukunda, H. S., Paul, P. J., Srinivasa, U. & Rajan, N. K. S. (1984) In: Proceedings of the 20th International Symposium on Combustion, pp. 1619-1628, the combustion institute
34. Reyes, S. & Jensen, K. F. (1986) Chem. Eng. Sci. **41**, p. 333-343
35. Reyes, S. & Jensen, K. F. (1987) Chem. Eng. Sci. **41**, p. 345-354
36. Morell, J.I., Amundson, N.R. & Park, S.K. (1990) Chem. Eng. Sci. **45**, p. 387-401
37. Calemma,V. & Radovic, L. R. (1991) Fuel, **70**, p. 1027
38. Kwon, T.W, Kim, S.D & Fung, D.P.C. (1988) Fuel vol. 67 , no. 4, p. 530-535
39. Walker Jr., P. L. Rusinko Jr. F. & Austin L.G. (1959) Advan. Catalysis. vol 11, s. 133, 1959.
40. Grønli, M. G., Antal, J. A, Jr. & Várhegyi, G. (1999) Ing. Eng. Chem. Res., **38**
41. Sørensen, L. H. (1996) Ph.D. disstertation, Risø national laboratory, Danmark, Risør-R-838(rev.)(EN)
42. Sørensen, L. H., Gjernes E., Jessen T. & Fjellerup J. (1996) Fuel, **75**, p. 31-38.
43. Rief, A. E. (1952) Journal of Phys. Chem., **56**, p. 785-788
44. Rodriguez-Mirasol, J., Cordero, T. & Rodriguez, J. J. (1993) Energy & Fuels **7**, p. 133-138
45. McKee, D. W. (1983) Fuel, **62**, p. 170-175
46. Moilanen, A. & Kurkela, E. (1995) Preprints of papers, American Chemical Society, Division of Fuel Chemistry, 40, p. 688-693
47. Rathmann, O. & Illerup J.B. (1996) Dep. of Combustion Research, RISØ National Laboratory, Denmark, RISØ R-873 (EN)
48. Hustad, J.E., Aho, M.J., Hupa M., Noopila, T., Sørensen, L.H., Clausen S., Kiørboe, L., Gromulski, J., Bengtsson M. & Leckner B. (1990) La Rivista dei Combustibili, **10**, 257.
49. Hustad, J. E. (1990) Ph.D. dissertation, Norwegian Institute of Technology
50. Miura, K., Hashimoto, K. & Siverston, P. L. (1989) Fuel, **68**, p. 1461-1475
51. Floess, J. K., Longwell, J. P. & Sarofim, A. F. (1988) Energy & Fuels **2**, p. 18-26

Paper III:

Steam gasification of wood char and the effect of hydrogen inhibition on the chemical kinetics. In proceedings: Progress in Thermochemical Biomass Conversion, September 2000, Tyrol, Austria

Included in Appendix II

Paper IV:

Risnes, H., Fjellerup, J., Henriksen, U., Moilanen, A., Norby, P., Papadakis, K., Posselt, D. and Sørensen, L. H. (2002) *Calcium addition in Straw Gasification*

Submitted for publication in FUEL

Calcium Addition in Straw Gasification

Risnes, H.[2], Fjellerup J.[1], Henriksen, U.[3], Moilanen, A.[4], Norby, P.[5], Papadakis, K.[1], Posselt. D.[6] and Sørensen, L. H.[1*]

[1]*ReaTech, Frederiksborgvej 399, P.O.Box 30, DK-4000 Roskilde, Denmark. Telephone +45 46775932*
[2]*Norwegian University of Science and Technology, Dep. of Thermal Energy and Hydropower, N-7491 Trondheim, Norway*
[3]*Technical University of Denmark, Dep. of Mechanical Engineering, Biomass Gasification Group, DK-2800 Kgs. Lyngby*
[4]*VTT Energy P.O.Box 1601, FIN-02044 VTT, Finland*
[5]*University of Oslo, Dep. of Chemistry, N-0315 Oslo, Norway*
[6] *Roskilde University, Dep. of Mathematics and Physics, P.O. Box 260, DK-4000 Roskilde, Denmark*
**: To whom correspondence should be addressed.*

ABSTRACT

The present work focuses on the influence of calcium addition in gasification. The inorganic-organic element interaction as well as the detailed inorganic-inorganic elements interaction has been studied. The effect of calcium addition as calcium sugar/molasses solutions to straw significantly affected the ash chemistry and the ash-sintering tendency but much less the char reactivity. Thermo balance test are made and high-temperature X-ray diffraction measurements are performed, the experimental results indicate that with calcium addition major inorganic–inorganic reactions take place very late in the char conversion process. Comprehensive global equilibrium calculations predicted important characteristics of the inorganic ash residue. Equilibrium calculations predict the formation of liquid salt if sufficient amounts of Ca are added and according to experiments as well as calculations calcium binds silicon primarily as calcium silicates and less as potassium calcium silicates.

Keywords: biomass gasification reactivity, ash sintering, global equilibrium calculations

1. INTRODUCTION

Gasification of biomass fuels is carried out in two steps, e.g. gasification in fixed or fluidised beds (normally from 700 to 1000°C) followed by combustion of the product gas. Alternatively the product gas can be co-combusted with other fuels such as coal, oil or natural gas[1].

In biomass gasification normally 70-80 wt.% of the fuel is rapidly released as volatile matter. The remaining char fraction is relatively reactive compared to coal chars. This is due to the chemical and physical structure of the carbonaceous material itself, as well as the large internal surface area and the availability of catalytic elements such as potassium (K), sodium (Na) and calcium (Ca).

The low-density char residue is easily elutriated from the bed in fluidised bed gasifiers or combustors. In order to maintain a stable bed, addition of other granular materials (e.g. sand, dolomite, lime or limestone) is required[2].

The catalytic elements K and Na are mobile and volatile at normal bed temperatures. The high potential to form molten salt layers as well as highly viscous (K, Ca) oxide/silicate melts on ash and bed particles, represents a high potential for adverse sintering and defluidisation. Additionally heat transfer surfaces are corroded from salt deposits. These salts are primarily composed of alkali-chlorides, carbonates, and hydroxides and under combustion conditions additionally also sulphates.

Operational measures to decrease the tendency of agglomeration, sintering and salt deposition in fluidised beds are[3]: 1) decrease process temperatures and avoiding hot spots 2) fuel refinement (e.g. through leaching, thus extracting Na and K), 3) co-firing with fuels having less problematic ashes, 4) modifying the bed material size distribution and composition, or as will be focused on in the present paper 5) using additives.

Additives typically react with parts of the fuel ash suppressing the formation of high-viscous melts. One example is kaolin[4, 5], reducing the sintering tendency through the reaction with fuel K; on the other hand this depletes the mobile catalysts from the carbon surfaces, which reduces char reactivity. Thus, increased gasification temperatures are required to obtain identical conversion rates, which potentially introduces other melts. Magnesium oxide is another well-known additive/bed material that is apparently relatively efficient and even exhibiting catalytic properties[4]. Unfortunately high quality kaolin and magnesium oxide are rather expensive.

The utilisation of additives easily becomes costly and addition of too small or just unbalanced amounts of additives may even aggravate the behaviour of problematic fuels. Therefore additive addition in biomass gasification and combustion requires a detailed knowledge about the inorganic composition of the fuels, the reactivity of the additive towards

the inorganic fuel elements, the target ash residues, and the process conditions.

The focus in this paper is directed towards the quantitative utilization of Ca as an anti agglomeration and anti sintering additive. The novel CAS/CAM solutions incorporate enhanced Ca-availability (i.e. higher efficiency) as compared to the traditionally used limestone or lime. Although both limestone and lime is known to be fairly inexpensive the CAS/CAM solutions are competitive in price, being based on residues from the sugar industry. Ca-based additives are also known to exhibit catalytic properties[2].

2. THE INFLUENCE OF THE INORGANIC ASH FRACTION AND THE EFFECT OF FUEL ADDITIVE UPON CHAR REACTIVITY

Char reactivity is generally determined as $R = dX/dt/(1-X)$, where X is the degree of conversion. Sørensen[6] found for a leached straw that the char reactivity decreased with the degree of conversion, while the reactivity for raw and enriched straws increased. The reactivity was modelled[7] as $R_0=r_c f_0(X)$, where R_0 is the reactivity at a specific degree of conversion of the pure uncatalysed carbonaceous fuel of relevance, r_c is a chemical kinetics term and $f_0(X)$ is a structural profile[8].

Furthermore, Henriksen[9] observed that the reactivity of a straw sample increased approximately linearly until a four fold salt enrichment of the straw. These results indicate that the straw reactivity increase linearly within relevant additive concentrations. This is in accordance with Mims and Pabst[10] who added aqueous solutions of alkali carbonates to high-purity carbon and activated charcoal as well as an Illinois #6 coal char. Gasification reactivity (at 975°C in a H_2O/H_2 mixture) increased almost linearly with the K/C ratio until it stabilized around K/C ≈ 0.08.
These findings prove that biomass char gasification reactivity is influenced by the inorganic elements in the fuel, which is known to be highly diverse[11, 12] (Ca, K and Si normally accounts for 60 to 90% of the ash calculated as oxides). The Si content is typically very low for slowly growing wood species while accounting for up to about 50wt% in straw ash, while the Ca and K contents are to some extent interchangeable[13]. Other important elements to be considered count Mg, Al, Na, Cl and S. (The elemental composition of the fuels studied in the present work is given in Table 1 and 2).

Although the concentration of catalytic elements is relatively high in biomass chars, the presence of Si might reduce char reactivity due to the

reaction with K and Ca and the subsequent formation of catalytic inactive silicates. This is reported by Moilanen et al.[4] (steam gasification of a wheat straw qualitatively very similar to Wheat97, Table 2) who observed a reduction in the total amount of potassium (K_{tot}) and the water soluble potassium (K_{ws}) to (X, K_{tot}, K_{ws}) = (0, ~90%, ~75%) during fuel pyrolysis. This reduction continued to (0.5, ~85%, 50%) and (1, ~80%, ~15%) during char gasification. Furthermore, Moilanen & Kurkela[14] and Moilanen & Saviharju[15] found an inverse correlation between biomass Si content and char reactivity, being most pronounced at high fuel conversions.

A voluminous literature exists concerning more fundamental studies embracing catalysis in carbon gasification, some relevant findings with regard to the catalytic effect of K and Ca is summarised below.

Several authors stated that the effectiveness of Ca depends on its distribution on the carbon surface[16, 17, 18, 19]. Leboda[20] investigated the effect of Ca and found that the reactivity increased significantly in the order: R(raw sample) < R(impregnate sample) < R(ion exchanged sample). For 5 wt.% pure catalyst loaded on spectroscopic grade graphite, McKee[21] found (steam gasification at 800°C & 900°C) the catalytic activity of K_2CO_3 to be ~2.8 times larger than of KCl, ~9 times larger than of K_3PO_4 and ~50 times larger than the pure graphite. Heinemann et al.[22] suggest that a mixture of alkali and earth alkali oxides (e.g. K_2O-CaO) gives a higher catalytic activity than the pure species alone. Pereira[23] found for a spectroscopic grade graphite impregnated by nitrate solutions of K and Ca (i.e. 10mmolK/molC_{input} $850 \leq T \leq 900$K) that the K-Ca-O_x impregnated graphite was significantly more reactive than K_2O or CaO alone. The catalytic activities appeared to obey simple additivity and the authors suggested that the high activity probably were due to the inhibition, as stable $CaCO_3$ formed when using Ca alone.

This condensed literature review shows that although catalysis is significant in biomass gasification, the catalytic activity is strongly dependent upon fuel ash chemistry. Especially interesting is the formation of catalytic inactive K-Ca silicates vs. the formation of catalytic active salts. This topic is especially addressed in this work through global equilibrium analysis and detailed experimental studies of the inorganic ash chemistry.

3. GLOBAL EQUILIBRIUM ANALYSIS (GEA)

The global equilibrium approach is useful for a first description of the complex reactions taking place during biomass gasification. Recently, Blander[24] has tested several multi-component chemical equilibrium programs commercially available and Backman et al.[13] have reviewed the state of the art, possibilities and application. The present GEA has been obtained by using the FACT equilibrium program[25], incorporating the CHEMSAGE algorithm for free energy minimisation.

How well GEA adequately reproduce reactor results depends on the completeness of the thermodynamic data set used. If important compounds or solution phases are not available within the database, or if the calculations include very thermodynamically stable compounds/phases that are kinetically prohibited within the relevant timescale of the considered process, this will inevitably lead to misleading results. This requires modelling and experimental verification to be conducted in an iterative procedure, based on detailed knowledge about the chemical systems of interest.

For the present gasification study the input for the equilibrium model is the input flows in terms of the elemental composition of the selected fuels and additives as given in Table 1 and 2, together with air and steam (air ratio of 0.26). The elements: C, H, N, O and K, Ca, Si, Al, Fe, Mg, Na, Cl, P and S, are studied. Additionally possible output species and compounds as well as 19 solution phases (Table 3) are evaluated during the calculations, made in the range from 700 to 1000°C in steps of 10°C.

A summary of the solution phases included in our analysis is given in Table 3. Of particular importance are the Si rich glass/liquid solution "SLAG"-phase, a solid KCl/NaCl mixture phase "ACLA", a solid and a liquid K_2CO_3–$CaCO_3$ "SCSO"/"LCSO"-phase respectively and a liquid alkali (K, Na) -chlorides/carbonates "SALT" solution phase. The chemically distinctive oxide/silicate and salt system are assumed to be non-miscible. Clearly the extrapolation of miscibility/non miscibility observed for well-defined limited compositions to multi-component systems is uncertain as are the kinetics of the possible reactions between inorganic compounds and the presence of carbonaceous material.

The SLAG database contains more than 20 oxide components and is obtained from optimisation of more than 150 binary, ternary and higher order systems. Not all of the ternary combinations have been optimised,

and only a few higher-order systems have been studied. The properties of higher-order systems are estimated automatically from low order systems using the quasi-chemical model [26].

4. EXPERIMENTAL

4.1 Apparatus and procedures

One barley sample and four wheat samples (Table 1 and 2) were tested experimentally. The water content was around 10 wt.% in all samples. The dry ash content varies from 3.5 to 8.4 wt.%. Straw pellets were each pressed with a pressure of 15 tons and had a weight of approximately 4.5 g with an inherent amount of water equal to 0.4 g.

Volatile matter and ash contents of the pulverized biomass samples were analysed on a LECO TGA-500. A LECO CHN-600 instrument was used to determine the C, H, N and S (O by difference) were determined using a LECO Sulphur Determinator SC432. The compositions of the ashes (prepared at 550°C) were analysed by X-ray fluorescence spectroscopy. A thermo balance was used for steam gasification reactivity tests of 5mg char samples. A Macro-TGA[27] was used for H_2O reactivity tests of 1g char samples between 700 and 850°C. Ash residues were visually characterized in a Leica MZ12,5 stereo microscope by a sintering and agglomeration index "SAI" similarly as by Moilanen et al.[28], and by electron microscopy (SEM-EDX). The sintering and agglomeration index (SAI) is defined in steps of 0.5 in an interval from 0* to 3* [28], SAI=0* and 3* representing no and strong sintering respectively. X-ray diffraction was used for the analysis of the crystalline compounds generated during gasification. These were performed on a Siemens (Bruker) D5000 powder diffractometer in Bragg-Brentano geometry using Cu-Kα_1 radiation. Time resolved in-situ synchrotron X-ray powder diffraction studies were performed at the Swiss-Norwegian beam line (BM01B) at the European Synchrotron Radiation Facility, ESRF, using a wavelength of 0.8001Å. Time resolved diffraction data were collected using a MAR345 imaging plate detector. The ash and Ca-additive mixtures were contained in a micro reaction cell and were heated from T=300°C to 900°C in oxygen flow [29].

Ca was added in the form of a 10 wt.% CaO + 55 wt% H_2O and 35 wt% sugar or molasses to "CAS" or "CAM" solutions. Fresh lime and water are mixed and well stirred, before sugar or molasses is added and the stirring continued for around 5 minutes in order to prepare a CAS/CAM (calcium saccharate) solution. The molasses contained around 50 wt.% sugar, 2-5 wt.% K and 0.5-1 wt.% Na and 0.1-0.5 wt.% Ca[29].

4.2 Reactivity versus agglomeration

Ca was added to the Barley 95 straw pellets as CAM or CAS in the amounts of 1, 2 and 3 wt.% $Ca(OH)_2$. From each pellet around ~1g of char was prepared in a muffle oven by pyrolysing the pellets at 600°C in N_2. The chars were subsequently gasified in steam at 850°C in the macro-TGA and the conversion time "τ (min)" was taken as a reactivity measure. A SAI value was determined using a light microscope. The results are shown in Table 4. Within the apparatus resolution of the Macro-TGA, the reactivity for Barley 95 seems only little affected by the addition of the CAS and the CAM solution, while SAI decreased significantly from 3* to 0.5* as the amount of added Ca increased. We suggest that the addition of Ca to biomass may primarily have an indirect catalytic effect, e.g. by reacting with Si and hereby increasing the concentration of mobile K and Na. Apparently Ca does not significantly affect the behaviour of the inherent K_{ws}-catalyst until late in the char conversion process. This supports the observations made by Moilanen et al[4]. Viscous slag generation is suppressed due to interactions between the added Ca and the inherent inorganic fuel components.

Wheat 2000 was tested with 0, 1, 2 and 3 wt.% $Ca(OH)_2$ (added as CAM) the reactivity was not significantly affected and in all cases SAI=3*. Wheat 2000 being only 20% richer in K_2O but almost three times richer in SiO_2 than Barley95 might explain this. Hence, reducing SAI by Ca addition requires significantly larger amount of Ca-additive. (With respect to the [Ash, K_2O, SiO_2] in wt.% of dry fuel we have for Barley95: [4.8, 1.52, 1.49] and Wheat2000: [8.4, 1.83, 4.36].)

The reactivity of Wheat #2 and Wheat #4 was measured in the VTT thermobalance (experimental procedure described in Moilanen et al[4]) at 750 and 850°C (see Figure 1). SAI indicators are included in Figure 1 and Table 2). Wheat #4 is rich and Wheat #2 is moderate in K_2O and CaO. This explains the relatively high reactivity of Wheat #4. However in spite of the high K_2O content in Wheat #4, a low SAI index is obtained (SAI=1). This might be explained as due to the low SiO_2 content or more precisely the large K_2O/SiO_2 and CaO/SiO_2 ratios, which favours salt formation instead of silicate slag formation.

4.3 Characterisation of the ash residue

Beside K_2O, SiO_2 and CaO several inorganic components participate in the reaction. Therefore a more complex experimental and theoretical

data analysis was made in order to gain a more detailed and quantitative understanding of the observations.

The ash residues from the gasified Barley 95 samples were analysed using SEM-EDX. Ternary projections of the ash sample compositions obtained from as well spot as area analysis are shown in Figure 2 (Ca enrichment is clearly observed). An overall mean composition of the sample is illustrated by a drop-line drawn from pure Barley to CaO. The symbols "•" located on the drop line illustrates expected individual average ash composition for the addition of 2.5, 5, 7.5 and 10 times ψ[I]. ψ is defined equal to 10^3 times the molar ratio of Ca (e.g. 2.5mmolCa_{CAM}/molC_{input}) in the CAM/CAS additive and carbon in the raw fuel. (Thus, 10 ψ correspond to about 3wt% $Ca(OH)_2$/kg,df.) All but one of the spot and area analysis shows a projection on the SiO_2 rich side of the drop line. This is in accordance with devolatilisation of KCl or KOH during the gasification process. X-ray diffraction was used for the analysis of the crystalline compounds generated. The results are shown in Table 5. In the untreated barley ash sample K_2CaSiO_4, $K_4CaSi_3O_9$ and $KAlSiO_4$ (all containing K) are observed. Upon Ca addition (as CAS) Si is mainly bound in binary calcium silicate compounds, Ca_2SiO_4 and Ca_3SiO_5 and quartz (SiO_2) become significant while $K_4CaSi_3O_9$ and $KAlSiO_4$ vanished. K_2CaSiO_4 remained in all tests.

In order to experimentally investigate the effect of Ca addition to wheat straw at high temperatures, the Wheat#2 straw ash (ashed at 500 ^oC) was mixed with 2 wt.% $Ca(OH)_2$ (CAM reference solution). The sample was contained in a capillary based micro reaction cell with an oxygen flow of 2 ml/min. The temperature was ramped to 925^oC with a heating rate of 20^oC/min while performing in-situ synchrotron X-ray powder diffraction studies (Figure 3). Crystalline phases originally present are Portlandite ($Ca(OH)_2$), sylvine (KCl), α-quartz (SiO_2) and low angle scattering material that likely originates from the organic CAM mixture. At about 400°C the low–angle background decreases and eventually disappears at 525°C. $Ca(OH)_2$ decomposes into amorphous or ionic Ca containing compounds and as the combustion of the saccharate initiates at 400-450°C, $CaCO_3$ (calcite) is formed. No decrease in the intensity from KCl is observed until between 500 and 550°C, where a dramatic change is observed in the diagram. The low angle background vanishes due to complete burnout of the saccharate, the amount of calcite diminishes and all chloride in KCl is either devolatilised or reacted and released as HCl.

[I] ψ is equal to 1000 times the molar ratio of Ca in the CAM/CAS additive and carbon in the raw fuel

K_2CaSiO_2 and one or more calcium silicate phases are detected (Ca_2SiO_4/Ca_3SiO_5). This indicates that the added Ca is greatly reactive. Also the binary calcium silicate phases are abruptly formed around 525°C. The results above indicate that Ca in the present case mainly reacts with Si and to a minor extent with K. More tests will be done in order to test the relative importance of the atmosphere, the temperature and the presence of carbonaceous matter for the inorganic reactions.

5. EVALUATION OF ASH CHEMISTRY BY GEA

In the following a global equilibrium approach (GEA) is used for a more complex evaluation of the experimental results concerning the biomass ash reactions. An introductory discussion about condensed and gas phases in bio ash chemistry is followed by a theoretical evaluation of the effect of enriching straw fuel with Ca.

In the calculations discussed below, the SLAG solution has been reduced to include oxides only (K_2O, CaO, SiO_2, MgO, FeO, Na_2O and Al_2O_3) an often-applied assumption[13,30]. Thus, carbonates are found as the pure stoichiometric compounds $K_2Ca_2(CO_3)_2$(s) and $K_2Ca(CO_3)_2$(s). In particular upon Ca addition, the solid (K, Ca)-carbonate solution (SCSO) also formed.

According to Levin[31] ternary eutectics are found around 700°C in all of the following systems: K_2O-CaO-SiO_2 (~720°C); K_2O-Na_2O-SiO_2 (~540°C), K_2O-MgO-SiO_2 (~685°C) and K_2O-Al_2O_3-SiO_2 (~695°C). While the multi-component FACT-model predict formation of liquid/glass oxides (SLAG) even around 500°C, with Al_2O_3 included in the SLAG model. However, the SLAG prediction is based on equilibrium assumptions (no ternaries have been evaluated for the K_2O-CaO-SiO_2 system, on contrary to the K_2O-Na_2O-SiO_2 system). Reducing the SLAG model by excluding Al_2O_3, increased the SLAG formation temperature significantly. Al was found mainly as $KAlSi_2O_6$(s) and $KAlSiO_4$(s).

Figure 4a illustrates the SLAG formation for the studied straw qualities (no Ca added). Total melt formation (i.e. SLAG+SALT+LSCO) is shown in Figure 4b. The reduced SLAG solution (pure oxide phase) was present within the whole temperature interval.

Zevenhoven et al.[30] predicted a theoretical melting point for the complex oxide/silicate system by estimating the melting point for the corresponding ternary K_2O-CaO-SiO_2 system. Thus, assuming Mg and

Na to act as Ca and K respectively, and ignoring the minor components Al and Fe (i.e. Fe=Al=Mg=0, Ca=Ca+Mg and K=K+Na).

A similar approach has been used in the present study, however only Al was excluded from the multi component oxide model (i.e. reducing the SLAG solution to consist of K_2O, CaO, SiO_2, MgO, FeO and Na_2O) in order to estimate the SLAG melting point. Both approaches are based on the limited validity of the model input data for Al.

The chemical composition and ash melting behaviour differs significantly among the selected fuels. A simple sensitivity analysis illustrates the validity of the model prediction (Figure 5). Increasing the Ca content by 5ψ, for Wheat#2 (i.e. by 167%), results in significant increased SLAG formation and reduces the melting temperature by approximately 100°C, while the opposite is seen for Wheat #4. Note that the SLAG formed for Wheat#2 has a composition very close to the stoichiometric component $K_2Si_2O_5$(s). Initial Ca-addition to Wheat2000 (high in Si) slightly increases SLAG formation, and a significant amount of SLAG is still formed after adding 10ψ.

The predicted effects of Ca addition (from 2.5ψ to10ψ) upon melt formation for Barley95 is shown in Figure 6a. Corresponding SALT and total melt formation is shown in Figure 6b and 6c respectively. Ca addition exceeding 5ψ results in gradually decreasing SLAG formation and is followed by an increase in liquid SALT formation.
However, the total amount of liquid melt remains approximately constant between 750-850°C.

The arrows along the SiO_2-K_2O and SiO_2-CaO binary in Figure 7 indicate the relative change in the SLAG composition upon Ca addition, i.e. towards Ca-enriched SLAG. (Note that the axes of a ternary system show all possible compositions, not only that of the liquid slag.) Ca enrichment in the SLAG solution (model assumptions as in Figure 6a) is also illustrated by projecting the multi-component SLAG into the ternary K_2O-CaO-SiO_2 system. This is accomplished by normalising the number of moles of the respective components, as found in the model output (e.g. X_{K2O} = $K_2O/(K_2O+CaO+SiO_2)$), which clearly represents a simplification. The solid lines denote increasing temperature, at constant wt% Ca in fuel input, dashed lines: isothermal with increasing Ca-addition, displayed at a temperature interval of 50°C (from 750 to 950°C). Increasing temperature and amount of additive shifts the mean SLAG composition towards higher Ca content and reduced content of

Si. Below a molar SiO_2 fraction of about 0.4 the SLAG solution is split into the SALT solution.

Increased K-carbonate formation within the liquid SALT solution (eventually dominated by carbonates) resulted in significant amounts of molten SALT being present between 600 and 900°C. The SALT system is, during the present calculations, mainly composed of carbonates and chlorides of K (up to 90 mol%) and Na (up to 9 mol%) and additionally small amount of KOH (less than 1 mol%). At lower temperatures a solid solution of alkali-chlorides, ACLA, is formed mainly comprising KCl and NaCl. Figure 8 illustrates the influence of the original ash composition and addition of Ca upon the increased SALT formation. It is evident from these results that Wheat#4, representing the highest reactivity of the investigated chars, also gives the highest level of catalytic SALT formation.

All P are found either as $Ca_5HO_{13}P_3(s)$ / $Ca_3(PO_4)_2(s)$ (present in the FACT database) or as $K_3PO_4(s)$ (included in the database by the authors, source HSC[32]). Zevenhoven et al.[30] found $Ca_3(PO_4)(s)$ as the dominating P-species. No thermodynamic data are available for ternary (Ca, K)–phosphate and little information is available for P-species in solutions. Furthermore, Cl is found as chlorides of K and Na (KCl and NaCl) being very stable in the gas phase. Minor, but significant, amounts of KOH(g) and NaOH(g) are formed at higher temperatures. Earth alkaline metals (Ca and Mg) are present in very small concentrations in the gas phase (around 1000°C), primarily as hydroxides or chlorides. The dominating S-species are H_2S and COS.

6. DISCUSSION

Addition of 1, 2 and 3 wt.% $Ca(OH)_2$ (as CAS or CAM solutions) to a barley straw, moderate in Si, subsequently reduced the sintering tendency from SAI = 3^* down to about 0.5^*. This is quantitatively in accordance with the behaviour predicted by GEA, from which the addition of around 3 wt% $Ca(OH)_2$ ($10\,\psi$) is sufficient to diminish the amount of SLAG. For a wheat #4 sample, poor in Si, almost complete SLAG reduction is predicted upon addition of 0.75 wt% $Ca(OH)_2$ ($2.5\,\psi$), while increased SLAG formation was found for the Si rich Wheat 2000. Upon enhanced addition (maximum level about 3 wt% $Ca(OH)_2$, $10\,\psi$) the SLAG formation reduced slowly. (Generally the molar K_2O/SiO_2 ratio in the SLAG solution increased until saturation was obtained around a molar ratio of about 2/3). The influence of fuel ash composition upon the

predicted viscous oxide/silicate melt formation is in accordance with the experimentally determined SAI index.

K_2CaSiO_4, $K_4CaSi_3O_9$ and $KAlSiO_4$ (all containing K) were observed in the untreated barley ash sample (by X-ray diffraction). When adding Ca, Si was primarily bound into binary calcium silicate compounds (Ca_2SiO_4 and Ca_3SiO_5), quartz (SiO_2) appears and $K_4CaSi_3O_9$ and $KAlSiO_4$ vanished, while no reduction of K_2CaSiO_4 was observed.

As no ternaries have been evaluated for the K_2O-CaO-SiO_2 system, FACT predicts formation of the binary compounds (e.g. $K_2Si_2O_5$, K_2SiO_3 and $Ca_3Si_2O_7$), solid solutions (e.g. α'$CaSiO_3$ (SIO3?) and Ca_2SiO_4 (CASI)) and the viscous oxide/silicate melt (SLAG). SiO_2 and Ca_3SiO_5 were observed (both by X-ray diffraction) but not predicted. The predicted ash compositions are thus qualitatively in accordance with the experimental results, despite model limitations.

A SALT fraction generally co-existed with the SLAG phase. The presence of potentially catalytic SALT was especially pronounced for the reactive wheat#4. (The low SAI index, SAI=1*, corresponds to the low amount of SLAG.) This indicates a high catalyst/carbon ratio and increasing reactivity as $X \rightarrow 1$ (experimentally observed for T = 750°C, Figure 1). The same tendency is not observed for the much less reactive wheat #2 ($SAI_{850°C}$=3*) where only a small SALT fraction co-exists with the SLAG. At 850°C Wheat #2 and Wheat #4 both showed increasing reactivity as $X \rightarrow 1$. This behaviour should be further investigated.

7. CONCLUSION

In the present work the influence of Ca addition in straw gasification has been investigated. The char reactivity measured in a thermal gravimetric analysis was little affected by Ca added as CAS/CAM. In-situ high-temperature X-ray diffraction and combustion measurements indicate that major parts of the inorganic-inorganic reactions take place late in the char conversion process. The results support the suggestions that in the present case the catalytic activity of the mobile K is significantly larger than that of Ca. Ca may, however, indirectly affect the reactivity by primarily binding silicon as calcium silicates and less into potassium calcium silicates and hereby generate potassium salts.

Fuels with silica rich ash tends to produce a viscous K and Si-oxide/silicate slag with a low melting point. Although small amounts of Ca results in a low melting point (due to ternary eutectics), the present

work shows that abundant Ca-enrichment of the inorganic straw ash in general leads to decreased formation of K-rich SLAG (experimentally observed through the reduced SAI-index), and increased formation of calcium-silicates within solid solutions, co-existing with a binary (K, Ca)-carbonate solid (SCSO) and liquid (LCSO) solution and an increasing water-soluble and potentially catalytic liquid SALT melt fraction. The fact that a significant reactivity enhancement was not observed in the present study support the assumption that formation of viscous oxide/silicate melt and the catalytic salt mainly takes place at the end of the char conversion process. Hence, the presence of carbon is prohibiting inorganic ash reactions in reaching equilibrium.

For the Si-poor barley sample experimentally addition of 2 to 3 wt.% $Ca(OH)_2$ was sufficient to obtain a low sintering and agglomeration index. While experimentally addition of 3 wt.% $Ca(OH)_2$ was not enough for the Si-rich Wheat 2000, in agreement with the theoretical calculations. However, as Wheat 2000 has about three times higher Si-content, addition of about 2-3 times more of the CAM solution (i.e. about 6-9 wt% $Ca(OH)_2$) is expected to reduce the slag formation to an acceptable level.

Equilibrium calculations predict the formation of liquid salt if sufficient amounts of Ca are added. In several combustion and gasification systems salt formation may by itself cause problems. Hence, an adverse slag formation problem might be replaced by increased corrosion on heat transfer surfaces.

The observation of the in-situ K_2CaSiO_4 and Ca_2SiO_4/Ca_3SiO_5 formation from Ca enriched straw ash we considered important with respect to improved modelling of the viscous oxide/silicate melt.

Acknowledgements
The research was supported by the Danish Ministry of Energy, RITTS Greater Copenhagen, Nordic Energy Research Programme (Biomass combustion programme) and Energy E2. Special thanks to Rainer Backman Åbo Academy University, Finland for valuable discussions concerning bio-ash chemistry and equilibrium calculations.
Furthermore, Esa Kurkela VTT, Finland, is acknowledged for his support on aspects concerning experiments and analysis. Per Rosenberg, GEUS, Copenhagen, Denmark are thanked for participation in the sampling and evaluation of the SEM data and Erik Winter, Energy E2,

Denmark is acknowledged for valuable discussions with special emphasis upon practical implications.

References

1 Palonen, J. Lahti biomass and REF gasification project. Foster Wheeler Energia Oy, Finland. Waste-to Energy. The latest technical development. Malmö, Sweden. 1999

2 Kurkela, E., Laatikainen-Luntama, J., Ståhlberg, P. and Moilanen, A. Espoo; VTT, VTT Publications 291, 1996, 41 p. + app. 5 p.

3 Hallgren, A. In: Proceedings to the 3rd Biomass conference of the Americas, Montréal, Quebeck, Canada, 571

4 Moilanen A., Sørensen L.H., Gustafsson T.E., Laatikainen-Luntama J. and Kurkela E. In: 'Progress In Thermochemical Biomass Conversion', Tyrol, Austria 2000, 122

5 Steenari B.-M., Lindqvist O., *Biomass and Bioenergy* 1998, **14**, 67

6 Sørensen, L. H., Henriksen U., Risnes H., Poulsen K.T., Hansen L.K., Olsen A. and Rathman O. In: 'Nordic Seminar on Thermochemical Conversion of Solid Fuels', Chalmers University of Technology, Sweden, December 1997

7 Sørensen L.H., Saastamoinen J. and Hustad J.E. *Fuel* 1996, **75**, 1294

8 Sørensen, L. H., Fjellerup, J., Henriksen, U., Moilanen, A., Kurkela, E. and Winther, E., EFP-98 1383/98-0003, ReaTech, ISBN 87-988105-0-2, September 2000, Roskilde, Denmark.

9 Henriksen U., Jacobsen M.P., Lyngbech T. and Hansen M.W. In: 'Developments in Thermochemical Biomass Conversion' Banff, Canada 1998, 891

10 Mims C.A. and Pabst J.K. *Journal of Catalysis* 1987, **107**, 209

11 Nordin, A. *Biomass & Bioenergy* 1994, **6** (5), 339

12 Wilen, C., Moilanen, A and Kurkela, E. VTT publications 282, 1996, 25p.

13 Backman, R. and Nordin, A. International Biomass Ash Workshop, Technical University of Graz, Austria, October 1-2, 1998

14 Moilanen, A. and Kurkela, E. Am. Chem. Soc. Div. of Fuel Chem., **40**(3), Preprints of Papers Presented at the 210th ACS National Meeting Chicago, August 20-24, 1995 Chicago, 688

15 Moilanen, A. and Saviharju, K. In: 'Developments in Thermochemical Biomass Conversion', Ed. by A. V. Bridgwater and D.G.B. Boocock Blackie Academic & Professional. Glasgow 1997, 828

16 Cazarola-Amoróz D., Linares-Solano A., Salinas-Matínez de Lecea C., Nomura M., Yamashita H. and Tomita A. *Energy & Fuels* 1993, **7**, 625

17 Kapteijn F., Porre H., Moulijn J.A. *AIChe Journal* 1986, 32(**4**), 691

18 Ohtsuka, Y. and Asami, K. *Energy & Fuels* 1996, **10**, 431

19 Salinas-Martínez de Lecea C., Almela-Alarcón M. and Linares-Solano A. *Fuel* 1990, **69**, 21

20 Leboda R., Skubiszewska-Zieba J., Grzegorczyk W. *Carbon* 1998, **36**, 417

21 McKee D.W. *Carbon* 1982, **20**, 59

22 Heinemann H., Somojai G.A., Pereira P. and Carrazza J. Am. Chem. Soc. (Div. Fuel Chem.) 1989, **34**(1), 121

23 Pereira P., Csencsits R., Somorjai G.A., Heinemann H. *Journal of Catalysis* 1990, **123**, 463

24 Blander, M., Milne, T.A., Dayton, D.C., Backman, R., Blake, D., Kühnel, V., Linak, W., Nordin, A. and Ljung, A. *Energy & Fuels* 2001, **15**, 344

25 Bale, C. W., Pelton, A. D. and Thompson, W. T., FACT-Win® Version 3.05, Software with extensive Thermochemical Database, Ecole Polytechnique de Montreal , Quebec, Canada. H3C3A7, 2000

26 Pelton, A. D. and Blander, M. *Met. Trans. B* 1986, **17B**, 805

27 Henriksen, U., Jacobsen, M.P., Lyngbech, T. and Wittrup Hansen M. In: 'Developments in Thermochemical Biomass Conversion'. Banff, Canada. 20-24 May 1996. **2**. 881

28 Moilanen, A., Kurkela, E. and Laatikainen-Luntama, J. In: 'Impact of mineral impurities in solid fuel combustion' (Eds Gupta et al.). New York: Kluwer Academic / Plenum Publishers 1999, 555

29 Norby P., Posselt D. and Sørensen L.H. To be published 2002.

30 Zevenhoven, M. and Backman, R. Internal report from the Åbo Akademi University Process Chemistry Group (Report 98-2, ISBN 952-12-0236-X)

31 Levin, E. M., Robbins, C. R. and McMurdie, F. *Phase diagrams for ceramists.* Vol. I. 5th print. Washington: American Chemical Society 1985. 601 p.

32 Roine A. HSC Chemistry® for Windows. Chemical Reaction and Equilibrium Software with extensive Thermochemical Database 1999, Version 3.0

TABLES

Table 1. Proximate and ultimate analysis of Danish straws (dry basis).

Sample	Ash %	Volatile matter %	Fixed carbon %	LHV, MJ/kg	C %	H %	N %	O %	S %
#1 Barley95	4.8	76.1	19.1	17.40	47.5	5.9	0.7	41.2	0.16
#2 Wheat	5.4	77.1	17.5	17.36	46.4	5.9	0.6	41.6	0.13
#3 Wheat97	6.1	75.8	18.1	17.30	46.5	5.7	1.4	40.1	0.12
#4 Wheat	3.5	78.2	18.3	17.53	47.2	5.9	0.5	41.5	0.13
#5 Wheat2000	8.4	72.6	19.9	15.06	45.2	6.0	0.54	39.9	0.17

Table 2. Ash chemical composition (wt% dry), and ash sintering test results obtained from steam gasification tests at 750 ^{o}C and 850 ^{o}C.

Sample	K_2O	CaO	SiO_2	Al_2O_3	Fe_2O_3	MgO	Na_2O	TiO_2	Cl	P_2O_5	SO_3	$Sint_{750}$	$Sint_{850}$
#1 Barley95	31.7	13.3	31.0	1.0	1.5	3.0	2.0	0.12	4.8	2.9	2.6		***
#2 Wheat	32.5	10.4	29.9	0.2	0.2	4.1	0.5	0.03	11	3.9	6.0	**	***
#3 Wheat 97	27.7	10.6	29.9	0.8	1.3	5.6	1.5	0.07	4.2	10.8	5.5	**(*)	***
#4 Wheat	41.0	15.4	16.3	0.2	0.6	4.1	0.4	0.03	12	1.8	7.5	*	*
#5 Wheat 2000	21.9	9.2	52.0	0.6	1.1	1.8	0.3	-	5.6	3.2	4.0		***

n.d.: not determined, u: unburned carbon present

Table 3. FACT solution phases evaluated in the calculations. The notation used for the solutions (e.g. MONOB) is identical to that applied in the FACT-program.

#	Solution	Species	Comments
1	MONOB	MgO, CaO, $MgAl_2O_4$	Bmonoxide
2	MONT	$CaMgSiO_4$, Mg_2SiO_4, $CaFeSiO_4$	Monticellite-forsterite
3	CFSM	$CaMgSiO_4$, Fe_2SiO_4, Ca_2SiO_4	(Ca,Fe)SiO4-CaMgSiO4
4	SIO3?	$MgSiO_3$, $FeSiO_3$, $CaSiO_3$	$MSiO_3$-ss
5	CASI	Mg_2SiO_4, Fe_2SiO_4, Ca_2SiO_4	a'Ca_2SiO_4 new in FS: ‘’C2S
6	NCSO	$Na_2Ca_2Si_3O_9$, $Na_4CaSi_3O_9$	(Na_2,Ca)$Na_2CaSi_3O_9$ solid solution
7	OLIV	Mg_2SiO_4, Fe_2SiO4, Ca_2SiO_4	Olivine new in FS: Oli2
8	MELI	$CaMgSiO_4$, Mg_2SiO_4, $CaFeSiO_4$	Melilite solution
9	SLAGA	MgO, FeO, Na_2O, SiO_2, CaO, Al_2O_3, K_2O, MgS, CaS, FeS, Na_2S, K_2S, $NaCl$, KCl, $CaCl_2$, $MgCl_2$, $FeCl_2$	Slag-liq/glass oxide
	SLAGD	MgO, Na_2O, SiO_2, CaO, Al_2O_3, K_2O, MgS, CaS, Na_2S, K_2S, Na_2SO_4, K_2SO_4, $CaSO_4$, $MgSO_4$, $NaCl$, KCl, $CaCl2$, $MgCl_2$	Slag-liq/glass oxide
	SLAGF	Na_2O, SiO_2, CaO, Al_2O_3, K_2O, CaS, Na_2S, K_2S, Na_2SO_4, K_2SO_4, $CaSO_4$, $NaCl$, KCl, $CaCl_2$, Na_2CO_3, K_2CO_3, $CaCO_3$	Slag-liq/glass oxide
**	SLAG?	MgO, FeO, Na_2O, SiO_2, CaO, K_2O	Slag-liq/glass oxide
10	ACLA	$NaCl$, KCl	Alk-Cl solid new in FS: AClA
11	CSOB	Na_2CO_3, K_2CO_3, Na_2SO_4, K_2SO_4	CO_3,SO_4/Na,K
12*	KCO	Na_2CO_3, K_2CO_3, Na_2SO_4, K_2SO_4	K_2CO_3 solid, NaK/CO_3,SO_4
13	NKXA	KOH, KCl	ANa,K/OH,F,Cl high temperature solid binary solution
14*	NCOA	$NaCl$, $NaOH$	Na/Cl,OH high NaOH content solid binary solution
15	SALT	$NaCl$, KCl, $NaOH$, KOH, Na_2SO_4, K_2SO_4, Na_2CO_3, K_2CO_3, $NaNO_3$, KNO_3	Salt-liq, new in FS: SALTA/SALTB/SALT?
16	LCSO	K_2SO_4, $CaSO_4$, K_2CO_3, $CaCO_3$	liq-K,Ca/CO_3,SO_4
17	SCSO	K_2SO_4, $CaSO_4$, K_2CO_3, $CaCO_3$	s-K,Ca,/CO_3,SO_4
18*	SCMO	$CaSO_4$, $MgSO_4$	s-Ca(SO_4),Mg(SO_4)
19*	LSUL	$CaSO_4$, $MgSO_4$, Na_2SO_4	liq-Ca,Mg,Na/SO_4

* Solution did not form in any of the cases studied
** Reduced composition used in this study

Table 4. Experimental results for Barley 95, the effect of $Ca(OH)_2$-addition: Total conversion time, τ (min) and SAI index as a function of CAS and CAM addition.

$Ca(OH)_2$-addition (wt% d.b)		τ (min)	SAI
0.0		7.4, 6.05	3*, 3*
1.0	CAS	8.85, 5.15	1.5*, 1.5*
	CAM	5.5, 5.0	1.5*, 1.5*
2.0	CAS	9.0, 6.65	1*, 1*
	CAM	4.4	0.5*, 0.5*
3.0	CAS	5.8	0.5*
	CAM	6.05	0.5*

Table 5. Crystalline compounds found in Barley 95 ash after gasification at 850 °C, in 1 bar H_2O.

	Main components				Minor components	
	Binary compounds		Ternary compounds			
Sample	Ca_2SiO_4	Ca_3SiO_5	K_2CaSiO_4	$K_4CaSi_3O_9$	$KAlSiO_4$	α-SiO_2
Pure			x	x	x	
1wt% Ca	Increasing	increasing	x	decreasing	decreasing	
2wt% Ca	x	x	x			x
3wt% Ca	x	x	x			x

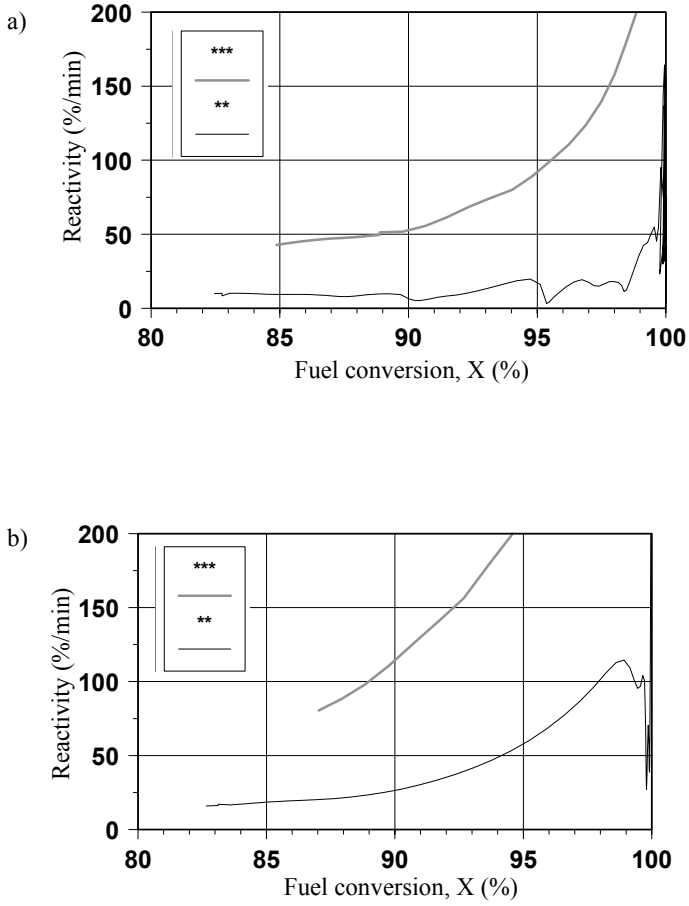

Figure 1: Reactivity measured in 1bar H_2O at 750 °C (lower curve) and 850 °C (upper curve) for: a) Wheat #2 and b) Wheat #4.

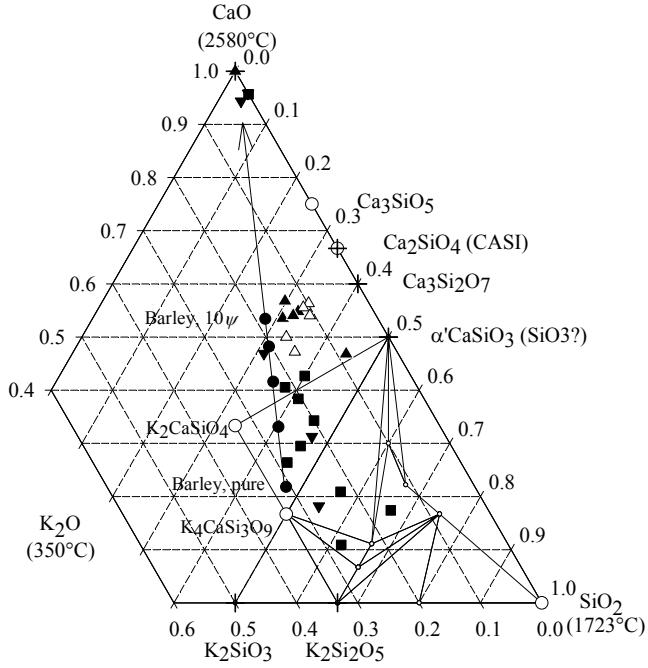

Figure 2: Barley95: Ternary projections of the relative ratio of the normalised main ash components (K, Ca and Si) as analysed on the raw fuel and on ash samples collected after gasification. The arrow drawn from pure Barley towards CaO illustrates the effect of overall Ca enrichment on the fuel input. Symbols: SEM-spot analysis - 1wt% $Ca(OH)_2$-addition▼, 2wt% ■, 3wt% ▲ (corresponding open symbols indicates area analysis); ❍ - Components found by powder diffraction; + - Components found in the computer simulations; ● - Mean average ash composition as measured on the raw fuel and stepwise (from 2.5ψ to 10ψ) altered composition towards the Ca rich corner.

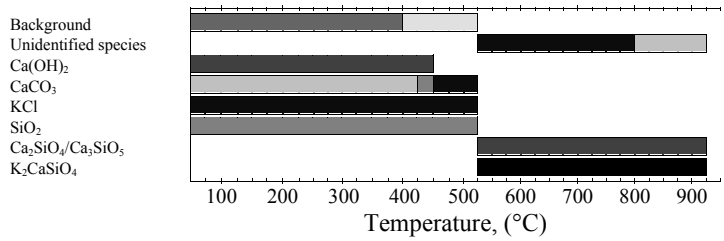

Figure 3: In-situ synchrotron X-ray powder diffraction studies conducted on wheat ash (originating from Wheat #2, ashed at 500 ^{o}C) mixed with a 2 wt.% $Ca(OH)_2$ (CAM reference solution). (The sample was heated up to 925 ^{o}C, with a heating rate of β = 20 ^{o}C/min in a 2 ml/min O_2 flow.)

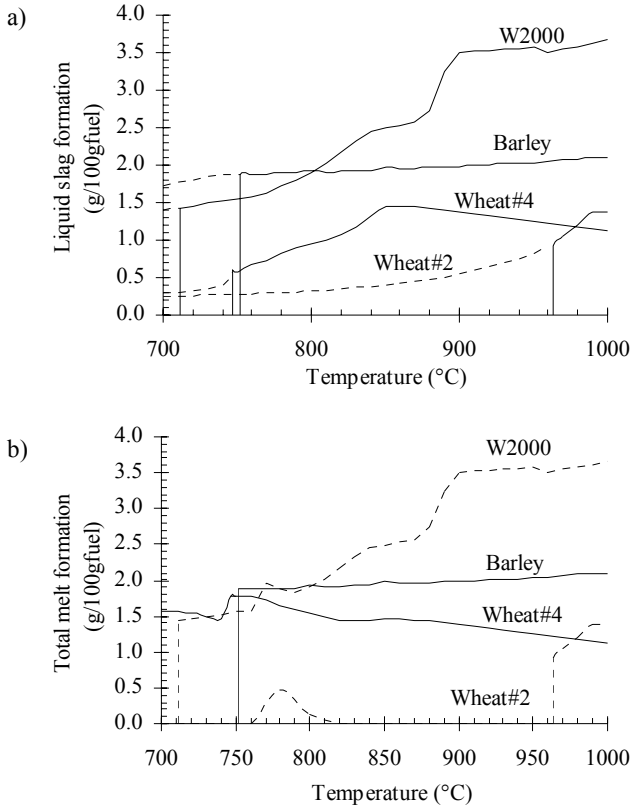

Figure 4: Theoretically predicted melting curves for the raw fuels. a) Liquid slag (assumed to consist of oxides only K_2O, CaO, SiO_2, MgO, FeO, Na_2O and Al_2O_3), the melting point is estimated by excluding Al from the model input. Dotted lines indicate slag formation when Al is included. b) Total melt formation (SLAG+SALT, note no SALT formation for Barley95). SLAG is not included in the model input below the predicted slag formation temperature (i.e. for $T<T_{melt,\,SLAG}$). Dotted lines for Wheat2000 and Wheat#2.

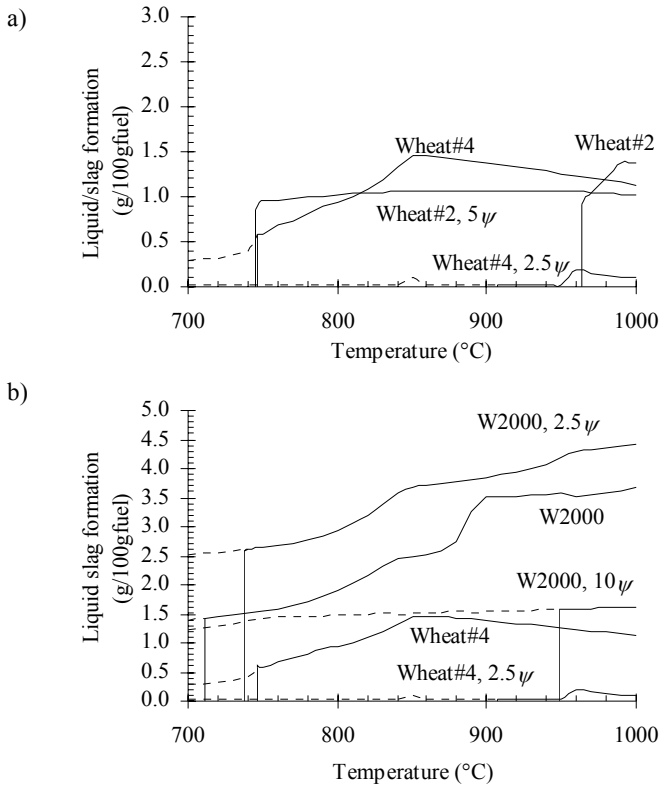

Figure 5: Illustrates how the original fuel ash composition influences upon the effect of Ca addition. Model sensitivity: a) Comparison of Wheat#2 vs. Wheat#4 and b) Wheat#4 vs. Wheat2000 (especially high Si content in the original fuel ash).

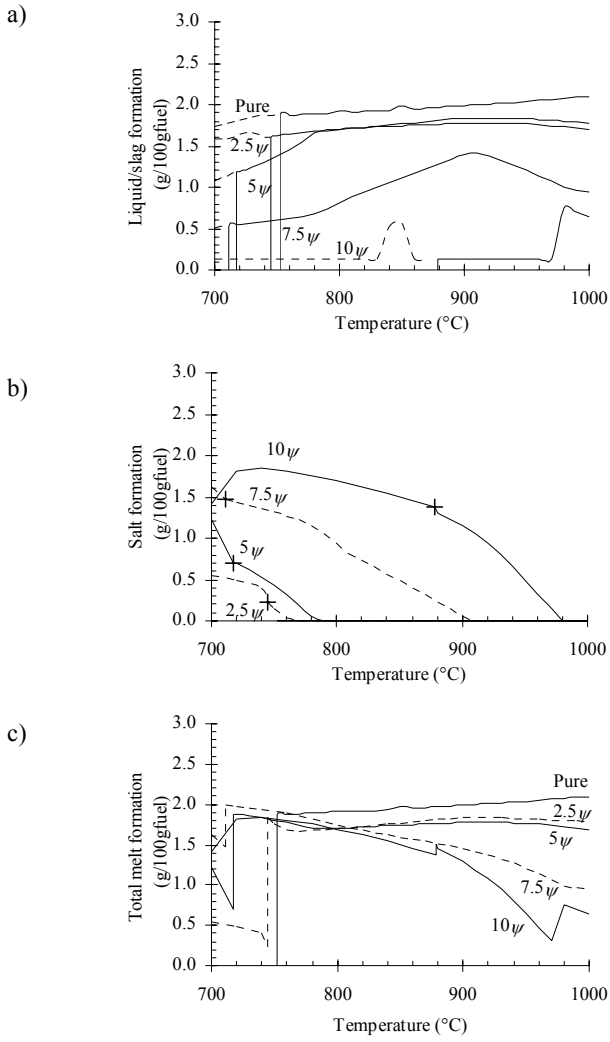

Figure 6: Addition of Ca to Barley95 results in: a) reduced formation and eventually disappearing liquid/slag, b) increased salt formation (slag formation temperature indicated by cross hairs). The total melt formation is shown in c).

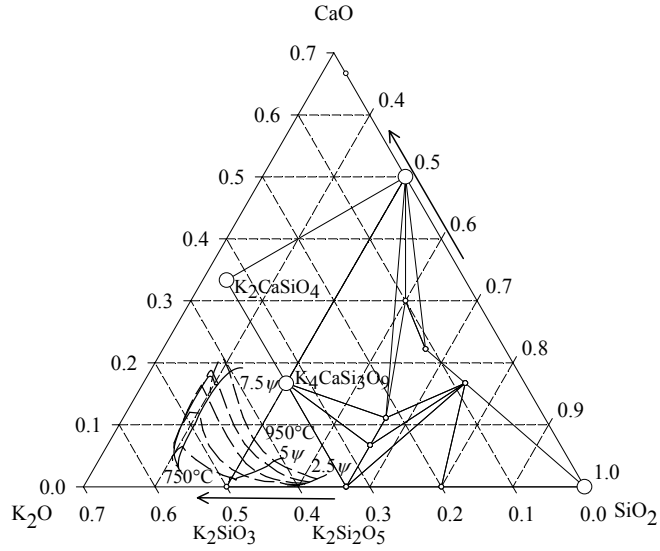

Figure 7: Barley95: Ternary projections of the relative ratio of the normalised main ash components (K, Ca and Si) as predicted by the SLAG solution model (pure oxide). Melting point estimations are conducted by excluding Al from the input file.

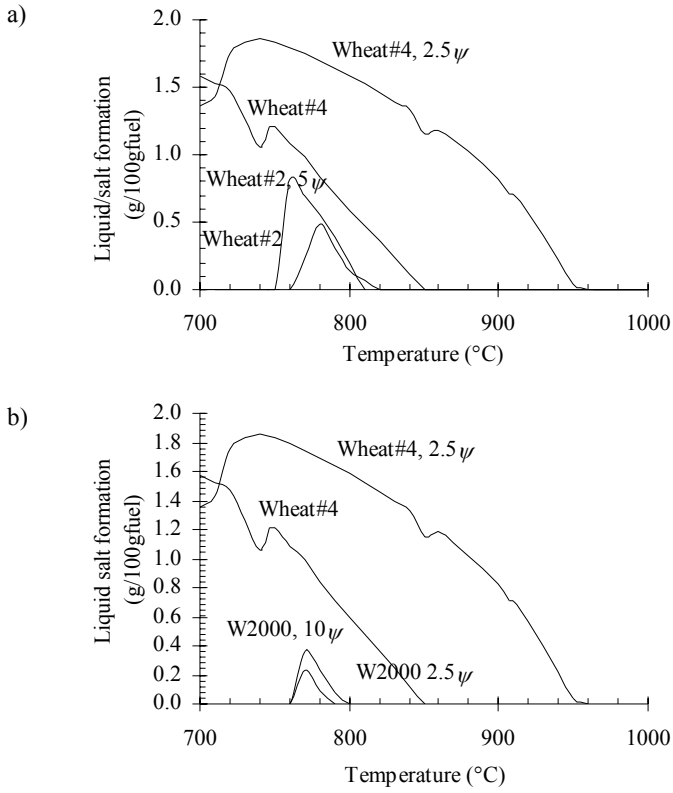

Figure 8: Illustration of the increased salt formation as Ca is added to the raw fuel. Model sensitivity: a) Comparison of Wheat#2 vs. Wheat#4 and b) Wheat#4 vs. Wheat2000 (especially high Si content in the original fuel ash).

5 High temperature cleaning of biomass gasification product gas

The process of product gas cleaning is still one of the major technical challenges with regard to the utilisation of biomass producer gas in high temperature applications, such as gas-fired engines and gas turbines. Granular bed filters are insensitive to hot particles, temperature fluctuations and corrosive elements in the impinging gas, this combined with the possibility to provide chemical processing of the gas makes the Panel Bed Filter a promising alternative for high temperature cleaning of gasification product gas.

5.1 General

Investigations of the technical feasibility and economical and environmental performance of different biomass gasification systems (in integrated gasification combined cycle (IGCC)) systems are published by Bridgewater (1995) and Faaji et. al. (1997). Bridgewater (1995) concluded that hot gas filters can be considered the least developed and most likely to create problems in a demonstration plant. Hence, claims for effectiveness and the consequences of failure of such devices require careful evaluation. Hot-gas clean up is thus a very important system-development issue for biomass gasification systems.

Various groups have carried out research and development work on hot gas cleaning during the 1980's and 1990's, resulting in the development of several filter concepts for high temperature and high-pressure operation. Published work embraces evaluations of granular bed filters (deep bed and cake forming filters), rigid metallic and ceramic candle elements of silicon carbide / oxide-based and cross flow filter elements (monolithic structure).

The gas cleaning requirements, as shown in Table 5.1, are process specific and for example for gas utilisation in gas turbines, particulates and alkali metals have to be removed. In this application tars can cause blocking problems in particulate filters, gas coolers and other downstream equipment. In the gasification-diesel engine process in turn, the gas has to be cooled to around 50 °C and hence, requirements for tar removal are even more stringent than in an IGCC process. However, the cleaning process can be done with a scrubbing process at low temperatures. The combustion of fixed bed producer gases in conventional burners generally does not need gas cleaning.

Table 5.1: Acceptable gas quality for producer gases [Hasler P. et al 1997]

Producer gas application	Particles [mg/Nm^3]	Particle size [um]	Tar [mg/Nm^3]	Alkali metals [mg/Nm^3]
IC engine	<50	<10	<100	
Gas turbine	<30	<5		0.24
Methanol synthesis	0.01		100	

Thermal decomposition of pyrolysis products also leads to a formation of high-molecular-weight components (tars) and soot, which may cause blinding of the filters. Furthermore, tars are a serious environmental problem when they persist and require recovery and disposal.

High levels of particulates and alkalis in the product gas can negatively impact IC engine, turbine and syngas applications, and can also represent a significant environmental problem. These contaminants can cause erosion, corrosion and pitting of the surfaces of downstream equipment (including piping, internals, lines, cylinders, blades and bearings), and can also cause fouling of engine lubricants and catalysts (in synthesis gas operations).

5.2 Experience on high temperature filtration of biomass gasification product gas

Many of the small carbon-containing particles being elutriated from the gasifier are difficult to remove by cyclones or by deep bed granular filtration (Kurkela 1996). System evaluations conducted in the early 1990s indicated that the rigid ceramic barrier filter concept would be the best choice for hot gas particle filtration (Lippert 1992 ref. in Wiant et al. (1993)). However, a critical problem is the mechanical and chemical durability of ceramic filters. In particular at higher temperature alkali metals may react with binder materials and deformation of the crystal structure may lead to reduction of the strength of the elements (Nieminen et al. 1996).

Literature documenting experience from high temperature filtration of biomass gasification product gas is scarce. A short introduction to systems described in the available literature is given below.

Kurkela et al. (1990 and 1993) compared SiC-based candle filters with homogeneous pore size (Didier Filtertechnik) and two-layer elements, which consisted of a thin fiber-containing layer with small pores outside the coarser SiC support structure (Dia Schumalith by Schumacher Gmbh). The major drawback of the homogeneous filter elements was their high pressure drop, which resulted in low permeability. Only the layered elements seemed to reach a stable pressure drop within the first 500 cleaning cycles. Filtration temperatures up to about 800 °C were tested, but the most stable operation was found at 400-500 °C. The applied filtration velocity was reported to be 1.8-4 cm/s.

This finding is supported by Malmgren-Hansen et al. (1996) who studied metallic (Pall PSS and Sintertech PORAL) and ceramic (BWF, Cerafil S-1000, Schumalith 40 and Dia-Schumalith40) filter elements operating on product gas from wood chip gasification in a 200 kW counter-current gasifier. These experiments showed that operating in surface filtration mode (480-550 °C) gave best results.

Engstrom (1998) reported 2000 hours successful operation of high temperature Schumacher (SiC) candel filter installed on the Bioflow IGCC demonstration plant (19MW fuel input), gasifying crushed wood and wood waste at 950-1000 °C. The filtration temperature was held within 320 to 400 °C, typically around 340-370 °C. Stable operation/pressure drop was obtained and no ash bridging observed.

Alvin (1998) presents a review of the Westinghouse Advanced Particulate Filtration (APF) system, operating with ceramic SiC filters, installed at the IGT fluidized-bed gasification facility (gasification of bagasse).

Hindsgaul (2000) used Polyester bag filters at 90 °C (average filtration velocities (U_S) of 2 cm/s) in filtration tests conducted on product gas from a 100 kW_{th} two-stage downdraft gasifier at DTU (gasification of wood chips). Stable operation was successfully demonstrated during a 50 hour test. No sign of filter blockage was reported.

Hofbauer and Rauch (2001) applied a PTE bag house filter, operated at about 200 °C, for the cleaning of product gas from a 100 kW_{th} gasifier operated on wood chips (at the Technical University in Vienna). Operational problems were encountered due to the condensation of polycyclic aromatic hydrocarbons.

5.3 Gas Contamination/Target Constituents

5.3.1 Operational problems related to alkali metals

Much work remains to be done with respect to analyses and quantification of alkali compounds in biomass derived producer gas, including characterisation of their physical and chemical properties.

Alkali metal containing components from biomass gasification act as fluxing agents due to their relatively low melting points compared to other ash components. Alkali metals released to the gas phase can react with the mineral phase of the fuel or condense (normally on entrained particles, as aerosols or directly on reactor surfaces). Particles enriched by alkali metal species may get a sticky surface, which can trap fly ash particles.

Alkali metal rich deposits (sodium (*Na*) and potassium (*K*)) are known to be highly corrosive and components as SO_x, H_2S, HCl and Cl_2 are believed to participate in the corrosion reactions. This might also be the case for gaseous alkali metal species. *Na* and *K* compounds are particularly harmful in turbine applications where they accelerate hot corrosion of the turbine blades and also contribute to deposition and cementing on the blades. Alkalis, particularly *Na* compounds, can also cause technical problems in long-term IC engine operation.

The alkali compounds, which are of principal concern in gas cleaning operations, are those which are present as aerosols and in the gas phase at the reactor outlet. The most common scheme for hot gas alkali metal control and removal is based on gas cooling followed by filtration in ceramic or metallic filters.

Vapour-phase alkali metal measurements, with several different types of biomass and coal, have shown that cooling the gas from 800-900 °C (at the gasifier outlet) to 500-550 °C, followed by filtration, reduces the alkali metal content of the product gas to the level of 0.1 ppm (m) or below (Kurkela et al. 1990, 1993 and 1995). VTT has verified this phenomenon even in co-gasification of straw and coal (Kurkela et al. (1996)), despite the high fuel alkali metal and chlorine content. Gas cooling and filtration at about 500 °C resulted in a total alkali content about 0.03-0.1 ppm-wt. Kurkela concluded that higher gas cleaning temperatures requires specific sorbents to remove alkalis.

Engstrom (1998), gasification of crushed wood and wood waste (950-1000 °C), measured alkali levels below 0.1 ppm(w) when operating the filter system at typically 340-370 °C.

5.3.2 Tars

Tars formed in gasification is a complex mixture of organic compounds ranging from light compounds like benzene to heavy polyaromatic hydrocarbons. The temperature at which fuel pyrolysis takes place has a very pronounced effect on tar composition and accordingly tars can be divided into low- and high temperature tars. Low temperature tar is formed at temperatures lower than about 650 °C and it is mainly composed of components that are primary decomposition products of the fuel structure. Hence, the used feedstock has strong influence on the low temperature tar composition. High temperature tar in turn is composed of mono- and polyaromatic compounds formed mainly in the secondary reactions of the primary products of the fuel. Low temperature tar is typically formed in updraft gasifiers and high-temperature tar in fluidized-bed, downdraft and entrained-bed gasifiers. A more thorough discussion about the nature, formation an conversion of tars is given in Hasler et al. (1997) and Milne et al. (1998).

Practically all end-uses of the product gas, with the exception of close-coupled combustion, are adversely affected by the presence of tars. They lead to fouling of valves, mixers, turbochargers, fuel lines, turbine blades, catalysts, lubricants and crystallisation of highly aromatic compounds (e.g. naphthalene) in lines and on other surfaces can occur.

One of three basic approaches can be taken to deal with the tars/oils: i) remove the tars/oils before passing them through the filter by either condensing them out at lower temperatures, ii) cracking them in a reactor at high temperature, iii) keeping the fuel gas at a high enough temperature, so that the tars/oils remain in the vapour state and don't condense out in the filter system.

Condensing out of tars/oils prior to the filter system has the disadvantage of reducing system efficiency and removing the heating value of the tars/oils from the combustion process. This heating value can be as much as 10% of the overall heating value of the fuel (Wiant et al. 1993). Therefore, retaining the tars/oils in the fuel is advantageous from a system efficiency point of view.

Filtration of wood derived product gases seem to be much more problematic than filtration of peat or coal derived gases (Kurkela et al. 1990). Simell et al. (1993) found the total tar concentration in the PFG product gas to depend mainly on the feedstock and on the gasification temperature. Wood gasification typically produces tars high in naphthalene and heavier PAH components. The relative portion of PAH components seem to increase in wood gasification as the gasification temperature increases. This indicates that these components, if formed, are rather stable and difficult to decompose without catalysts. According to Simell et al. (1993) one possible explanation of the feed-stock dependency upon tar formation might be related to the difference in mineral matter contents of these feedstocks. Main tar components in the wood gasification tests were benzene (representing 60-98%) and naphtalene. The second group represents a sum of benzene derivatives, pyridine and phenol, the major single component of this group being toulene.

According to Wiant et al. (1993) operating the filter system at > 540 °C, without catalyst/tar cracker, increases the possibility of carbon laydown within the filter. This is supported by Kurkela (1996) who experienced complete blocking of the

ceramic filter unit for wood gasification, at a filter temperature of 690-720 °C. They concluded that this rapid and severe blocking was due to cracking, polymerisation or condensation of heavy molecular weight tars, this despite a relatively high gasification temperature (900 °C). Even at 950 °C a sticky dust cake formed, due to tar condensation. Severe soot formation was detected within the dust cake and inside the pores of the filter. Furthermore, some of these tars did penetrate through the filter creating a potential emission source. This was however very much dependent on the gasification feedstock.

In 1991, better results were achieved in sawdust test runs, where dolomite was added to the gasifier. The operation of the ceramic filter at a slightly lower face velocity (about 2.4 cm/s) resulted in much better filtration behaviour than in the first wood gasification test. The most stable operation was obtained by decreasing the filter temperature to 400-500 °C.

Malmgren-Hansen et al. (1996) reported that operating at a filtration temperature of 400 °C resulted in a sticky filter cake consisting of ash, char and condensed tar. (Wood chip gasification in a 200 kW counter-current gasifier.) Tar components with boiling point up to about 525 °C was identified. Increasing the filter temperature up to 480-550 °C resulted in a porous filter cake and improved filter stability.

No severe blinding of the filter elements was found by Kurkela et al. (1996) in cogasification of danish wheat straw and coal. However, Kurkela found it likely that tars of straw alone gasification would cause operation problem. But no test on straw alone gasification was reported.

The porous dust cake obtained by Alvin (1998) (gasification of bagasse, filter temperature 675-915 °C) was enriched by carbon, especially along the outer dust cake surface.

Hofbauer and Rauch (2001) published preliminary results from gasification of wood chips in a 100 kW_{th} Fast Internal Circulating Fluidised Bed (FICFB). The tars produced contained various mono and poly-cyclic aromatic hydrocarbons, mainly being BTX, Naphthalene, Fluoranthene and Pyrene.

The filter bags (PTFE) applied by Hofbauer and Rauch (2001) collapsed due to severe deposition of fly coke/ash on the bag surface. The temperature of the gas at the exit of the product gas heat exchanger was around 220-240 °C. The N_2 pulses (having a temperature of 90-100 °C) additionally cooled the filter bags. Polycyclic aromatic hydrocarbons condensed thus creating a mist with charcoal, acting as glue. Material collected from the bags and the bin below the filter was analysed, and especially the deposit on the filter bags was found to be highly organic (22% extracted with dichloromethane) compared to the 1% in the bin. The main components of the solutions were polycyclic aromatic hydrocarbons, at three, four or fifth cycle. The boiling point of these constituents of tar was in the range 300-500 °C.

Simell et al. (1993) reported total tar concentration up to 18 g/Nm^3. While Fercher et al. (1998) and Hofbauer and Rauch (2001) reported around 2 and 3 g/Nm^3 respectively (main higher hydrocarbon was ethene) Tar content increased with decreasing temperature and decreasing steam-fuel ratio. Applying a catalytic bed material (NiO/Olivine) Hofbauer and Rauch (2001) reduced the tar concentrations to below 0.6 g/Nm^3

Engstrom (1998) measured tar levels below 5 g/Nm^3. And states that the formation of tars was minimised by thermal cracking due to the high gasification

temperature (950-1000 °C) and the catalytic effect of the bed material. Hindsgaul (2000) reports a tar load below 100 mg/Nm^3 in the product gas from the two-stage gasifier (gasification of wood chips).

Sampling and analytical methods used for tar, light hydrocarbons, gases and fuel have been described in more detail in other publications (Neeft et al. (2000) and Abatzoglou et al. (2000))

5.3.3 Particulates

Particulates typically consists of inorganic ash which was present in the feedstock, but can also include entrained char, soot and, where applicable, entrained fines derived from the attrition of the bed material (for example, the sand or dolomite used in fluidised beds).

The inorganic fraction of the entrained ash consists primarily of alkali chlorides (i.e. *NaCl* and *KCl*), carbonates ($CaCO_3$, K_2CO_3) and silicate compounds. Persistent aerosols and mists, which are in a condensed phase, but are nevertheless entrained in the gas phase, are often considered to be particulate components.

During combustion/gasification, the inorganic constituents undergo a variety of physical and chemical changes that depend on their original mode of occurrence, their time-temperature history, and interactions among the constituents. This might lead to strong adhesion forces within the dust cake and at the interface dust cake-filter.

Generally, fixed bed gasifiers exhibit particle contents in the range of 0.1 to 6 g/Nm^3 whereas in fludised bed the particle level can be as high as 100 g/Nm^3 (Hasler and Nussbaumer (1998)).

Usually, the particulate concentration determined after the cyclone in CFB gasification of wood (Kurkela 1996 and Kurkela et al. 1990) was of the order of 1 g/Nm^3, while typical particulate concentrations in straw, peat and coal gasification were at least one order of magnitude higher. Kurkela (1996) obtained particulate removal efficiencies higher than 99.9%, i.e. lower than 10 mg/Nm^3 and alkali concentrations < 0.1 ppm-w. The presence of porous char and ash particles in the gas provided a positive filter aid by creating a shielding cake for tar and soot blinding.

Kurkela (1996) also reported that filter fines derived from filtration (ceramic filters) of wood-derived gas at 500 °C adsorbed heavy tar compounds and the BET surface area could be increased from the original 85 m^2/g up to 280 m^2/g by heat treating the sample at 900 °C to remove tars.

Engstrom (1998) measured outlet dust concentration (CFB gasification of wood chips, hot gas clean up by ceramic filters) less than 2 mg/Nm^3. Hindsgaul (2000), fibrous filter obtained particle removal efficiencies of 96-99%, outlet dust concentration < 40 mg/Nm^3 (two-stage fixed bed gasification of wood-chips). However, the dust concentration increased for short periods when the bottom grid was activated. The inorganic content of up to 35% was found after burn out in air at 550 °C.

Only a limited amount of data on the particle size distribution from biomass gasifiers has been published. Hasler and Nussbaumer (1998 and 1999) published particle size distributions of the fly ash from biomass gasification. The particle measurements were

conducted before the cyclone and both the sample tubes and the impactor were heated to 270°C to limit tar condensation. Particle mass with diameters greater than 5μm is attributed to unconverted wood char. They concluded that both the fixed bed and the fluidized bed gasifier exhibit bimodal size distributions in the raw product gas. Size distribution measurements by Coulter counter (Kurkela et al. 1990) gave medium particle diameters (d_{50}) of 2-7 micron. A bimodal size distribution is also reported by Malmgren-Hansen et al. (1996), wood chip gasification in a 200kW counter-current gasifier.

A comparison of these distributions and those published by (Brown et al. (1986), Larson and Svenningsson (1990) and Hasler and Nussbaumer 1998) is shown in Figure 5.1.

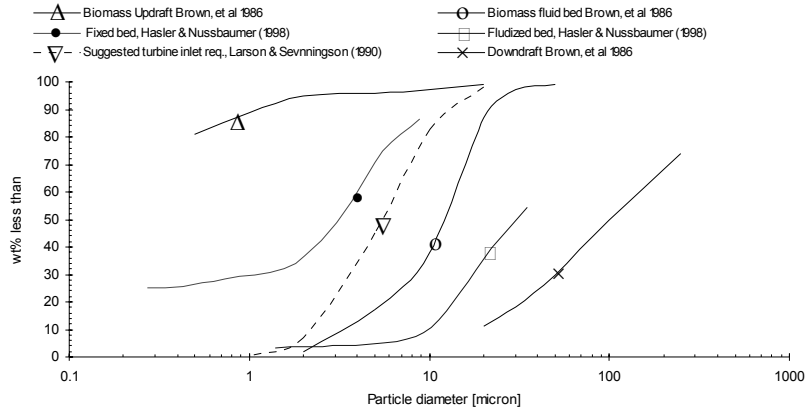

Figure 5.1: Characterisation of gasifier fly ash. Size distributions derived from the reviewed literature.

5.3.4 Short summary of the reviewed literature

Literature concerning operational experience on high temperature filtration of gasification product gas is mainly available on the filtration of coal derived product gases. However, a limited number of publications has been found and reviewed.

Both fixed bed and fluidized bed gasifiers exhibit particulate emissions (typically with a bimodal size distribution) into the raw product gas. Particle loadings reported from fixed bed gasifier is generally within the range of 0.1 to 6 g/Nm^3 whereas those from fludised bed gasifiers can be as high as 100 g/Nm^3.

It is essential to choose gas cleaning systems, incorporating high collection efficiency for micron and sub-micron particles, ensuring acceptable particle levels for gas turbines and IC engines. Cyclones or simple wet cleaning systems (e.g. spray towers) does not meet these requirements. The most promising results are reported from filter systems operating in surface filtration mode, where the carry over particles (e.g. char and inorganic particles) creates a filter cake incorporating high filter efficiency, simultaneously providing a positive filter aid for tar and soot blinding. Applying efficient catalysts (e.g. carbonate rocks and nickel catalysts) have proven to reduce problems related to tars, although parts of the most stable compounds, like benzene, toulene and naphthalene might survive.

The reviewed literature describes filtration experiments conducted at widely different conditions. According to Williams and Larson (1993) there appears to be a practically realisable exit-gas temperature window of 500-600 °C, for fixed-bed gasifiers, whitin which problems with both condensed tars and vaporised alkalis may be avoided. This is in accordance with Kurkela (1996) who found that the alkali vapour concentration was reduced to a level close to the target value of 0.1 ppm-wt by cooling the gas to below 500-550 °C (steam gasification in a CFB). Kurkela obtained the most stable operation of the filter system when operating between 400 and 500 °C (CFB steam gasification of a wide variety of fuel qualities; wood, straw and peat) while Malmgren-Hansen et al. reports the best results between 480-550 °C (wood chip gasification in a counter-current gasifier) and Engstrom obtained stable operation within the temperature range 340-370 °C (CFB gasification of crushed wood and wood waste). Hindsgaul (2000) states that stable filtration was obtained at temperatures as low as 90 °C (gasification of wood chips in a steam blown two stage gasifier (downdraft)).

It is concluded, based on the reviewed literature, that the gas cleaning efficiency and filter stability for commercial available technologies must be improved to safely achieve the postulated gas quality requirements for both gas turbines and IC engines, and also solid oxide fuel cells (SOFC) in the future. Alternatively new technologies must be developed.

5.4 Experimental set-up, procedure and results when connecting the horizontal bed filter to the stratified downdraft gasifier

In total 3 experiments have been conducted with the horizontal bed unit coupled to the gasifier. The gasification product gas was filtered at temperatures ranging from 300 to about 540 °C, and face velocities up to about 20 cm/s.

5.4.1 The gasifier

The air blown stratified downdraft gasifier is illustrated in Figure 5.2, which shows the assembly of the fuel feeding system, air supply, reaction chamber and gas outlet section. The relative location of the thermocouples and air inlets are shown in Figure 5.2b. The fuel (wood pellets, see Table 5.2) is supplied through a pseudo-continuous feeding system (a hopper and two pneumatic sliding valves). The analysis given in Table 5.3 and 5.4 indicate slightly higher ash content and significantly higher amounts of Si, Al and Fe in birch pellets as compared to heartwood. This might partly be attributed to the presence of soil contamination as the heartwood originates from a sample free of bark and which has not been exposed to the ambient. Pure heartwood was not used in the gasification experiments, but is included in order to support the analysis of the carry over particles collected in the high temperature filter unit.

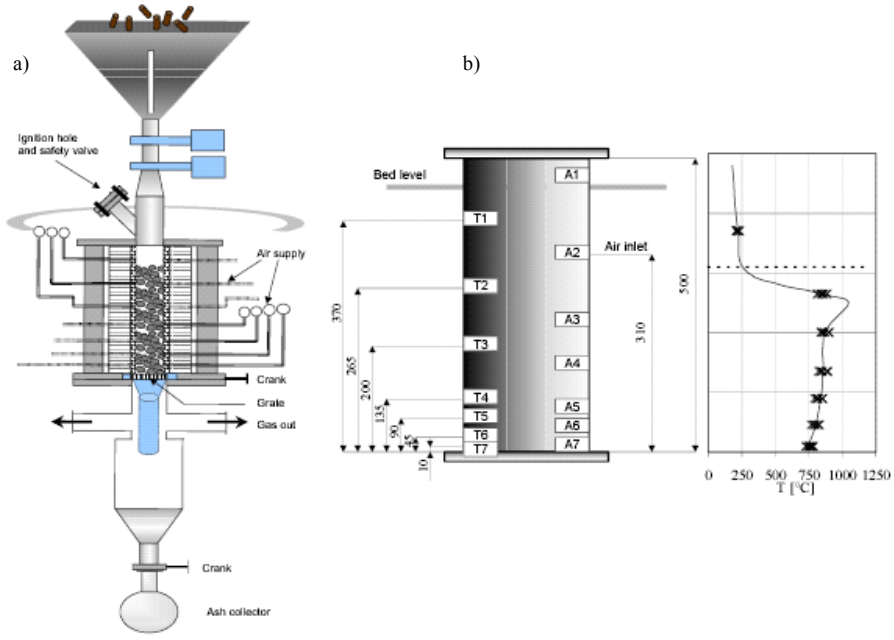

Figure 5.2: a) Stratified downdraft gasifier design b) Location of air nozzles and thermocouples, including a typical temperature profile (Barrio et al. 2001a).

Compressed air at about 7 bar passes through a filter. Dry and particulate free air is preheated before it enters a manifold and is distributed to 7 independent channels for air supply (arranged as circular distributors around the gasifier). Five nozzles evenly distribute the air (225 °C) from each of these to the reactor. The volume flow through each channel is measured with a rotameter and controlled with a valve. The air pressure at the reactor is slightly above atmospheric pressure, depending on the pressure losses downstream the reactor.

The location of the air levels is shown in Figure 5.2b, together with the position of the temperature measurements. The first two experiments reported here (experiment # 14 and #16) have been conducted using only one of the air levels, situated 310 mm above the grate (marked A_2 in Figure 5.2b). Using both A_1 and A_2 (supplying 80 and 20% of the total volume flow respectively) increased the gasifier stability in experiment (#23) (Guhl (2002) and Botnevik (2002))

The reactor itself is a cylinder 100 mm in diameter and 500 mm high. A view port (also acting as a safety pressure release valve) placed between the feeding system and the reactor is used to ignite the bed. The bed level has been maintained above the location of the first temperature measurement (T_1). The grate (a net made of steel rods, 5mm in diameter, with square openings of 15x15 mm) is placed between the reactor and the bottom section. Blockage of the grid is avoided by manually shaking it at a predefined pressure build-up.

Table 5.2 – NTNU-gasifier: Ultimate analysis and other fuel data. Also including characteristic paramters for the gasifier operation, product gas quality and product gas line/high temperature filter.

Fuel quality	
-Ultimate analysis	50.7wt%, mf C, 42.4%O, <0.3% N and 6.9% H
-Moisture content	7.5 wt%
-Ash content	0.39wt%, mf
-Calorific value	18.86 MJ/kg raw pellets
-Bulk density	668 kg/m3
-Pellet diameter	6mm
-Pellet length	6-16mm
Gasifier operation	
-Air excess ratio*	0.25-0.3
-Air to fuel ratio*	1.6 kg air / kg fuel
-Gas to fuel ratio*	2.3 kg gas / kg fuel
Product gas quality	
-amount	Approx. 12.5Nm3/h
-composition [%vol]	16% H_2, 25.3% CO_2, 1.6% CH_4, 9.5% CO_2 & 47.6% N_2
-Heating value	5.3-5.7 MJ/Nm3
-Tar content	3 g/Nm3
-Particle concentration	10.5 g/Nm3
Product gas line temperature	Approx. 600°C
Filter temperature	300-520°C
Superficial velocity	10-20 cm/s
Bed material	Olivin sand (AFS30)

* independent on gasifier load

Table 5.3: Fact-input[mol]

Sample	Gasification air			Steam	C	H	N	O
	N2	O2	CO2	H2O				
Birch Pellets	50.2	13.3	0.0191	5.14	44.2	62.5	0.214	26.5
Birch hw	Assumed equal to Birch Pellets							

Table 5.4: Elemental ash composition [mol]

	Si	Al	Fe	Ca	Mg	K	Na	S	P	Cl
Birch Pellets	7.14e-3	2.07e-3	1.17e-3	2.16e-2	5.23e-3	1.08e-2	6.92e-4	9.26e-4	6.04e-4	3.3e-5
Birch hw	4.17e-5	1.45e-5	1.19e-4	2.92e-2	7.70e-3	2.79e-2	1.36e-4	7.79e-4	4.28e-3	3.3e-5

The temperature inside the reactor is measured with seven thermocouples (Type K), placed only 5 mm into the bed. The temperature inside the manifold is also measured, as well as at several points at the outlet pipe. The pressure at the manifold and inside the reactor is measured with the help of pressure transducers.

A more detailed description and characterisation of the gasifier system is given by Barrio et al. (2001a and 2001b), Barrio (2002) and Guhl (2002).

5.4.2 The pipeline, sampling point and filter unit

Erroneous particle size distributions and particle concentrations is sought minimised by constructing the product gas line, sampling point and slip stream-line (Figure 5.3) according to available standards (the Norwegian standard (NS 4861), the German VDI 2066, and ISO 5221, 7194 and 12103-1). The gas velocity through all horizontal pipe lines was > 20 m/s, and the velocity at the sampling point was approx. 5 m/s. An "étoile" flow straightener is installed at the inlet of the vertical sampling section, in order to minimise swirl at the sampling point. The volume flow control and measurement system consisted of a reduction valve and a calibrated nozzle.

A back-up filter and a simplified tar sampling line were placed downstream of the granular filter. The water content of the gas is condensed out together with the tar as passing through the sampling line. Additional moisture was removed in the silica gel box.

The heating system consisted of four separate heating elements (Figure 5.3): i) the bottom section of the gasifier, ii) the pipe-line from the bottom-section until the sampling point, iii) the pipeline from the sampling point and through to the inlet cone and iv) the test section. Elements i and ii are welded directly on to the gas line, while indirect heating was applied for iii and iv.

Zone iii and iv: The heating elements were placed concentric around each part of the system. Thus, heat transfer was accomplished through natural convection and radiation (no direct contact between heating elements and filter unit). All heating elements were used during the pre-heating of the system. The heating element surrounding the test section was switched off during filtration in experiment #16. (This procedure was used in order to minimize the electromagnetic field surrounding the filter, as in the filtration experiments with standard dust qualities, Section 3.2.5). However, despite compensation through heating element iii the filtration temperature fell from 520 to about 420 °C during filtration. It was therefore chosen to use heating element iv also during filtration in experiment #23.

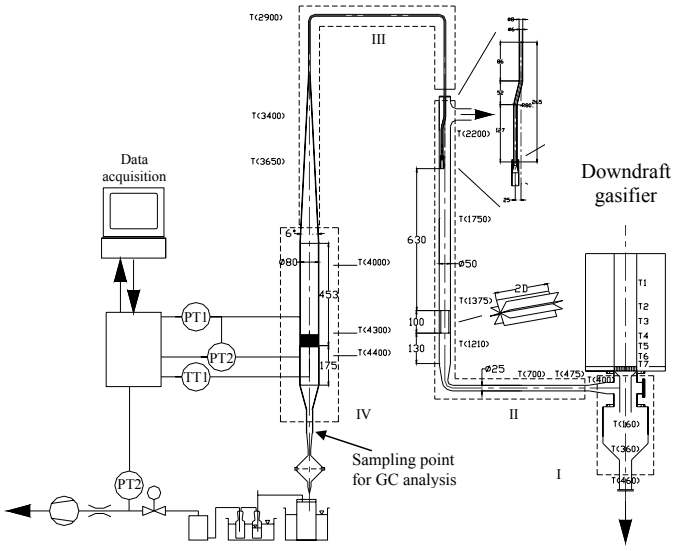

Figure 5.3: Illustration of the product gas line, sampling point and the location of the most essential temperatures are indicated on the drawing (notation: T(mm)).

The following signals were recorded continuously, and used to evaluate the filter operation: The relative pressure just above the filter surface (PT1); the pressure difference between the dirty and clean gas sides of the filter (PT2); the volume flow (calculated based on the absolute pressure (PT3) at the inlet of the calibrated nozzle installed upstream of the blower); and the temperature measured just beneath the wire-mesh (TT1).

5.4.3 Experimental procedure

The gasifier, product gas line and filter are preheated to 250 °C, 600 °C and the pre-defined filtration temperature respectively. Ignition of the gasifier is accomplished by charging it with small pieces of charcoal (approx. one fifth of its height) and thereafter entrain some few pieces of glowing charcoal onto these. Once the view port is closed and ignition has been observed from the temperature readings, the reactor is filled with raw pellets. Air being supplied from level A_2, the pyrolysis front climbs up through the reactor until it reaches its final position, close to air level A_2. The bed level is maintained above T_1 but its exact location is unknown because it cannot be measured. Stable operation is normally reached approximately two hours after ignition. (The notation used when referring to the experiments (e.g. exp. #14) is identical to the notation used by Barrio et al. (2001b).)

Filter operation: In experiment #14 and #16 the filter was operated with approximately 250 ml of granular material (Olivin sand, $X_{50,3}$ = 545 μm), corresponding to a bed thickness of about 4cm. The bed rested upon a wire mesh and was slightly fluidised with a reversed flow of air (in order to accomplish a homogeneous bed) after mounting and isolating the test section. Thereafter a new back up filter was installed, the first impinging bottle filled with acetone, and the silica gel holder re-filled with virgin silica gel. Both the steel condenser and the

impinging bottles were placed in a ice/salt bath in order to protect the blower by maximising the condensation of both tars and water.

Experiment #23: This experiment was conducted with two layers of granular material, a fine sand layer (about 250 ml of Olivin AFS50, $X_{50,3}$ = 351μm) backed with a coarser granule (about 250 ml of catalytic material (G-56A from Süd-Chemie AG, München, Germany) 1 to 2 mm in diameter). The fluidisation procedure was not used in this experiment, an empty impinging bottle replaced the steel condenser and no salt was used in the ice bath.

The product gas was enriched with steam (up to about 20 vol.%) in order to enhance the stability of the steam reforming catalyst (suppressing deactivation by carbon lay down). Steam generation was accomplished through an electric heater, and the injection point was located just below the gasifier grate.

The catalytic material was activated by flowing a mixture of hydrogen in nitrogen through the filter system during heating up (in the opposite direction to normal flow). The following procedure was used: i) purging the system with pure nitrogen (262 l/h) for about 50 minutes (while the temperature in the filter unit rose from room temperature up to approx. 60 °C), ii) catalyst activation was started by adding 4.5 vol.% hydrogen to the purge gas (total flow 274 l/h) while the filter temperature was increased from 100 to approx. 500 °C (about 60 minutes), iii) increasing hydrogen content to 13 vol. % (T_{filter} 500 °C, total flow 240 l/h) duration about 60 minutes, iv) decreasing the flow to 180 l/h (13 vol.% H_2 in N_2) for 80 minutes, v) purging the system with pure nitrogen (160 l/h) for 15minutes before starting filtration.

Inlet and outlet gas quality was measured by gas chromatography. Determination of the major gas components: A gas sample was manually injected (using a syringe) into a gas chromatograph from SRI Instruments, equipped with a TCD detector and a Supelco column (Carboxen 1000). The instrument was calibrated for H_2, N_2, CO, CH_4 and CO_2. A Chrompack, refinery gas analyser (three channels) was used for the determination of minor components/tars: The first channel is designed for the light hydrocarbons separation, C1-C5 (Alumina plot capillary column). Channel 2 (HaySep (T/Q) and MolSieve 5A packed column in combination) was used for the analysis of permanent gases and C1, C2 hydrocarbons. Channel 3 (Haysep Q / MolSieve 5A in combination) was used for hydrogen determination. Sample injection was accomplished both on-line (syringe) and using a gas-mouse. Further details about the experimental set-up is given by Skoblja (2002) and Botnevik (2002).

The reduction valve located just up-stream of the nozzle was closed until the gasifier had reached stable operation and the filtration experiment started.

5.4.4 Experimental results on high temperature filtration, filter cake formation

Stable operation of the gasifier was reached in all three experiments (#14, #16 and #23) and the granular filter was operated for 9 hours in total.

Excess air ratio during exp. #14 was equal to 0.29, air supply equal to 6.0Nm^3/h and the amount of product gas produced was equal to 12.6 Nm^3/h. The gasifier operation during exp. #16 was similar to #14 (and exp. #13a). Hence, the product gas quality is assumed to be equal. The product gas dependency upon air supply is shown in Figure 5.4. (Cabeza (2001) gives a more detailed description of the gasifier operation during these two experiments.)

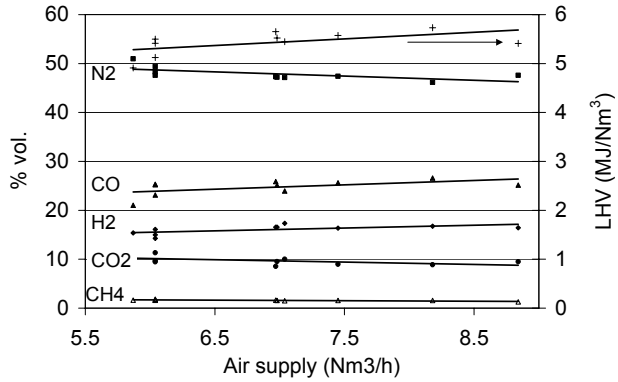

Figure 5.4: Product gas composition as a function of air supply (Barrio et al. 2001b)

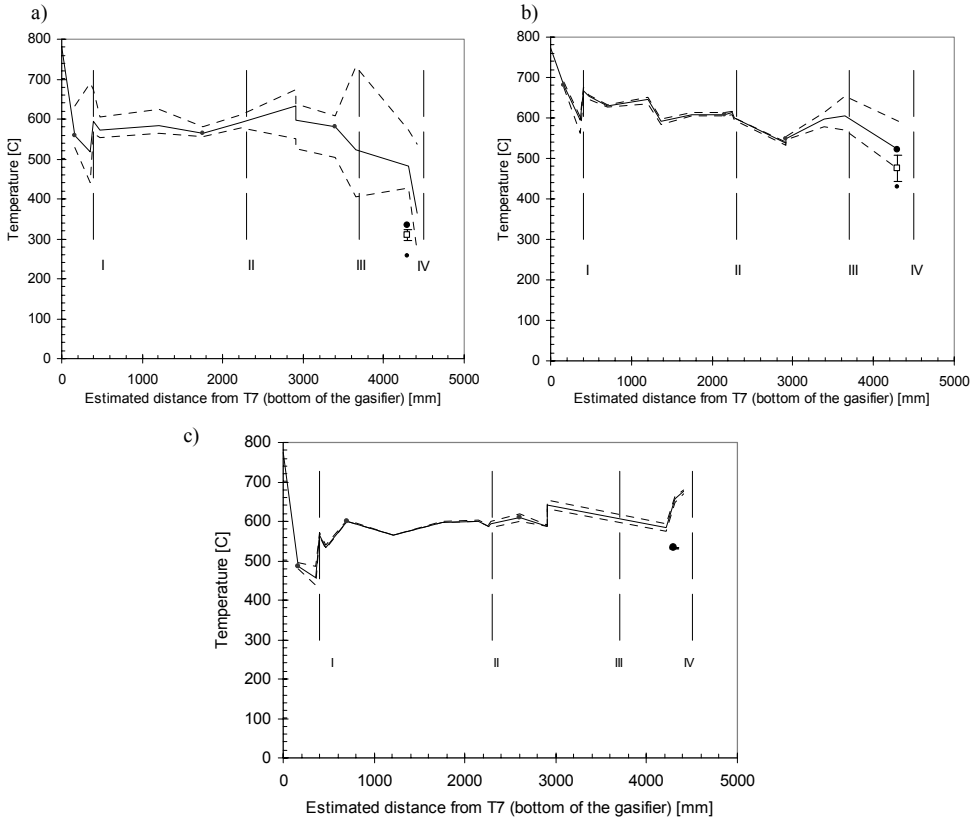

Figure 5.5: Temperature along the pipeline from the gasifier outlet (T7) to the filter bed: a) experiment #14, b) experiment #16 and c) experiment #23. Both maximum and minimum temperature, measured during filtration, is displayed together with the averaged value. Note that only the filtration temperature is measured directly in the gas stream (□-average and •-maximum/minimum). Temperatures used to regulate the different zones are marked with: •.

Heating element iv has normally just been applied during the pre-heating of the filter unit (Section 3.2.5) but an exception was made in exp. #14 and #23. Here, both the zone iii and iv was used to keep the filter temperature constant.

The uniformity of the temperature profiles along the product gas line and filter unit is shown in Figure 5.5. The uniformity of the temperature profile obtained in exp. #14 was rather bad (short pre-heating period) compared to the uniformity obtained in exp. #16 (reduced uniformity in zone iv as this was switched off during filtration) and #23 (due to instabilities in the electric circuit zone i had to be switched off prior to ignition).

Filtration of the product gas started after the gasifier had reached stable operation (Figure 5.6). However, malfunctions in the fuel feeding system (lock-hopper operated with sliding valves) generated significant fluctuations in the recorded temperatures and pressures within both the gasification reactor and the high temperature filter (exp. #14 and #16).

Experiment #14: The first minutes of filter operation was influenced by velocity fluctuations and increasing filtration temperature. Stable filter operation was reached after approximately 20 minutes ($T_{filter} \approx 300$ °C). A slightly decreasing pressure drop rate is seen at the end of the experiment (Figure 5.7).

Experiment #16: The pressure build-up (Figure 5.7) increased sharply after about 30 minutes of filtration. In addition to some velocity fluctuations (as reported for exp. #14) this period coincides with unstable gasifier operation (malfunctioning in the lock-hopper system). The sudden increase in the pressure drop after 130minutes of operation is due to increased filtration velocity. The pressure build up rate during stable operation was generally low and steadily decreasing. Note that the decreasing filtration temperature enhances this decrease in the pressure drop rate ($dP_{filter} \propto \mu$, hence roughly proportional to $T_{filter}^{0.75}$.)

Experiment #23: The total pressure build up was about four times higher than for exp. #14 (Figure 5.7). The observed fluctuations in the pressure drop are due to increased gas throughput resulting from the gas sampling (for GC analysis) downstream of the filter unit. Shaking of the gasifier grate resulted in some additional pressure build up, also seen in the preceding experiments.

Figure 5.8 shows experimental calibration curves as obtained at room temperature for the two different bed configurations (exp. #14 and #16 vs. #23, solid lines). Included in the figure is also the temperature corrected pressure drop, shown for 300 °C (dashed lines, long) and 500 °C (dashed line, short), as is some data points extracted from the very beginning of the filtration experiments. A significant deviation is seen between the temperature corrected pressure drop and the data points extracted from exp. #14 and #16. This indicates erroneous velocity calculations in these experiments, partly explaining the low resulting pressure build-up. A closer evaluation of the experimental set-up used in exp. #14 and #16 showed that the critical nozzle used in these experiments (ø 5 mm) was too large to obtain accurate flow control. A smaller nozzle (ø 3 mm) was installed prior to exp. #23, the improved accuracy is evident from Figure 5.8 (the pressure drop for 3.3 cm/s is obtained during catalyst activation).

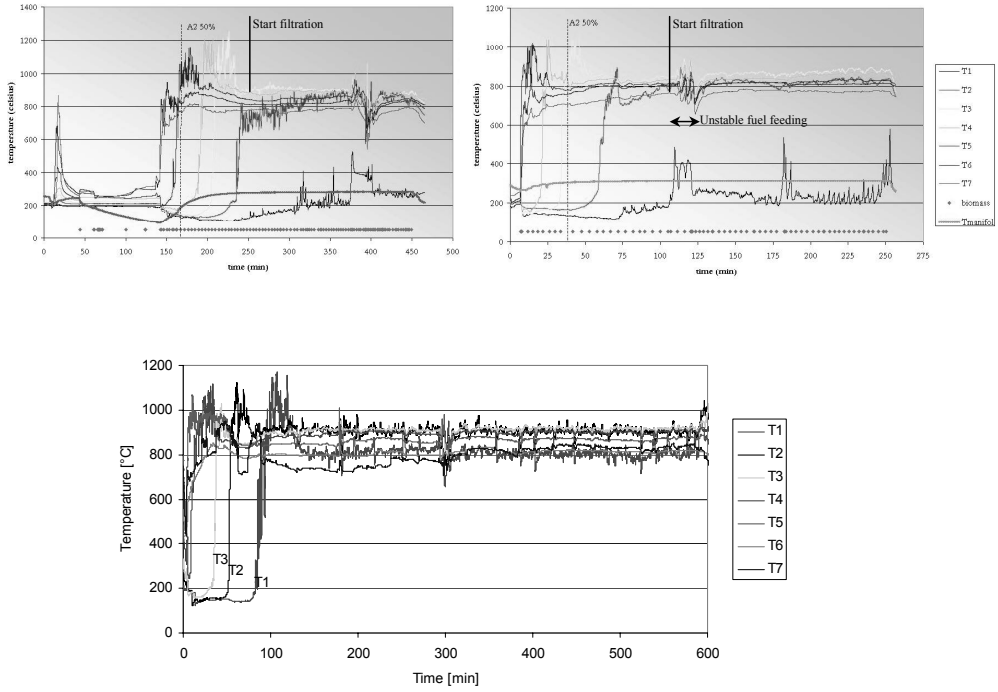

Figure 5.6: Temperature history for the gasifier during experiments #14 (upper left) and #16 (upper right) and #23 (lower).

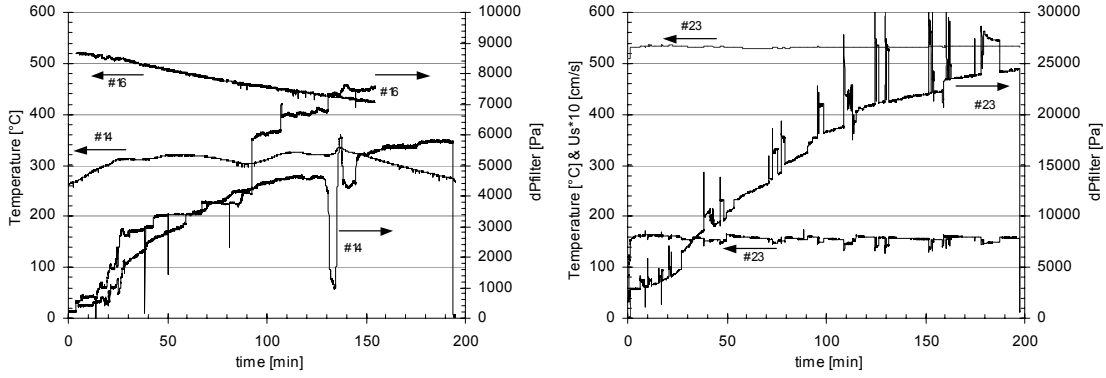

Figure 5.7: Comparison of the temperature and pressure profiles in the initial two experiments (#14 and #16) and the final experiment (#23)

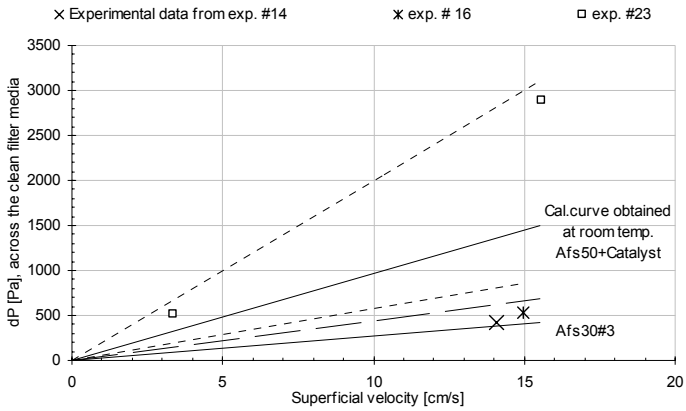

Figure 5.8: Pressure drop through the clean filter bed: calibration curves obtained at room temperature and experimentally measured values.

The decreasing pressure build up rate at the end of the experiments might be explained as due to a change in the raw gas dust concentration/composition with time, the nature of the filter cake build up or minor gas leakages downstream of the filter caused by the increasing under pressure in the filter system (this should be further investigated).

The filter test section was cooled down before dismantling. During cooling the filter was purged with nitrogen in order to preserve the filter cake for further analysis (exp. #16 and #23). Estimation of the inlet dust concentration based upon the collected filter cake, shows a very low dust concentration in exp. #16 (about 2.7 g/Nm^3, dry gas) compared to exp. #23 (10.6 g/Nm^3, dry gas). The latter dust concentration is very close to the value reported by Barrio (2001b), 10.5 g/Nm^3 (dry gas).

Instabilities in the gasifier operation and erroneous filtration velocity reduced the outcome of exp. #14 and #16, however evidence of filtercake formation was found. The picture taken through the crystal walls surrounding the filter (exp. #16, Figure 5.9) clearly documents cake formation (2-3 mm high). This filtercake formation was confirmed in exp. #23 (Figure 5.10 and 5.11) where stable gasifier operation, uniform and stable filter temperature and improved regulation of the volume flow through the filter allowed for a better evaluation of filter performance.

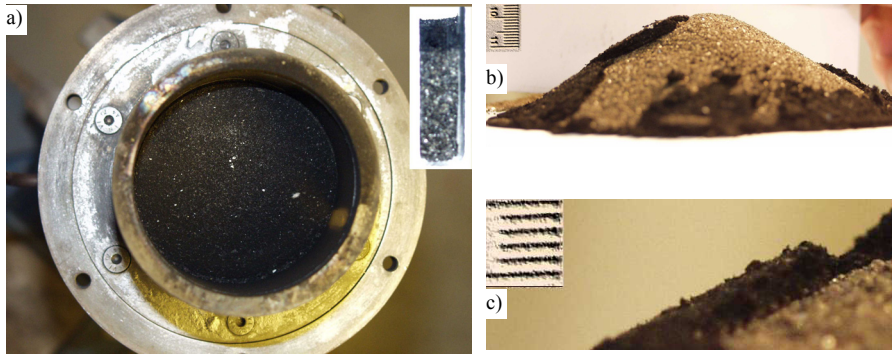

Figure 5.9: Experiment #16: a) Top view of the deposited particles, including a cross section of the cake b) Bed material and cake fragments, after removal of the supporting wall, dimensions as indicated by the ruler displayed in the upper left corner. c) Indication of filter cake height. Ruler included in upper left corner, mm spacing.

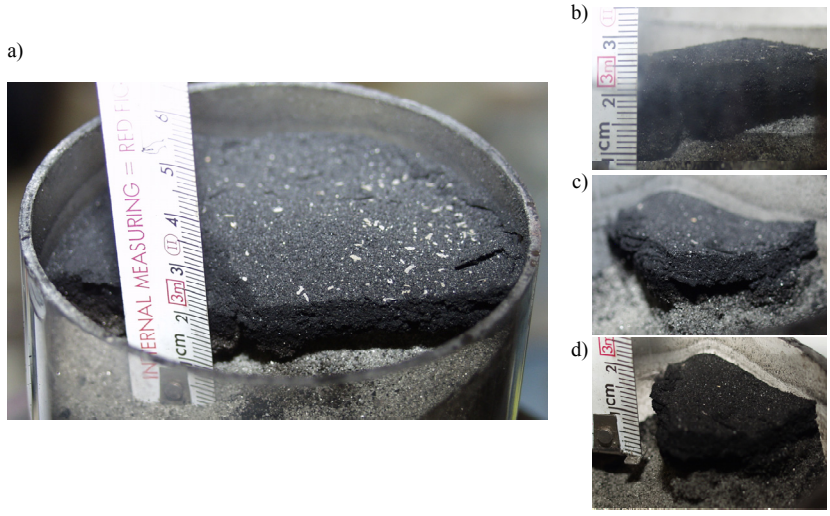

Figure 5.10: Experiment #23: Top view of the filter cake. The cake had a typically two-layered structure, the upper part consisting of thin "layers" of carry over particles and having a "textile" like characteristic, while the lower part consisted of typically coarser particles. The latter layer being partly mixed with bed material.

Figure 5.11: The two filter cake layers had a clear cut and could easily be separated (upper layer to the left and lower layer to the right). The thickness was estimated to be about 3 and 5 mm respectively.

5.4.5 Experimental results on high temperature filtration, catalytic conversion of tars.

Experiment # 23: Major gas components (H_2, CO, CO_2, CH_4 and N_2) were measured before and after the high temperature filter unit (Figure 5.12). The shift towards a higher content of H_2 and CO_2 (a minor increase in CH_4 is also seen), and lower content of CO and N_2 is evident. This catalytic effect is consistent with the results from the Chrompack analyser, including both major and minor components. Significant levels of etan (C_2H_6), etan/etylen (C_2H_4), etyn/acetylen (C_2H_2), propen/propylene (C_3H_6), benzen and toulen, together with some trace amounts of other species are seen before the filter (Table 5.5) while only trace amounts, mainly etan/etylen (C_2H_4), benzene and toluene are seen after the filter. Skoblja (2002) gives further details about the gas sampling and analysis.

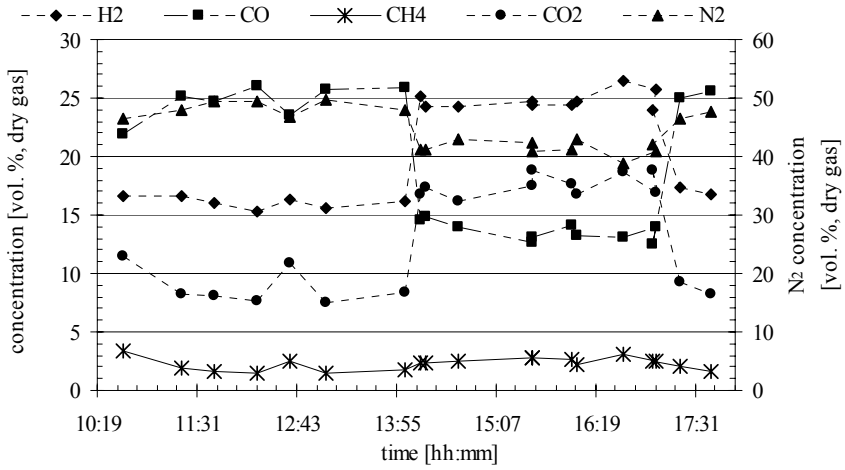

Figure 5.12: Major gas components (SRI-analysis) as measured before (until 13:55 and after 17:30) and after the high temperature filter unit (from 13:55 until 17:30).

Table 5.5 Gas components from experiment #23, analysis conducted with the Chrompack GC.

Sampling time [1)]	277	340	411	462	519	519
Method used for sampling	on-line (syringe)	on-line (syringe)	on-line (syringe)	gas mouse	on-line (syringe)	gas mouse
Sampling #	3	4	8	11	13	14
Components	before filter	after filter	after filter	after filter	before filter	after filter
Main components [*)]						
O_2/lekkasjer	0.682	5.100	6.516	0.000	0.770	1.241
H_2	16.398	26.577	27.501	24.247	16.634	25.693
CO_2	7.458	19.384	20.457	16.084	8.028	17.152
O_2	0.000	0.000	0.000	0.000	0.000	0.000
N_2	47.563	36.128	34.467	43.213	45.795	40.123
CH_4	1.583	2.621	3.014	2.336	1.777	2.608
CO	26.574	15.268	14.556	14.116	27.255	14.421
Minor components						
Etan (C_2H_6)	0.021	0.002	0.000	0.000	0.028	0.000
Eten/Etylen (C_2H_4)	0.307	0.016	0.003	0.002	0.367	0.003
Etyn/Acetylen (C_2H_2)	0.020	0.000	0.000	0.000	0.037	0.000
Propan (C_3H_8)	0.001	0.000	0.000	0.000	0.001	0.000
Propen/Propylen (C_3H_6)	0.012	0.001	0.000	0.000	0.018	0.000
1.2-Propen (C_3H_4)	0.000	0.000	0.000	0.000	0.000	0.000
1-Propyn/Metylacetylen (C_3H_4)	0.002	0.000	0.000	0.000	0.000	0.000
Butener	0.000	0.000	0.000	0.000	0.000	0.000
1.3-Buten/Bivinyl (C_4H_6)	0.003	0.000	0.000	0.000	0.000	0.000
Syklopentan	0.000	0.000	0.000	0.000	0.000	0.000
C5-umettet	0.001	0.000	0.000	0.000	0.000	0.000
Heksan/Dipropyl	0.000	0.000	0.000	0.000	0.000	0.000
C6-umettet	0.002	0.000	0.000	0.000	0.002	0.000
Benzen	0.045	0.004	0.001	0.000	0.049	0.001
Toluen	0.007	0.001	0.000	0.000	0.008	0.000
Meta- og para-xylen	0.000	0.000	0.000	0.000	0.001	0.000
Styren [2)]	0.001	0.000	0.000	0.000	0.001	0.000
Unidentified components	0.001	0.000	0.000	0.000	0.000	0.000
SUM [3)]	100	100	100	100	100	100

The components from ethane is grouped after increasing number of carbon atoms

[*)] Normalised values in vol %

[1)] Number of minutes from ignition in the gasifier.

[2)] Unsertain identification

[3)] Normalised, O_2-free gas

5.5 *Experimental setup and procedure for The gasifier at TU-Wien (Fercher. et al. 1998)*

The FICFB-gasification process (Figure 5.13) consists of two zones. The gasification zone is fluidised with steam and the combustion zone is fluidised with air. The bed particles are separated from the riser gas stream using a U-beam separator. The fuel feeding system consists of a hopper and a multi-screw-conveyor. Air is supplied by blowers into the riser and during the start up period also into the gasification zone. Steam is produced by an electrical steam generator and overheated by an electrical heater. The product gas, which is cooled from 700 °C to 200 °C by a three-step heat exchanger, and the flue gas have separated exits from the reactor. A gas burner ensures that the product gas is completely combusted before entering a cyclone and a flue gas cooler. A product gas cyclone reduces the particle content of the product gas from 20 g/Nm³ to 3 g/Nm³. Figure 5.13 contains characteristic data and dimensions of the pilot plant. The reactor is manufactured with stainless steel and is isolated. The warm up is carried out with electrical preheating of all air streams.

The gas composition of the product gas depends on the gasification temperature and the fuel itself. With increasing temperature the H_2 content increases, the CO_2 content remains nearly constant and the CO and CH_4 content decreases. The N_2 content of the product gas is about 5%. This is very low compared to air blown gasifiers (45-50%). The calorific value is therefore much higher and lies above 13 MJ/Nm³ dry gas.

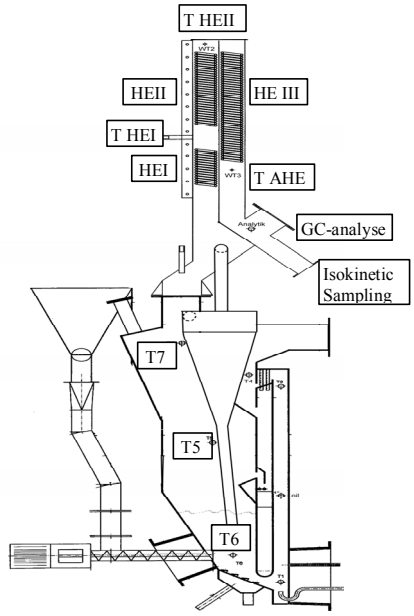

Characteristic data of the pilot plant		
thermal output	100 kW	
fuel	wood chips	
reactor	800 x 120	mm
riser	75 x 120	mm
riser height	2500	mm
bed material	olivine	
bed mass	37.5	kg
mean diameter	0.6	mm

Location	Temperature [°C]	
	run #1	run #2
T6	800	800
T5	750	750
T7	600	600
T HEI	~500	350-450
T HEII	250-350	350-400
T HEIII	250	200

Figure 5.13: The FICFB gasifier and its heat exchanger (Ferscher et at. 1998). T6: gasification temperature; T5: freeboard temperature; T7: cyclone inlet; HEI: heat exchanger 1. section; HEII: 2. section; HEIII: 3. section; THEI: temperature after HEI; THEII: temp after HEII; T AHE: temp after heat exchanger.

Samples from two different test-runs (#1 and #2) have been collected and analysed. The samples consist of deposits from the down-stream heat exchanger and isokinetic dust samples. Stable operating conditions lasted for approximately 4 and 7 hours, accounting for respectively 1/3 and 1/2 of the total run time. The gasification temperature was 800 °C in both runs.

Dust samples were collected through a slipstream connected after the heat exchanger (AHE), at stable operating conditions. While the deposits from the first and second section of the heat exchanger (HEI and HEII) were collected after plant shutdown, and thus affected by the whole test run (included heating up and cooling down). It is assumed that this has a non-negligible effect on the collected deposits.

5.6 Gasification of birch in the down draft stratified gasifier, chemical equilibrium analysis

The global equilibrium approach based on bulk input compositions only – although limited – is useful as a first estimate of the complex reactions inside a biomass conversion system. There are uncertainties in the numerical values of the equilibrium, but much greater errors may appear due to inconsistency in the thermochemical data, or simply missing compounds. (A more thorough discussion concerning equilibrium calculations was given in Chapter 4).

This section presents results from global equilibrium calculations performed in order to evaluate the ash chemistry relevant for the downdraft gasifier coupled to the high temperature filter unit (i.e. the HBU). The applied air ratio (0.3) corresponds to the experimental conditions. Equilibrium calculations were performed in the temperature range 500-1100 °C, on both birch pellets and birch heartwood. (The included model solutions are summarised in Table 5.6.) These two fuel qualities were used in order to evaluate the effect of fuel contamination and sensitivity of the fuel analysis upon the predicted results.

The fuel experiences a relatively sharp temperature gradient as it is introduced into the pyrolysing zone of the gasifier as does the product gas in the product gas line. Thus the inorganic ash particles will experience short residence times during heating up (when entering the flamming pyrolysis zone) and cooling down (flowing through down stream pipe lines and heat exchangers), while relatively long residence times are expected within the gasification zone and the high temperature filter unit. The latter typically allow the ash reactions to approach equilibrium to a greater extent. However, reactions in a condensed layer become slow at temperatures much below 600 °C and equilibrium might not be obtained.

Two different concepts might be relevant for the condensed phases: Pure nucleation or solid solutions. Which of the phenomena that will actually be controlling depends on the aerosol physics in the system, e.g governing the size distribution of the particulate emission. (This is not possible to predict by thermodynamic calculations.) If the system is assumed to consist of pure particles only, no liquid phase is present since the condensed compounds are stable at temperatures below their pure component melting temperature. Thus, the eutecticum is not considered.

Often one condensed compound will dominate leading to an almost pure phase of that compound. In other cases one compound starts condensing at much higher

Table 5.6: Solution phases evaluated in the calculations

#	Solution	Species	Comments
1	MONOB	MgO, CaO, $MgAl_2O_4$	BMonoxide
2	MONT	$CaMgSiO_4$, Mg_2SiO_4, $CaFeSiO_4$	Monticellite-forsterite replaced by Oli1
3	CFSM	$CaMgSiO_4$, Fe_2SiO_4, Ca_2SiO_4	(Ca,Fe)SiO4-CaMgSiO4 replaced by Oli1
4	SIO3?	$MgSiO_3$, $FeSiO_3$, $CaSiO_3$	$MSiO_3$-ss
5	CASI	Mg_2SiO_4, Fe_2SiO_4, Ca_2SiO_4	a'Ca_2SiO_4 new in FS: ‘’C2S
6	NCSO	$Na_2Ca_2Si_3O_9$, $Na_4CaSi_3O_9$	***$(Na_2,Ca)Na_2CaSi_3O_9$ solid solution***
7	OLIV	Mg_2SiO_4, Fe_2SiO4, Ca_2SiO_4	Olivine new in FS: Oli2
8	MELI	$CaMgSiO_4$, Mg_2SiO_4, $CaFeSiO_4$	Melilite solution
9	SLAGA	MgO, FeO, Na_2O, SiO_2, CaO, Al_2O_3, K_2O, MgS, CaS, FeS, Na_2S, K_2S, NaCl, KCl, $CaCl_2$, $MgCl_2$, $FeCl_2$	Slag-liq/glass oxide
	SLAGD	MgO, Na_2O, SiO_2, CaO, Al_2O_3, K_2O, MgS, CaS, Na_2S, K_2S, Na_2SO_4, K_2SO_4, $CaSO_4$, $MgSO_4$, NaCl, KCl, CaCl2, $MgCl_2$	Slag-liq/glass oxide
	SLAGF	Na_2O, SiO_2, CaO, Al_2O_3, K_2O, CaS, Na_2S, K_2S, Na_2SO_4, K_2SO_4, $CaSO_4$, NaCl, KCl, $CaCl_2$, Na_2CO_3, K_2CO_3, $CaCO_3$	Slag-liq/glass oxide
	SLAG?	MgO, FeO, Na_2O, SiO_2, CaO, K_2O	Slag-liq/glass oxide
10	ACLA	NaCl, KCl	Alk-Cl solid new in FS: AClA
11	CSOB	Na_2CO_3, K_2CO_3, Na_2SO_4, K_2SO_4	CO_3,SO_4/Na,K
12*	KCO	Na_2CO_3, K_2CO_3, Na_2SO_4, K_2SO_4	K_2CO_3 solid, NaK/CO_3,SO_4
13	NKXA	KOH, KCl	ANa,K/OH,F,Cl high temperature solid binary solution
14*	NCOA	NaCl, NaOH	Na/Cl,OH high NaOH content solid binary solution
15	SALT	NaCl, KCl, NaOH, KOH, Na_2SO_4, K_2SO_4, Na_2CO_3, K_2CO_3, $NaNO_3$, KNO_3	Salt-liq new in FS: SALTA/SALTB/SALT?
16	LCSO	K_2SO_4, $CaSO_4$, $K2CO_3$, $CaCO_3$	liq-K,Ca/CO_3,SO_4
17	SCSO	K_2SO_4, $CaSO_4$, K_2CO_3, $CaCO_3$	s-K,Ca,/CO_3,SO_4
18*	SCMO	$CaSO_4$, $MgSO_4$	s-Ca(SO_4),Mg(SO_4)
19*	LSUL	$CaSO_4$, $MgSO_4$, Na_2SO_4	liq-Ca,Mg,Na/SO_4

*Solution did not form in any of the cases studied

temperature than the rest, which means, that there will be almost pure condensed particles of this compound at these high temperatures.

-Assumptions and calculations

The discussion presented in this section includes two simplified scenarios: i) Global equilibrium is reached unconstrained, i.e. complete mixing and no kinetic limitations in the whole temperature interval (500-1100 °C). ii) The interactions between the dilute phase of condensed compounds present in the product gas is assumed to be negligible, as between the condensed compounds and the elements present in the gas phase. Thus, elements present in the gas phase will preferably form molten salt/carbonate or pure stoichiometric compounds and not lead to the formation of the solid solutions.

Note that the effect of partitioning between the bottom ash and carry over particles is not taken into account in this study. Although carry over particles deposited in the filter unit will experience enhanced contact, as compared to the dilute phase of condensed compounds present in the product gas, both the temperature level (in our case 300-500 °C) and particle mixing is limited.

-Results and discussion

Scenario i (global equilibrium reached, unconstrained) see Figure 5.14: Calculations performed on the birch pellets shows liquid potassium carbonate formation (SALT and LCSO) between 700 and 850 °C (mean temperature for the gasification zone and gasifier outlet was about 800 and 775 °C respectively). Mg is found as stoichiometric MgO(s), Si as Ca_2SiO_4 (CASI-solid solution) and excess Ca as CaO (Monoxide -solid solution). Phosphorus is found as $Ca_5HO_{13}P_3$(s) below some 750 °C and above some

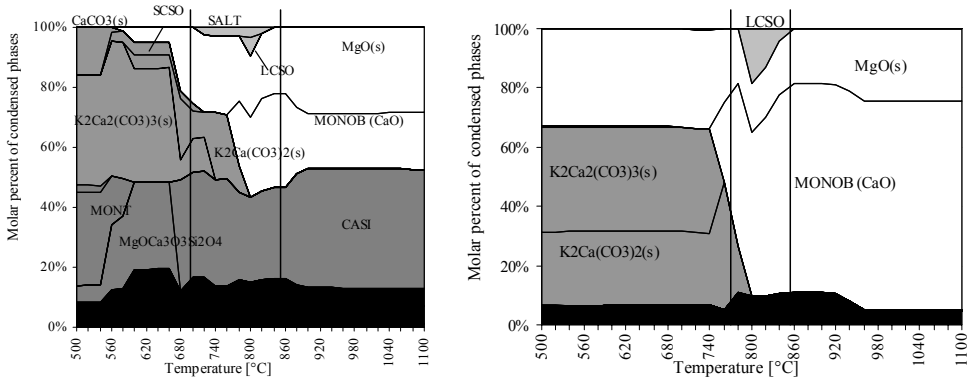

Figure 5.14: Results of the equilibrium calculations. Molar distribution of condensed phases for birch pellets (left) and birch heartwood (right). The drop lines indicate the temperature region within which liquid ash melt is formed.

950 °C, while K_3PO_4(s) is formed at intermediate temperatures. Al is present as $Ca_3Al_2O_6$(s) above 900 °C, as $MgAl_2O_4$(s) below some 700 °C and as $KAlO_2$(s) at intermediate temperatures.

Including Al in the SLAG model input (a viscous solution of pure silicate/oxides of K_2O, CaO, SiO_2, MgO, FeO, Na_2O and Al_2O_3) results in SLAG formation down to about 550 °C for both birch pellets and heartwood otherwise no SLAG formed. When present, this solution contained all Al present in the input fuel for birch pellets. Note the very low amounts of Si and Al in birch heartwood. However, its existence is considered to be questionable due to model limitations (see discussion in chapter 4). Si not included in the SLAG solution is found as Ca_2SiO_4 (CASI-solid solution) above, and as $MgCa_3O_3Si_2O_4$(s) below some 700 °C. Below some 600°C most of the Mg is found as $CaMgSiO_4$(s), while access Ca is found as carbonates ($CaCO_3$(s), $K_2Ca_2(CO_3)_3$(s) and $K_2Ca(CO_3)_2$(s)).

The very low Si content in birch heartwood results in virtually no silicates being formed (Figure 5.14). Carbonates are found both as stoichiometric components and as significant amounts of molten carbonates (LCSO) present between 750 and 850 °C, formation temperature slightly higher than for birch pellets.

Note that Ca is primarily present as liquid carbonate in the liquid solution LCSO, while SALT mainly contains (K,Na)-CO_3 where K is dominating. This means that Ca is preferably found either as stoichiometric $K_2Ca(CO_3)_2$(s), $K_2Ca_2(CO_3)_3$(s), or as CaO (Monoxide-solid solution). Thus, with substantial surplus of Ca, this should be present as CaO, with increasing amount of $CaCO_3$(s) below 600 °C. CSOB, a solid solution of Na and K carbonates, is stable between some 550-700 °C.

The high level of Mg in the input fuel results in significant oxide formation as stoichiometric MgO(s), over the whole temperature interval, except below some 550 °C if Monticellite is formed (i.e. for birch pellets).

Applying scenario ii is only appropriate from the gasifier outlet, through the product gas line and in the filter, which means that this only affects the elemental distribution

as calculated for temperatures below the gasifier outlet temperature (about 775 °C). This would imply that Ca_2SiO_4 (CASI) formed within the gasifier is transported as "inert" particles from the gasifier to the filter, and deposited as such. Furthermore, at typical gasifier conditions, Mg is most stable as MgO(s), and rest Ca as CaO (Monoxide-solid solution). These would be expected to deposit in the filter cake as MgO(s), CaO(s) and to some extent as $CaCO_3$(s). (CaO is accessible for reaction with the gas phase to form carbonates.)

If, despite the low filtration temperatures (about 500 °C) and the limited mobility (the particles are deposited in a stationary matrix/dendrites), chemical equilibrium is obtained in the filter unit the chemically more stable components of Mg_2SiO_4(s) and $CaMgSiO_4$(s) and $MgOCa_3O_3Si_2O_4$(s) would form. Some of the Ca would also form (K, Ca) –carbonates. However, considering the low temperature and the limited mobility it is found more likely that particles deposited as MgO(s), CaO(s), $CaCO_3$(s), K_2CO_3(s) and CASI (Ca_2SiO_4) would preferentially form the more stable (K, Ca)-carbonates ($K_2Ca(CO_3)_2$(s), $K_2Ca_2(CO_3)_3$(s)), although in limited amounts. And only minor amounts of Mg_2SiO_4(s), $CaMgSiO_4$(s) and the more complex $MgOCa_3O_3Si_2O_4$(s) is expected.

-*Conclusion*

The filtration experiments reported in this work were conducted at relatively low temperatures (300-540 °C) at which the kinetic limitations involved in the formation of complex binary and ternary compounds are expected to be considerable, thus significantly inhibiting the formation of complex (Ca, Mg) silicates present at equilibrium conditions. The existence of a liquid oxide/SLAG is questionable (although predicted in very small amounts). However, a significant amount of molten SALT and liquid carbonates (LCSO) is present in a temperature window between 700-850 °C, i.e. within the operating conditions of the gasifier (gasifier outlet – about 775 °C; gasification zone – about 800 °C; peak temperature in the flamming pyrolysis – about 1000-1100 °C).

The interaction between solid particles is expected to be significant within the gasifier bed and the filter cake, but limited when entrained in the gas phase. Hence, upon cooling of the product gas and the dilute phase of carry-over particles, partly conversion of CaO(s) to $CaCO_3$(s) is considered to be more likely than formation of more complex calcium silicates and (Ca, Mg) silicates (i.e. Ca_2SiO_3(s), Mg_2SiO_4(s), $CaMgSiO_4$(s) and $MgOCa_3O_3Si_2O_4$(s)).

Continuous operation of a high temperature filter system (e.g. the PBF) results in improved contact and mixing between the condensed particles. Especially effects as particle accumulation and re-entrainment (within the filter house) will encompass enhanced mixing and contact between the condensed phases.

5.7 Analysis of deposits, carry over particles and tars

The fly ash collected in experiment #13a, the filter cake formed in experiment #16 and the deposits collected downstream of the FICFB has been characterised using thermogravimetrical measurements (TGA), gas-chromatography (GC-MS) and scanning electron microscopy (SEM-EDX).

Parts of the untreated and ashed (in air at 450 °C for 6 hours) carry-over particles, filter cake material and FICFB samples were analysed semi quantitatively, by X-ray diffraction, on the elements *Si*, *Al*, *Fe*, *Ca*, *Mg*, *P*, *Na*, *K* and *Cl*. It is important to be aware of the limitation connected to this method. As these chemical analyses are performed on the surface of the particles only (maximum depth of about 1 μm). Despite this, the results are believed to give a qualitative description of the samples.

All the figures and chemical analyses obtained in connection to these analyses are included in Appendix III. But, some selected elemental analysis (averaged values of area measurements and point measurements (pp)) are presented in Figure 5.15 (elemental composition is given on a molar basis). Chemical analyses of the filter media, birch heartwood and birch pellets are included for comparison. (The chemical analysis of the fuel is identical to those published by Barrio et al. (2001b).)

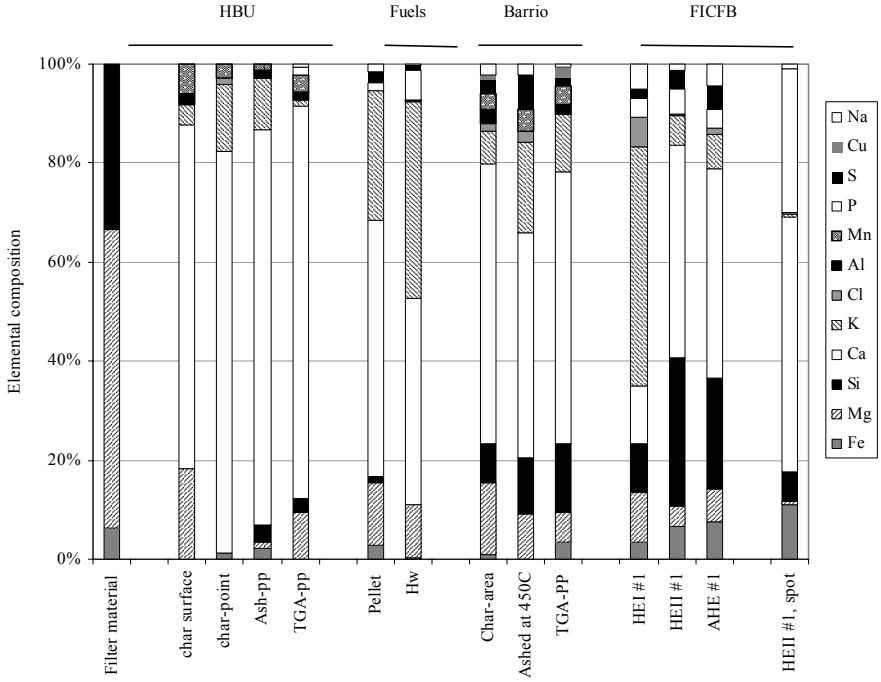

Figure 5.15: Chemical analysis of the filter material and filter cake from the HBU, carry over particles (collected by Barrio et al. (2001b)) and those collected after the FICFB.

5.7.1 Fly ash characterisation by electron microscopy and qualitative chemical analysis

SEM pictures of the bed material (olivine sand) applied in the horizontal bed filter (Figure 5.16a) reveals non-porous particles typically irregular in shape, the corresponding size distribution is given in Figure 3.12. Samples of the raw and ashed filter cake samples are included in this figure.

A large number of small and intermediate char particles (<10 and 10-100 μm) is found in the samples obtained from the filter cake material, Figure 5.16.b. The larger porous char particles (100-500μm) are believed to dominate with respect to the accumulated mass, while the small particles dominate in number. This is in qualitative agreement with the bimodal size distribution found by other authors (discussed in Section 5.3.2). Most of the large inorganic and non-porous particles present in the ashed sample (Figure 5.16c) are assumed to originate from the filter bed material. This presence of filter bed material within the filter cake sample is believed to enhance the levels of Mg, Si and Fe (in decreasing order), as determined by area analysis, i.e. beyond the actual level for the carry over particles alone.

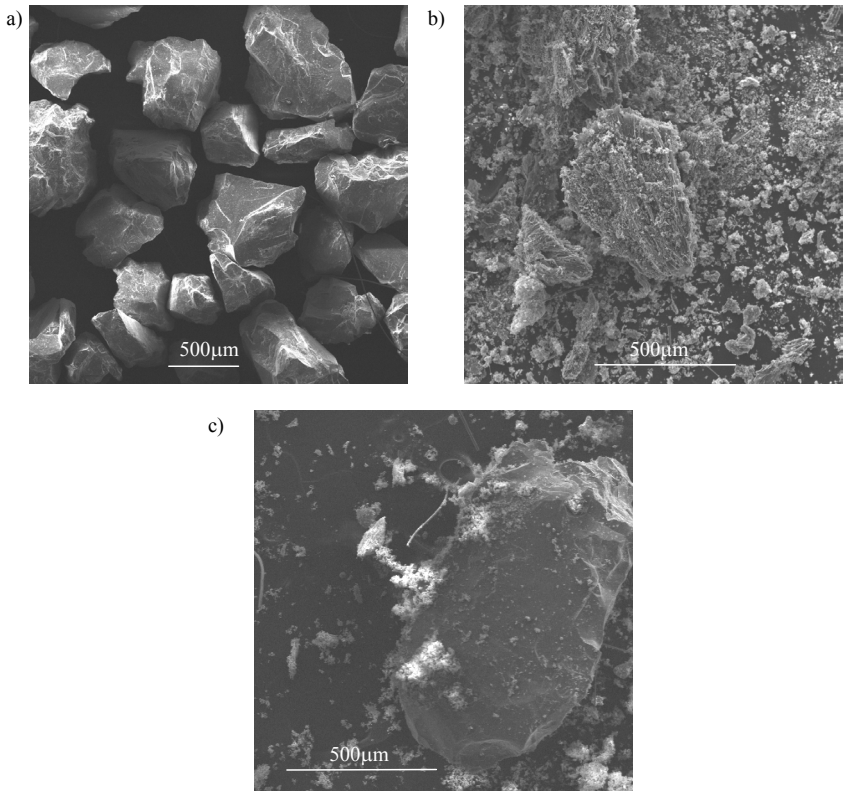

Figure 5.16: Pictures of particles collected from a) the filter bed material, b) the raw filter dust and c) the flocculation of ashed dust on the surface of a filter bed particle.

However these elements are also detected in the layer of small inorganic particles covering the surface of distinct char particles and in the light inorganic fume and porous network found in the samples ashed in air (at 450 °C). But, these molar ratios reveal a clear domination by Ca and Mg, which does not correspond to the bed material. Areas dominated by Ca and Mg indicate that these elements are present as carbonates or pure oxides. Point analysis conducted on these structures show almost pure Ca diluted with K and Mn. A distinct particle with a stoichimetric 1/1 ratio of Ca and Si was identified.

The sample of the particles collected isokinetically by Barrio et al. (2001b), Figure 5.17a, is clearly dominated by larger char structures (>100 μm) and the large number of small carbonaceous particles seen in the filter cake sample is not found here. It is interesting to note the high level of Mg (at about a molar ratio equal to that of the original fuel). This supports the assumption that Mg is present not only due to impurities from the filter bed material, but also as particles originating from the gasifier fuel.

Both inorganic dendrites/flocculations (about 200 μm) of micron/submicron particles and porous structures found in the ashed samples, clearly indicate the structure of the parent char (carry-over particles). However, evidence of ash melt formation and larger agglomerates was not found in the investigated samples. (The presence of molten silicates/oxides is neither supported by the equilibrium analysis.) Point measurements on these structures shows that the elements Mg, Ca, K and Mn dominates the distinct particles, with structures almost pure in Mg/Ca and Ca/Si, and some with dilute amounts of K and traces of Fe.

K is present also without Si, which strongly indicates that K to some extent has been deposited as carbonates (e.g as K_2CO_3, $K_2Ca(CO_3)_2$(s) and $K_2Ca_2(CO_3)_3$(s)). However, it is possible that some of the K is present as binary potassium silicates alternatively as ternary K-Ca-Si, although in minor amounts.

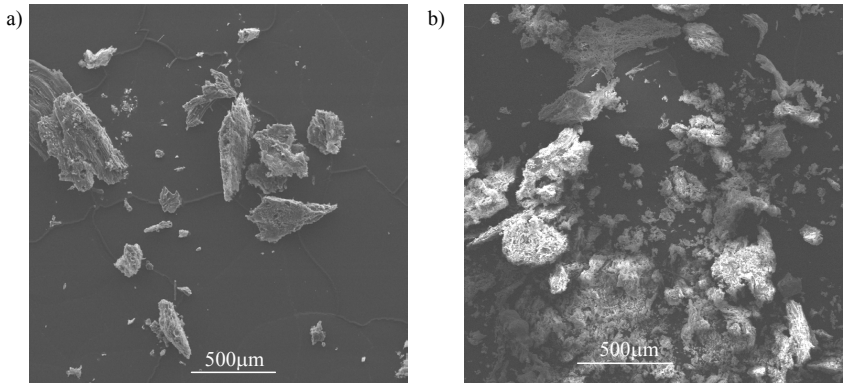

Figure 5.17: Dust sampled by Barrio et al. (2001b). a) raw dust (the sample indicate a higher fraction of the larger particles, compared to the raw dust from the HBU) b) fractions of ashed dust.

Also traces of Cl were found in two of the area analysis conducted on the raw samples. These results indicate a slightly higher Cl concentration in the samples collected by Barrio et al. (which are collected at a lower temperature, 250 °C vz. the 400-500 °C in the filter unit, exp#16). Cl is still present after ashing at 450 °C in air, but is not found in the samples heated up to 900 °C.

Some selected pictures of the particles collected after the FICFB heat exchanger is shown in Figure 5.18. The sample is dominated by coarse carryover particles (mainly char, 10-100 μm). The smaller inorganic particles (bright spots <10 μm) is believed to originate from the fuel, while the larger particles represents fuel contamination or CFB bed material. Both samples also contained sub micron sized fume (assumed to be soot), Figure 5.18b.

Almost pure calcium phosphate was found in the sample from HEII (present as a spherical particle, about one micron in diameter) remaining elements is assumed to originate from "background levels" / noise, as this particle was located on top of another solid particle (probably bed material).

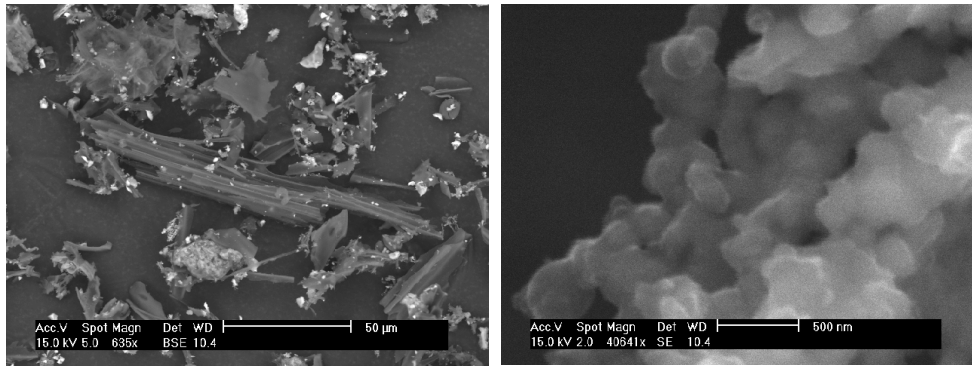

Figure 5.18: SEM picture of sample AHE #1 a)The picture reveals a domination of coarse carryover particles (mainly char , 10-100 μm). The bright areas indicate inorganic material. b) Flocculation of sub-micron sized fume (assumed to be soot.)

5.7.2 Thermogravimetric analysis

Some of the collected samples have been analysed by thermogravimetry. The test procedure and results are outlined below. After drying for 1 hour at 110 °C, the samples (approx. 5 mg) were heated (5 °C/min) up to 900 °C, under flowing nitrogen (200 ml/min), before being ashed at 450 °C in air. The resulting weight loss curves exhibit three characteristic peaks: i) below 500 °C, ii) 500-700 °C and iii) above 700 °C.

No significant mass loss is seen for the filter cake samples (exp #16, see Figure 5.19a, black lines) below some 550 °C. However, the observed mass loss is typically bimodal, with the second and main maximum located at about 650 °C. The low reproducibility is partly due to the occurrence of filter bed material within the sample. (A similar test conducted on bed material alone showed no weight loss up to 900 °C.)

Also some of the fly ash collected during experiment #13a, by Barrio et al. (2001b), was analysed. The filter cake and fly ash samples exhibit much the same behaviour, although the latter shows a much smaller weight loss (Figure 5.19a, grey lines).

A part of the sample was ashed at 450 °C (for 6 hours in air) before being analysed using the same test procedure. This resulted in the disappearance of the weight loss above 700 °C, while the second peak remained (Figure 5.19b). It is therefore reasonable to relate this peak to the ash fraction of the sample.

Deposits taken from the FICFB heat exchangers first part (HEI) does not show any significant weight loss below 500 °C, but reveals a sharp peak between 500 and 700 °C. (Results obtained from the raw FICFB samples are given in Figure 5.19c). This was as expected, since the deposits have been formed at temperatures above 500 °C. The deposits from the second part of the heat exchanger (HEII) show two distinct peaks: one covering the area below 500 °C and one between 500 and 700 °C, the latter is consistent with the one seen for the HEI-sample. The same pattern is seen for the dust sample collected after the heat exchanger, although not so pronounced. All samples show increasing weight loss above 700 °C. After ashing (same procedure as in b) only the weight loss between 500 and 700 °C remained.

Weight loss as coupled to the different peaks, and the sample ash fractions, are calculated and shown in Table 5.7. Both the samples originating from the HBU and Barrio et al. (2001b) shows a very low weight loss below some 500 °C, however the ash fraction is about seven times higher in the HBU sample. (The very small sample applied in the TGA (about 5 mg) makes it very sensitive for inhomogeneties. This explains the significant variation among the obtained ash fractions. The sample size used for direct ashing at 450 °C was about 0.05 and 1.0 g for exp. #13a and #16 respectively, thus far more homogeneous. However a slight over prediction of the ash content is certain, as filter bed particles were clearly present.) It is interesting to note that the weight loss between 500 and 700 °C was very similar for the HBU and Barrio et al. (2001b) samples.

Concerning the FICFB deposits the weight loss below 500 °C is especially pronounced for the HE2 sample. (This sample was also clearly stickier than the HEI and AHE samples.) Furthermore the HEI had highest ash fraction while AHE had the highest char fraction. This is in qualitative agreement with the HBU and Barrio et al. (2001b) samples.

5.7.3 Chromatography

Barrio et al. (2001b) analysed the tar content in the product gas both gravimetrically and by the SPA method. The tar content varied between 3-5 g/Nm^3, being quite high, compared to other stratified downdraft gasifiers (0.1-1.14 g/Nm^3). The two analysis methods agreed quite well although the SPA method predicted a slightly higher total tar content. The main tar components were identified as: benzene (45wt%), toulene (15%), naphthalene (7%), indan (8%), phenol (7%) and o-xylene (5%). Note that these numbers are only approximate.

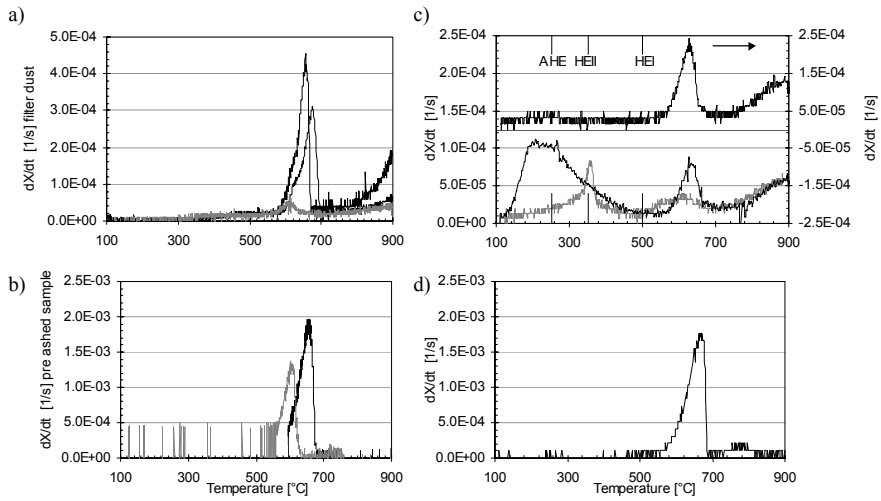

Figure 5.19: Resulting weight loss curves from the TGA experiments: a) Comparison of filter cake deposits from experiment #16 (black lines) and carry over particles from experiment #13a (grey lines). b) same particles as in a, but pre-ashed at 450 °C in air; c) deposit from HEI (upper curve), HEII (lower black curve) and particles collected isokinetically after the heat exchanger (lower grey curve); d) particles from HEI, but pre-ashed at 459 °C in air. (Temperatures at the outlet of HEI, HEII and the isokinetic sampling point (AHE) was as indicated in c) .)

Table 5.7: Thermogravimetrical analysis: Weight loss upon heating different samples (about 5mg) at 5 °C/min from 110 to 900 °C, in an inert atmosphere (N_2). The ash fraction after determined after burn-out is also included. (Amount of water is determined in-situ by keeping the sample for one hour at 110 °C before heating the sample to 900 °C.

	HBU		Barrio (2001b)		FICFB		
Weight fraction of	raw	ashed sample	Raw	ashed sample	HE1	HE2	AHE
Water	<0.01	<0.01	<0.01	<0.01	0.02	0.12	0.02
Volatiles released between			<0.01				
110 – 500 °C	#1 0.00	0.01	0.03	0.01	0.03	0.16	0.07
	#2 0.02		0.03				
500-700 °C	#1 0.07	0.11	0.05	11.15	0.05	0.05	0.04
	#2 0.14		0.05				
Volatiles (above 700 °C) and char	#1						
	#2 0.23	0.76	0.76	2.17	0.17	0.29	0.54
	0.48		0.74				
Ash fraction	#1 0.71	0.91	0.15	0.88	0.73	0.38	0.33
	#2 0.35		0.18				
Ash fraction obtained after ashing in air, at 450 °C for 6hours	0.74		0.11				

- refers to replicate sample

Analysis of the FICFB samples revealed both mono and poly-cyclic hydrocarbons (dominated by phenol, inden, naphthalene, phenanthren, antracen, fluoranthen and pyren) in the samples from HEI and HEII, while mainly higher PAH-compounds (flouranthen/pyren) was detected in the dust sample. Hofbauer and Rauch (2001) recently published preliminary results from gasification of wood chips in a 100 kW_{th} Fast Internal Circulating Fluidised Bed (FICFB). Tars sampled from the product gas stream contained various mono and poly-cyclic aromatic hydrocarbons, mainly being BTX (Benzene-Toulene-Xylene), Naphthalene, Fluoranthene and Pyrene.

Figure 5.20 shows a comparison between the measurements conducted by Barrio et al. (2001b) and analysis conducted on the FICFB samples collected in this work. It is interesting to note that while benzene and other light hydrocarbons are clearly dominating the tar found in the product gas from the stratified downdraft gasifier and the FICFB (as in the results published by Hofbauer and Rauch) no benzene and only minor amounts of other light hydrocarbons are present in the deposits and carry over particles. (These latter samples were dominated by heavier PAH). The high naphthalene concentration found in the deposits is in qualitative agreement with the measurements conducted on the material that accumulated inside the bag house filter operated by Hofbauer and Rauch (2001).

The low condensation temperature of the tars and the high temperature at which these deposits were formed explain the low content of benzene and other light hydrocarbons in the deposits and carry over particles.

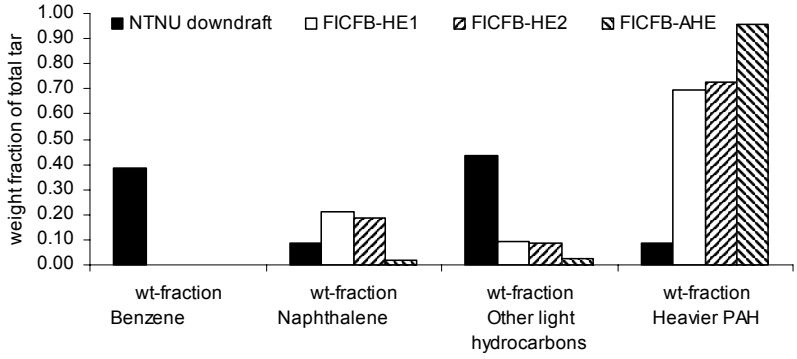

Figure 5.20: Comparison of the tar composition as analysed on the product gas from the downdraft gasifier, deposits from the FICFB and carry over particles from the FICFB.

It is important to note that the analysis conducted on the FICFB deposits, and carry over particles, were aimed towards a qualitative determination of the tar components present in the samples, and that no attempt was made to quantify the total amount of condensed compounds based on these chromatographic analysis. However, combining these results with those obtained by the thermogravimetric analysis gives an indication of the amount of tars deposited at the different locations.

5.7.4 Discussion

The chemical analysis (normalised to 100%, Figure 5.15) of the collected samples (deposits, filter cake and carry over particles) is compared to wet chemical analysis conducted on birch pellets and heartwood. The chemical characterisation of the carry over particles shows especially high contents of Ca (most pronounced in the filter cake sample) followed by K and Mg. The amount of Si was generally lower in the sample collected downstream of the downdraft gasifier, as compared to the FICFB samples. A higher ratio of Si in the latter sample is partly explained by particles originating from the gasifier (CFB) bed material. This is supported by the fact that Si is generally low in the porous structures (visually similar to the parent char structures) found in the ashed samples. S and P were present in small amounts and Cl occurred only in trace amounts in all but the HE1 sample.

The SEM-EDX analysis shows structures with an atomic ratio very close to MgSiO4(s) and $CaSiO_3$(s) in the raw and Ca_2SiO_4(s) in the ashed samples. Phosphate was only detected in one of the point measurements conducted on the ashed HBU sample. The presence of pure calcium phosphate is indicated by spot analysis conducted on the HEII deposit (ashed sample).

These analysis clearly indicate the presence of almost pure Ca structures, with dilute amounts of K. According to the equilibrium calculations these elements should be present mainly as stoichiometric $K_2Ca(CO_3)_2$(s) and $K_2Ca_2(CO_3)_3$(s). However, the domination of Ca in these structures suggests that Ca is mainly present as $CaCO_3$(s)/CaO(s). The presence of bright porous areas dominated by Ca and Mg also indicates that these particles have been deposited as CaO(s)/$CaCO_3$(s) and MgO respectively.

Furthermore, the equilibrium calculations show that Ca_2SiO_3 (CASI-solid solution) is a very stable component at the conditions typical for the gasification zone (about 800 °C). Distinct particles having a molar ratio of Ca and Si corresponding to this was not found.

Formation of molten silicates (e.g. ternary K-Ca-Si components) within the filter cake is not likely due to the low temperature (generally below some 500 °C). Such components are more likely to originate from carry over particles from the gasifier. Either formed in situ in the gasification zone or originating from fuel contamination. However, molten ash was not found within the studied samples, neither as silicates nor as salt solution.

Mg and Ca can be transported to the filter as MgO(s)/CaO(s)/$CaCO_3$(s). Additionally some Ca might be present as binary calcium silicates, eventually as potassium-calcium-silicates. If Mg should be present only as Mg-Ca-Si in the analysed samples, then the level of Mg should be lower than or equal to the amount of Si. However, the presence of Mg is measured to be generally higher than the amount of Si. This is in accordance with the significant amount of MgO(s) predicted by the equilibrium analysis, even at lower temperatures. Parts of the measured Mg might still be present, as ternary Mg-Ca-Si. But the formation of these components within the filter unit is most likely kinetically limited due to the relatively low temperature (generally below some 500 °C) and the rigid dendrite structure in which the particles are deposited.

It is interesting to note that the samples collected from the downdraft stratified gasifier, especially those from the filter cake, shows a strong Ca-enrichment as

compared to the parent fuel. Also the FICFB samples, except the one originating from the high temperature region of the heat exchanger (T > 500 °C) shows high content of calcium. However, the strong Ca-enrichment indicated by the filter cake sample is not confirmed in these samples.

Figure 5.21 shows the stability limit beween CaO and $CaCO_3$ as function of the CO_2 partial pressure and temperature. (Operational conditions corresponding to the gasifier and HBU filtration experiments are indicated in this figure.) The transportation of Ca from the gasification reactor to the down stream equipment represents a potential risk for unstable filter operation, as fluctuations in the operation conditions within the gasifier and thereby in the filter itself can lead to adverse sintering and filter degeneration through the recarbonisation cycle (Backman and Nordin (1998)).

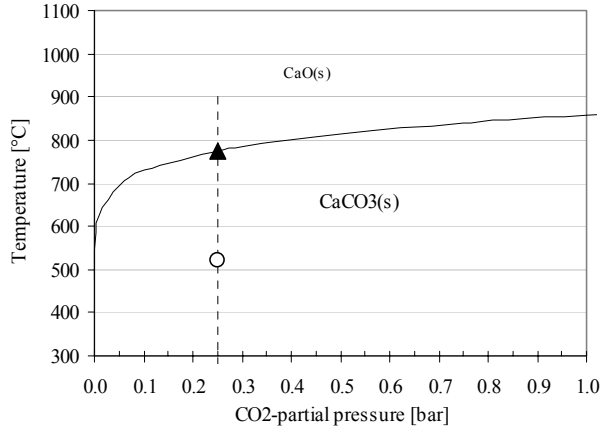

Figure 5.21: Stability diagram of CaO(s) vs. $CaCO_3$(s), as a function of temperature and the partial pressure of CO_2. The vertial drop line indicates the CO_2 level as measured in the product gas from the downdraft stratified gasifier. (Upward triangle gives approximate gasifier outlet temperature and the open circle gives maximum filtration temperature applied during experiment # 16.)

The deposits collected at the high temperature part of the FICFB heat exchanger and the carry-over particles accumulated in the filter cake shows much the same behaviour when heated in an inert atmosphere (100% nitrogen). No significant weight loss is seen before the pronounced change occurring between 500-700 °C, some additional weight loss is seen above 700 °C. Deposits and carry-over particles collected at significantly lower temperatures, about 250 °C, shows additional weight loss below 500 °C. However, the weight loss found for the sample collected by Barrio et al. (2001b) is significantly less than for the particles collected after the FICFB heat exchanger (both samples were collected at about 250 °C). The weight loss below 500 °C and above 700 °C disappears after ashing the samples at 450 °C (in air) while the intermediate weight loss remains. It is therefore likely that the corresponding weight loss seen for the raw samples is connected to the inorganic fraction of the ash.

The chronomatographic analysis of the FICFB samples reveals significant amounts of tars. The carry-over particles being clearly dominated by heavier PAH while significant amounts of naphthalene and minor amounts of light hydrocarbons are also found in the deposits. However, the weight loss between 110 and 500 °C is more than 5 times higher for the deposits collected in the low temperature part of the heat exchanger compared to the high temperature part, and about two times higher than for the carry-over particles collected after the heat exchanger. These results indicate that only minor amounts of tars are found in the samples collected above some 500 °C. These results are in general agreement with the thermogravimetric results obtained on the filter cake samples and the particles collected by Barrio et al. (2001b).

5.8 Summary and conclusions

The reviewed literature describes cleaning of biomass gasification product gas conducted at a variety of temperatures (from 90 to about 800 °C). Cooling the product gas from the typical gasifier outlet temperature, about 800 °C, to below some 550 °C reduces the alkali content in the gas to acceptable limits. Thus leaving tars as the more difficult component. Decreasing the filtration temperature to below 500 °C means moving into a temperature range where tar condensation can by detrimental. Removal of these tars is especially important for closed coupled engine application. As the gas have to be cooled down to about 50 °C before being combusted. Furthermore, operating filter systems above some 600 °C has been reported to cause filter blockage by carbon lay-down and ash sintering.

Although cooling the gas to below some 300 °C results in the tars being efficiently removed by condensation and adsorption, this results in lower plant efficiency as these components considerably contributes to the heating value of the product gas. Furthermore condensation of tars represents a potential risk for filter blinding and unplanned plant shut-down. This represents clear incentives for applying catalytic upgrading of the gas, thus ultimately cracking the tars into CH_4 and H_2.

The amount of tars condensing and their influence upon the stability of the gas cleaning operation is closely coupled to gasifier operation and tar composition/concentration. While Malmgren-Hansen et al. (1996) reported serious blocking of the ceramic filter system when operating at about 500 °C, and related this to tar condensation, Hindsgaul (2000) reports no operational problems when operating a bag house filter at 90 °C. Considering that both systems operate on down draft wood gasification systems, this clearly demonstrates differences in the resulting product gas quality. Hofbauer and Rauch experienced complete blocking due to tar condensation when operating at about 200 °C (CFB steam gasification of wood). Furthermore, Engstrom reports successful (long term) operation at 340-370 °C. These findings clearly show that the gas cleaning operation is heavily influenced upon by the gasifier operation.

It is of outmost importance to be aware of the diversity among the biofuels (especially ash composition and amount of the most abundant components K, Ca and Si) which highly influence upon the properties of the resulting ash and carry over particles.

A ternary diagram comparing some of the fuels studied in this thesis is shown Figure 5.22. Generally the content of Si is low in slow growing (e.g. wood) while often high in fast growing (e.g. straw). However, the content of Si, Mg and Al is

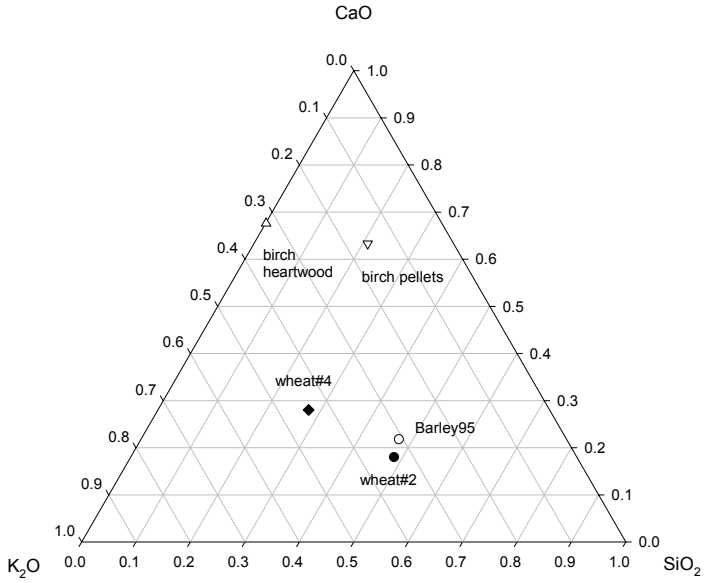

Figure 5.22: Projection of the ash composition of some selected fuels into the ternary K_2O-CaO-SiO_2 diagram (Δ-birch heartwood; ∇-birch pellets; ♦-wheat#4; ●-wheat#2 and ○-Barley95). Fuels with ashes rich in Silicon typically produce considerably amounts of a viscous silicate/oxide liquid (e.g. Wheat #2, SIA – index equal to 3*), while fuels dominated by calcium typically form both solid and liquid carbonate solutions (e.g. birch heartwood).

typically increased through fuel contamination by soil. It is thus interesting to note the higher content of Si and Al in birch pellets vs. birch heartwood.

Fuels with a high Si-content (e.g. straw) typically have low ash melting temperatures, due to silicate/oxide glas/liquid (SLAG) formation. While a low Si content in the fuel ash (e.g. birch heartwood) typically lead to liquid salt/LCSO (high in K_2CO_3) formation.

Summarising these effects shows that cooling the product gas to below some 550 °C results in the alkali level being reduced to acceptable limits while further cooling might introduce operational problems due to tar condensation, although the critical temperature limit is being highly dependent upon gasifier operation.

Furthermore, this work successfully demonstrates filter cake formation upon a free horizontal surface of unbound filter media (sand with a mass mean particle diameter of about 500 μm) when filtering product gas from an air blown down draft stratified gasifier (fuelled with birch pellets) at elevated temperatures (300-540 °C). A slightly decreasing pressure drop rate is seen at the end of both experiments.

Preliminary measurements estimate the tar and particle content of the raw product gas to be about 3-5 g/Nm^3 and 10 g/Nm^3, respectively (Barrio et al. 2001b). These carry over particles, particles accumulated within the high temperature filter unit, and samples originating from the FICFB were all analysed by scanning electron microscopy. This reveals char particles with a clearly bimodal size distribution (in

accordance with distributions available in the literature, embracing both fixed bed and fluidized bed reactors) and a Ca rich ash.

Thermogravimetric analysis (heating the dry samples (5 °C/min) under flowing nitrogen (200 ml/min)) revealed three distinct regions with respect to the resulting weight loss vs. temperature. i) below 500 °C, ii) between 500-700 °C and iii) above 700 °C. These are assumed to be due to the evaporation of tars (i), decomposition of the ash and iii) ash/rest pyolysis. This is generally in agreement with the discussion outlined above. However, these thermogravimetric analyses are preliminary of nature and used for physical characterisation of the sample only.

No melt formation was detected either through ashing, heat treatment or through visual inspection, applying scanning electron microscope.

Furthermore, tars and heavier hydrocarbons were efficiently converted when applying catalytic bed material (G-56A from Süd-Chemie AG) in the high temperature filter unit. Despite the relatively low filter temperature (about 535 °C) no deactivation of the catalyst was detected during the three hours for which the filter was operated.

It is important to stress the operational differences between the horizontal bed filter used in this study and continuous operation of a filter system operating in surface filtration mode (e.g. the panel bed filter). Long term operation of this latter system typically incorporate accumulation of micron/sub-micron particles within the filter vessel, with extensive mixing of the particles due to the mechanisms involved in filter regeneration (e.g. particle re-entrainment). These parameters, especially in combination with elevated filtration temperature, typically allow the system to approach global equilibrium to a greater extent than within the horizontal bed filter.

5.9 References

Abatzoglou et al. (2000) *The development of a draft protocol for the sampling and analysis of particulate and organic contaminants in the gas from small scale biomass gasifiers,* Biomass and Bioenergy, v 18, pp. 5-17.

Alvin, M.A. (1998) *Impact of char and ash fines on porous ceramic filer life.* Fuel Processing Technology 56 (1998), pp. 143-168.

Backman, R. and Nordin, A. (1998). *High temperature equilibrium calculations of ash forming elements in biomass combustion/gasification systems - state of the art, possibilities and applications*. International Biomass Ash Workshop, Technical University of Graz, Austria, October 1-2, 1998

Barrio, M., Fossum, M. and Hustad. J. E. (2001a) *A small-scale stratified downdraft gasifier coupled to a gas engine for combined heat and power production.* In proceedings: Progress in Thermochemical Biomass Conversion, September 2000, Tyrol, Austria, pp. 426-440.

Barrio, M., Fossum, M. and Hustad, J.E. (2001b) *Operational characteristics of a small-scale downdraft gasifier*.Sixth international conference on technologies and combustion for a clean environment, 9-12 July, 2001, Porto, Portugal, pp. 1269-1276.

Barrio, M. (2002) *Biomass gasification for the production of heat and power in small scale applications.* Academic dissertation, Norwegian University of Science and Technology. Dep. of thermal energy and hydropower, 2002.

Botnevik (2002) *A theoretical and experimental study of gas cleaning by the use of a granular filter, with special emphasis upon the removal of particulate and gaseous emissions from combustion and gasification processes*. Diploma report, Norwegian University of Science and Technology. Dep. of thermal energy and hydropower, Report nr. 02:20.

Bridgewater, A. V. (1995) *The technical and economic feasibility of biomass gasification for power generation.* Fuel 1995, v 74, n 5, pp. 631-635.

Brown, M. D., Baker, E. G. and Midge. L. K. (1986) *Evaluation of Processes for Removal of Particulates, Tars, and Oils from Biomass Gasifier Product Gases*, In Energy From Biomass and Wastes X. Edited by D. L. Klass. Institute of Gas Technology, Chicago, Illinois

Cabeza, J.G. (2000) *Biomass gasification in Small-Scale Applications.* Project report (00:43) Norwegian University of Science and Technology. Dep. of thermal energy and hydropower, 2000.

Engstrom, F. (1998) *Hot gas clean-up Bioflow ceramic filter experience*. Biomass and Bioenergy, v 15, n 3, 1998, pp. 259-262.

Faaij, A., van Ree, R., Waldheim, L., Olsson, E., Oudhuist, A., van Vijk, Ad., Daey-Ouwens, C. and Turkenburg, W. (1997) *Gasification of Biomass Wastes and Residues for Electricity Production*, Biomass & Bioenergy, v 12, n 6, pp. 387-407

Fercher, E. , Hofbauer, H., Fleck, T., Rauch, R. and Veronik, G. (1998) *Two Years Experience with the FICFB-Gasification Process,* Proc. of the 10th European Conference and Technology Exhibition, June, 1998, Wurtzburg

Guhl, S. (2002) *Gasification of biomass in a small-scale downdraft gasifier using air and steam as gasification agents*. Project report, The Norwegian University of Science and Technology. Dep. of thermal energy and hydropower, 2002.

Hasler, Ph., Ruedi, B. and Nussbaumer, Th. (1997) *Evaluation of gas cleaning technologies for small scale biomass gasifiers*. Final report, Swiss Federal Office of Energy and Swiss Federal Office for Education and Science, July 1997, 53 p.

Hasler, Ph. and Nussbaumer, Th. (1998) *Particle sized distribution of the fly ash from biomass gasification*. Biomass for Energy and Industry,1998, pp. 1623-1625.

Hasler, Ph, and Nussbaumer, Th. (1999) *Gas cleaning for IC engine applications from fixed bed biomass gasification.* Biomass and Bioenergy 16 (1999) pp. 385-395.

Hindsgaul, C. (2000) *Low temperature particle filtration of producer gas with low tar content.* Department of Energy Engineering, DTU, ET-ES-2000-05.

Hofbauer, H. and Rauch, R. (2001) *Hydrogen-rich gas from biomass steam gasification*. In: the European Commision, in the framework of the Non Nuclear Energy Programme, JOULEIII, Contract JOR3CT970196.

Kurkela, E., Stahlberg, P. Laatikainen, J. and Nieminen, M. (1990) *Removal of Particulates and Alkali Metals from Pulverized Fluid-Bed Gasification of Peat and Biomass - Gas Cleanup for Gas Turbine Applications,* In Energy From Biomass and

Wastes XIV. Edited by D. L. Klass. Institute of Gas Technology, Chicago, Illinois, pp. 947-970.

Kurkela, E., Stahlberg, P. Laatikainen, J. and Simell, P. (1993) *Development of Simplified IGCC-Process for biofuels: Supporting Gasification Research at VTT*, In: Bioresource Technology United Kingdom, 1993, v 46 (1-2), pp. 37-47.

Kurkela, E., Ståhlberg, P. and Laatikainen-Luntama, J. (1995) *Pressurised fluidised-bed gasification experiments with wood, peat and coal at VTT in 1991-1994, Part 2. Experience from peat and coal gasification and hot gas filtration.* Espoo 1995, Technical Research Centre of Finland, VTT Publications 249, 58 p.

Kurkela, E. (1996) *Formation and removal of biomass-derived contaminants in fluidized-bed gasification processes.* Espoo 1996, Technical Research Centre of Finland, VTT Publications 287. 47p.

Kurkela, E., Laatikainen-Luntama, J., Ståhlberg, P. and Moilanen, A. (1996) *Pressurised fluidised-bed gasification experiments with biomass, peat and coal at VTT in 1991-1994, Part 3. Gasification of Danish wheat straw and coal.* Espoo 1996, Technical Research Centre of Finland, VTT Publications 291, 41p.

Larson, E. D. and Svenningsson, P. M. (1990) *Development of Biomass Gasification Systems for Gas Turbine Power Generation, In Energy From Biomass and Wastes XIV.* Edited by D. L. Klass. Institute of Gas Technology, Chicago, Illinois

Malmgren-Hansen, B., Kristiansen, A. E. & Zielke, U. (1996) *Particulate Filtration from Hot Generator Gas.* In danish. Energiminsteriets Forskningsprogram. Anvendelse af biomasse til energiformaal, Report No. NEI-DK--2469, Denmark, Sept. 1996, 119p.

Milne, T.A., Abatzoglou, N. and Evans, R.J. (1999). *Biomass gasifier "tars". Their nature, formation and conversion.* NREL/TP-570-25367, November 1998.

Neeft, J.P.A. et al. (2001) *Guideline for sampling and analysis of "tars" and particles in biomass producer gases*, Progress in Thermochemical Biomass Conversion, Tyrol, Austria, 17-22 Sept. 2000.

Nieminen, N., Simell, P., Leppälahti, J., Ståhlberg, P. and Kurkela, E. (1996) *High-temperature Cleaning of Biomass-Derived Fuel Gas.* In: Proceedings of the 9th Eurpean Bioenergy Conference, Edited by P. Chartier et al., June 24-27, Copenhagen, Denmark, pp. 1080-1086.

Nieminen, M. Kangasmaa, K., Kurkela, E. and Ståhlberg, P. (1996) *Durability of metal filters in low sulphur gasification gas,* In Proceedings: 3rd Symposium and Exhibition Gas Cleaning at High Temperatures, Sep 18-20, 1996, Karlsruhe, Germany, pp. 120-131.

Simell, P., Kurkela, E. and Ståhlberg, P. (1993) *Formation and catalytic decomposition of tars from fludized-bed gasification.* In: Bridgewater A.V. (ed.). Advances in thermochemical biomass conversion. Glasgow: Blackie Academic & Professional, 1993. v 1. pp. 265-279.

Skoblja, S. (2002) Personal communication. Dep. of Gas, Coke and Air Protection, Faculty of Environmental Technology, Inst. of chemical technology, Prague

Williams, R.H. and Larson, E. D. (1993) *Biomass-Gasifier Gas Turbine Power Generating Technology*, Proceedings, Strategic Benefits of Biomass and Waste Fuels, 1993, pp. 7.1-7.26.

Wiant, B. C., Carty, R. H., Horazak, D., and Ruel, R. H. (1993) *Biomass Gasification Hot Gas Cleanup For Power Generation*, First Biomass Conference of the Americas, 1993, pp. 571-582.

6 Summary, conclusions and recommendations for further work

6.1 Summary and conclusions

The increased focus upon the environmental impact of industrial off-gases has led to an ever more strict legislation. Thus industrial heat and power production, being one of the major contributors, has faced steadily decreasing emission limits. This represents a strong incentive for the research and development of novel gas cleaning technologies, as well as environmentally friendly and more efficient ways to produce energy. The utilisation of biomass, being a renewable and CO_2 neutral fuel, in advanced combustion and gasification systems is an interesting alternative in this respect. Special attention has been directed towards gasification due to the need for higher power-to-heat ratios, governed by a less increase in the heat loads in district heating and process industry, than in the electricity demand.

The work outlined in this thesis focus on key issues related to high temperature filtration in both combustion and gasification processes, with special emphasis laid upon evaluation and further development of the Panel Bed Filter technology. The experimental part covers both industrial scale and more fundamental laboratory scale research. Hence a broad span of fundamental and empirical theory related to filtration of the off gases, as well as the thermochemical conversion of the solid fuel itself, has been reviewed and discussed.

The Panel Bed Filter utilises the transient behaviour of granular filtration and operates in surface filtration mode. It is basically similar to cake forming filters as bag house filters and ceramic/metallic candles, but fundamentally different from the bulk of granular filters based on deep bed filtration. Therefore a comprehensive literature review of state of the art within cake forming filters is given. Furthermore the main parameters controlling the operational characteristics of these systems are discussed. It should be noted that the reported values found in the reviewed literature are highly scattering.

The filter developed by Lee et al. had three columns of louvers, which defined two separate sand beds. The sand layer exposed for the dust laden gas typically having a smaller grain size (mass median diameter of about 500 μm or below) compared to the second and coarser (d_p about 1-2 mm) back up layer. The Folla design represented a modification of this design, by incorporating a simplified front louver design and replacing the remaining two sets of louvers with two sets of wire-mesh.

The field tests demonstrate successful operation of a commercial scale Panel Bed Filter element. Stable operation, i.e. a stable residual pressure drop was maintained within a wide range of filtration velocities (U_S = 4-14 cm/s). The filter capacity (325 m^3/m^2h) and efficiency (better than 99.8%) at design conditions is within the upper range of those reported for fabric and rigid media filters. This has been verified in an industrial scale pilot plant connected to a 5 MW bark boiler (designed for a capacity of 30000 m^3/h at 200 °C). The experience gained through operation at industrial scale documented the necessity of developing a more rugged

construction incorporating simplified production and maintenance as well as reduced costs.

The filter development embraces the design, erection, instrumentation and operation of a series of model filters. The early work conducted by Squires and Lee is used as a reference for this thesis, as is established filtration standards. Despite a skilled operator and accurate handling of the equipment some scattering in the experimental data is to be expected. However, reproducibility in the different set-ups was high. And a fairly good documentation of the enhanced filter capacity and filter stability was obtained.

Removing the second sand layer and thereby excluding the necessity of the wire mesh applied in the commercial scale filter elements, represents a clearly enhanced ruggedness with respect to the filter construction, as does the simplicity of the novel L10-56 louver. However, replacing the coarse sand-box with a rack of louvers introduced the potential of local destabilisation of the filter bed, i.e. local fluidisation, and entrainment of the filter bed material into the clean gas duct. As expected, this upper stability limit was highly dependent upon bed material characteristics and the geometry defining this granular filter bed (i.e. the louvers). The experimental investigations undertaken to quantify this phenomenon show a close relationship between the upper stability limit and the theoretical minimum fluidisation velocity.

An accurate measurement of the actual gas entry surface of the filter (i.e. the exposed sand surface) is difficult. This influence upon the calculation of the specific sand spill (g/cm^2) and the actual velocity of the gas impinging the filter cake. This in combination with particle sedimentation (i.e. for the dust) in the inlet cone makes the predicted specific cake resistance partly instrument specific and complicates direct comparison with tests reported in the literature. However, utilising the superficial velocity (based on the face area of the filter elements) and operating at comparable conditions (i.e. filter temperature, capacity and raw gas concentration) makes the comparison of the wishbone louver design and the novel L10-56 louvers adequate.

The process of product gas cleaning is still one of the major technical challenges with regard to the utilisation of biomass producer gas in gas turbines or other high temperature applications. Granular bed filters are insensitive to hot particles, temperature fluctuations and corrosive elements in the impinging gas. These advantages combined with the possibility to provide chemical processing of the gas makes the Panel Bed Filter a promising alternative for high temperature cleaning of gasification product gas.

Furthermore, characterisation of the chemically diverse biomass fuel is of major concern if the promising gasification technology is to be developed into a technologically as well as commercially mature technology. It is thus important to realise the interaction between the different processes involved and ensure optimised integration of these rather than solely sub-optimising the different process steps. This has been sought accomplished through laboratory scale studies aimed towards improving models for reactor simulations and thereby increase the accuracy in the prediction of product gas quality. This subsequently provides a better understanding of the environment defining the operational conditions for the equipment installed down stream of the gasification reactor (e.g. heat exchanger surfaces and gas cleaning equipment).

Experiments conducted to obtain biomass gasification reactivity data embraces selected char samples derived from a variety of biomass qualities, ranging from well-defined heartwood to highly problematic straws. Thus representing very different fuels with respect to ash content and inorganic composition, i.e. having highly different properties with respect to ash fusion/agglomeration and the catalytic influence upon char conversion.

A simple n^{th} order reaction scheme and an assumption about invariant reactivity development versus char conversion (structural profile $f(X)$) was successfully applied for gasification reactivity determinations, conducted at atmospheric conditions, in different partial pressures of CO_2 in N_2 and H_2O in N_2. Note that significant melt formation, due to reactions among the inorganic components present in the raw fuel, might influence upon the validity of the structural profile assumption.

However, hydrogen inhibition was observed when adding hydrogen together with steam at the reactor inlet and Langmuir-Hinshelwood kinetics was used to take this into account. The reactivity development versus conversion was found to be consistent within one fuel/reactant combination, but different reactants gives reactant specific reactivity profiles.

The experiments conducted on reactivity determination indicate that a more complex mechanism must be considered if the results, even for a single pure gas, are to be extrapolated to their limits for the purposes of modelling reactor data under realistic conditions.

Most of the alkali metals present in the raw input fuel are released into the gas phase or converted into water insoluble particles at high char conversion levels. Which is of major importance both with respect to reactions among the ash elements (e.g. Ca, K and Si) and reductions in the catalytic effect.

Fuels with a high Si-content (e.g. straw) typically have low ash melting temperatures, due to silicate/oxide glas/liquid formation. While a low Si content in the fuel ash (e.g. birch heartwood) typically lead to liquid salt (high in K_2CO_3) formation. In this work moderate amounts of a Ca-based additive have been successfully applied to control the agglomeration tendency (i.e. the generation of potassium rich silicate/oxide slag and liquid salt melts) of various straws.

Furthermore, these investigations documents the formations of a viscous oxide/slicate melt, including the formation of ternary K-Ca-Si compounds. The added Ca participates significantly to the inorganic element transformation and calcium enrichment of the oxide/silicate slag is clearly observed in the samples. Furthermore, both experiments and theoretical evaluations (global equilibrium calculations) document the positive influence of the novel Ca-based additive by significantly reducing sintering and agglomeration while preserving fuel reactivity. Availability of the added Ca is shown to depend on how Ca is added to the raw fuel.

No pronounced reactivity enhancement was observed within the resolution of the equipment applied in this study (a slight increase was found for the calcium molasses supported samples). We therefore suggest that the mutual inorganic reactions do not abundantly take place or affect reactivity, until late in the char conversion process.

The reviewed literature shows that cooling the product gas to below some 550 °C results in the alkali level being reduced to acceptable limits, while further cooling might introduce operational problems due to tar condensation. The critical

temperature limit with respect to detrimental tar condensation is found to be highly dependent upon gasifier operation. While some investigators report stable filter operation at about 100 °C, others report unstable operation due to tars even at temperatures about some 500 °C.

This work successfully demonstrates filter cake formation upon a free horizontal surface of unbound filter media (sand with a mass mean particle diameter of about 500 μm) when filtering product gas from an air blown down draft stratified gasifier (fuelled with birch pellets) at elevated temperatures (300-540 °C).

Application of catalytic material in the granular filter resulted in efficient cracking of the tars and higher hydrocarbons. Despite the low temperature used in this experiment (about 535 °C) no catalyst deactivation was observed during the three hours of filter operation.

The carryover particles which accumulated within this high temperature filter unit was compared with samples originating from a steam blown fast internal circulating fluidised bed gasifier (FICFB), both systems fuelled with wood. Scanning electron microscopy with x-ray diffraction revealed char particles with a clearly bimodal size distribution and a Ca rich ash. This particle distribution is in qualitative accordance with distributions available in the literature.

Thermogravimetric analysis (heating the dry samples (5°C/min) under flowing nitrogen (200 ml/min)) revealed three distinct regions with respect to the resulting weight loss vs. temperature. i) below 500 °C, ii) 500-700 °C and iii) above 700 °C. These are assumed to be mainly effects of the evaporation of tars (i), decomposition of the ash and iii) ash/rest pyolysis. This is generally in agreement with the discussion outlined above. However these thermogravimetric analysis are preliminary in nature and used for physical characterisation of the sample only.

Although no melt formation was detected in the collected samples it is important to stress the operational differences between the horizontal bed filter used in this study and continuous operation of a filter operating in surface filtration mode (e.g. the panel bed filter). Long term operation of this latter system typically incorporate accumulation of micron/sub-micron particles within the filter vessel, with extensive mixing of the particles due to the mechanisms involved in filter regeneration (e.g. particle re-entrainment). These parameters, especially in combination with elevated filtration temperature (typically above some 600 °C) allow the system to approach global equilibrium to a greater extent than within the horizontal bed filter.

Thus, the great diversity in ash properties among the biofuels has to be taken into account before changing the fuel on which the system is operating. As this represent a potential risk both concerning gasfier operation, stability of the filter unit and the resulting product gas quality. Generally, increasing the filtration temperature above some 550 °C leads to reduced alkali removal efficiency and requires careful attention to the ash melting properties, as both liquid carbonates (e.g. wood) and silicate/oxide melt (e.g. straw) might be formed.

6.2 Recommendations for further work

The first step in the process of scale-up and commercialisation of the novel louver design is to ensure an even sand spill distribution during puff-back, efficient cleaning and a sufficiently stable filter bed. However, it is considered essential that the voluminous literature published, on fundamental filtration mechanisms governing particle collection and retention in particulate, fibrous and ceramic structures, involved in deep bed (e.g. traditionally granular bed filters) as well as in surface filtration (e.g. bag house filters, ceramic and metallic candles) is thoroughly reviewed, and that its relevance with respect to application in the further development of the panel bed filter is evaluated. The experience and knowledge accumulated in connection to the development of these systems, represents valuable inputs for future work on the PBF. The present thesis has emphasised upon creating a reference for the comparison with these technologies and exploits the limits for maximum filter capacity and stability. Hence, aiming towards improved performance in full-scale systems, developing a simplified and rugged filter construction suitable for commercialisation.

Important issues when optimising the filter design is the interaction between filter geometry, stability of the filter bed (at relevant filter loads) and the system for filter material regeneration and re-circulation. Particle size distribution, mass median diameter and specific density directly influence these through dust migration, filter bed fluidisation and the efficiency in separating dust and filter material in the re-circulation loop. Therefore information concerning physical characteristics such as specific density, angularity, hardness and fragility is required in order to evaluate alternative filter materials. Obviously parameters such as availability and price are crucial with respect to commercialisation.

This thesis embrace extensive experimental testing of the resulting pressure build up when depositing dust upon the surface of a laboratory scale panel bed filter and a free unbound horizontal surface of sand. A more detailed analysis of the difference between these test units (applying alternative filter media) and commercially available and highly efficient total-filters would give essential information about particle migration within the granular filter media. Thus enlighten the difference in the pressure build up in these systems and support the evaluation of long term operation and stability. In particular the fact that the Panel Bed Filter is generally operated in the pressure range up to 2000 Pa, typically ten times lower than for the Horisontal Bed Unit. A better understanding of this is considered to be crucial in the further development of the filter unit.

Furthermore, focus should be directed upon obtaining long term operational experience through the integration of a full scale PBF with a representative system (e.g. an industrial scale biomass, waste or coal boiler) thus evaluate the impact of natural system variations (e.g. boiler operation and fuel quality) upon the conditions within the filter vessel (importance of particle accumulation and effect of re-entrainment) its influence upon selection of practically realisable and optimised design-conditions (i.e. filter load at a specified ideal gas flow and particle load). This emphases the importance of a rugged construction, including efficient filter material recycling and development of efficient and cost effective procedures for system operation and maintenance. Furthermore, routines for filter cleaning in case of adverse filter blinding (i.e. worst case scenario) should be developed.

In addition to parameters directly connected to the gasifier/boiler (e.g. working principle and geometry) emissions are closely connected to the operation of the reactor, e.g. fuel quality and load variations. An accurate prediction the amount and chemical/physical characteristics of these gaseous, molten and solid components are important in the development of high temperature filter operation. This embrace modelling of the thermochemical conversion, as well as fractionation and particle deposition through transport lines and heat exchangers.

Scientific literature released during, the last decade, on the topic of thermal conversion of biomass through pyrolysis, combustion and gasification, gives a significantly improved background for the modelling of these processes. This literature is generally based on experiments conducted in pure N_2, CO_2 in N_2 and H_2O in N_2, some authors also reports experiments with external addition of H_2 and/or CO. However, information available on reactivity measured in more complex gas mixtures (e.g. a typical gasification atmosphere) is scarce.

The present work supports the findings that especially the latter stages of char conversion is important with respect to the reaction between the inorganic compounds, hence the generation of molten silicates and slag being favoured at high degrees of conversion. More accurate reactivity analysis focusing upon the late stages of char burn-out and more fundamental knowledge of the water soluble potassium content (i.e. how it is coupled to the carbonaceous material) and improved understanding of the inorganic reactions in biomass ash is considered to be important. Hence, both improved modelling of the fuel conversion process itself and accurate and reliable experimental data on char reactivity in different gas mixtures is still needed.

Although powerful, the global equilibrium programs available today is far from complete. Important chemical compounds are missing, e.g. very little information is available on phosphorous species and thermodynamic data on ternary K-Ca-Si compounds is missing. Furthermore, information about the viscosity of silicate melts and improvement of the theoretical models available for the chemical modelling of silicate system and the miscibility of the carbonate systems.

The fact that the panel bed filter is based upon the utilisation of granular filter media also facilitates the application of catalytic material / adsorbents within the filter bed, incorporating the possibility for simultaneous removal of particulate and gaseous emissions (catalytic conversion of tars, collection of volatilised ash components through gettering materials or even sulphur removal (combustion processes)). This can also be accomplished through the injection of reactive particulate material upstream of the filter system (a proven and well-known technology applied for bag house filters) generating a reactive dust cake wherein the conversion occurs. However, the contact between the entrained particles and the gaseous contaminants is rather limited as is the residence time within the resulting dust cake. Furthermore, the substantial increase in dust load would imply a higher pressure build-up rate and reduced filter capacity. Application of this alternative must therefore be evaluated vs. the increased load on the system for filter material re-circulation.

This thesis includes preliminary filtration tests on biomass gasification product gas, at elevated temperatures (up to 540 °C) and successful catalytic cracking of tars and

higher hydrocarbons is demonstrated at a relatively low filtration temperature (about 535 °C). Increasing the filtration temperature even further would ease the catalytic conversion of tars (catalyst deactivation being less severe). However, the presence of molten ash components would complicate filter operation. And additional effects such as high temperature corrosion and its implications for the steel construction used for the PBF would need closer examination.

Appendix I

Experimental results from the Panel Bed Filter tests

A comprehensive summary of experimental data collected during the filtration tests is included in this appendix. An overview of the experimental matrix is shown in Table I.1, including the total filtration time (dt [min]), superficial velocity (U_S [cm/s]), volume flow (q [m^3/h]), the pressure drop through the clean filter (dP_0 [Pa]), the residual pressure drop (dP_r [Pa]), piston feed rate for the rotating brush particle dispenser [mm/h], the resulting inlet dust concentration [g/m^3], total number of filtration cycles, the discharged material upon puff-back [g/cm^3], the dust to sand ratio [-], apparent outlet dust concentration [mg/m^3] and the apparent cleaning efficiency [-]. This matrix embraces 30 separate experiments, conducted on two different louver geometries, four different dust qualities and an accumulated filtration time of 142 hours. (Table I.1 is grouped chronologically with respect to the date on which the experiment was conducted, while Table 3.4 is arranged with increasing filtration velocity.)

A graphical presentation of the corresponding pressure build-up curves (including the filtration velocity (U_S)) vs. time is given in Section I.1. And a summary of the resulting cycle time (t_c), residual pressure drop (dP_r) and the transient behaviour of the specific cake resistance (K_2') versus filtration time is included in Section I.2. A complete table of experimental parameters (such as t, t_c, U_S, v_f, c, dP_0, dP_{max}, dP_r, $dP_{cake,max}$ and K_2') for each experiment and filtration cycle is included in Section I.3.

I.1 Pressure build-up vs. time, summary of the filtration experiments conducted in the High temperature Panel Bed Filter Unit.

The applied pressure build up range was chosen in order to comprise the VDI-3926 (guidline for testing of filter media for cleanable filters) and to cover the experimental conditions applied in the earlier work conducted on the PBF, illustrated in Figure I.1

Each graph includes the total pressure drop across the filter and the superficial velocity. Furthermore, each graph is supplied with an "identification label" (i.e. experimental number – PanelBedFilter/Louver geometry/Dust quality). The experimental number is composed of the date (ddmmyy) and the test number on this specific date (e.g. 020201#1-PBF/Wishbone/SAE). The duration of each filter test was limited by the maximum load capacity of the rotating brush feeder. The applied dust qualities are discussed in Section 3.5.1) (No detailed experimental data (except those included in Table I.1) is available for experiment number 310101, due to initial problems with the data logging.) The amount of discharged material upon puff-back (Table I.1) is calculated vs. the estimated exposed filter surface (approximate values).

The filtration velocity was kept close to constant (as seen in the presented graphs) by installing a critical nozzle downstream of the filter. A variable resistance just upstream of the nozzle was used to manually compensate for the minor velocity variations along the filtration test.

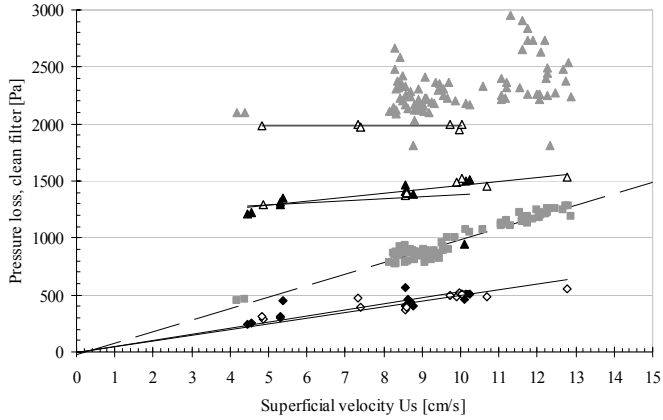

Figure I.1: Maximum pressure drop before regeneration vs. clean/cleaned filter pressure drop, as a function of superficial velocity. The velocity and pressure loss ranges applied in the small-scale panel bed filter is compared with the experimental conditions applied in the commercial scale filter element. (Triangles – dP_{max}; Rectangular symbols- dP_{clean}; Filled black symbols for Wishbone, open symbols for L10-56 and grey symbols for Folla louvers (Risnes and Sønju (2000)).

Some instability in the pressure build-up (sudden pressure drops) was experienced at high pressure drops (above some 1500Pa) during the first experiment (number 310101). Unfortunately no detailed experimental data (except those included in Table I.1) is available for this experiment. Based on this observation the maximum pressure drop in the consecutive tests were about 1000 Pa above the clean pressure drop. However, a maximum pressure drop of about 2000Pa was used in some of the experiments in which the L10-56 louver was applied. Instabilities similar to those found in the initial Wishbone experiment appeared here.

The PuralNF dust is highly agglomerative and caused unplanned shut down in experiment number 030201#1 and 050201#1. Successful operation was achieved after cleaning of the brush and changing to the special top cover (type B). PuralNF and SAE-fine gave much the same pressure build up. The PuralSB gave no problems with the particle feeding or filter regeneration, but the resulting pressure build-up was low.

The pressure valve became instable (reduced puff-back intensity) if the duration between each activation (i.e. each puff-back) was to long. This is clearly seen in experiment number 080301#1 (filtering of PuralSB dust) where the first cycle lasted for about 170minutes. Resulting in a very fast initial pressure increase during the second cycle, while the consecutive two cycles showed a close to linear pressure build up. Note that this gave a resulting average sand spill of 0.09g/cm^2, being the lowest sand spill registered during the filtration tests. (Assuming this sand spill to be distributed over three cycles would raise this number to about 0.12g/cm^2.)

Table I.1: Summary of filtration tests conducted in the high temperature panel bed filter (about 200°C).

dust	file	dt	Us	q	dP_{clean}	dP_r	dP_{max}	Feed rate [mm/h]	C_{raw}	Cycles	Discharged material upon puff-back Theoretical, average values tot	ex. Dust	dust/sand	Apparent outlet dust conc	eff.
	Exp#	[min]	[cm/s]	[m^3/h]	[Pa]	[Pa]	[Pa]	average	[g/m^3]		[g/cm^2]	[g/cm^2]	[-]	[mg/m^3]	[-]
Wishbone															
SAE	310101	165.7	13.67	11.42	400	413	1470	51.44	6.15	14	0.75	0.73	0.090		
	010201	355.2	8.75	7.31	399	399	1380	27.87	3.26	18	-	-	-		
	020201#1	707.4	4.44	3.70	241	239	1214	13.31	3.07	17	0.70	0.64	0.093		
	020201#2	313.2	4.57	3.82	250	298	1227	27.11	6.07	15	0.50	0.43	0.134		
	020201#3	89.8	8.63	7.21	461	429	1399	94.94	11.26	16	0.62	0.55	0.102	5.55	0.9995
NF	030201#1	40.0	5.37	4.49	447	452	1353	70.00	8.68	2.5					
	050201#1	101.6	8.55	7.14	563	478	1412	29.43	2.29	4					
	050201#2	133.0	10.25	8.56	513	552	1515	70.44	4.58	13	0.63	0.58	0.088	12.63	0.9972
	060201#1	496.4	5.30	4.42	303	340	1291	18.23	2.29	11	0.81	0.75	0.078	5.05	0.9978
	060201#2	259.1	5.30	4.43	313	315	1312	37.95	4.77	10	0.83	0.83	0.084	9.35	0.9980
		298.7	8.57	7.16					2.32	12				6.48	0.9972
		197.1	8.59	7.17				30.33	2.35	8	0.78	0.69	0.111		
SB	030201#1	60.0	8.71	7.28	437										
	070201#1	190.0	10.15	8.48	507	617	1499	57.26	4.62	2.5	0.89		0.384		
	080201#1	184.5	10.09	8.42	459	503	949	57.74	4.69	3	1.03		0.327		
max			10.25						11.26						
min			4.44						2.29						
	Total	56.8	[h]												
	Exp#	[min]	[cm/s]	[m^3/h]	[Pa]	[Pa]	[Pa]	mm/h average	[g/m^3]		[g/cm^2]	[g/cm^2]	[-]	[mg/m^3]	[-]
L10/56															
SAE	270201#1	216.3	8.57	7.90	368	446	1372	42.86	4.64	7	0.54	0.50	0.074	3.02	0.9993
	280201#1	417.1	8.60	7.92	394	496	1396	21.42	2.31	8	0.58	0.48	0.066	1.21	0.9995
	280201#2	298.9	12.77	11.77	549	693	1537	32.47	2.36	18	0.25	0.23	0.066	3.92	0.9983
	020301#1	318.3	10.69	9.85	486	509	1455	27.16	2.36	9	0.50	0.47	0.057		
	020301#2	355.6	10.02	9.24	512	649	1519	27.21	2.52	16	0.21	0.19	0.086	3.12	0.9988
	030301#1	346.7	4.86	4.47	293	486	1288	27.21	5.20	6	0.23	0.18	0.204	-3.17	1.0006
	060301#1	789.9	9.89	9.12	483	664	1488	13.43	1.26	16	0.20	0.19	0.097	-0.43	1.0003
	070301#1	380.8	9.74	8.97	500	766	1995	27.49	2.62	9	0.18	0.16	0.111	1.53	0.9990
	070301#2	176.9	9.98	9.19	514	666	1952	53.54	4.98	8	0.19	0.15	0.189	3.01	0.9994
	070301#3	354.6	10.03	9.25	510	737	2001	27.29	2.52	9	0.19	0.15	0.173	1.75	0.9993
	080301#1	352.7	4.84	4.46	310	520	1981	27.01	5.18	4	0.16	0.09	0.452	1.38	0.9997
	080301#2	224.8	7.34	6.76	469	807	1994	40.00	5.06	6	0.16	0.13	0.167	1.09	0.9996
	090301 #1-4	871.7	7.40	6.82	390	619	1970	40.14	5.03	22	0.36	0.31	0.133	1.81	0.9996
NF	180301#1	234.4	4.47	4.12	301	0	1979	40.78	5.51	3	0.33		0.190	4.18	0.9992
VDI	20501		4.80	4.42				24.00	4.49						
	030501#1		9.77	9.00				111.10	10.20						
	030501#2		9.75	8.99				55.22	5.08						
	Total	85.1	[h]												
Wishbone + L10/56		141.9	[h]												

All experiments on filtration of SAE dust in the Wishbone louver showed linear pressure build-up. Although the bulk of filtration experiments showed a close to linear pressure build-up rate, some of the experiments showed a clearly downward sloping pressure bulid-up. In two out of three experiments where PuralSB was used on the Wishbone configuration, the initial pressure build up rate gradually increased before becoming linear, while the intermediate experiment (070201#1) showed a distinct downward sloping pressure increase not observed in any of the other Wishbone louver tests.

However, this behaviour is clearly seen in the bulk of experiments conducted on the L10-56 louver. In these tests also the consecutive pressure build-up rates showed a typical downward sloping pressure increase at low filter loading.

The high but downward sloping pressure build up rate seems most pronounced at low filter loading (i.e. low pressure drop) Above some 1200Pa the overall pressure build up is close to linear in all experiments. Exceeding a pressure build-up of some 1500Pa introduce some instabilities (seen as sudden pressure drops) in the filter operation. These are similar to what would have been expected in connection to pinhole formation, or bad filter cleaning. It is important to underline that further investigation is necessary in order to determine the reason for this behavior. The filter was generally operated at under pressure (2000-4000Pa), measured behind the filter. This lead to a decreasing pressure difference between the particle feeder and the filter surface as the pressure build up increased. Increasing the under pressure seemed to result in a more stable operation (i.e. the instabilities at high pressure drops decreased). The system supplying pressurised air gave a variable pressure at the inlet, due to cyclic compression. The cyclic variation became more pronounced during periods with low consumption of air (e.g. after working hours). Thus reducing the average under pressure in the filter house seemed to result in more stable operation.

The most stable operation of the L10-56 louver was obtained at a sand spill of 0.18 and 0.31 g/cm^2 (experiment 030301#1 and 090301#1 respectively, filtration of SAE-fine), being highest for the experiment operated with the highest filtration velocity. Further investigations are necessary in order to gain a clear understanding of how filter loading (filtration velocity and raw gas dust concentration) influences upon the most favorable sand spill.

Graphs showing the resulting pressure build-up is included in the following pages (the order of appearance corresponds with Table I.1.).

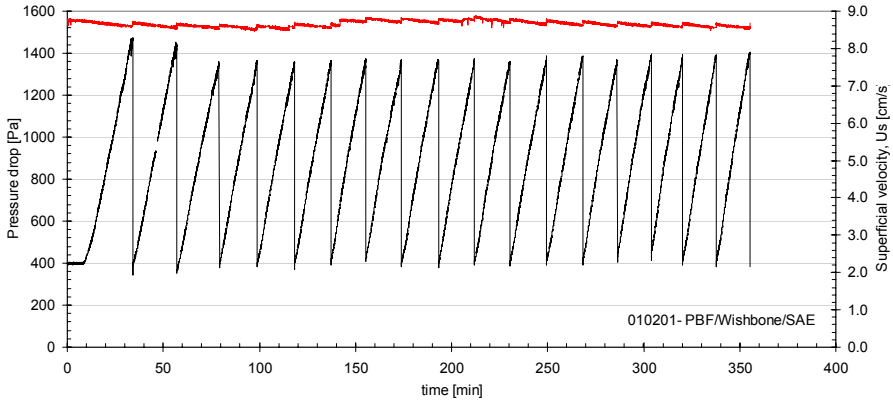

The interruption seen at about 400min, in experiment number 020201#1, is due to mal-functioning of the data acquisition system and not connected to the filter stability.

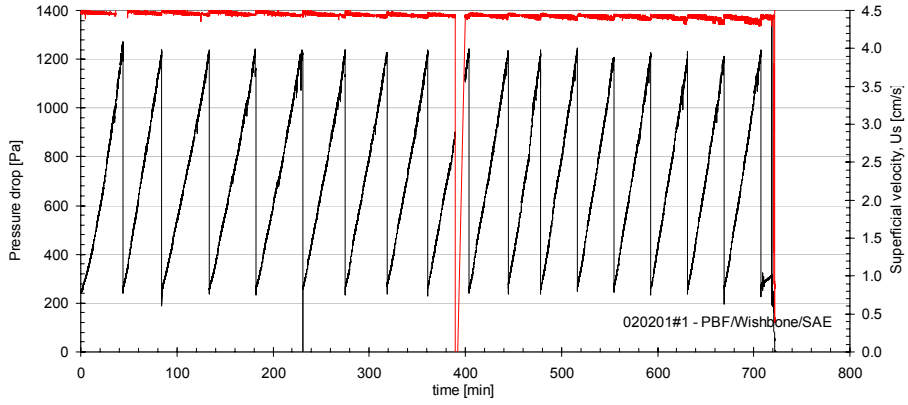

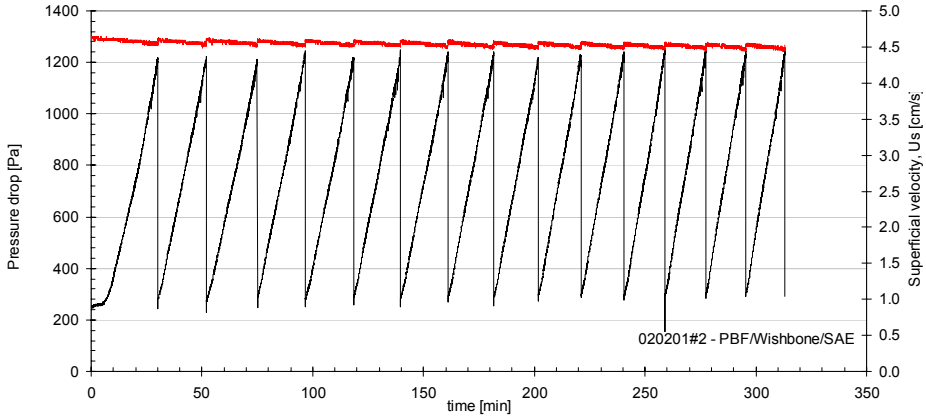

The interruption seen at about 400min, in experiment number 020201#1, is due to mal-functioning of the data acquisition system and not connected to the filter stability.

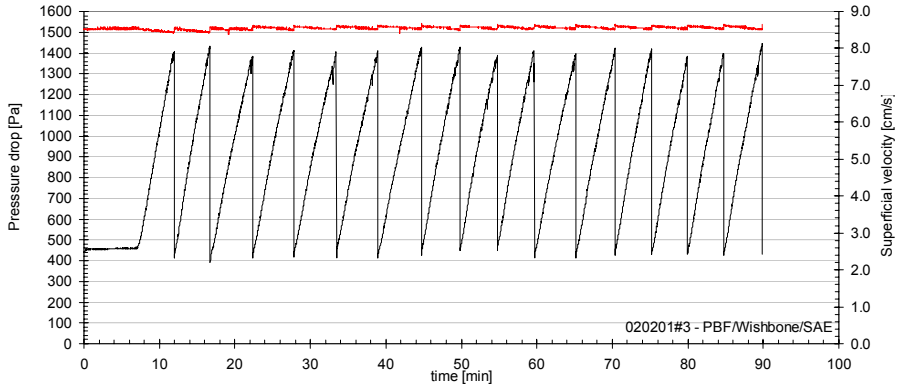

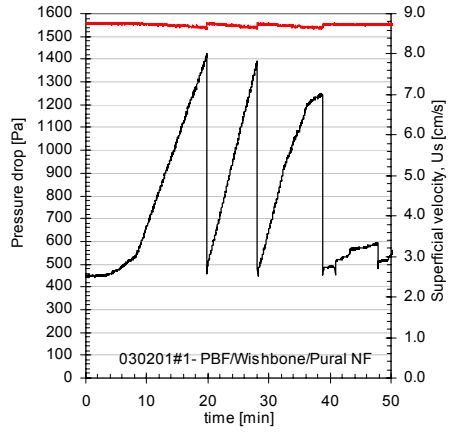

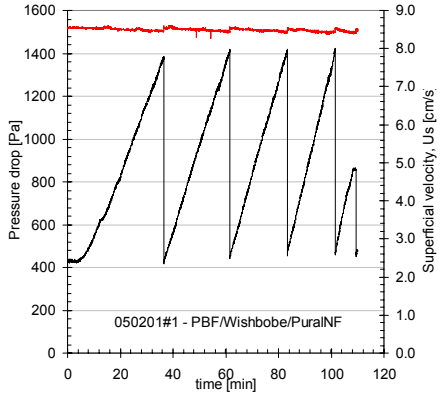

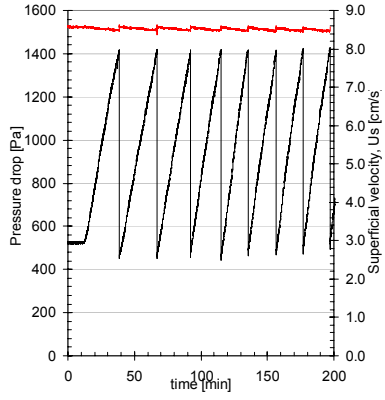

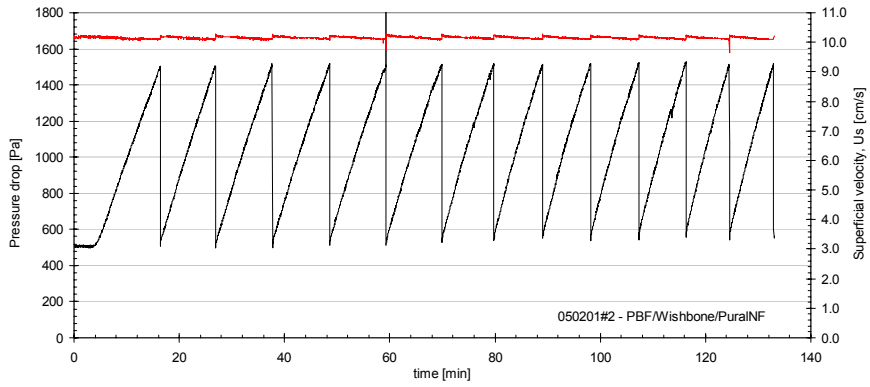

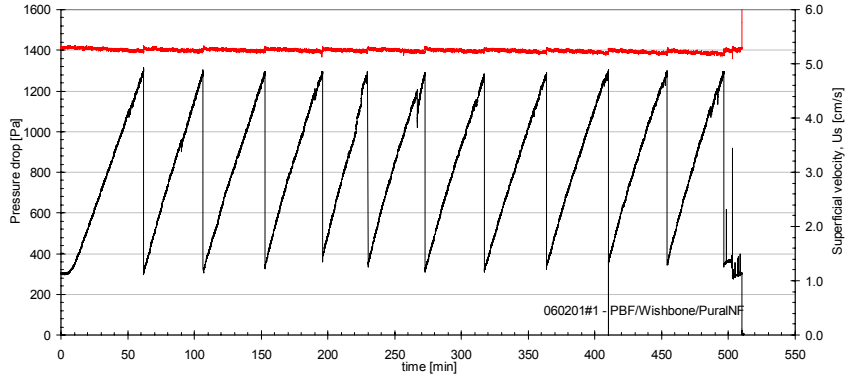

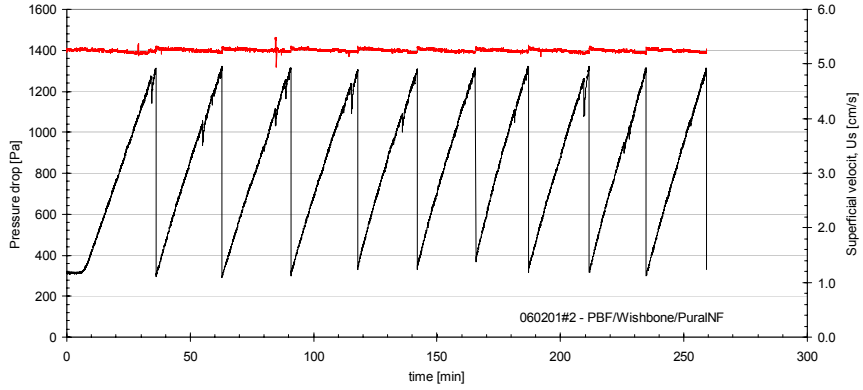

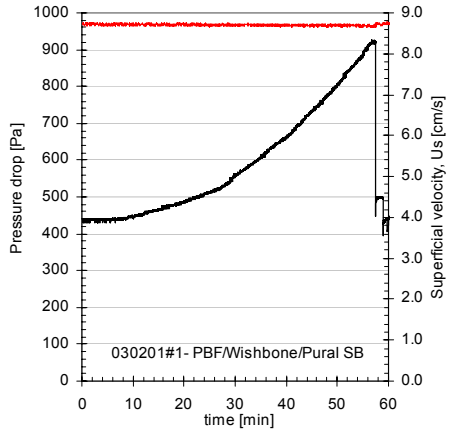

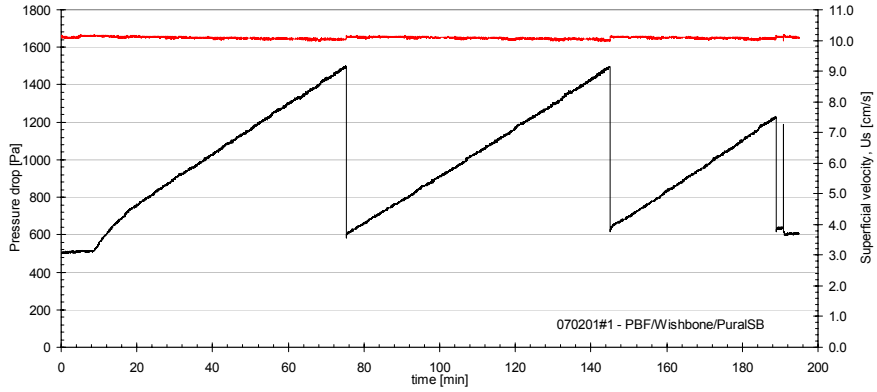

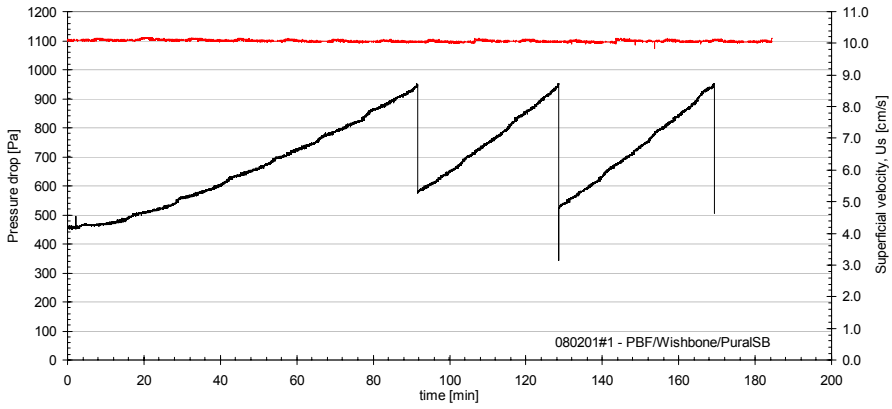

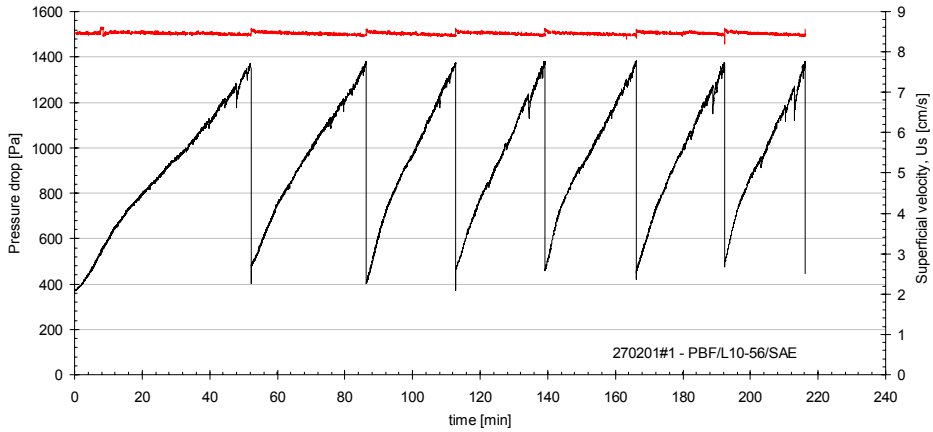

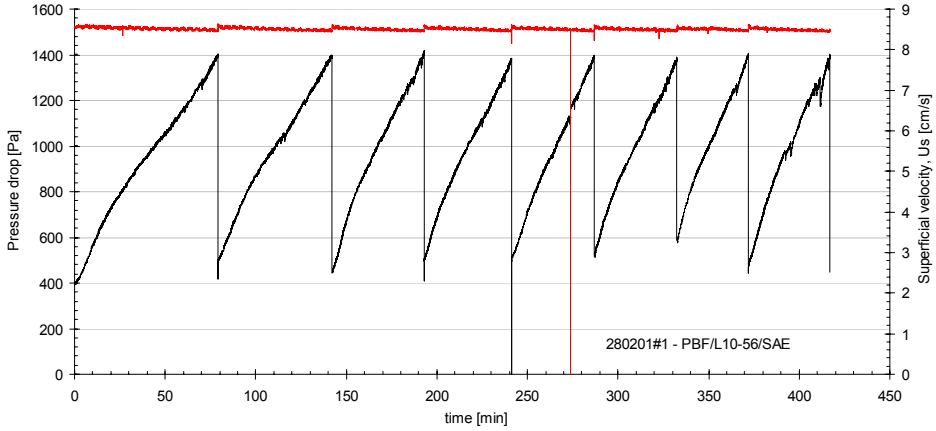

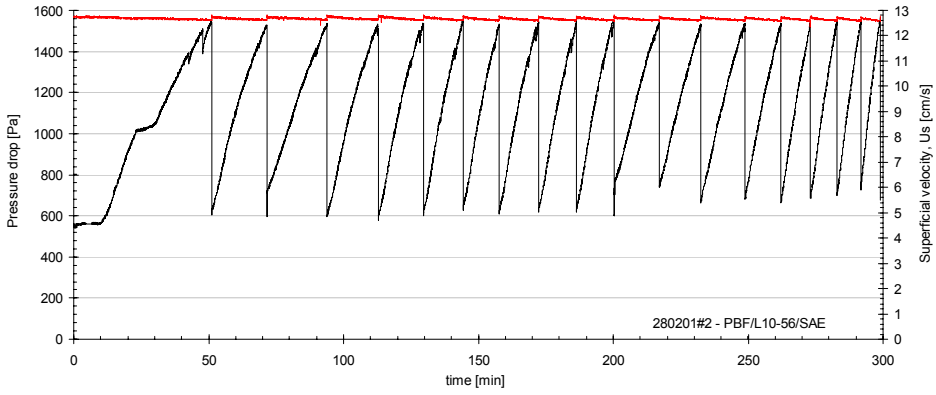

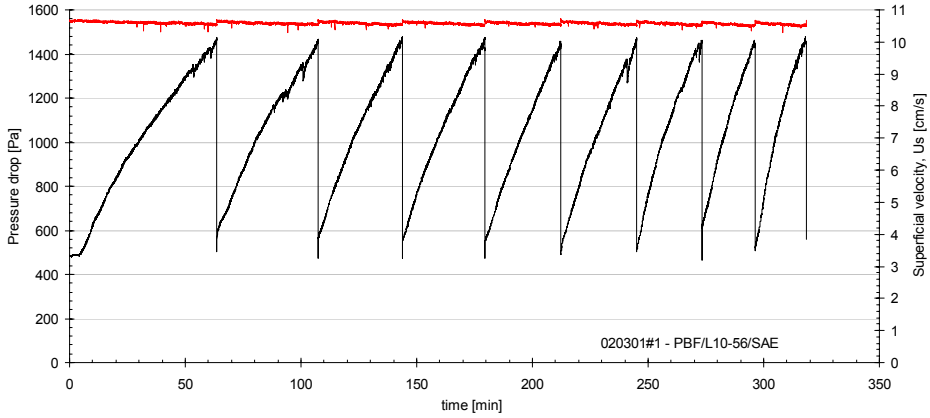

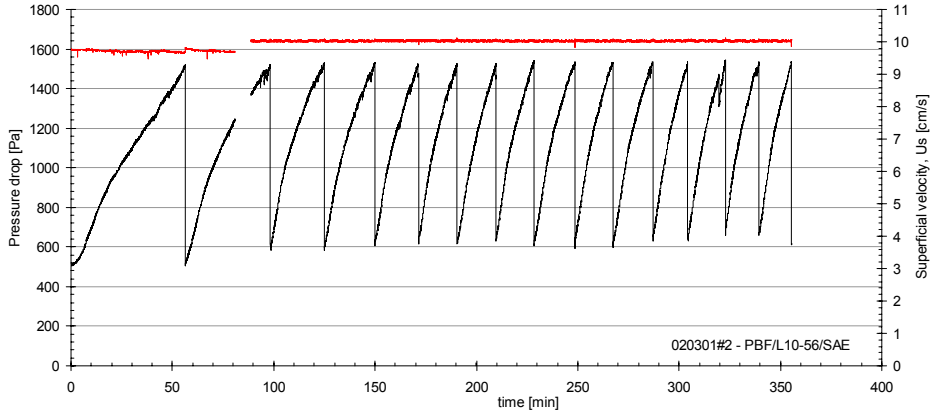

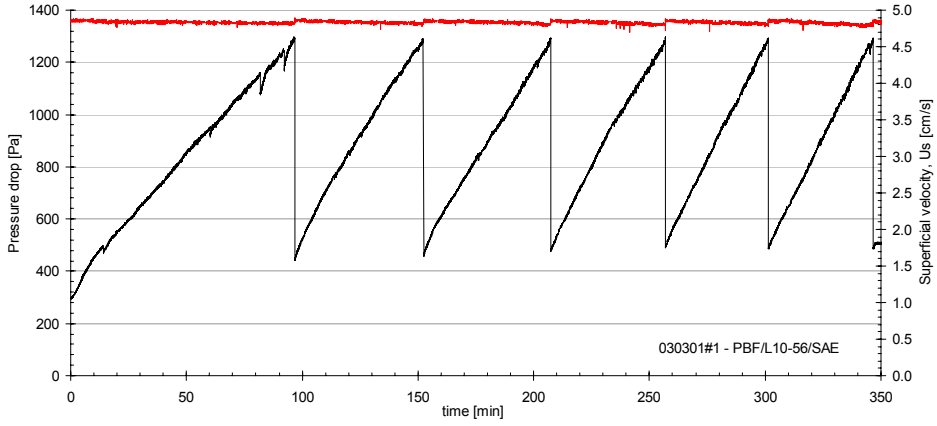

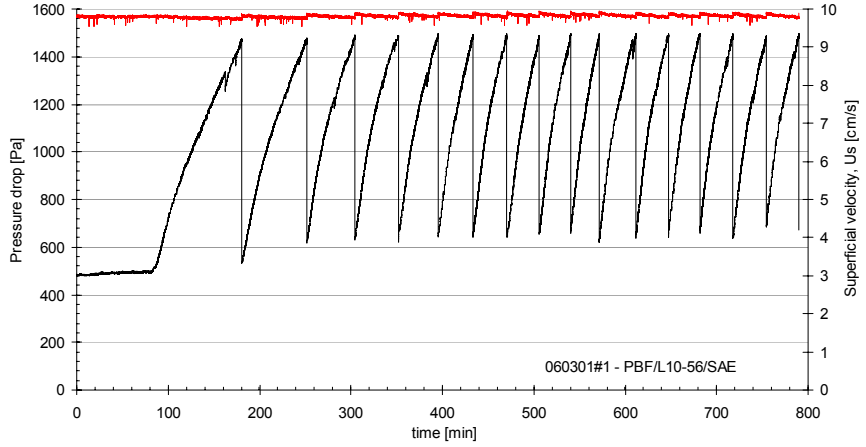

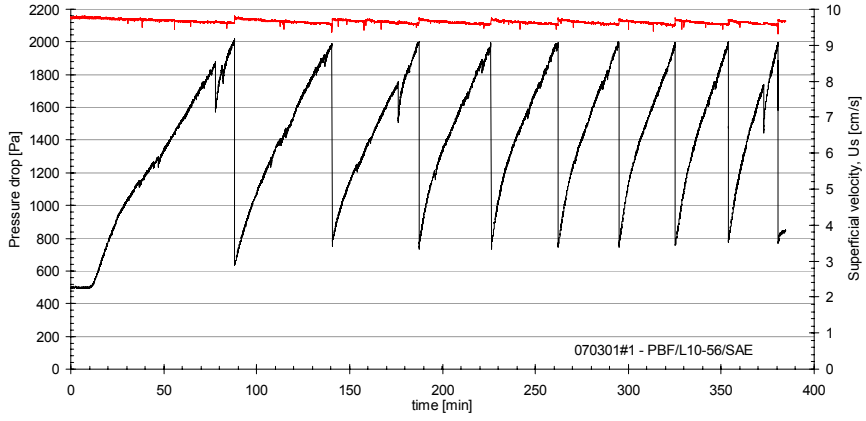

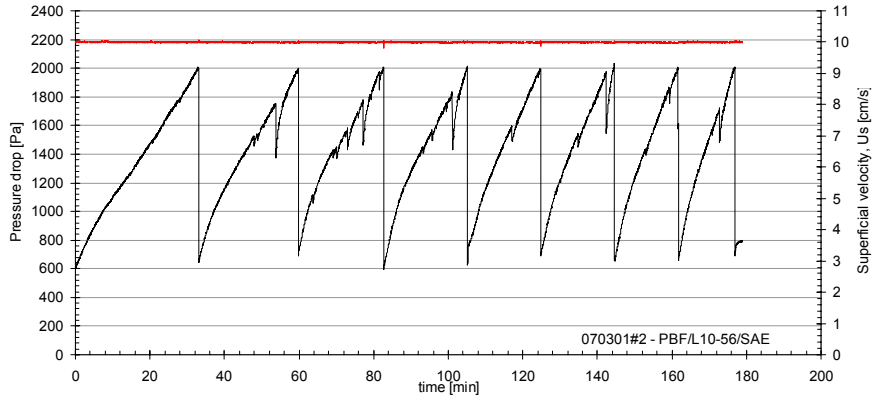

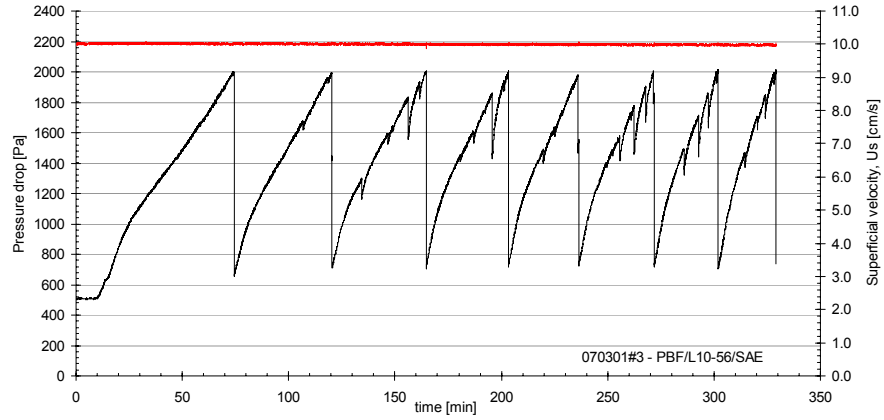

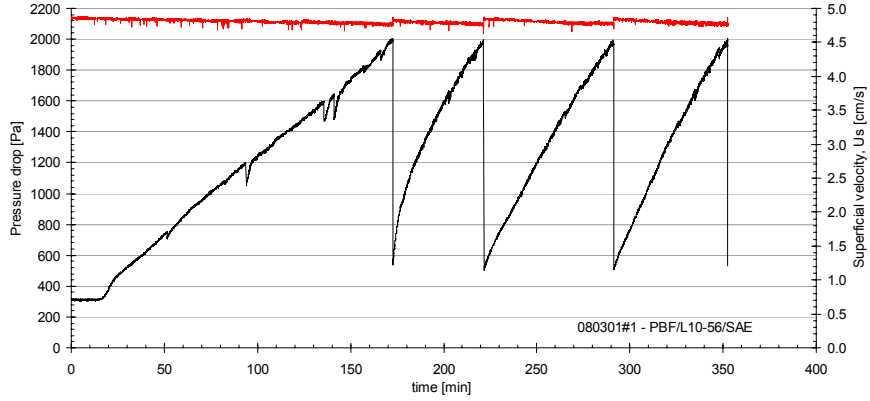

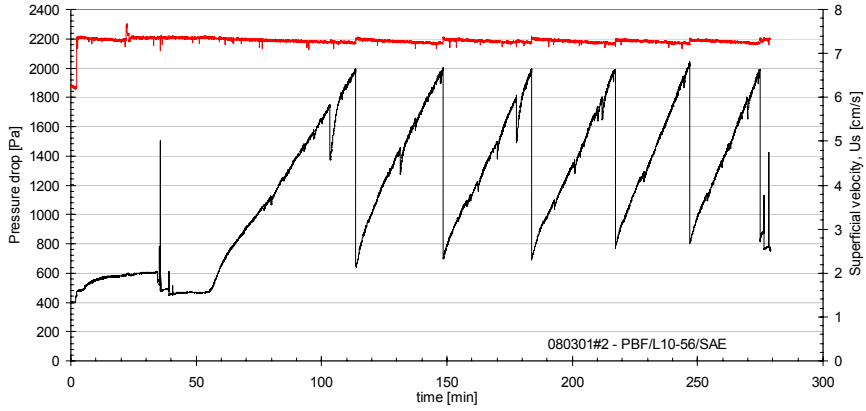

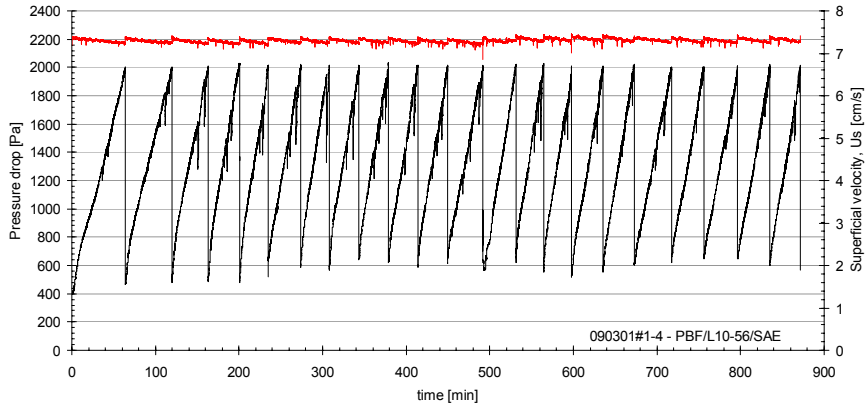

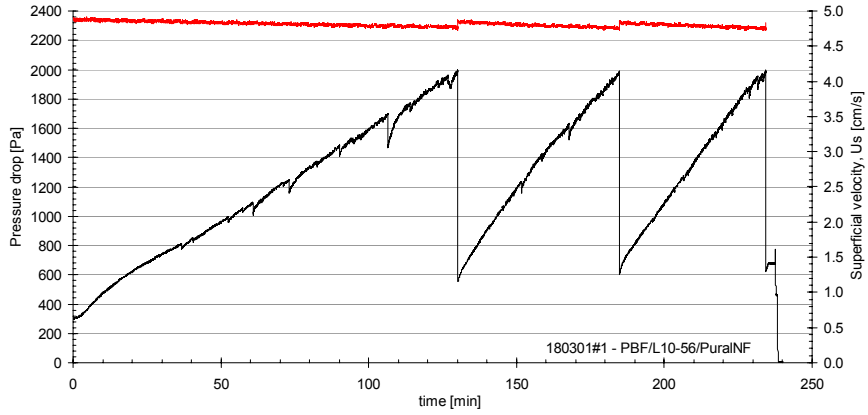

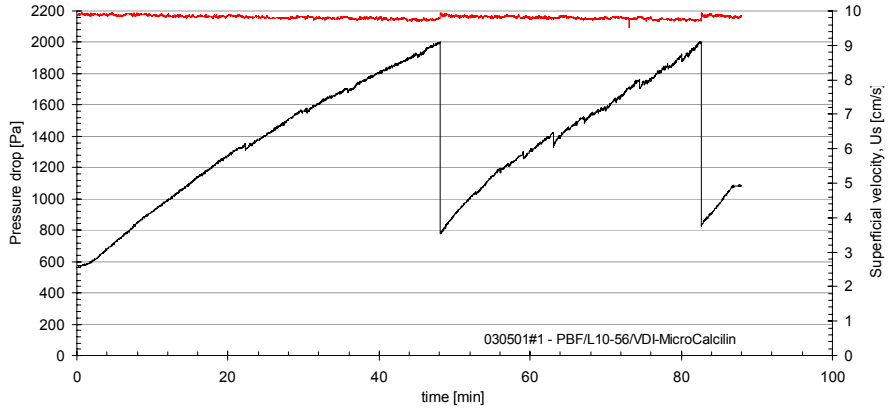

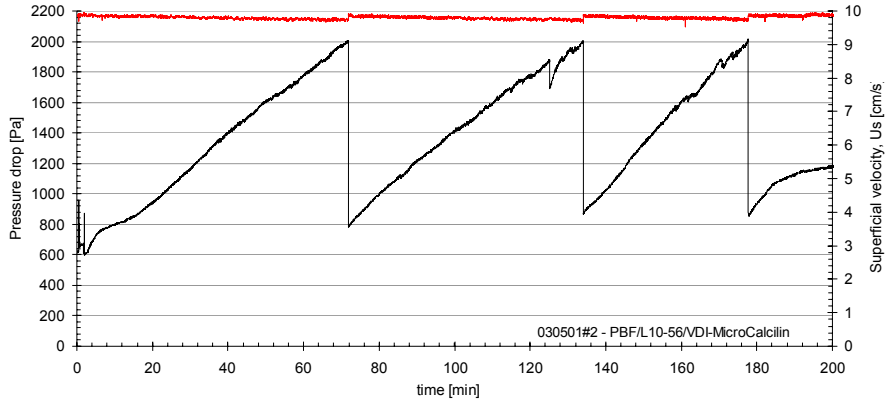

I.2 Resulting cycle time (tc) residual pressure drop (dPr) and specific cake resistance (K2') vs. filtration time.

As expected from the bulk of experimental data published in the literature (Chapter 2) both the cycle time and the residual pressure drop changed during the initial filtration cycles.

The consecutive pages contains graphical presentation of how the cycle time (t_c) developed with time (one graph for each combination of louver geometry and dust quality), followed by similar graphs for the residual pressure drop (dP_r) and the specific cake resistance (K_2').

- t_c and dP_r:
It is interesting to note the low increase in the residual pressure drop for the Wishbone louver (compared to the L10-56 louver) despite this stable operation was achieved.

Cleaning intensity in the Wishbone louver tests resulted in a theoretically average sand spill in the range of 0.43-0.83g/cm^2. The corresponding range for the L10-56 louver tests is 0.09 to 0.50. The relatively high cleaning intensity applied in the Wishbone explains the relatively low residual pressure build up seen for this louver. (The variations in the specific sand spill are listed in table I.1)

The applied dust qualities showed very different characteristics with regard to the resulting pressure build-up. This resulted in generally the same duration of the filtration cycles when using SAE-fine and PuralNF dust, while significantly longer cycles was obtained when using the PuralSB and Micro Calcilin dust. Hence, the transient pressure build up and increase in the residual pressure drop when using these dusts is less well documented.

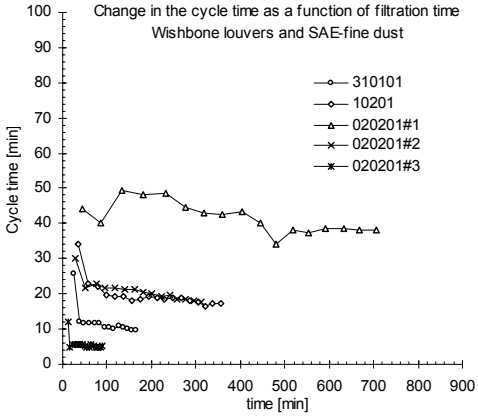

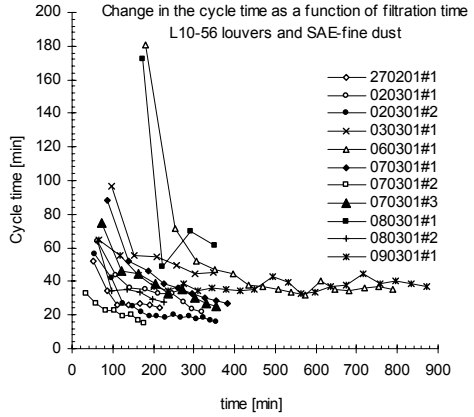

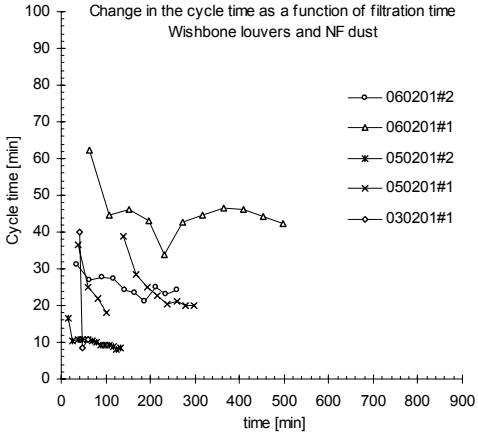

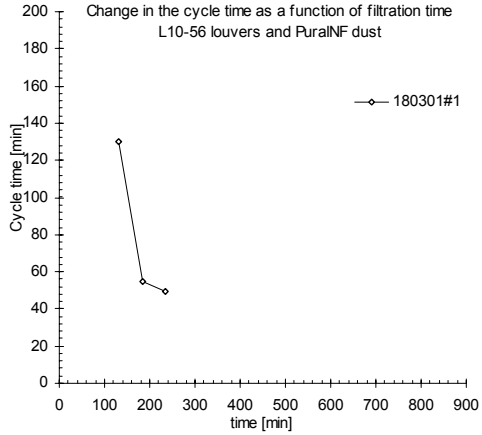

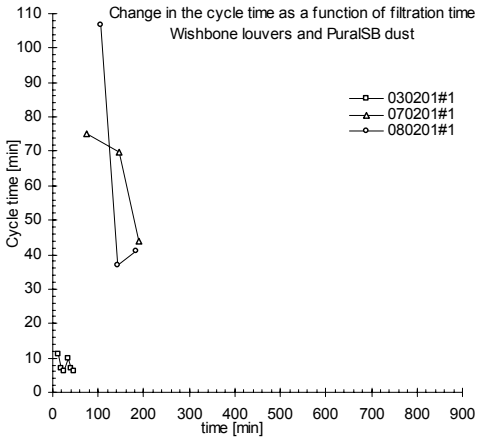

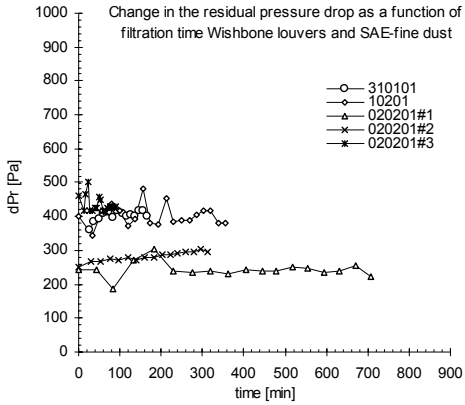

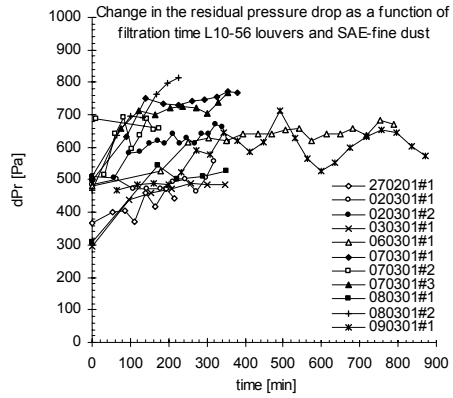

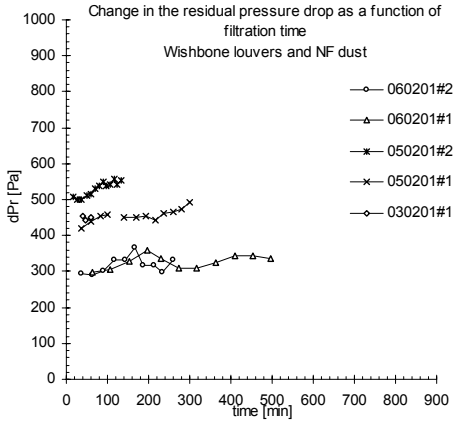

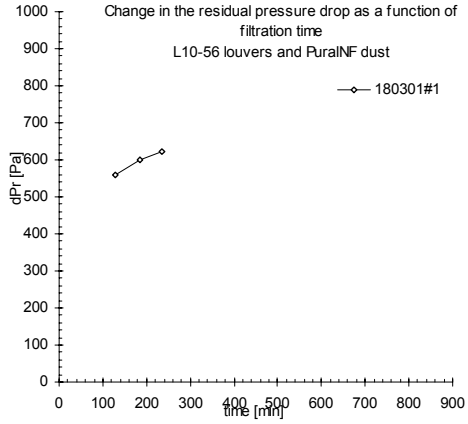

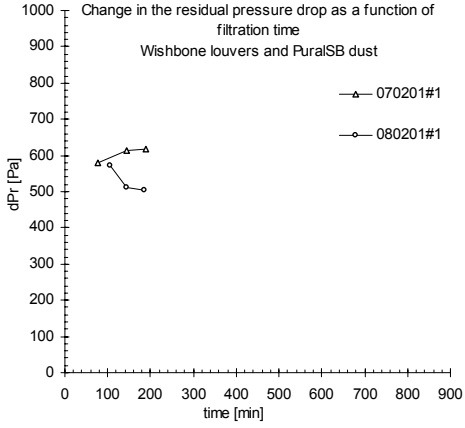

- K_2':

The calculation of an average specific cake resistance (K_2') can lead to misleading results if effects such as the non-linearity in the initial pressure build-up (at low filter loadings) and the instabilities at the higher pressure build up (higher filter loadings) are not taken into account. Hence, in order to investigate the effect of using different approaches, in general three different values of K_2' was calculated: i) based on the total pressure build up (from start to end of one filtration cycle), ii) based on the last five minutes and iii) from 70-90% of the pressure build up across the filter cake.

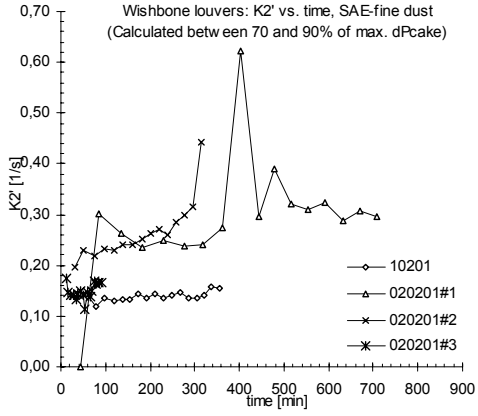

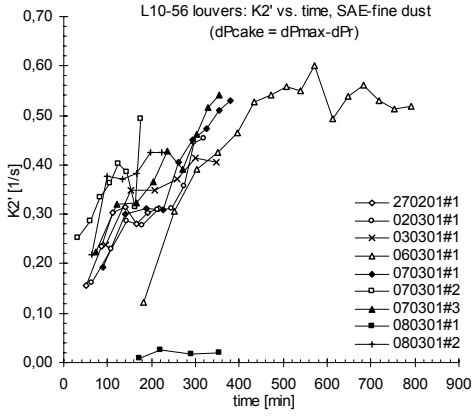

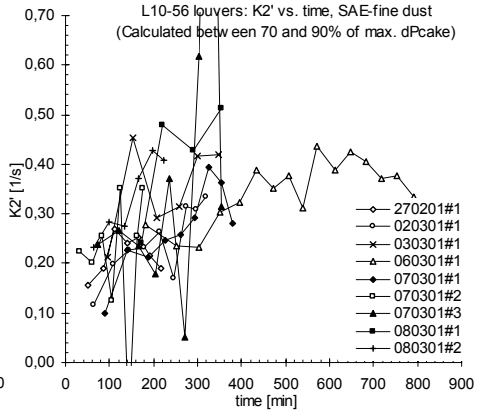

I.3 Some essential parameters characterising the filtration experiments.

The consecutive pages contains tabulated values (such as t, t_c, U_S, v_f, c, dP_0, dP_{max}, dP_r, $dP_{cake,max}$ and K_2') characterizing each filtration experiment in general and each specific pressure build up in special (i.e. each cycle). In order of appearance: Wishbone – SAE-fine; L10-56 – SAE-fine; L10-56 – PuralNF; Wishbone – Pural NF and finally Wishbone – PuralSB.

Note that the initial transient pressure build up registered after cleaning also complicates the derivation of the residual pressure drop (dPr). This effect is illustrated by calculating the total pressure build up just after cleaning and compare this to the pressure build up 10 seconds later (denoted as +10s in the included tables).

Furthermore, values derived at typically unstable filter operation (i.e. clearly influenced by the initial non-linearity, the instabilities at higher pressure build up and before the filter operation became "stable" are indicated with red and *italic* numbers. These values are not used when deriving maximum and minimum values, as well as average and standard deviations.

The following figure explains some of the most important parameters included in the preceding tables.

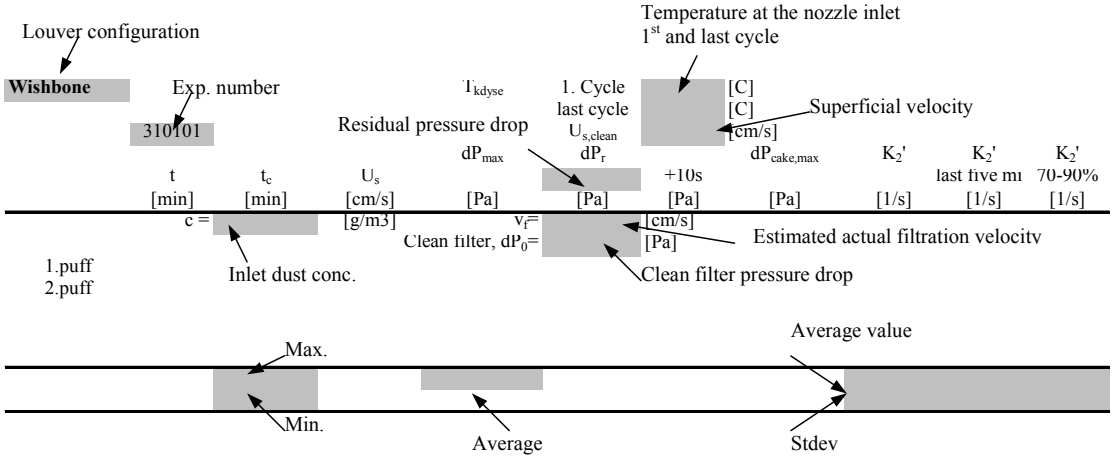

Wishbone				$\dot{T}_{kdyse}$	1. Cycle	22,56	[C]	SAE-fine	1063	[kg/m3]					$\dot{T}_{kdyse}$	1. Cycle	22,50	[C]	SAE-fine	1063	[kg/m3]
SAE-fine					last cycle	22,73	[C]									last cycle	21,72	[C]			
310101				$U_{s,clean}$		8,57	[cm/s]	VelFactor	0,65	[-]	**010201**				$U_{s,clean}$		8,75	[cm/s]	VelFactor	0,65	[-]
				dP_{max}	dP_r		$dP_{cake,max}$	K_2'	K_2'	K_2'					dP_{max}	dP_r		$dP_{cake,max}$	K_2'	K_2'	K_2'
	t	t_c	U_s		412,66	+10s			last five min	70-90%	t	t_c	U_s		398,6	+10s				last five min	70-90%
	[min]	[min]	[cm/s]	[Pa]	[Pa]	[Pa]	[Pa]	[1/s]	[1/s]	[1/s]	[min]	[min]	[cm/s]	[Pa]	[Pa]	[Pa]	[Pa]	[1/s]	[1/s]	[1/s]
	c =	6,15	[g/m3]	v_f=	13,67	[cm/s]					c =	3,26	[g/m3]	v_f=	13,5	[cm/s]				
	0		Clean filter, dP_0=		399,6	[Pa]					0		Clean filter, dP_0=		399,0	[Pa]				
1.puff	25,75	25,73	8,84	1491,7	360,0	426,1					34,13	34,13	8,73	1462,3	345,3	400,4		*0,088*	*0,124*	*0,135*
2.puff	37,72	11,98	8,99	1469,7	385,7	422,5					57,10	22,97	8,64	1440,3	415,1	378,4		*0,134*	*0,122*	*0,144*
3.puff	49,17	11,45	8,96	1425,6	393,1	440,8					79,10	22,00	8,62	1359,5	437,2	400,4		0,121	0,120	0,120
4.puff	60,78	11,62	8,97	1458,7	407,8	448,2					98,82	19,72	8,60	1355,8	415,1	400,4		0,131	0,133	0,137
5.puff	72,23	11,45	8,91	1458,7	411,4	440,8					118,19	19,37	8,70	1359,5	371,0	400,4		0,137	0,137	0,131
6.puff	84,02	11,78	8,81	1469,7	396,7	451,8					137,37	19,18	8,68	1366,8	393,1	426,1		0,146	0,145	0,132
7.puff	94,58	10,57	8,89	1473,4	418,8	451,8					155,49	18,12	8,81	1366,8	481,2	426,1		0,152	0,133	0,131
8.puff	105,15	10,57	8,90	1469,7	407,8	451,8					173,97	18,48	8,84	1370,5	382,1	404,1		0,136	0,135	0,143
9.puff	115,18	10,03	8,88	1466,0	400,4	448,2					193,15	19,18	8,79	1355,8	378,4	407,8		0,143	0,124	0,135
10.puff	126,10	10,92	8,88	1502,7	404,1	440,8					211,97	18,82	8,75	1374,2	451,8	411,4		0,149	0,149	0,143
11.puff	136,48	10,38	8,87	1473,4	400,4	437,2					230,45	18,48	8,80	1355,8	385,7	415,1		0,138	0,135	0,134
12.puff	146,52	10,03	8,88	1469,7	418,8	462,9					249,45	19,00	8,80	1366,8	389,4	411,4		0,146	0,135	0,142
13.puff	156,02	9,50	8,80	1488,0	418,8	451,8					268,29	18,83	8,75	1377,8	389,4	418,8		0,148	0,139	0,146
14.puff	165,70	9,68	8,81	1458,7	400,4	429,8					286,24	17,95	8,72	1366,8	404,1	440,8		0,154	0,143	0,136
15.puff											303,84	17,60	8,70	1385,2	415,1	448,2		0,157	0,139	0,135
16.puff											320,37	16,53	8,60	1388,9	415,1	418,8		0,166	0,145	0,141
17.puff											337,80	17,43	8,68	1392,5	382,1	411,4		0,158	0,157	0,157
18.puff											355,24	17,43	8,67	1403,6	382,1	411,4		0,165	0,155	0,154
max		25,73	8,9	1469,7								34,13	8,72	1380,49				0,147	0,139	0,139
min		9,50										16,53						0,083	0,072	0,066

Wishbone				$\dot{T}_{kdyse}$	1. Cycle	17,72	[C]	SAE-fine	1063	[kg/m3]					$\dot{T}_{kdyse}$	1. Cycle	18,77	[C]	SAE-fine	1063	[kg/m3]
SAE-fine					last cycle	18,62	[C]									last cycle	18,15	[C]			
020201#1				$U_{s,clean}$		4,47	[cm/s]	VelFactor	0,65	[-]	**020201#2**				$U_{s,clean}$		4,62	[cm/s]	VelFactor	0,65	[-]
				dP_{max}	dP_r		$dP_{cake,max}$	K_2'	K_2'	K_2'					dP_{max}	dP_r		$dP_{cake,max}$	K_2'	K_2'	K_2'
	t	t_c	U_s		238,8	+10s			last five min	70-90%	t	t_c	U_s		297,56	+10s				last five min	70-90%
	[min]	[min]	[cm/s]	[Pa]	[Pa]	[Pa]	[Pa]	[1/s]	[1/s]	[1/s]	[min]	[min]	[cm/s]	[Pa]	[Pa]	[Pa]	[Pa]	[1/s]	[1/s]	[1/s]
	c =	3,05	[g/m3]	v_f=	6,9	[cm/s]					c =	6,07	[g/m3]	v_f=	7,0	[cm/s]				
	0		Clean filter, dP_0=		241,0	[Pa]					0		Clean filter, dP_0=		250,0	[Pa]	0,0			
1.puff	44,33	44,33	4,63	1256,6	242,5	*271,8*		*0,265*	*0,374*	*0,000*	30,08	30,08		1219,9	268,2	*282,9*	*18,2*	*0,179*	*0,290*	*0,197*
2.puff	84,48	40,15	4,47	1227,2	187,3	*253,5*		*0,283*	*0,272*	*0,301*	51,92	21,83		1223,5	268,2	*271,8*	*18,2*	*0,243*	*0,273*	*0,229*
3.puff	133,90	49,42	4,52	1238,2	271,8	*260,8*		*0,246*	*0,272*	*0,262*	74,95	23,03		1212,5	275,5	290,2	*25,5*	0,226	0,273	0,217
4.puff	181,92	48,02	4,52	1161,1	304,9	*253,5*		*0,214*	*0,170*	*0,234*	96,62	21,67		1238,2	271,8	282,9	*21,8*	0,248	0,278	0,231
5.puff	230,65	48,73	4,46	1223,5	238,8	*257,1*		*0,218*	*0,221*	*0,248*	118,45	21,83		1212,5	279,2	290,2	*29,2*	0,237	0,269	0,229
6.puff	275,37	44,72	4,48	1131,7	235,1	*271,8*		*0,231*	*0,051*	*0,237*	139,75	21,30		1238,2	271,8	286,5	*21,8*	0,252	0,278	0,240
7.puff	318,47	43,10	4,48	1227,2	238,8	*275,5*		*0,266*	*0,280*	*0,241*	161,05	21,30		1212,5	279,2	293,9	*29,2*	0,243	0,249	0,240
8.puff	360,93	42,47	4,47	1216,2	231,4	*271,8*		*0,266*	*0,297*	*0,275*	181,65	20,60		1234,6	279,2	293,9	*29,2*	0,258	0,278	0,253
9.puff	404,19	43,26	4,47	1241,9	242,5	*268,2*		*0,270*	*0,807*	*0,623*	201,90	20,25		1216,2	286,5	301,2	*36,5*	0,255	0,265	0,262
10.puff	444,44	40,25	4,46	1227,2	238,8	271,8		0,283	0,314	0,295	221,08	19,18		1197,8	286,5	297,6	*36,5*	0,264	0,261	0,272
11.puff	478,71	34,27	4,46	1150,1	238,8	268,2		0,307	0,178	0,390	240,63	19,55		1238,2	290,2	297,6	*40,2*	0,269	0,282	0,261
12.puff	516,91	38,20	4,44	1245,6	249,8	275,5		0,305	0,306	0,322	258,93	18,30		1245,6	293,9	301,2	*43,9*	0,289	0,318	0,284
13.puff	554,42	37,52	4,44	1205,2	246,1	271,8		0,294	0,314	0,311	277,43	18,50		1249,3	293,9	301,2	*43,9*	0,287	0,310	0,298
14.puff	592,96	38,53	4,45	1227,2	235,1	268,2		0,294	0,357	0,325	295,58	18,15		1216,2	304,9	308,6	*54,9*	0,279	0,265	0,315
15.puff	631,34	38,38	4,41	1223,5	238,8	257,1		0,298	0,416	0,288	313,17	17,58		1256,6	297,6	308,6	*47,6*	0,303	0,339	*0,441*
16.puff	669,36	38,02	4,43	1212,5	253,5	268,2		0,296	0,323	0,307										
17.puff	707,37	38,02	4,39	1230,9	224,1	268,2		0,297	0,297	0,296										
18.puff																				
max		49,42	4,5	1214,5				0,297	0,313	0,317		30,08		1227,5				0,262	0,282	0,259
min		34,27						0,025	0,213	0,102		17,58						0,085	0,090	0,115

Wishbone T_{kdyse} 1. Cycle 22,61 [C] SAE-fine 1063 [kg/m3]
SAE-fine last cycle 23,32 [C]
020201#3 $U_{s,clean}$ 8,54 [cm/s] VelFactor 0,65 [-]

	dP_{max}	dP_f		$dP_{cake,max}$	K_2'	K_2'	K_2'
	t	t_c	U_s	428,58	+10s			last five min	70-90%
	[min]	[min]	[cm/s]	[Pa]	[Pa]	[Pa]		[1/s]	[1/s]	[1/s]
	c =	11,26	[g/m3]	v_f=	13,3	[cm/s]				
	0			Clean filter, dP_0=	460,6	[Pa]				
1.puff	11,97	11,97		1396,2	418,8	*459,2*		*0,066*	*0,156*	*0,175*
2.puff	16,72	4,75		1425,6	466,5	*429,8*		*0,178*	*0,009*	*0,146*
3.puff	22,35	5,63		1381,5	503,3	451,8		0,136	*0,027*	0,142
4.puff	27,82	5,47		1410,9	418,8	462,9		0,139	*0,154*	0,141
5.puff	33,45	5,63		1403,6	415,1	477,6		0,147	*0,146*	0,131
6.puff	38,90	5,45		1399,9	426,1	444,5		0,152	*0,149*	0,144
7.puff	44,72	5,82		1418,2	426,1	477,6		0,143	*0,148*	0,149
8.puff	49,82	5,10		1425,6	455,5	477,6		0,165	*0,164*	0,142
9.puff	54,75	4,93		1377,8	448,2	488,6		0,157	*-0,006*	0,113
10.puff	59,68	4,93		1319,1	415,1	451,8		0,148	*-0,007*	0,147
11.puff	65,13	5,45		1388,9	411,4	448,2		0,150	*0,150*	0,139
12.puff	70,33	5,20		1410,9	426,1	470,2		0,161	*0,162*	0,148
13.puff	75,23	4,90		1414,6	429,8	462,9		0,169	*0,004*	0,170
14.puff	79,98	4,75		1377,8	429,8	470,2		0,168	*0,002*	0,162
15.puff	84,73	4,75		1396,2	426,1	455,5		0,171	*0,010*	0,166
16.puff	89,83	5,10		1432,9	429,8	455,5		0,166	*0,167*	0,166
17.puff										
18.puff										
max		11,97		1398,73				0,155		0,147
min		4,75						0,075		0,104

050201#1 ν/s & 2.2-2.3g/m3

	t	tc
	[min]	[min]
1.puff	36,62	36,62
2.puff	61,62	25,00
3.puff	83,47	21,85
4.puff	101,62	18,15
5.puff	38,85	38,85
6.puff	67,20	28,35
7.puff	92,37	25,17
8.puff	115,25	22,88
max		38,85

050201#2 10.5cm/s & 4.5g/m3

	t	tc
	[min]	[min]
1.puff	16,38	16,38
2.puff	26,93	10,55
3.puff	37,67	10,73
4.puff	48,58	10,92
5.puff	59,32	10,73
6.puff	69,87	10,55
7.puff	79,82	9,95
8.puff	89,07	9,25
9.puff	98,17	9,10
10.puff	107,30	9,13
11.puff	116,28	8,98
12.puff	124,53	8,25
13.puff	132,98	8,45
max		16,38

060201#1 5.5cm/s & 2.2g/m3

	t	tc
	[min]	[min]
1.puff	62,20	62,20
2.puff	106,72	44,52
3.puff	152,85	46,13
4.puff	195,88	43,03
5.puff	272,63	42,75
6.puff	317,10	44,47
7.puff	363,65	46,55
8.puff	409,98	46,33
9.puff	454,23	44,25
10.puff	496,42	42,18
max		62,20

060201#2 5.5cm/s & 4.6g/m3

	t	tc
	[min]	[min]
1.puff	36,23	31,23
2.puff	63,00	26,77
3.puff	90,83	27,83
4.puff	117,95	27,12
5.puff	142,07	24,12
6.puff	165,65	23,58
7.puff	186,95	21,30
8.puff	211,77	24,82
9.puff	234,83	23,07
10.puff	259,13	24,30
max		31,23

L10-56				T_{kdyse}	1. Cycle	20,32	[C]	SAE-fine	1063	[kg/m3]					T_{kdyse}	1. Cycle	19,62	[C]	SAE-fine	1063	[kg/m3]
SAE-fine					last cycle	19,82	[C]									last cycle	21,23	[C]			
	270201#1				$U_{s,clean}$	8,46	[cm/s]	VelFactor	1,30	[-]						$U_{s,clean}$	8,57	[cm/s]	VelFactor	1,30	[-]
				dP_{max}	dP_r		$dP_{cake,max}$	K_2'	K_2'	K_2'				dP_{max}	dPr		$dP_{cake,max}$	K_2'	K_2'	K_2'
	t	t_c	U_s		445,7	+10s			last five min	70-90%	t	t_c	U_s		495,9	+10s			last five min	70-90%
	[min]	[min]	[cm/s]	[Pa]	[Pa]	[Pa]	[Pa]	[1/s]	[1/s]	[1/s]	[min]	[min]	[cm/s]	[Pa]	[Pa]	[Pa]	[Pa]	[1/s]	[1/s]	[1/s]
	C=	4,64	[g/m3]	vf=	6,59	[cm/s]					C=	2,32	[g/m3]	vf=	6,6	[cm/s]				
	0		Clean filter, dP_0=		367,9	[Pa]					0,0		Clean filter, dP_0=		394,3	[Pa]				
1.puff	52,22	52,22	8,56	1348,5	400,4	484,9		*0,155*	*0,170*	*0,157*	79,23	79,23	8,64	1396,2	418,8	492,3		*0,209*	*0,219*	*0,176*
2.puff	86,42	34,20	8,55	1377,8	404,1	415,1		*0,236*	*0,213*	*0,191*	142,32	63,08	8,61	1396,2	444,5	455,5		*0,256*	*0,219*	*0,217*
3.puff	112,80	26,38	8,58	1374,2	371,0	477,6		0,304	0,261	0,271	192,98	50,67	8,61	1410,9	407,8	503,3		*0,316*	*0,365*	*0,192*
4.puff	139,22	26,42	8,58	1374,2	459,2	470,2		0,314	0,243	0,241	241,08	48,10	8,62	1385,2	415,1	499,6		0,336	0,316	0,272
5.puff	166,18	26,97	8,56	1377,8	418,8	459,2		0,282	0,255	0,253	287,03	45,95	8,61	1392,5	514,3	521,6		0,352	0,340	0,364
6.puff	192,27	26,08	8,58	1374,2	473,9	495,9		0,303	0,292	0,215	332,65	45,62	8,57	1385,2	576,8	587,8		0,316	0,304	0,213
7.puff	216,32	24,05	8,56	1377,8	444,5	492,3		0,311	0,292	*0,189*	372,17	39,52	8,59	1407,2	444,5	481,2		0,348	0,389	0,269
8.puff											417,05	44,88	8,51	1396,2	448,2	484,9		*0,351*	*0,632*	*0,162*
9.puff																				
10.puff																				
11.puff																				
12.puff																				
13.puff																				
14.puff																				
15.puff																				
16.puff																				
17.puff																				
18.puff																				
max		52,22	8,572	1372,07				0,303	0,269	0,245		79,23	8,599	1396,21				0,338	0,337	0,279
min		24,05	0,001					0,042	0,082	0,094		39,52	0,003					0,048	0,112	0,223

L10-56				T_{kdyse}	1. Cycle	22,52	[C]	SAE-fine	1063	[kg/m3]					T_{kdyse}	1. Cycle	21,02	[C]	SAE-fine	1063	[kg/m3]
SAE-fine					last cycle	21,52	[C]									last cycle	20,10	[C]			
	280201#2				$U_{s,clean}$	12,74	[cm/s]	VelFactor	1,30	[-]	**020301#1**					$U_{s,clean}$	10,67	[cm/s]	VelFactor	1,30	[-]
				dP_{max}	dPr		$dP_{cake,max}$	K_2'	K_2'	K_2'				dP_{max}	dPr		$dP_{cake,max}$	K_2'	K_2'	K_2'
	t	t_c	U_s		693,1	+10s			last five min	70-90%	t	t_c	U_s		509,4	+10s			last five min	70-90%
	[min]	[min]	[cm/s]	[Pa]	[Pa]	[Pa]	[Pa]	[1/s]	[1/s]	[1/s]	[min]	[min]	[cm/s]	[Pa]	[Pa]	[Pa]	[Pa]	[1/s]	[1/s]	[1/s]
	C=	2,36	[g/m3]	vf=	9,8	[cm/s]					C=	2,36	[g/m3]	vf=	8,2	[cm/s]				
	0,0		Clean filter, dP_0=		549,0	[Pa]					0,0		Clean filter, dP_0=		485,9	[Pa]				
1.puff	51,13	51,13	12,80	1543,2	606,1	628,4		*0,14*			63,68	63,68	10,69	1466,0	503,3	595,1	980,1	*0,161*	*0,154*	*0,115*
2.puff	71,57	20,43	12,70	1528,5	595,1	712,9		*0,33*			107,47	43,78	10,71	1462,3	473,9	569,4	959,1	*0,230*	*0,208*	*0,198*
3.puff	93,98	22,42	12,80	1535,8	595,1	613,7		*0,31*			143,88	36,42	10,70	1473,4	473,9	554,7	999,5	0,288	0,246	0,227
4.puff	112,85	18,87	12,81	1502,7	576,8	598,8		*0,35*			179,58	35,70	10,70	1421,9	473,9	558,4	948,0	0,278	0,139	0,232
5.puff	129,60	16,75	12,82	1535,8	602,5	628,4		0,42			212,40	32,82	10,72	1440,3	492,3	521,6	966,4	0,309	0,216	0,264
6.puff	144,40	14,80	12,77	1554,4	628,4	654,1		0,47			245,13	32,73	10,68	1466,0	503,3	521,6	973,7	0,312	0,239	0,171
7.puff	157,80	13,40	12,78	1532,1	609,8	639,4		0,49			273,22	28,08	10,61	1462,3	462,9	613,7	959,1	0,358	0,231	0,315
8.puff	172,40	14,60	12,77	1546,8	617,4	643,1		0,47			296,37	23,15	10,68	1447,6	507,0	529,0	984,8	0,446	0,285	0,308
9.puff	186,48	14,08	12,78	1543,2	617,4	650,5		0,48			318,33	21,97	10,68	1458,7	558,4	676,2	951,7	*0,454*	*0,285*	*0,333*
10.puff	200,23	13,75	12,80	1546,8	598,8	709,2		0,50												
11.puff	217,17	16,93	12,76	1546,8	738,6	753,3		0,41												
12.puff	232,50	15,33	12,78	1528,5	661,5	683,5		0,38												
13.puff	248,90	16,40	12,76	1506,4	679,8	698,2		0,38												
14.puff	262,28	13,38	12,76	1532,1	665,2	690,9		0,47												
15.puff	273,20	10,92	12,75	1539,5	683,5	705,6		0,59												
16.puff	283,07	9,87	12,73	1546,8	698,2	735,0		0,64												
17.puff	291,88	8,82	12,73	1543,2	742,3	775,4		0,70												
18.puff	298,92	7,03	12,77	1558,1	676,2	705,6		0,85												
max		51,13	12,77	1537,3				0,52				63,68	10,69	1455,39				0,35	0,23	0,26
min		7,03	0,00									21,97	0,00					0,21	0,21	0,22

L10-56 SAE-fine — T_{kdyse} 1. Cycle 28,20 [C] SAE-fine 1063 [kg/m3]; last cycle 27,88 [C]; $U_{s,clean}$ 9,77 [cm/s] VelFactor 1,30 [-]

020301#2

	t [min]	t_c [min]	U_s [cm/s]	dP_{max} [Pa]	dPr +10s [Pa]	$dP_{cake,max}$ [Pa]	K_2' [1/s]	K_2' last five min [1/s]	K_2' 70-90% [1/s]
	C=	2,58	[g/m3]	vf=	7,5	[cm/s]			
	0,0		Clean filter, dP_0=		511,9	[Pa]			
1.puff	56,58	56,58	9,83	1510,1	507,0	521,6	998,2	*0,201*	*0,201*	*0,171*
2.puff	98,48	41,90	10,04	1521,1	584,1	606,1	1014,2	*0,276*	*0,134*	*1,988*
3.puff	125,00	26,52	10,01	1528,5	587,8	598,8	944,4	*0,407*	*0,210*	*0,269*
4.puff	149,95	24,95	10,04	1532,1	609,8	635,8	944,4	*0,432*	*0,285*	*0,252*
5.puff	171,40	21,45	10,04	1469,7	621,1	639,4	859,9	*0,458*	*0,210*	*0,372*
6.puff	190,55	19,15	10,04	1521,1	613,7	632,1	900,0	0,537	0,411	*0,383*
7.puff	209,87	19,32	10,02	1462,3	639,4	661,5	848,6	0,502	0,285	*0,402*
8.puff	228,43	18,57	10,01	1539,5	609,8	628,4	900,0	0,554	0,403	*0,441*
9.puff	248,70	20,27	10,03	1528,5	628,4	650,5	918,6	0,518	0,327	*0,393*
10.puff	267,35	18,65	10,01	1510,1	609,8	617,4	881,7	0,540	0,302	*0,371*
11.puff	287,03	19,68	10,03	1532,1	639,4	654,1	922,3	0,535	0,369	*0,394*
12.puff	304,37	17,33	10,02	1535,8	639,4	650,5	896,4	0,591	0,420	*0,411*
13.puff	322,72	18,35	10,03	1532,1	668,8	683,5	892,7	0,556	*0,327*	*0,171*
14.puff	339,58	16,87	10,02	1532,1	661,5	679,8	863,3	0,585	0,403	*0,460*
15.puff	355,58	16,00	10,04	1535,8	617,4	635,8	874,3	0,624	0,462	*0,446*
16.puff										
17.puff										
18.puff										
max		56,58	10,02	1519,4				0,554	0,376	0,411
min		16,00	0,001					0,066	0,157	0,075

030301#1

	t [min]	t_c [min]	U_s [cm/s]	dP_{max} [Pa]	dPr +10s [Pa]	$dP_{cake,max}$ [Pa]	K_2' [1/s]	K_2' last five min [1/s]	K_2' 70-90% [1/s]
	C=	5,19	[g/m3]	vf=	3,7	[cm/s]			
	0,0		Clean filter, dP_0=		293,3	[Pa]	0,0			
1.puff	96,73	96,73	4,89	1293,3	440,8	444,5	147,5	1000,0	*0,237*	*0,253*	*0,214*
2.puff	152,40	55,67	4,84	1289,7	459,2	462,9	165,9	848,8	*0,350*	*0,287*	*0,454*
3.puff	207,32	54,92	4,88	1293,3	473,9	477,6	180,6	834,1	0,349	0,405	0,292
4.puff	257,03	49,72	4,86	1278,7	488,6	499,6	195,3	804,8	0,371	0,320	0,314
5.puff	301,42	44,38	4,84	1289,7	484,9	488,6	191,6	801,1	0,414	0,388	0,418
6.puff	346,72	45,30	4,84	1282,3	484,9	488,6	191,6	797,4	0,404	0,320	0,419
7.puff											
8.puff											
9.puff											
10.puff											
11.puff											
12.puff											
13.puff											
14.puff											
15.puff											
16.puff											
17.puff											
18.puff											
max		96,73	4,855	1287,83					0,385	0,358	0,361
min		44,38	0,004						0,078	0,124	0,187

L10-56 SAE-fine — T_{kdyse} 1. Cycle 21,17 [C] SAE-fine 1063 [kg/m3]; last cycle 19,98 [C]; $U_{s,clean}$ 9,81 [cm/s] VelFactor 1,30 [-]

060301#1

	t [min]	t_c [min]	U_s [cm/s]	dP_{max} [Pa]	dPr +10s [Pa]	$dP_{cake,max}$ [Pa]	K_2' [1/s]	K_2' last five min [1/s]	K_2' 70-90% [1/s]
	C=	1,26	[g/m3]	vf=	7,6	[cm/s]			
	0		Clean filter, dP_0=		482,7	[Pa]			
1.puff	180,80	180,80	9,84	1469,7	529,0	540,0	987,0	*0,121*	*0,229*	*0,276*
2.puff	252,33	71,53	9,87	1473,4	617,4	635,8	944,4	*0,307*	*0,239*	*0,235*
3.puff	304,45	52,12	9,89	1488,0	628,4	643,1	870,7	*0,391*	*0,327*	*0,234*
4.puff	351,72	47,27	9,89	1488,0	621,1	643,1	859,6	*0,425*	*0,206*	*0,302*
5.puff	395,90	44,18	9,88	1495,4	643,1	657,8	874,3	*0,465*	*0,328*	*0,323*
6.puff	433,63	37,73	9,90	1488,0	643,1	654,1	844,9	0,527	0,381	0,390
7.puff	470,75	37,12	9,92	1491,7	643,1	654,1	848,6	0,541	0,365	0,351
8.puff	506,33	35,58	9,90	1488,0	654,1	668,8	844,9	0,559	0,381	0,378
9.puff	540,08	33,75	9,92	1491,7	657,8	679,8	837,6	0,550	0,423	0,311
10.puff	571,93	31,85	9,93	1484,4	621,1	639,4	826,6	0,602	0,409	0,435
11.puff	611,87	39,93	9,90	1499,1	639,4	657,8	878,0	0,492	*0,214*	0,389
12.puff	647,42	35,55	9,87	1491,7	643,1	657,8	852,3	0,538	0,363	0,425
13.puff	681,72	34,30	9,90	1488,0	657,8	668,8	844,9	0,562	0,352	0,404
14.puff	717,97	36,25	9,86	1495,4	635,8	646,8	837,6	0,530	0,421	0,371
15.puff	754,72	36,75	9,88	1484,4	683,5	694,5	848,6	0,514	0,344	0,377
16.puff	789,90	35,18	9,87	1491,7	672,5	679,8	808,2	0,518	0,397	0,334
17.puff										
18.puff										
max		180,80	9,894	1488,0				0,539	0,384	0,379
min		31,85	0,002					0,054	0,074	0,097

070301#1

	t [min]	t_c [min]	U_s [cm/s]	dP_{max} [Pa]	dPr +10s [Pa]	$dP_{cake,max}$ [Pa]	K_2' [1/s]	K_2' last five min [1/s]	K_2' 70-90% [1/s]
	C=	2,61	[g/m3]	vf=	7,5	[cm/s]			
	0		Clean filter, dP_0=		499,8	[Pa]			
1.puff	88,17	88,17	9,81	2009,9	632,1	643,1	1510,1	*0,192*	*0,353*	*0,099*
2.puff	140,62	52,45	9,75	1987,9	749,6	768,0	1355,8	*0,300*	*0,213*	*0,226*
3.puff	187,25	46,63	9,76	1998,9	735,0	757,0	1249,3	*0,312*	*0,402*	*0,214*
4.puff	226,15	38,90	9,73	1995,2	731,3	757,0	1260,3	0,309	0,224	0,246
5.puff	262,23	36,08	9,75	1973,2	742,3	760,7	1241,9	0,406	0,251	0,259
6.puff	294,82	32,58	9,72	1995,2	746,0	764,3	1252,9	0,451	0,397	0,293
7.puff	325,45	30,63	9,77	1995,2	757,0	775,4	1249,3	0,472	0,442	0,393
8.puff	353,98	28,53	9,71	2002,6	771,7	793,7	1245,6	0,509	0,454	0,364
9.puff	380,75	26,77	9,71	1998,9	768,0	786,4	1227,2	*0,529*	*0,585*	*0,279*
10.puff										
11.puff										
12.puff										
13.puff										
14.puff										
15.puff										
16.puff										
17.puff										
18.puff										
max		88,1667	9,738	1995,2				0,429	0,354	0,311
min		26,7667	0,003					0,180	0,307	0,209

L10-56				T_{kdyse}	1. Cycle	21,17	[C]	SAE-fine	1063	[kg/m3]					T_{kdyse}	1. Cycle	20,27	[C]	SAE-fine	1063	[kg/m3]
SAE-fine					last cycle	20,62	[C]									last cycle	20,10	[C]			
	070301#2				$U_{s,clean}$	10,01	[cm/s]	VelFactor	1,30	[-]	**070301#3**					$U_{s,clean}$	10,02	[cm/s]	VelFactor	1,30	[-]
				dP_{max}	dPr		$dP_{cake,max}$	K_2'	K_2'	K_2'				dP_{max}	dPr		$dP_{cake,max}$	K_2'	K_2'	K_2'
	t	t_c	U_s		666,4	+10s			last five min	70-90%	t	t_c	U_s		737,4	+10s			last five min	70-90%
	[min]	[min]	[cm/s]	[Pa]	[Pa]	[Pa]	[Pa]	[1/s]	[1/s]	[1/s]	[min]	[min]	[cm/s]	[Pa]	[Pa]	[Pa]	[Pa]	[1/s]	[1/s]	[1/s]
	C=	4,96	[g/m3]	vf=	7,7	[cm/s]					C=	2,53	[g/m3]	vf=	7,7	[cm/s]				
	0		Clean filter, dP_0=		513,8	[Pa]					0,00		Clean filter, dP_0=		509,6	[Pa]				
1.puff	33,02	33,02	10,06	1995,2	643,1	665,2	1481,5	*0,251*	*0,018*	*0,224*	74,47	74,40	10,03	2002,6	657,8	672,5	1493,0	*0,224*	*0,019*	*0,239*
2.puff	59,78	26,77	10,04	1995,2	690,9	723,9	1352,1	*0,287*	*0,033*	*0,202*	120,52	45,80	10,07	1991,6	712,9	731,3	1319,1	0,320	*0,020*	0,267
3.puff	82,67	22,88	9,81	2006,3	595,1	628,4	1315,4	*0,335*	*0,036*	*0,255*	164,67	44,15	10,04	1998,9	701,9	723,9	1267,6	0,322	*0,025*	0,236
4.puff	105,20	22,53	10,00	2006,3	635,8	749,6	1411,1	0,361	*0,021*	*0,125*	203,53	38,87	10,05	2006,3	720,3	742,3	1282,3	0,365	*0,038*	*0,179*
5.puff	124,75	19,55	9,86	1991,6	687,2	705,6	1355,8	0,404	*0,026*	0,351	236,43	32,45	10,02	1980,5	723,9	746,0	1238,3	0,428	*0,029*	0,371
6.puff	144,65	19,90	10,03	2028,3	654,1	672,5	1341,1	0,384	*0,021*	*-0,115*	271,95	35,18	10,04	2002,6	720,3	738,6	1256,6	0,392	*0,027*	*0,052*
7.puff	161,72	17,07	10,01	1598,5	657,8	683,5	944,4	0,315	*-0,007*	0,256	302,03	30,08	10,01	2006,3	705,6	723,9	1267,6	0,461	*0,026*	*0,618*
8.puff	176,85	15,13	9,99	1995,2	687,2	723,9	1337,4	0,494	*0,031*	0,351	329,30	27,27	10,04	2006,3	738,6	760,7	1282,3	0,516	*0,040*	*1,595*
9.puff											354,63	25,33	10,03	2009,9	768,0	790,1	1249,3	0,540	*0,047*	0,314
10.puff																				
11.puff																				
12.puff																				
13.puff																				
14.puff																				
15.puff																				
16.puff																				
17.puff																				
18.puff																				
max		33,0167	9,976	1952,1				0,392	0,000	0,320		74,4	10,035	2000,5				0,418	0,000	0,297
min		15,1333	0,009					0,169	0,000	0,172		25,3333	0,002					0,200	0,000	0,198

L10-56				T_{kdyse}	1. Cycle	19,74	[C]	SAE-fine	1063	[kg/m3]					T_{kdyse}	1. Cycle	20,8	[C]	SAE-fine	1063	[kg/m3]
SAE-fine					last cycle	20,53	[C]									last cycle	20,0	[C]			
	080301#1				$U_{s,clean}$	4,85	[cm/s]	VelFactor	1,30	[-]	**080301#2**					$U_{s,clean}$	7,4	[cm/s]	VelFactor	1,30	[-]
				dP_{max}	dPr		$dP_{cake,max}$	K_2'	K_2'	K_2'				dP_{max}	dPr		$dP_{cake,max}$	K_2'	K_2'	K_2'
	t	t_c	U_s		519,8	+10s			last five min	70-90%	t	t_c	U_s		806,6	+10s			last five min	70-90%
	[min]	[min]	[cm/s]	[Pa]	[Pa]	[Pa]	[Pa]	[1/s]	[1/s]	[1/s]	[min]	[min]	[cm/s]	[Pa]	[Pa]	[Pa]	[Pa]	[1/s]	[1/s]	[1/s]
	C=	5,16	[g/m3]	vf=	3,7	[cm/s]					C=	5,06	[g/m3]	vf=	5,6	[cm/s]				
	0,00		Clean filter, dP_0=		309,7	[Pa]					0		Clean filter, dP_0=		468,5	[Pa]				
1.puff	172,67	172,67	4,82	2002,6	543,7	562,1	1692,9	*0,008*	*0,445*	*0,242*	63,75	63,75	7,35	1991,6	635,8	646,8	1344,8	*0,218*	*0,311*	*0,233*
2.puff	221,55	48,88	4,85	1987,9	503,3	514,3	1425,8	*0,025*	*0,343*	*0,479*	98,62	34,87	7,36	1987,9	694,5	705,6	1282,3	*0,378*	*0,302*	*0,283*
3.puff	291,25	69,70	4,84	1973,2	510,6	518,0	1458,9	0,018	0,345	0,427	133,83	35,22	7,36	1976,9	690,9	705,6	1271,3	*0,372*	*0,636*	*0,275*
4.puff	352,68	61,43	4,83	1962,2	529,0	532,7	1444,2	0,020	0,377	0,512	167,12	33,28	7,30	1991,6	764,3	779,0	1212,5	0,381	*0,723*	0,371
5.puff											196,85	29,73	7,34	2028,3	797,4	808,4	1219,9	0,425	0,433	0,428
6.puff											224,82	27,97	7,34	1987,9	815,8	834,1	1153,8	0,426	0,387	0,407
7.puff																				
8.puff																				
9.puff																				
10.puff																				
11.puff																				
12.puff																				
13.puff																				
14.puff																				
15.puff																				
16.puff																				
17.puff																				
18.puff																				
max		172,667		1981,466				0,019	0,361	0,470		63,75	7,340	1994,02				0,411	0,410	0,402
min		48,8833						0,076	0,063	0,128		27,97	0,003					0,062	0,080	0,072

L10-56				T_{kdyse}	1. Cycle	20,48	[C]	SAE-fine	1063	[kg/m3]	
SAE-fine					last cycle	18,86	[C]				
	090301#1				$U_{s,clean}$	7,39	[cm/s]	VelFactor	1,30	[-]	
				dP_{max}	dPr			$dP_{cake,max}$	K_2'	K_2' last five min	K_2' 70-90%
	t	t_c	U_s		619,1	+10s					
	[min]	[min]	[cm/s]	[Pa]	[Pa]	[Pa]		[Pa]	[1/s]	[1/s]	[1/s]
	C=	5,03	[g/m3]	vf=	5,7	[cm/s]					
	0		Clean filter, dP_0=		389,8	[Pa]	0,0				
1.puff	64,35	64,35	7,39	1991,6	466,5	473,9	76,8	0,0	0,000		*0,000*
2.puff	119,48	55,13	7,41	1987,9	484,9	495,9	95,1	1521,4	0,282		*0,113*
3.puff	163,13	43,65	7,35	1987,9	488,6	499,6	98,8	1503,0	0,352		*0,233*
4.puff	200,47	37,33	7,40	1359,5	484,9	495,9	95,1	870,9	0,239		*0,227*
5.puff	234,80	34,33	7,35	2013,6	521,6	529,0	131,9	1528,7	0,456		*0,170*
6.puff	273,80	39,00	0,00	0,0	591,4	0,0	201,7	0,0	0,000		*0,000*
7.puff	308,08	34,28	7,39	2013,6	576,8	591,4	187,0	1422,2	0,425		*-0,653*
8.puff	343,80	35,72	7,38	2013,6	646,8	657,8	257,0	1436,9	0,412		*0,474*
9.puff	379,17	35,37	7,38	2021,0	621,1	632,1	231,3	1374,2	0,398		*-0,101*
10.puff	413,63	34,47	7,39	2013,6	587,8	595,1	198,0	1392,5	0,414		*-0,098*
11.puff	449,33	35,70	7,37	2013,6	617,4	628,4	227,6	1425,8	0,409		*0,232*
12.puff	491,78	42,45	0,00	0,0	712,9	0,0	323,1	0,0	0,000		*0,000*
13.puff	531,15	39,37	7,44	2009,9	628,4	643,1	238,6	1297,0	0,337		*0,224*
14.puff	564,20	33,05	7,43	2032,0	565,7	576,8	175,9	1403,6	0,435		*1,235*
15.puff	598,13	33,93	7,45	1951,2	525,3	532,7	135,5	1385,4	0,418		*0,150*
16.puff	635,23	37,10	7,41	2002,6	554,7	562,1	164,9	1477,3	0,408		*0,213*
17.puff	672,68	37,45	7,41	2013,6	598,8	609,8	209,0	1458,9	0,399		*0,191*
18.puff	717,12	44,43	0,00	0,0	632,1	0,0	242,3	0,0	0,000		*0,000*
19.puff	756,15	39,03	7,39	1998,9	654,1	657,8	264,3	1366,8	0,358		*0,246*
20.puff	796,77	40,62	7,41	1991,6	646,8	654,1	257,0	1337,4	0,337		*0,148*
21.puff	835,08	38,32	7,41	2006,3	602,5	613,7	212,7	1359,5	0,363		*0,196*
22.puff	871,65	36,57	7,41	2009,9	573,1	580,4	183,3	1407,5	0,394		*0,170*
		64,35	7,39842	1970,094					0,393		
		33,05							0,080		

L10-56				T_{kdyse}	1. Cycle	18,2923815	[C]	NF	692	[kg/m3]	
Pural NF					last cycle	17,9459842	[C]	area	0,0256	[m2]	
					$U_{s,clean}$	4,87147914	[cm/s]	VelFactor	1,3	[-]	
	180301#1			dP_{max}	dP_r			$dP_{cake,max}$	K_2'	K_2' last five min	K_2' 70-90%
	t	t_c	U_s		592,75	+10s					
	[min]	[min]	[cm/s]	[Pa]	[Pa]	[Pa]		[Pa]	[1/s]	[1/s]	[1/s]
	c =	5,51	[g/m3]	v_f =	3,44	[cm/s]					
	0		Clean filter, dP_0=		301,23	[Pa]					
1.puff	130,133333	130,133333	4,46910748	1984,22	558,385			1682,99	0,30976941	0,4326	0,1947
2.puff	184,933333	54,8	4,47635558	1969,526	598,795			1411,141	0,62062256	0,5267	0,3605
3.puff	234,433333	49,5	4,45870979	1984,22	621,067			1385,425	0,67392364	0,5643	0,4272
		130,13	4,46805762	1979,32					0,6473	0,5455	0,3939
		49,50	0,00198512						0,0582	0,0488	0,1198

Wishbone NF 692 [kg/m3] T_{kdyse} 1. Cycle 20,24 [C]
Pural NF area 0,0232 [m2] last cycle 19,99 [C]
060201#2 VelFactor 0,65 [-] $U_{s,clean}$ 5,26 [cm/s]
Clean filter 313,40 [Pa] vf 8,15 [cm/s]
c 4,77 [g/m3]

	t [min]	t_c [min]	U_s [cm/s]	dP_{max} [Pa]	dP_f 314,70 [Pa]	+10s [Pa]	$dP_{cake,max}$ [Pa]	K_2' [1/s]	K_2' last five min [1/s]	K_2' 70-90% [1/s]
1.puff	36,23	31,23	5,32	1315,4	293,9	308,6	1003,1	0,148	0,166	0,179
2.puff	63,00	26,77	5,32	1319,1	290,2	304,9	1025,2	0,204	0,189	0,173
3.puff	90,83	27,83	5,30	1311,7	301,2	319,6	1021,5	0,196	0,185	0,187
4.puff	117,95	27,12	5,30	1289,7	330,6	349,0	988,4	0,195	0,147	0,182
5.puff	142,07	24,12	5,29	1308,0	330,6	349,0	977,4	0,217	0,212	0,188
6.puff	165,65	23,58	5,28	1315,4	367,4	385,7	984,8	0,224	0,193	0,262
7.puff	186,95	21,30	5,34	1319,1	315,9	334,3	951,7	0,238	0,228	0,204
8.puff	211,77	24,82	5,29	1315,4	315,9	330,6	999,5	0,215	0,170	0,206
9.puff	234,83	23,07	5,29	1315,4	297,6	312,3	999,5	0,232	0,235	0,218
10.puff	259,13	24,30	5,28	1311,7	330,6	341,6	1014,2	0,224	0,216	0,199
11.puff										
		31,23	5,30	1312,08	320,01		995,79	0,22	0,20	0,20
		21,30	0,00343		0,07293		0,02341	0,070718	0,14458491	0,1302

Wishbone NF 692 [kg/m3] T_{kdyse} 1. Cycle 25,50 [C]
Pural NF area 0,0232 [m2] last cycle 26,39 [C]
050201#2 VelFactor 0,65 [-] $U_{s,clean}$ 10,17 [cm/s]
Clean filter 513,44 [Pa] vf 15,76 [cm/s]
c 4,58 [g/m3]

	t [min]	t_c [min]	U_s [cm/s]	dP_{max} [Pa]	dP_f 552,26 [Pa]	+10s [Pa]	$dP_{cake,max}$ [Pa]	K_2' [1/s]	K_2' last five min [1/s]	K_2' 70-90% [1/s]
1.puff	16,38	16,38	10,20	1506,4	507,0	540,0	1003,1	0,091	0,120	0,113
2.puff	26,93	10,55	10,29	1506,4	499,6	536,3	1003,1	0,142	0,130	0,130
3.puff	37,67	10,73	10,27	1513,8	499,6	540,0	1010,5	0,140	0,129	0,128
4.puff	48,58	10,92	10,23	1517,4	510,6	554,7	1014,2	0,138	0,127	0,121
5.puff	59,32	10,73	10,27	1513,8	514,3	554,7	1010,5	0,140	0,125	0,125
6.puff	69,87	10,55	10,28	1506,4	529,0	562,1	1003,1	0,142	0,123	0,130
7.puff	79,82	9,95	10,26	1517,4	536,3	584,1	1014,2	0,152	0,130	0,132
8.puff	89,07	9,25	10,28	1513,8	551,0	587,8	1010,5	0,163	0,140	0,140
9.puff	98,17	9,10	10,21	1521,1	536,3	584,1	1017,8	0,167	0,141	0,145
10.puff	107,30	9,13	10,25	1521,1	543,7	595,1	1017,8	0,166	0,144	0,127
11.puff	116,28	8,98	10,25	1524,8	558,4	602,5	1021,5	0,170	0,144	0,177
12.puff	124,53	8,25	10,25	1510,1	543,7	591,4	1006,8	0,182	0,155	0,143
13.puff	132,98	8,45	10,18	1517,4	554,7	595,1	1014,2	0,179	0,155	0,150
average		16,38	10,25	1514,6			1011,3	0,152	0,136	0,135
stdev[-]		8,25	0,00332				0,00596	0,157867	0,08588334	0,1184

060201#1 NF 692 [kg/m3] T_{kdyse} 1. Cycle 19,73 [C]
area 0,0232 [m2] last cycle 20,52 [C]
VelFactor 0,65 [-] $U_{s,clean}$ 5,30 [cm/s]
Clean filter 302,60 [Pa] vf 8,15 [cm/s]
c 2,29 [g/m3]

	t [min]	t_c [min]	U_s [cm/s]	dP_{max} [Pa]	dP_f 340,42 [Pa]	+10s [Pa]	$dP_{cake,max}$ [Pa]	K_2' [1/s]	K_2' last five min [1/s]	K_2' 70-90% [1/s]
	62,20	62,20	5,34	1308,0	297,6	315,9	1003,1	0,179	0,225	0,200
	106,72	44,52	5,33	1300,7	304,9	315,9	1003,1	0,250	0,233	0,235
	152,85	46,13	5,31	1293,3	326,9	338,0	988,4	0,237	0,217	0,227
	195,88	43,03	5,32	1293,3	360,0	382,1	966,4	0,248	0,233	0,220
	229,88	34,00	5,30	1293,3	334,3	345,3	933,3	0,306	0,362	0,408
	272,63	42,75	5,27	1278,7	308,6	323,3	944,4	0,245	0,354	0,118
	317,10	44,47	5,28	1278,7	308,6	315,9	970,1	0,243	0,281	0,231
	363,65	46,55	5,29	1278,7	323,3	338,0	970,1	0,232	0,209	0,216
	409,98	46,33	5,28	1304,4	345,3	356,3	981,1	0,236	0,185	0,208
	454,23	44,25	5,26	1278,7	341,6	352,7	933,3	0,235	0,137	0,195
	496,42	42,18	5,28	1293,3	334,3	345,3	951,7	0,254	0,209	0,172
		62,20	5,29	1291,0	328,2		965,6	0,25	0,25	0,23
		34,00	0,00427		0,05763		0,0252	0,090877	0,3035476	0,33296

050201#1 NF 692 [kg/m3] T_{kdyse} 1. Cycle 23,79 [C]
area 0,0232 [m2] last cycle 23,72 [C]
VelFactor 0,65 [-] $U_{s,clean}$ 8,40 [cm/s]
Clean filter 563,36 [Pa] vf 13,15 [cm/s]
c 2,29 [g/m3]

	t [min]	t_c [min]	U_s [cm/s]	dP_{max} [Pa]	dP_f 477,56 [Pa]	+10s [Pa]	$dP_{cake,max}$ [Pa]	K_2' [1/s]	K_2' last five min [1/s]	K_2' 70-90% [1/s]
1.puff	36,62	36,62	8,59	1385,2	418,8	437,2	959,1	0,111	0,139	0,097
2.puff	61,62	25,00	8,57	1418,2	440,8	459,2	999,5	0,171	0,167	0,154
3.puff	83,47	21,85	8,52	1392,5	455,5	481,2	951,7	0,186	0,170	0,191
4.puff	101,62	18,15	8,51	1418,2	459,2	477,6	962,7	0,226	0,222	0,208

050201#1 NF 692 [kg/m3] T_{kdyse} 1. Cycle [C]
area 0,0232 [m2] last cycle [C]
VelFactor 0,65 [-] $U_{s,clean}$ [cm/s]
Clean filter [Pa] vf 13,21 [cm/s]
c 2,35 [g/m3]

	t [min]	t_c [min]	U_s [cm/s]	dP_{max} [Pa]	dP_f min [Pa]	+10s [Pa]	$dP_{cake,max}$ [Pa]	K_2' [1/s]	K_2' last five min [1/s]	K_2' 70-90% [1/s]
5.puff	140,47	38,85	8,60	1414,6	451,8	470,2	889,3	0,094	0,122	0,140
6.puff	168,82	28,35	8,60	1421,9	451,8	473,9	970,1	0,140	0,143	0,501
7.puff	193,98	25,17	8,58	1418,2	455,5	481,2	966,4	0,158	0,155	0,499
8.puff	216,87	22,88	8,60	1410,9	444,5	473,9	955,4	0,172	0,161	0,502
9.puff	237,10	20,23	8,59	1418,2	462,9	484,9	973,7	0,199	0,173	0,499
10.puff	258,40	21,30	8,58	1414,6	466,5	488,6	951,7	0,184	0,176	0,499
11.puff	278,53	20,13	8,57	1418,2	473,9	499,6	951,7	0,195	0,164	0,511
12.puff	298,70	20,17	8,57	1414,6	492,3	521,6	940,7	0,192	0,158	0,507
average		38,85	8,58	1412,13				0,169	0,162	0,359
stdev[-]		18,15	0,00338					0,22419	0,150272	0,49975

Wishbone
Pural NF
030201#1
Clean filter 447,42 [Pa]

NF	692	[kg/m3]	T_{kdyse}	1. Cycle	23,90	[C]
area	0,0232	[m2]		last cycle	24,07	[C]
VelFactor	0,52	[-]		$U_{s,clean}$	8,76	[cm/s]
vf	10,36	[cm/s]				
c	2,34	[g/m3]				

	t	t_c	U_s	dP_{max}	dP_r 451,85	+10s	$dP_{cake,max}$	K_2'	K_2' last five min	K_2' 70-90%
	[min]	[min]	[cm/s]	[Pa]	[Pa]	[Pa]	[Pa]	[1/s]	[1/s]	[1/s]
1.puff	39,88	39,88	5,40	1425,6	455,5	507,0	977,4	0,055	0,518	0,490
2.puff	48,17	8,28	5,32	1392,5	444,5	481,2	937,0	0,126	0,719	0,723
3.puff	58,90	10,73	5,39	1241,9	451,8	488,6	797,4	0,000	0,000	
average		39,88	5,37	1353,3				0,090	0,618	0,607
stdev[-]		8,28	0,00824					0,558345	0,22917998	0,2709

Wishbone
Pural SB
070201#1
Clean filter 507,41 [Pa]

SB	850	[kg/m3]	T_{kdyse}	1. Cycle	27,16	[C]
area	0,0232	[m2]		last cycle	27,53	[C]
VelFactor	0,65	[-]		$U_{s,clean}$	10,10	[cm/s]
vf	15,61	[cm/s]				
c	4,62	[g/m3]				

	t	t_c	U_s	dP_{max}	dP_r 617,39	+10s	$dP_{cake,max}$	K_2'	K_2' last five min	K_2' 70-90%
	[min]	[min]	[cm/s]	[Pa]	[Pa]	[Pa]	[Pa]	[1/s]	[1/s]	[1/s]
	75,33	75,32	10,15	1499,1	580,4	602,5		0,020	0,020	0,021
	145,15	69,80	10,14	1499,1	613,7	635,8		0,020	0,022	0,020
	188,97	43,80	10,15	1227,2	617,4	632,1		0,021	0,020	0,024
average		75,32	10,15	1499,1				0,020	0,020	0,022
stdev[-]		69,80	0,00063					0,0320	0,0619	0,1044

Wishbone
Pural SB
030201#1
Clean filter 437,34 [Pa]

SB	850	[kg/m3]	T_{kdyse}	1. Cycle		[C]
area	0,0232	[m2]		last cycle		[C]
VelFactor	0,65	[-]		$U_{s,clean}$	8,71757864	[cm/s]
vf	13,41	[cm/s]				
q	7,28	[m3/h]				

	t	t_c	U_s	dP_{max}	dP_r min	vf	$dP_{cake,max}$	K_2'	K_2' last five min	K_2' 70-90%
	[min]	[min]	[cm/s]	[Pa]	[Pa]	[cm/s]	[Pa]	[1/s]	[1/s]	[1/s]
1. Intervall	10,98	10,98	8,71	451,8	440,8	13,40		0,008		
2.intervall	17,98	7,00	8,71	481,2	455,5	13,40		0,015		
3.intervall	23,98	6,00	8,74	518,0	484,9	13,45		0,012		
4.intervall	33,98	10,00	8,72	632,1	525,3	13,42		0,012		
5.intervall	40,98	7,00	8,70	746,0	650,5	13,39		0,013		
6.intervall	46,98	6,00	8,70	892,9	790,1	13,38		0,014		
average			8,71							
stdev[-]			0,00176							

)80201#1
Clean filte 459,37 [Pa]

SB	850	[kg/m3]	T_{kdyse}	1. Cycle	27,18	[C]
area	0,0232	[m2]		last cycle	27,24	[C]
VelFactor	0,65	[-]		$U_{s,clean}$	10,11	[cm/s]
vf	15,52	[cm/s]				
c	4,69	[g/m3]				

t	t_c	U_s	dP_{max}	dP_r 503,28	+10s	$dP_{cake,max}$	K_2'	K_2' last five min	K_2' 70-90%
[min]	[min]	[cm/s]	[Pa]	[Pa]	[Pa]	[Pa]	[1/s]	[1/s]	[1/s]
106,68	106,68	10,15	948,0	573,1	580,4	374,9	0,005		0,011
143,55	36,87	9,97	948,0	510,6	525,3	437,4	0,018		0,018
184,45	40,90	10,15	951,7	503,3	510,6	448,4	0,016		0,017
	106,68	10,09	949,2				0,017		0,017
	36,87	0,01024					0,0558		0,0733

Appendix II

Paper III – *Steam gasification of wood char and the effect of hydrogen inhibition on the chemical kinetics.* In proceedings: Progress in Thermochemical Biomass Conversion, September 2000, Tyrol, Austria

Steam gasification of wood char and the effect of hydrogen inhibition on the chemical kinetics.

M. Barrio, B. Gøbel[+], H. Risnes, U. Henriksen[+], J.E. Hustad and L.H. Sørensen[*]

Norwegian University of Science and Technology, Department of Thermal Energy and Hydro Power, 7491 Trondheim, Norway

[+]Technical University of Denmark, Department of Energy Engineering, Nils Koppel Allé, DTU-Building 403, DK-2800 Kongens Lyngby

**ReaTech c/o Centre for Advanced Technology (CAT), Postbox 30, DK-4000 Roskilde*

ABSTRACT: Gasification kinetics parameters have been derived for birch and beech char samples (45μm<d<60μm) pyrolysed under identical conditions. Reactivity experiments were made in steam-hydrogen-nitrogen mixtures at atmospheric pressure. Reactivity profiles have been obtained in the temperature range from 750 °C to 950 °C, for H_2O partial pressures of 0.05, 0.1, 0.2, 0.5 and 1.0 bar and H_2 partial pressures of 0.1, 0.2 and 0.3 bar. Assuming n^{th} order kinetics for pure steam experiments, the activation energy and the reaction order are E=211 kJ/mol and n=0.51 for beech and E=237 kJ/mol and n=0.57 for birch. A kinetic expression based on Langmuir-Hinshelwood kinetics fairly describes the observed hydrogen inhibition effect on the steam-carbon reaction. The differences between the kinetics determined for the two fuels are relatively small and partly due to the origin and quality of the raw wood. The kinetic parameters obtained are presented using a kinetic compensation diagram; they are compared with literature data and discussed. The influence of the calculation procedure on the results is also discussed. It is found that the data evaluation procedure mostly influences the pre-exponential factor and less the activation energy and reaction order.

INTRODUCTION

The gasification process requires an oxidising agent that provides oxygen for the formation of CO from solid fuel. The oxidising, or gasifying, agents are air, oxygen, steam and CO_2. CO_2 is produced during the pyrolysis and early oxidation processes and generally not externally added. The most common agent is air because of its availability at zero cost. Air, though cheap, is not a perfect agent because of its nitrogen content. The product gas from air gasification has generally a low heating value of 4-7 MJ/Nm^3. Oxygen gasification produces a higher heating value (10-18 MJ/Nm^3) but has a drawback due to the high production cost of oxygen.

Steam is another alternative. It also generates a medium calorific value gas (10-14 MJ/Nm^3) and moreover increases the hydrogen content of the product gas. The presence of steam is important in case of further catalytic upgrading of the product gas[1]. Steam gasification is however a highly endothermic reaction and requires a temperature above 800 °C to take place[2] if no catalyst is present[3,4]. The heat required for the reaction has to be transferred either by partial char combustion in the same reactor –mixing H_2O with oxygen/air[1,5]- or by indirect heating[6,7].

Because of biomass moisture, and steam from pyrolysis in downdraft gasification, steam will always be present in gasification whether it is used or not as a gasification agent. Hydrogen is one of the products of steam gasification and its effect on the reaction is also relevant. Some kinetic data for steam gasification of biomass have been published[2,8,9,10,11,12,13,14,15,16,17,18], but very few considering the effect of H_2 inhibition[19,20,21,41].

The diversity in evaluation of the results from char reactivity experiments is large. The definition of gasification rate varies among researchers and so does the criteria to select the reactivity values from the experiments. Few authors[16,22] have concerns regarding this.

This study presents the kinetic parameters and reactivity profiles for steam gasification of birch and beech char. The inhibition effect of hydrogen is also studied using Langmuir-Hinshelwood kinetics. In addition, the influence of the treatment of the experimental results is analysed by comparing the kinetic parameters differently obtained from the same experiments.

The same birch char has been used for CO_2/CO gasification[23]. The kinetic study of char gasification in $H_2O/H_2/CO_2/CO$ mixtures will be a continuation of the work presented.

THEORETICAL BACKGROUND

H_2O/H_2 REACTION MECHANISMS

The overall steam gasification reaction can be represented by:

$$C_f + H_2O \rightleftharpoons CO + H_2 \quad (1)$$

However, the reaction is much more complex and involves several steps. Numerous studies have been conducted in order to understand the mechanisms of the steam gasification reaction. The catalytic activity of the ash plays an important role in this discussion[24,19,25]. H_2O gasification is more complex than CO_2 gasification because not only H_2O is involved but also H_2, CO_2 and CO due to the equilibrium of the water gas shift reaction[19,25].

Hüttinger and Merdes[26] give a comprehensive description of the models proposed in the literature for the carbon-steam reaction. Basically, there are two models of the reaction mechanism: the oxygen exchange model and the hydrogen inhibition model. The equations involved are:

$$C_f + H_2O \underset{k_{1b}}{\overset{k_{1f}}{\rightleftharpoons}} C(O) + H_2 \quad (2)$$

$$C(O) \xrightarrow{k_3} CO + C_f \quad (3)$$

$$C_f + H_2 \underset{k_{4b}}{\overset{k_{4f}}{\rightleftharpoons}} C(H)_2 \quad (4)$$

$$C_f + \frac{1}{2}H_2 \underset{k_{5b}}{\overset{k_{5f}}{\rightleftharpoons}} C(H) \quad (5)$$

The oxygen exchange model is based on equations 2 (reversible -k_{1f} and k_{1b}-) and 3, the traditional hydrogen inhibition model is based on equations 2 (irreversible -only k_{1f}-), 3

and 4 and a different version of the hydrogen inhibition model substitutes equation 4 by equation 5. Each model has a different explanation of the inhibition effect of hydrogen. According to the oxygen exchange model, it is due to the equilibrium of the dissociation reaction (Eq. 2). For the traditional hydrogen inhibition model, the formation of the $C(H)_2$ complex is the reason for inhibition. Finally, the second version of the hydrogen inhibition model involves a dissociative chemisorption of hydrogen on the active sites[27,28], blocking them for the oxygen transfer reaction with steam.

The reaction rate for the models presented is similar, with the exception of dependency on hydrogen partial pressure:

$$r_c = \frac{k_{1f}\, p_{H2O}}{1 + \frac{k_{1f}}{k_3} p_{H2O} + f(p_{H2})} \tag{6}$$

where $f(p_{H2}) = \frac{k_{1b}}{k_3} p_{H2}$, oxygen exchange model (6.1.)

$f(p_{H2}) = \frac{k_{4f}}{k_{4b}} p_{H2}$, hydrogen inhibition model (traditional) (6.2.)

$f(p_{H2}) = \frac{k_{5f}}{k_{5b}} p_{H2}^{0.5}$, hydrogen inhibition model (second version) (6.3.)

According to Hüttinger and Merdes[26], it is not possible to determine which is the dominating hydrogen inhibiting mechanism by looking at the reaction rate because the equations are identical, with exception of the second version of the hydrogen inhibition model.

It is quite common to reduce equation 6 to the following expression[20,24]:

$$r = \frac{K_1 p_{H2O}}{1 + K_2 p_{H2O} + K_3 p_{H2}} \tag{7}$$

where K_2 and K_3 represent a ratio between rate constants but are not rate constants themselves.

Other authors[19,29] rather use empirical equations to model the chemical kinetics. In this work, the kinetic parameters have been obtained according to the oxygen exchange model, equations 2 and 3, and also according to n^{th} order kinetics.

INFLUENCE OF FUEL TYPE

Several studies have focused on the influence of wood type on CO_2 gasification[30,31,32] and steam gasification[2,14,17,20,33,34,35]. A general conclusion is that the ash content, composition and its catalytic properties explain the differences among the fuels. In particular, Hansen et al.[20] refer to the potassium content of the ashes as being especially relevant.

Moilanen et al.[14] present their results from steam atmospheric gasification of chars from different origins: wood, black liquor, cellulose fibres, peat and coal. All chars, apart from peat, present an increasing reaction rate with conversion, especially wood.

Stoltze et al.[17] find that the gasification of hardwood is 2-3 times slower than straw, probably due to the different char structure and composition. However, since the density of the hardwood char is 5 times higher than the one of straw, in a volume basis the reactivity of wood char is double than of straw. The direct consequence of this fact is that the gasifiers for wood char only require half the volume of a straw gasifier.

Finally, it is important to mention that the pyrolysis conditions also have influence on the char reactivity, as several investigations have proved.

TREATMENT OF THE EXPERIMENTAL RESULTS

There are two definitions of the reactivity commonly used:

$$r = -\frac{1}{(m(t)-m_f)} * \frac{d(m(t)-m_f)}{dt} \quad (8)$$

$$r_w = -\frac{1}{(m_0-m_f)} * \frac{d(m(t)-m_f)}{dt} \quad (9)$$

where m_o is the char mass at the beginning of the gasification and m_f is either negligible, or represents the mass of ash, or – as in this work- the residual mass after gasification. The degree of conversion is obtained as:

$$X(t) = 1 - \frac{m(t)-m_f}{m_0-m_f} \quad (10)$$

Therefore, the relation between the two definitions of reactivity presented above is:

$$r_w = r*(1-X) \quad (11)$$

It is widely accepted that the reactivity depends on the degree of conversion but there is no agreement about how to define one representative value of reactivity for each experiment.

The representative value of reactivity from an experiment is most frequently obtained as the average reactivity between two degrees of conversion: 0-50%[36], 0-70%[16], 0-75%[10], 40-60%[20], 10-50%[37], 60-80%[30].

Bandyopadhyay et al.[38] selects the representative value of reactivity as the reactivity at 5% conversion. Using an earlier value might introduce error because of the gas changing, but a later value would not correspond to a known condition of the sample inside the sample cup holder (depth, mainly).

Stoltze et al.[16] propose a mass-weighed mean reactivity in order to give less importance to the latest stages of conversion.

Finally, other researchers consider the reactivity as a function of the chemical reactivity, dependent of temperature and reactants partial pressure but independent of conversion, and of a structural factor, solely dependent on the degree of conversion[13,39].

Still, it is possible to find other methods to obtain reactivity[11,19].

EXPERIMENTAL SECTION

Kinetics for a Norwegian birch and a Danish beech have been determined. Apart from their origin there are also other differences between the woods. The beech sample is first received as wood chips whose surface has been exposed to the ambient and that partially contains bark. The birch sample comes from a wood log that has been cut into small cubes of 1x1x1cm, removing the bark. The proximate and ultimate analysis is shown in Table 1 and the ash analysis in Table 2.

Table 1 Proximate and ultimate analysis of birch and beech wood.

Proximate analysis	Moisture	Volatile matter*	Fixed carbon	Ash
Birch wood	11.13%	78.7%, mf	20.9%, mf	0.37%, mf
Beech wood	14.16%	75.2%, mf	24.2%, mf	0.56%, mf
Ultimate analysis	C	H	N	O (by diff.)
Birch wood (wt%, mf)	48.7	6.4	0.078	44.45
Beech wood (wt%,mf)	48.1	6.4	0.081	44.82

* Pyrolysis conditions: Heating at 24 °C/min until 600 °C, held for 30 min, natural cooling.

Table 2 Ash analysis of birch and beech wood (%).

Species	Si	Al	Fe	Ca	Mg	K	Na	Ti	S
Beech	1.2	0.14	1.8	25	7.1	28	2	0.029	0.75
Birch	0.03	0.01	0.17	30	4.8	28	0.08	0.007	0.64
Species	P	Cl	Cu	Zn	Ni	Pb	Cd	Hg	
Beech	2	0.29	0.03	0.2	0.02	0.01	<0.001	<0.001	
Birch	3.4	0.03	0.06	0.06	0.01	0.02	<0.001	<0.001	

Both woods have been pyrolysed at the Technical University of Denmark, Department of Energy Engineering (DTU, ET), in a macro-TGA, heated at 24 °C/min to 600 °C, held at that temperature for 30 min and then cooled down to room temperature naturally. Both chars were thereafter crushed and sieved to 45-63 μm.

The instrument used for the reactivity study is a Pressurised Thermogravimetric Analyser (PTGA) at ReaTech, a modified Du Pont Thermogravimetric Analyser. The sample (~5 mg) is placed on a small platinum tray, hanging on a horizontal balance arm. The sample temperature is measured with the help of two thermocouples, near to, but not in contact, with the sample. This investigation is limited to atmospheric pressure although the instrument is prepared for high pressure operation. Rathmann et al.[40] and Sørensen[35] give a detailed description of the PTGA and Hansen et al.[20] describe the modifications required for the instrument to tolerate steam.

Once the char sample is introduced into the PTGA, it is first dried in N_2 during 10 min at 200 °C, then is heated at 24 °C/min to 1000 °C and held at this temperature for 30 min. After this the sample is cooled to the gasification temperature and when conditions are stable, the steam is allowed into the reaction chamber. The sample is hold isothermal until the gasification reaction is complete and then the temperature is raised to 1000 °C to complete the reaction. The sample size is ca. 10 mg and the gas flow 1000 ml/min.

The objective of increasing the temperature up to 1000 °C previous to gasification is to simulate the history of the particle in the two-stage gasifier at DTU, ET. This is also the reason for the heating rate of 24 °C/min. During the 30 min. period at 1000 °C

in the nitrogen atmosphere some fraction of the catalytic species K and Na devolatilise and are carried away from the sample and therefore the char could be less reactive.

The experimental matrix for this investigation is shown in Table 3.

Table 3 Experimental matrix for H_2O gasification experiments

	T(°C)							
P_{H2O}	750	800		850		900		950
(bar)			With H_2		with H_2		with H_2	with H_2
0.1	○●	○●●	①	○○●	①❶❸	○●	①❶❸	③❸
0.3	○○●●	○●	❷❷❸	○●	❸	●	②❸	
0.5	○●	○○●	①❶	○●	①❶		③	③

(○,①,②,③) Birch char; (●,❶,❷,❸) Beech char. The numbered symbols indicate the partial pressure of hydrogen (x10 bar).

The design of the installation is described in Fig. 1.

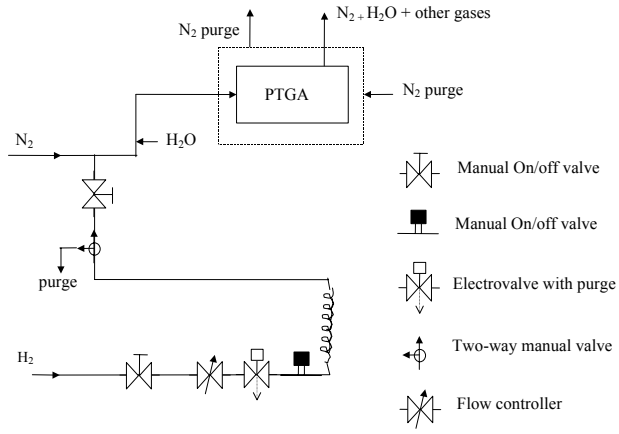

Fig. 1 Schematic drawing of the installation set-up.

RESULTS AND DISCUSSION

GASIFICATION RATE

Fig. 2 shows the mass loss curve for one of the experiments. The initial and final weights for the gasification reaction are also indicated. Fig. 3 shows the reactivity as a function of the degree of conversion, i.e. the reactivity profile, for the same experiment according to equations 8 and 9. In addition, the figure shows the average reactivity (from eq. 8) between 20 and 80% conversion.

It is important to notice that the shape of the reactivity profile is very dependent on the reactivity definition. For the following discussion, the reactivity has been obtained according to equation 8.

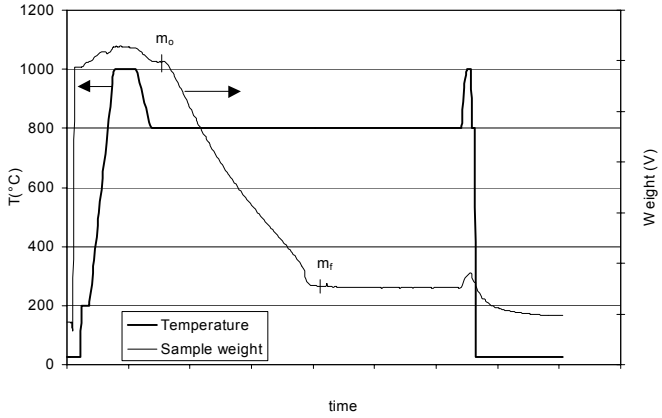

Fig. 2 Temperature and weight signal as a function of time. Experimental data.

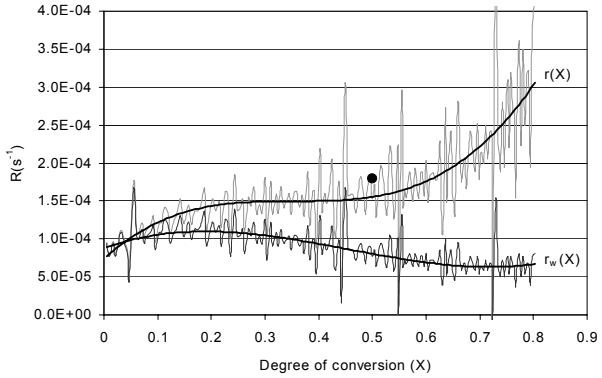

Fig. 3 Reactivity as a function of conversion.
(●: Average reactivity between 20 and 80% conversion).

PURE STEAM EXPERIMENTS

Fig. 4 shows the reactivity of the pure steam experiments as a function of temperature and steam partial pressure. The representative reactivity value has been obtained as the reactivity at 50% conversion. The continuous line shows the n^{th} order reaction model for the birch experiments. The figure shows that beech is more reactive than birch at

low temperatures (750-800 °C). The kinetic parameters obtained according to n^{th} order kinetics are shown in Table 4 together with results from other references.

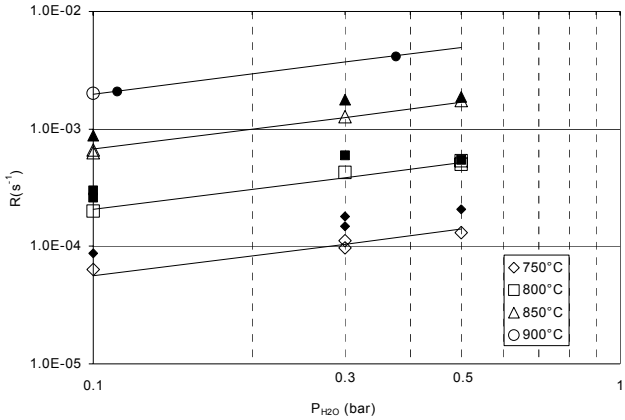

Fig. 4 Reactivity as a function of steam partial pressure and temperature.
(Filled symbols: beech, hollow symbols: birch).

Table 4 Kinetic parameters comparison for steam gasification experiments.

		N^{th} order kinetics		
Reference	Char origin	E(kJ/mol)	k_o	n
This work*	Birch	237± 0.4	$2.62\cdot10^{8}\pm5\cdot10^{6}$ $s^{-1}bar^{-n}$	0.57± 0.03
This work+	Beech	211± 6.1	$1.71\cdot10^{7}\pm1\cdot10^{7}$ $s^{-1}bar^{-n}$	0.51±0.05
Capart et al.[12]	Woodchar	138	$1.79\cdot10^{3}$ $s^{-1}atm^{-n}$	1.00
Hemati et al.[13]	Woodchar	198	$1.23\cdot10^{7}$ $s^{-1}atm^{-n}$	0.75
Richard et al.[8]	Fir wood	104.5±8		
Li et al.[9]	Black liquor	210±10		
Whitty[19]	Black liquor	230		0.56
Timpe et al.[10]	Poplar	271		
	Cattails	262		
Moilanen et al.[14,15]	Wood	196, 217		
	Black liquor	226		
Stoltze et al.[16,17]	Straw	151	$4.77\cdot10^{7}$ %/min	~0.5
(Large TGA)	Wood chips	119	$1.76\cdot10^{6}$ %/min	~0.5
Rensfelt et al.[2]	Poplar wood	182	$1.2\cdot10^{8}$ min^{-1}	
	Straw	182	$5.9\cdot10^{7}$ min^{-1}	
Groeneveld [18]	Wood char	217	$10^{6} – 10^{7}$ $s^{-1}m^{2.1}mol^{-0.7}$	0.7

* $R_{sqr} = 0.9919$, + $R_{sqr} = 0.9784$

From the above comparison one can see that the activation energy varies between 105 and 270 kJ/mol. Most values for E lie between 180 and 270 kJ/mol and the parameters obtained in this investigation are well within this range. The reaction order obtained is

also similar to the values found in literature, eventually among the lower values. These data will be further discussed in Fig. 7.

H_2 INHIBITION EFFECT

The experiments show that the presence of hydrogen inhibits the steam gasification reaction, as presented in Fig. 5.

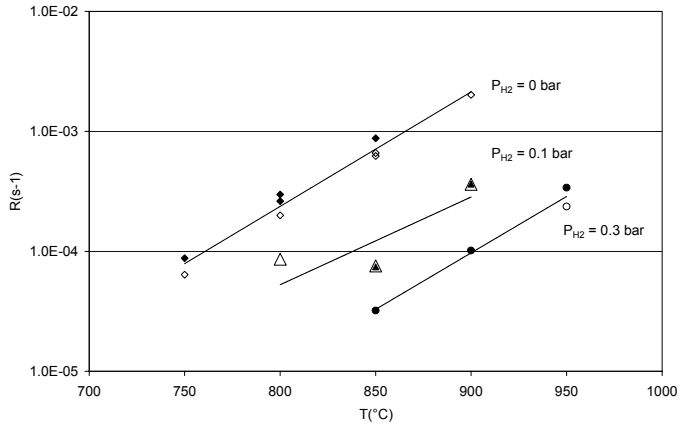

Fig. 5 Inhibition effect of H_2 as a function of temperature and H_2 partial pressure. (P_{H2O}= 0.1 bar, filled symbols: beech, hollow symbols: birch)

The equations 6 and 6.1 have been used to model the reaction. Table 5 shows the kinetic parameters obtained in this investigation. In spite of the high uncertainty of the model parameter calculation, the model fits well the experimental results (See Fig. 6).

Table 5 Kinetic constants for H_2O/H_2 gasification of birch and beech char.

Wood species	E_{1f} (kJ/mol)	k_{o1f} ($s^{-1}bar^{-1}$)	E_{1b} (kJ/mol)	k_{o1b} ($s^{-1}bar^{-1}$)	E_3 (kJ/mol)	k_{o3} (s^{-1})
Beech	199	$2.0 \cdot 10^{7}$	146	$1.8 \cdot 10^{6}$	225	$8.4 \cdot 10^{7}$
Birch	214	$7.6 \cdot 10^{7}$	284	$2.1 \cdot 10^{12}$	273	$1.6 \cdot 10^{10}$

Table 6 compares these results with the few kinetic parameters found in the literature. Although there is a certain agreement in the value of E_3, the other values are somewhat different. This could be explained by the high uncertainty of the calculation, as also mentioned by Hansen et al.[20] or by the differences in char origin.

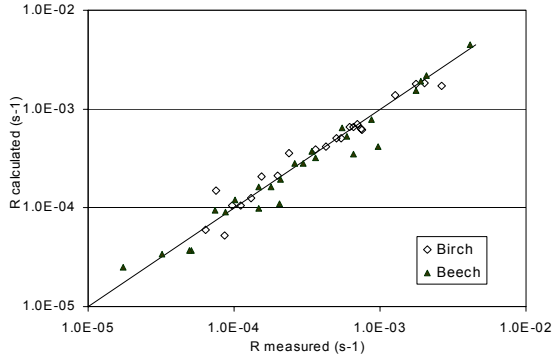

Fig. 6 Calculated reactivity values versus experimental values.

Table 6 Comparison of kinetic parameters for H_2O/H_2 gasification.

		Langmuir-Hinshelwood kinetics				
Reference	Char origin	E_{1f} (kJ/mol)	E_{1b} (kJ/mol)	E_3 (kJ/mol)	E_{1f}-E_3 (kJ/mol)	E_{1b}-E_3 (kJ/mol)
This work	Birch	214	284	273	-59	11
This work	Beech	199	146	225	-26	-79
Hansen et al. [20]	Wheat straw	149	140*	257*	-108	-117
Sørensen et al.[41+]	Wheat straw	158	126	269	-111	-143

* Calculated values, implied in the kinetic model.
+ Recalculation from Hansen et al.[20] experiments.

Fig. 7 compares all the kinetic parameters obtained with those found in literature, with and without hydrogen inhibition, by means of a kinetic compensation diagram. A solid line has been drawn for each of the Langmuir-Hinshelwood constant. Most of the values lie within the same line what might be a sign of consistency in spite of the disparity in activation energies. The kinetic parameters according to n^{th} order kinetics are somewhat more scattered although still aligned. The differences between kinetic parameters can be also due to parameters not studied in this investigation like the number of active sites or the effect of temperature on the active sites behaviour. The three sets of kinetic parameters for birch (Langmuir-Hinshelwood kinetics) represent three valid numerical solutions in the model fitting.

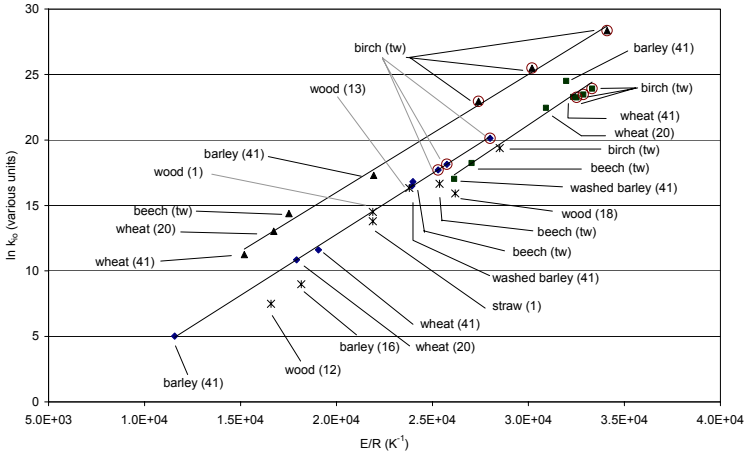

Fig. 7 Kinetic compensation diagram for H_2O and H_2O/H_2 gasification.
(✳: n^{th} order, ◆: k_{1f}, ▲: k_{1b}, ■: k_3, tw: this work)

EFFECT OF FUEL TYPE

With respect to reactivity, the results have shown no large differences between birch and beech. There are however certain differences regarding the effect of temperature on the reactivity profile, and the shape of the profile itself. Fig. 8 shows several reactivity profiles, normalised with respect to their reactivity at 20% conversion to allow comparison. The final increase in gasification rate is more drastic for beech than for birch, especially noticeable for beech at lower temperatures.

Moilanen and his co-workers[14,21] also obtain increasing reactivity profiles with conversion, except for peat. They expect such increasing reactivity because of pore development structure, enhanced by the catalytic effect of the ash, since the ratio catalyst/carbon increases with char conversion. Stoltze et al.[16] obtain similar profiles with barley straw. Rensfelt et al.[2] find as well increasing reactivity with conversion, and a characteristic shape of the reactivity profile for each fuel, having each fuel the same curve independent of temperature. However, for washed barley chars, Sørensen et al.[41] find a decreasing reactivity as a function of conversion.

The ash analysis presented in Table 2 shows very similar values for the potassium content of both woods, but there is some variation regarding other ash components. It cannot be known from the experiments whether the differences in the reactivity profiles are due to these other ash components or to a different porosity evolution as the conversion proceeds.

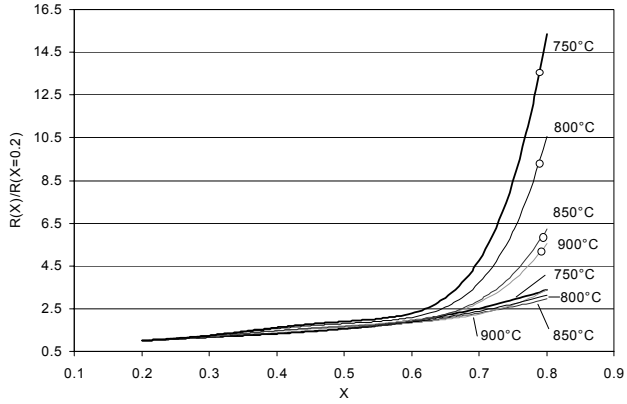

Fig. 8 Reactivity profiles for H_2O experiments. (O: beech experiments).

INFLUENCE OF REACTIVITY DEFINITION

In this section, six different procedures are used to select a representative reactivity value (r_c) from the same experiments, using the reactivity definition (eqn. 8). All the definitions are explained in Table 7.

Table 7 Representative reactivity definitions compared in this section.

	Description	X	Definition of r_c
1	Reactivity at 20% conversion	0.2	$r_c = r\ (X=0.2)$
2	Reactivity at 50% conv.	0.5	$r_c = r\ (X=0.5)$
3	Reactivity at 80% conv.	0.8	$r_c = r\ (X=0.8)$
4	Average reactivity (20-80% conv.)	0.2-0.8	r_c= average r between X=0.2 and 0.8
5	Structural profile f(X) assumed [35,39,42]	0.2-0.8	$r=r_c(T, P_{H2O})*f(X)$
6	Time for 80% conversion	0-0.8	$r_c=1/t(X=0.8)$

The kinetic parameters for the n^{th} order kinetic model have been obtained using these definitions of reactivity for the pure steam gasification experiments of birch. All the activation energies lie between 228-238 kJ/mol and the reaction orders between 0.54 and 0.58, apart from definition 3. The frequency factors are somewhat more scattered, lying between $5 \cdot 10^7$ and $3 \cdot 10^8$. Regarding the uncertainty of the calculation, definitions 2, 5 and 4 seem to give more precise results and it is interesting to notice that the error of the reaction order calculation does not depend on how a representative reactivity value is defined.

It is very important to analyse the influence of the reactivity definition (eqn. 8 and 9) on the kinetic parameters. Since all representative reactivity definitions are related to a fixed degree of conversion (or a fixed interval), the difference between r and r_w will be a multiplying factor, independent of temperature and pressure, and therefore absorbed in the frequency factor. This means that whether equation 8 or 9 is used, the activation energy and the reaction order calculation will give the same result.

CONCLUSIONS

(1) The kinetic parameters according to the n^{th} order reaction model for steam gasification of wood char are E= 237 kJ/mol, k_0= $2.62 \cdot 10^8$ and n= 0.57 for birch, E= 211 kJ/mol, k_0= $1.71 \cdot 10^7$ and n= 0.51 for beech char.

(2) Hydrogen inhibits the steam gasification reaction. The char gasification reaction with steam and hydrogen can be modelled based on Langmuir-Hinshelwood kinetics. The model fits well the results.

(3) The type of wood affects very little the kinetic parameters but shows some influence on the reactivity profile.

(4) The definition of the reactivity will not affect the activation energy or the reaction order calculation.

(5) The method to select a representative reactivity value from one experiment has more influence on the frequency factor than on the activation energy and reaction order. The accuracy of the calculation might also be affected.

ACKNOWLEDGMENTS

The work was supported by the Norwegian Research Council, the Danish Ministry of Energy and EK Energy A.m.b.A. The authors want to thank Torben D. Pedersen, Peter Mørk and Torben Lyngbech for their help during the experimental work.

REFERENCES

1. Gil, J., Aznar, M.P., Caballero, M.A., Francés, E. & Corella, J. (1997). Biomass gasification in fluidized bed at pilot scale with steam-oxygen mixtures. Product distribution for very different operating conditions, Energy and Fuels, Vol. 11, pp. 1109-1118.
2. Rensfelt, E., Blomkuist, G., Ekstrom, S., Espenäs, B.G. & Liinanki, L. (1978). Basic gasification studies for development of biomass medium-btu gasification processes, Energy from Biomass and Wastes, IGT, 14-18 August 1978. Paper No. 27, pp. 466-494.
3. Bilbao, R., García, L., Salvador, M.L. & Arauzo, J. (1998). Steam gasification of biomass in a fluidized bed, effect of a Ni-Al catalyst, Biomass for Energy and Industry. 10th European Conference and Technology Exhibition, 8-11 June 1998, Würzburg, Germany, pp. 1708-1711.
4. Rapagnà, S., Jand, N. & Foscolo, P.U. (1998). Utilisation of suitable catalysts for the gasification of biomasses, Biomass for Energy and Industry. 10th European Conference and Technology Exhibition, 8-11 June 1998, Würzburg, Germany, pp. 1720-1723.
5. Evans, R., Knight, R. A., Onischak, M. & Babu, S.P. (1987). Process performance and environmental assessment of the Renugas process, Energy from Biomass and Wastes X, IGT, pp. 677-696.
6. Paisley, M.A. et al. (1999). Commercial demonstration of the Battelle/FERCO biomass gasification process: Startup and initial operating experience,Proceedings of the 4th Biomass Conference of the Americas, Oakland, CA,USA, pp.1061-1066.
7. Zschetzsche, A., Hofbauer, H. & Schmidt, A. (1998). Biomass gasification in an internal circulating fluidized bed, Proceedings of the 8th EC on Biomass for Agriculture and Industry, Vol. 3, pp. 1771-1777.

8. Richard, J.R., Cathonnet, M. & Rouan, J.P. (1982). Gasification of charcoal: Influence of water vapor, Fundamentals of Thermochemical Biomass Conversion, pp. 589-599. Elsevier Applied Science Publishers.
9. Li, J. & van Heiningen, A.R.P. (1991). Kinetics of gasification of black liquor char by steam,Industrial & Engineering Chemistry Research, Vol. 30, No, 7, pp. 1594-1601.
10. Timpe, R.C. & Hauserman, W.B. (1993).The catalytic gasification of hybrid poplar and common cattail plant chars, Energy from Biomass and Wastes XVI, Institute of Gas Technology, March 2-6, 1992, pp. 903-919.
11. Kojima, T., Assavadakorn, P. & Furusawa, T. (1993).Measurement and evaluation of gasification kinetics of sawdust char with steam in an experimental fluidized bed, Fuel Processing Technology, Vol. 36, pp. 201-207.
12. Capart, R. & Gélus, M. (1988). A volumetric mathematical model for steam gasification of wood char at atmospheric pressure, Energy from Biomass 4. Proceedings of the 3rd contractors'meeting, Paestum, 25-27 May, pp. 580-583.
13. Hemati, M. & Laguerie, C. (1988). Determination of the kinetics of the wood sawdust Steam-gasification of charcoal in a thermobalance, Entropie, No. 142, pp. 29-40.
14. Moilanen, A., Saviharju, K. & Harju, T. (1993). Steam gasification reactivities of various fuel chars, Advances in Thermochemical Biomass Conversion, Blackie Academic & Professional, 1993, pp. 131-141.
15. Moilanen, A. & Saviharju, K. (1997). Gasification reactivities of biomass fuels in pressurised conditions and product gas mixtures, Developments in Thermochemical Biomass Conversion, Blackie Academic & Professional, 1997, pp 828-837.
16. Stoltze, S., Henriksen, U., Lyngbech, T. & Christensen, O. (1993). Gasification of straw in a large-sample TGA, Nordic Seminar on Solid Fuel Reactivity, Chalmers University of Technology, Gothenburg, Sweden, 24 November 1993.
17. Stoltze, S., Henriksen, U., Lyngbech, T. & Christensen, O. (1994). Gasification of straw in a large-sample TGA, Part II Nordic Seminar on Biomass Gasification and Combustion, NTH, Trondheim, 21 June 1994.
18. Groeneveld, M.J. (1980). The co-current moving bed gasifier, Ph.D.thesis, Twente University of Technology, Enschede, Netherlands.
19. Whitty, K.J. (1997). Pyrolysis and gasification behaviour of black liquor under pressurized conditions, Academic Dissertation, Report 97-3, Åbo Akademi, Department of Chemical Engineering.
20. Hansen, L.K., Rathmann, O., Olsen, A. & Poulsen, K.(1997). Steam gasification of wheat straw, barley straw, willow and giganteus, Risø National Laboratory, Optics and Fluid Dynamics Department, Project No. ENS-1323/95-0010
21. Moilanen, A. & Mühlen, H.J. (1996). Characterization of gasification reactivity of peat char in pressurized conditions. Effect of product gas inhibition and inorganic material, Fuel, Vol. 75, No. 11, pp. 1279-1285.
22. Whitty, K.J. (1993). Gasification of black liquor char with H2O under pressurized conditions, Report 93-4, Department of Chemical Engineering, Combustion Chemistry Research Group.
23. Barrio, M.& Hustad, J.E. CO2 gasification of birch char and the effect of CO inhibition on the calculation of chemical kinetics, *This conference*.
24. Mühlen, H-J., van Heek, K.H. & Jüntgen, H. (1985). Kinetic studies of steam gasification of char in the presence of H2, CO2 and CO, Fuel, Vol.64, July, pp. 944-949.

25. Meijer, R., Kapteijn, F. & Moulijn, J.A.(1994).Kinetics of the alkali-carbonate catalysed gasification of carbon: H_2O gasification, Fuel,Vol.73,No.5, pp.723-730.
26. Hüttinger, K.J. & Merdes, W.F. (1992). The carbon-steam reaction at elevated pressure: formations of product gases and hydrogen inhibitions, Carbon, Vol. 30, No. 6, pp. 883-894.
27. Weeda, M., Abcouwer, H.H., Kapteijn, F. & Moulijn, J.A. (1993).Steam gasification kinetics and burn-off behaviour for a bituminous coal derived char in the presence of H_2, Fuel Processing Technology, Vol. 36, pp. 235-242.
28. Linares-Solano, A., Mahajan, O.P. & Walker, P.L. (1979). Reactivity of heat-treated coals in steam, Fuel, Vol. 58, May, pp. 327-332.
29. Liliedahl, T. & Sjöström, K. (1997). Modelling of char-gas reaction kinetics, Fuel, Vol. 76, No. 1, pp. 29-37.
30. DeGroot, W.F. & Shafizadeh, F.(1984). Kinetics of gasification of Douglas Fir and cottonweed chars by carbon dioxide, Fuel, Vol. 63, February, pp. 210-216.
31. Kannan, M.P. & Richards, G.N.(1990). Gasification of biomass chars in carbon dioxide: dependence of gasification rate on the indigenous metal content. Fuel, Vol. 69, June, pp. 747-753.
32. Illerup, J.B.& Rathmann, O.(1995).CO2 gasification of Wheat straw, barley straw, willow and giganteous, Department of Combustion Research, RISØ National Laboratory, 12th December.
33. Espenäs, B.G. (1993). Reactivity of biomass and peat chars formed and gasified at different conditions, Advances in Thermochemical Biomass Conversion, Blackie Academic & Professional, 1993, pp. 142-159.
34. Moilanen, A. & Kurkela, E. (1995). Gasification reactivities of solid biomass fuels, Preprints of papers, American Chemical Society, Division of Fuel Chemistry, Vol. 40(3), pp. 688-693.
35. Sørensen, L.H.(1994). Fuel reactivity as a function of temperature, pressure and conversion, Ph.D. thesis, Risø National Laboratory, Denmark.
36. Chen, G., Yu, Q. & Sjöström, K.(1997). Reactivity of char from pyrolysis of birch wood, Journal of Analytical and Applied Pyrolysis, Vol. 40-41, pp. 491-499.
37. Zanzi, R., Sjöström, K. & Björnbom, E. (1995). Rapid pyrolysis of agricultural residues at high temperature, Proceedings of the 2nd Biomass Conference of he Americas: Energy, Environment, Agriculture, pp. 630-636.
38. Bandyopadhyay, D., Chakraborti, N. & Ghosh, A.(1991). Heat and mass transfer limitations in gasification of carbon by carbon dioxide, Steel Research, Vol. 62, No. 4, pp. 143-151.
39. Sørensen, L.H., Gjernes, E., Jessen, T. & Fjellerup, J. (1996). Determination of reactivity parameters of model carbons, cokes and flame-chars, Fuel, Vol. 75, No. 1, pp. 31-38.
40. Rathmann, O., Stoholm, P. & Kirkegaard, M. (1995). The pressurized thermogravimetric analyzer at the Department of Combustion Research,, Risø: Technical description of the instrument, Roskilde: Risø National Laboratory, Risø-R-823(EN), Denmark.
41. Sørensen, L.H. et al. (1997). Straw - H2O gasification kinetics. Determination and discussion, Nordic Seminar on Thermochemical Conversion of Solid Fuels, 3rd December, 1997, Chalmers University of Technology, Sweden.
42. Risnes, H., Sørensen, L.H. & Hustad, J.E. CO_2 reactivity of char from Danish wheat, Norwegian spruce and Longyear coke. *This conference*.

Appendix III

High temperature filtration of biomass product gas, SEM-EDX analysis

This appendix contains the experimental results obtained from the SEM-EDX analysis of filter bed material and the filter cake obtained from experiment #16. The different samples were analyzed for 14 chemical elements (Fe, Mg, Si, Ca, K, Cl, Mn, Ce, P, S, Cu, Na, Ni and Zn).

It is important to be aware of the limitation connected to this method. As these chemical analyses are performed on the surface of the particles only (maximum depth of about 1μm). Despite this, the results are believed to give a qualitative description of the samples.

The table contains all 14 elements, while the 6 most important are extracted and shown in the figures. The following notation has been used in order to enhance readability.

Notation:

a - area analysis
p - point analysis

Bed – bed material
BPP – bright porous particle
Char – char particle
DP – dense particle
DBP- dense bright particle
Glass – particle with a glassy appearance
PP- porous particle
SOC – surface of a char particle

6516-1 Filter bed materiale AFS(Olivin)

	Fe	Mg	Si	Ca	K	Cl	Mn	Cr	P	S	Cu	Na	Ni	Zn
1a	2	26	14											
2a	3	26	14											
3a	3	25	15											
	3	26	14											

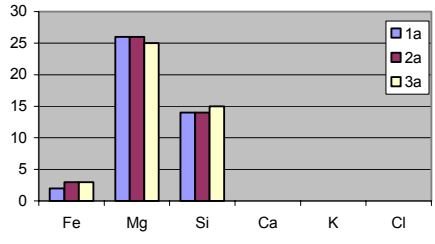

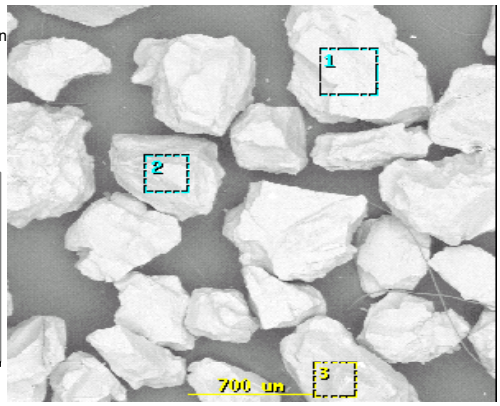

6516-1 Varmebehandlet AFS30; 900 °C i nitrogen og 450 °C i luf

	Fe	Mg	Si	Ca	K	Cl	Mn	Cr	P	S	Cu	Na	Ni	Zn
1a	2	26	14											
2a	4	25	13											
3a	2	26	14											
	3	26	14											

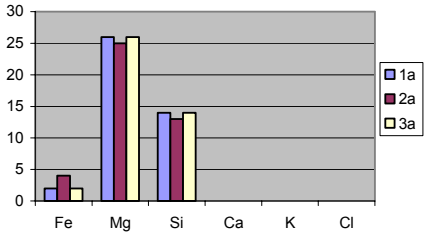

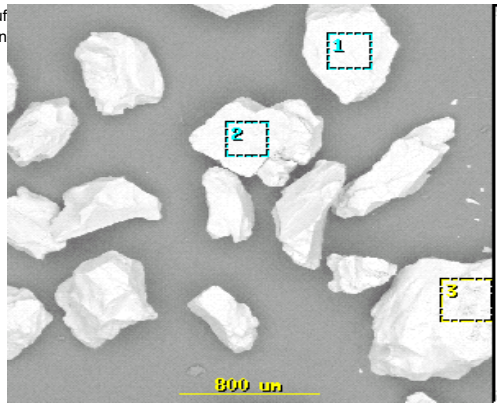

6517-1 HBU Gasif. filter dust **raw**, 0.397 g

	Fe	Mg	Si	Ca	K	Cl	Mn	Cr	P	S	Cu	Na	Ni	Zn
1p-DBP	4	5	12	15	6									
2p-DBP		3	9	30										
3p-SOC				43	4		1							
4p-SOC				46	2									
5p-SOC	2			30		2	3							

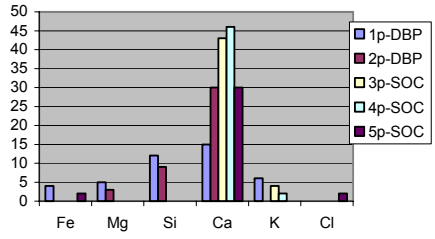

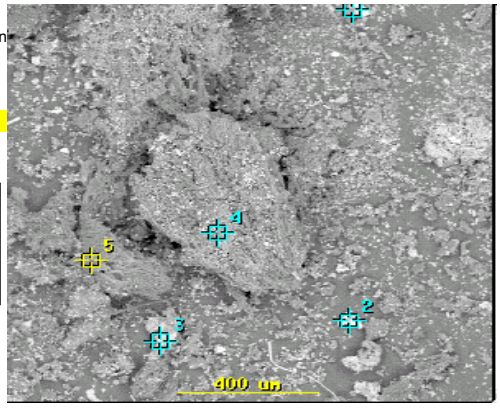

6517-2 HBU Gasif. filter dust **raw**, 0.397 g

	Fe	Mg	Si	Ca	K	Cl	Mn	Cr	P	S	Cu	Na	Ni	Zn
1a-SOC		9		34	2		3							

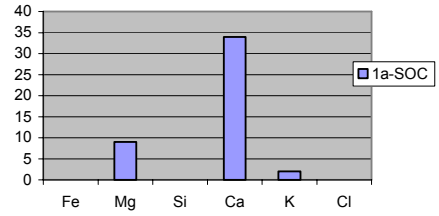

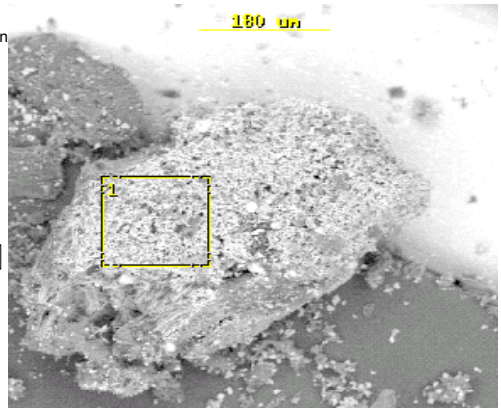

6518-1 Askerest HBU Dust #1 (Heated in sdt 900C/N2)

	Fe	Mg	Si	Ca	K	Cl	Mn	Cr	P	S	Cu	Na	Ni	Zn
1p-DP			19	19			1							
2p-BPP				46			2							
3p-Bed	2	26	14											
4p-DP	18	9						28						
5p-DP		3	23	11										
6p-BPP		10	4	25	2		2		2					

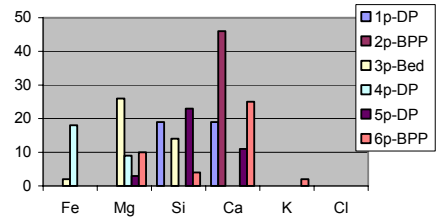

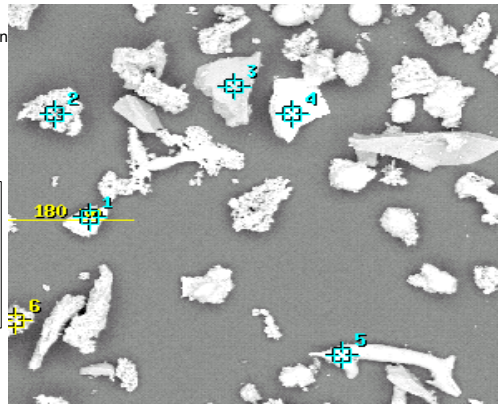

6519-1 HBU Dust #2 (Heated in sdt 900C/N2)

	Fe	Mg	Si	Ca	K	Cl	Mn	Cr	P	S	Cu	Na	Ni	Zn
1p		6	4	36	1									
2p		5		28	13		1				1			
3p	12		2	29										
4p	5	6	5	24	1		2							
5p		3	2	37	6		1							

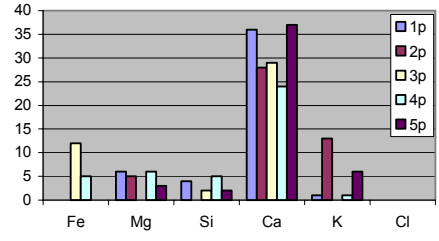

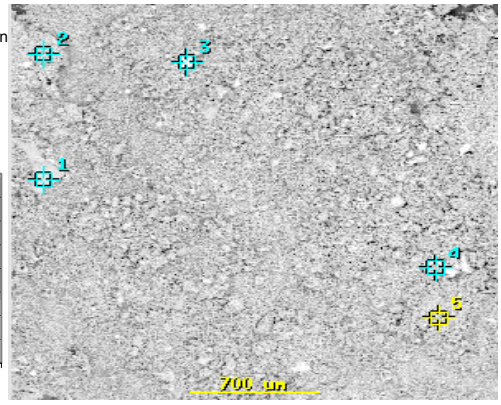

6520-1 280401 HBU Gasif. Filter dust ash (in air 450C)

	Fe	Mg	Si	Ca	K	Cl	Mn	Cr	P	S	Cu	Na	Ni	Zn
1p-BPP	1			43	4									
2p			2	42			3							
3p-DP			21	14	4									
4p-DP		10	4	29			2							
5p-PP	2		1	40	3		2							
6p-?		2	12	7	4					2	11			
7p-PP		2	4	33	9									

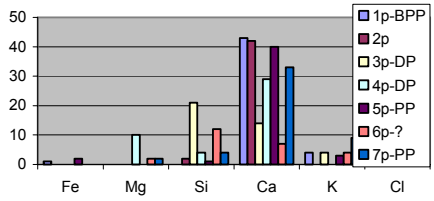

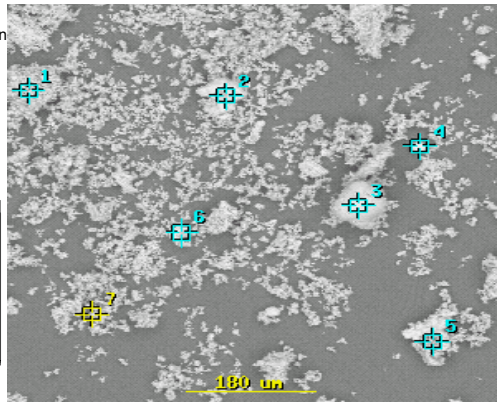

6521-1 Ash Dust, 13.07.01 (SDT 900C)

	Fe	Mg	Si	Ca	K	Cl	Mn	Cr	P	S	Cu	Na	Ni	Zn
1a+DP		6	2	35			2							
2a-PP		3		40			1					1		

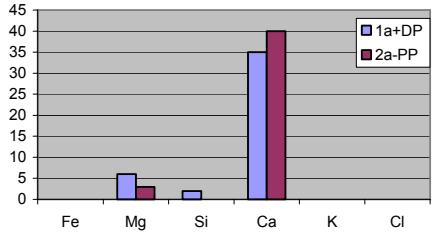

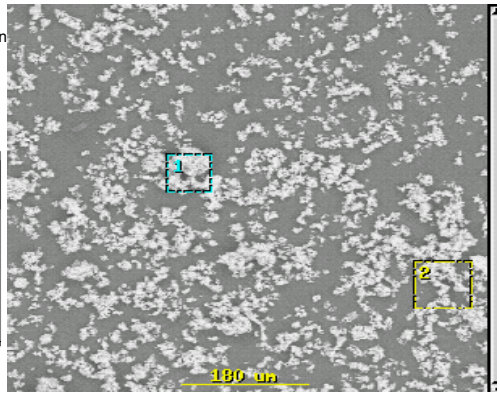

6522-1 Stov fra gasifier prod. gas, Exp. 13a MB **raw**

	Fe	Mg	Si	Ca	K	Cl	Mn	Cr	P	S	Cu	Na	Ni	Zn
1a-Char		5	3	19	9	3				3	2	1	1	
2a-Char	1	9	4	28	1		2							
3a-Char		6	3	32	2		2			1				
4a-Char	1	6	5	25			2			1		3		

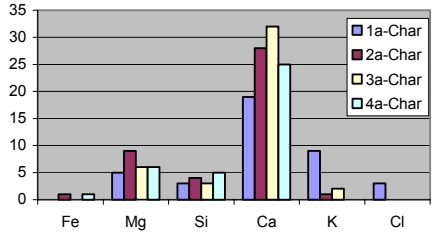

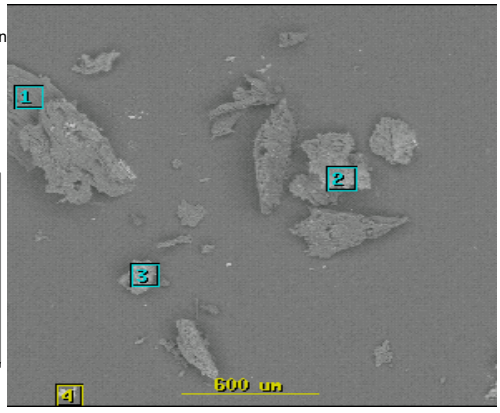

6523-1 Stov fra exp. 13a forasket ved 450°C i 6 timer

	Fe	Mg	Si	Ca	K	Cl	Mn	Cr	P	S	Cu	Na	Ni	Zn
1a-PP		4	5	20	8	1	2			3		1		
2a+DP		5	4	23	7		2			2		1		

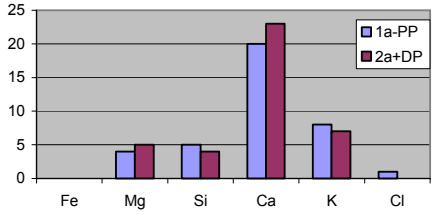

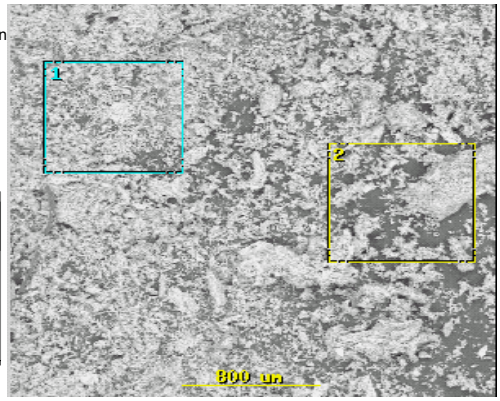

6524-1 Askerest #13a, 16.07.01 (SDT 900C)

	Fe	Mg	Si	Ca	K	Cl	Mn	Cr	P	S	Cu	Na	Ni	Zn
1p-PP	25	7		6						2				
2p-DP?	6	6	1	24	5		2			2				
3p-PP		6		41			1							
4p-PP	3	3		26	8		2				4			

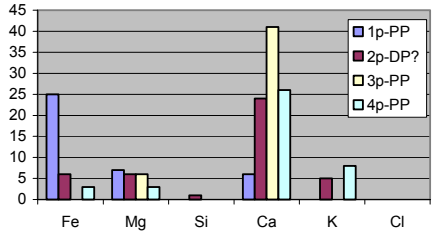

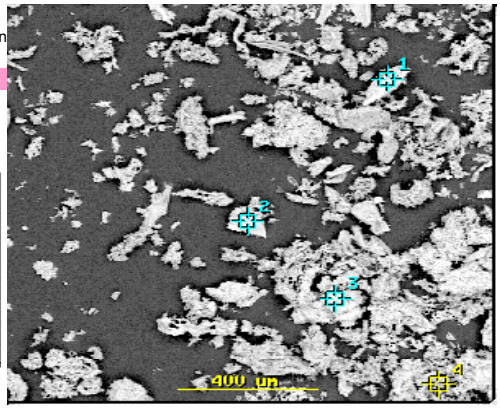

6525-1 6525_1 Askerest #13a-003, 16.07.01 (SDT 900C)

	Fe	Mg	Si	Ca	K	Cl	Mn	Cr	P	S	Cu	Na	Ni	Zn
1p-Glass	4	7		27			3			5				
2p-Glass	3	8		23			3			6				
3p-BPP			20	9	10					1		KCaSi		
4p-DP?	6	8	13		8							2		
5p-PP	1	5	3	28	2		2			2		1		

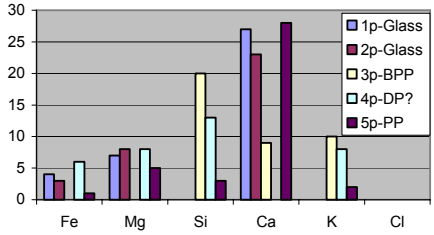

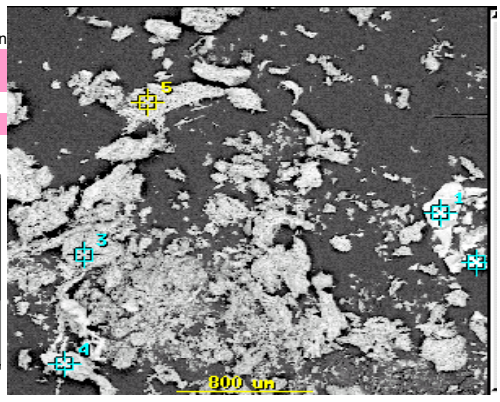

6526-1 Ash, 17.07.01 (SDT 900C, av støv 450C)

	Fe	Mg	Si	Ca	K	Cl	Mn	Cr	P	S	Cu	Na	Ni	Zn
1p+DP		5	15	11	6		2					5		
2p-DP			20	2	12				KSi			5		
3p-DP	3	9	1	15	4		2			3		3		7
4p-PP	2	3	2	36	1		3							

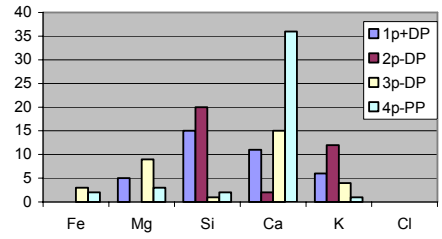

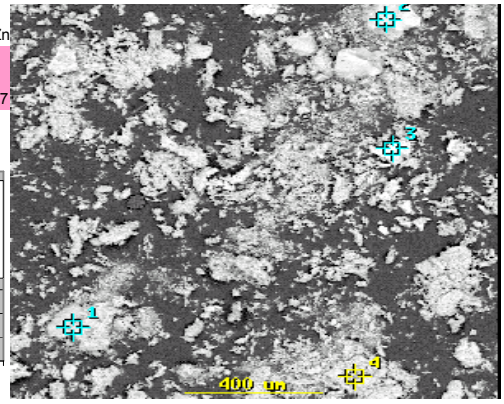

URN:NBN:no-3322